



THÈSE

En vue de l'obtention du

DOCTORAT DE L'UNIVERSITÉ DE TOULOUSE

Délivré par :

Institut Supérieur de l'Aéronautique et de l'Espace

Présentée et soutenue par :

Syed Mohd Fairuz Bin SYED MOHD DARDIN

le vendredi 19 juin 2015

Titre :

Étude d'algorithmes de poursuite du signal GNSS permettant d'améliorer le positionnement en environnement urbain

New adaptive tracking loop algorithm for reliable positioning in harsh environment

École doctorale et discipline ou spécialité :

ED MITT : Signal, image, acoustique et optimisation

Unité de recherche :

Équipe d'accueil ISAE-ONERA SCANR

Directeur(s) de Thèse :

M. Jean-Yves TOURNERET (directeur de thèse)

M. Vincent CALMETTES (co-directeur de thèse)

Jury :

M. Olivier BESSON Professeur ISAE-SUPAERO - Président

M. Emmanuel DUFLOS Professeur d'Université - Rapporteur

M. Serge REBOUL Maître de Conférence - Rapporteur

Mme Juliette MARAIS Chargée de Recherche

M. Jean-Yves TOURNERET Professeur d'Université - Directeur de thèse

M. Vincent CALMETTES Ingénieur Chercheur ISAE-SUPAERO - Co-directeur de thèse

Acknowledgement

First and foremost, it is with immense gratitude that I acknowledge the help and support of my supervisors, Dr. Vincent Calmettes and Prof. Jean-Yves Tournieret for taking me under their wings and guide me with their wisdom and patience throughout my study here. I dare say that without your vision, guidance and persistent help, this dissertation would not have been possible. Special thanks to my “pseudo” advisor, Mr. Benoit Priot for all your continuous support whose enthusiasm in the field of navigation had a lasting effect.

I would like to express my appreciation to my thesis committee member, Prof. Emmanuel Duflos, Dr. Serge Reboul, Dr. Juliette Marais and Dr. Olivier Besson for taking the time to be part of my defense. For the record, I want to thank you for letting my Ph.D defense to be an enjoyable with ‘good’ stressful moments at least for me personally, and also for your brilliant comments and suggestions which I am very grateful for.

My many thanks also goes to all the great people in DEOS department especially the SCAN team which have been home for me for the past 3 and half years. I wanted to take this opportunity to acknowledge the past and present colleagues, friends inside the group who are kind enough to share beautiful crazy moments that somehow coloured my life here in ISAE. Special thanks to my very good friends, Paulo and Hakim for keeping me in check and continue to do so even when you guys have left. In addition, I am extremely thankful to the Malaysian community here in Toulouse which help me unconditionally in my time in need and make me feel that I have a home here. I will never forget each and every one of you. In addition, I also need to express my gratitude to all my volleyball friends here which in some weird way keep me sane throughout my journey.

Finally, I cannot find words to describe my gratitude to my family back home especially Yoep, Nyah, and Adik for your continuous love, support and above all, your beliefs in me. To my little rascals, Afif, Nabil, Auni, Elman, Aqeel, Damia and Danial, I hope somehow my work here will ignite your imagination and instil a love of learning in your life. To my one and only Ayah, no word in the world can express my appreciation or no gesture is enough for me to repay you. You shaped me into the man I am today and I thank god every day for choosing you to be my dad.

Dedication

To my *ibu*... who I miss every single day!

Résumé

Cette activité de recherche concerne le domaine de la navigation par satellite qui utilise les systèmes GNSS (Global Navigation Satellite Systems). Elle vise à améliorer les performances globales d'un système de navigation, c'est à dire la robustesse, la disponibilité et l'intégrité d'un récepteur utilisant les signaux GNSS pour élaborer sa position et sa vitesse. L'enjeu est important et on note que les représentations des nouveaux signaux proposés pour GPS et GALILEO visent à diminuer la corrélation entre les signaux, faciliter la poursuite de ces signaux en abaissant le niveau des seuils de poursuite, réduire l'effet des interférences. La navigation basée sur les signaux GNSS reste toutefois dépendante du canal de propagation et est particulièrement affectée en cas réflexion, réfraction, diffraction, diffusion, et de blocage du signal émis par le satellite. Il en résulte une dégradation importante des performances en environnement urbain. L'objectif de cette recherche est ainsi de proposer, d'analyser et de caractériser des architectures de récepteur robuste, permettant d'adresser efficacement le problème de la navigation dans des environnements difficiles où le signal GNSS est affecté par de fortes perturbations.

De nombreux travaux de recherche visant à améliorer les performances des algorithmes de poursuite du signal au sein d'un récepteur ont été conduites, en particulier pour adresser le problème de cette poursuite dans des environnements difficiles, en présence de multi-trajets. Les approches les plus connues traitent le signal de post-corrélation. Ainsi l'utilisation de corrélateurs étroits permet de réduire l'impact des multi-trajets générant un retard important. De même des techniques utilisant un banc de corrélateurs pour estimer les paramètres des multi-trajets ont été étudiées. La présence de multi-trajets demeure toutefois une importante source d'erreur pour des récepteurs opérant en environnement urbain. L'amélioration des performances des récepteurs dans ce contexte reste un enjeu important et de nombreuses études sont conduites en vue d'améliorer la disponibilité, la robustesse, la fiabilité et l'intégrité de ces récepteurs.

Le principal objectif de cette thèse est de proposer une architecture de poursuite adaptative exploitant des techniques de poursuite vectorielle (Vector Tracking Loop – VTL). Les récepteurs conventionnels utilisent une architecture directe où une poursuite scalaire du signal (Scalar Tracking Loop – STL) est réalisée en amont du navigateur. Cette architecture n'utilise pas les informations élaborées par le navigateur pour améliorer les performances de la poursuite. Au contraire l'architecture vectorielle permet à la poursuite de bénéficier de la connaissance de la position et de la vitesse estimées par le récepteur. Il peut en résulter une dégradation de la poursuite lorsque le

navigateur ne sait pas isoler une mesure contaminée. Cette architecture rend donc les performances d'un canal très dépendantes des mesures utilisées par le navigateur, et donc en particulier des autres canaux. L'approche qui est explorée ici vise à combiner les approches de poursuite STL et VTL pour améliorer les performances des récepteurs en environnement urbain, dans un contexte multi-constellation.

Abstract

Present research activities in the field of Global Navigation Satellite Systems (GNSS) aim at enhancing the overall navigation performance by providing better and more robust navigation signals compared the ones available today. These GNSS signals are designed to provide better improved cross-correlation protection, lower tracking thresholds and reduced susceptibility to narrow band interferences. However navigation based on GNSS signals remains sensitive to propagation impairments such as reflection, refraction, diffraction and scattering, and sometimes blockage of the line of sight signals. These effects are especially important in urban environment. Therefore, a better and more robust receiver design and implementation is crucial to meet an appropriate navigation performance using GNSS signals.

Improving signal tracking algorithms inside the receiver is an attractive approach. This is particularly true in the case of urban environments where interference and multipath severely degrade the performance of the GPS positioning. Despite the many efforts of performance enhancement, multipath still remains as the dominant source of error and the limiting factor for many applications. Consequently improving the performance of a receiver in multipath environment is a great challenge and many studies are carried out to satisfy the above requirements in term of availability, reliability and integrity.

The main goal of this PhD thesis is to propose a new adaptive tracking algorithm based on vector tracking loop (VTL) approach. Currently, the conventional technique (i.e., Scalar Tracking Loop (STL)) is implemented in a forward-only strategy which doesn't exploit the position, velocity and time (PVT) solution provided by the Navigation System (NS). Standard VTL on the other hand, suffers from measurements contamination from the exploitation of PVT provided by the NS. This adaptive approach will take advantage of both tracking methods for providing reliable measurements in a multi-constellation context.

Table of Contents

List of Figures.....	v
List of Tables.....	ix
CHAPTER 1 – Introduction.....	1
1.2 History and background on GNSS.....	1
1.2 Motivation.....	3
1.3 Research Objectives.....	4
1.4 Thesis Structure.....	5
CHAPTER 2 – GPS Fundamentals.....	7
2.1 GNSS Signal.....	8
2.1.1 Signal Structure.....	9
2.1.2 Signal Model.....	11
2.2 Tracking Loop Fundamentals.....	12
2.2.1 Correlators.....	15
2.2.2 Discriminators.....	20
2.2.3 Loop Filter.....	24
2.3 Tracking Loop Implementation.....	26
2.3.1 Carrier Tracking Loop.....	28
2.3.2 Code Tracking Loop.....	30
2.3.3 Tracking Loop Assessment.....	31
2.4 Summary.....	34
CHAPTER 3 – Channel Analysis.....	35
3.1 Propagation Impairments.....	36
3.2 MP Channel Model.....	37
3.2.1 MP Effect on Tracking Loop.....	40
3.2.2 In-House Simulator.....	46
3.3 Land-Mobile Satellite Channel.....	52
3.3.1 Statistical Channel Model (SCM).....	52
3.3.2 Physical-statistical Channel Model (PSCM).....	55
3.3.3 Weakness of existing models.....	57
3.3.4 Integrating LMS channel model in our Simulator.....	57
3.3.5 Simulation Environment of the DLR Channel.....	59

3.4 Summary	64
CHAPTER 4 – Signal tracking in GNSS Receivers	65
4.1 GNSS receiver architecture	66
4.2 Navigation Solution (NS)	69
4.2.1 Least Mean Square (LMS) PVT Estimation	70
4.2.2 Extended Kalman Filter (EKF).....	75
4.3 Scalar Tracking Loop (STL) Configuration.....	79
4.3.1 Local Estimator.....	81
4.3.2 Parameters affecting STL Performance	82
4.4 Vector Tracking Loop (VTL) Architecture	83
4.4.1 Principal of Vector Tracking Architecture	84
4.4.2 Centralized Architecture	85
4.4.3 Decentralized Architecture	89
4.4.4 Summary of the VTL Approach	93
4.5 VTL Implementation.....	94
4.5.1 Measurement Model	95
4.5.2 NS Outputs	97
4.6 Performance Evaluation for STL vs. VTL.....	97
4.6.1 Simulation Methodology	98
4.6.2 Impact of MP.....	99
4.6.3 Impact of Masking.....	106
4.6.4 Possible Enhancement of the Current Tracking Architecture.....	108
4.7 Summary	110
CHAPTER 5 – Adaptive Vector Tracking Loop (AVTL).....	113
5.1 Urban Environment – Perspective for Adaptive MP Scenarios	114
5.2 Time-Frequency Processing	115
5.2.2 Frequency Analysis.....	116
5.2.3 Time-Delay Analysis	122
5.3 Adaptive Tracking Architecture and Implementation	128
5.3.1 Navigation System	130
5.3.2 NCO Control	133
5.3.3 Correlators and Discriminators	134
5.3.4 Local Estimator.....	135

5.3.5 Monitoring and Control	146
5.4 Adaptive Tracking Performance Analysis.....	154
5.4.1 Simulation using an In-house simulator	154
5.4.2 Simulation using DLR Model	160
5.5 Summary	165
CHAPTER 6 – Conclusions	167
6.1 Perspective.....	167
6.2 Future Work.....	169
Bibliography	171
Rédaction De Mémoire De Thèse	179
CHAPITRE 1: Introduction	181
Objectif.....	181
Contexte.....	182
CHAPITRE 2 : Principe des systèmes GNSS	185
CHAPITRE 3 : Canal de transmission	187
Modèle déterministe	187
Modèle physico-statistique.....	188
Mise en œuvre du simulateur du DLR	189
Effets des multi-trajets.....	193
CHAPITRE 4 : Poursuite du signal dans les récepteurs GNSS.....	193
Navigateur.....	194
Boucles de poursuite	198
CHAPITRE 5 : Poursuite des signaux en présence de multi-trajets.....	207
Détection des multi-trajets	209
Stratégie pour la gestion des multi-trajets	211
Performance du récepteur proposé	218
CHAPITRE 6 : Conclusion.....	223
Bibliographies	225

List of Figures

Figure 1: Scenario illustration of received path for a GNSS receiver.	3
Figure 2: DSSS Modulation.	8
Figure 3: Example of (a) Auto-correlation and (b) Cross-correlation function of NRZ sequence based on Gold codes.	10
Figure 4: Illustration of received signal at the receiver.	11
Figure 5: Basic demodulation scheme	13
Figure 6: Generic model of tracking Loop.	13
Figure 7: Complete Conventional Tracking Loop Architecture.	14
Figure 8: Complex correlator for 'carrier wipe-off'.	15
Figure 9: Phasor diagram of various conditions for I and Q components.	16
Figure 10: Early-Prompt-Late Correlation for I-arm.	17
Figure 11: Code Correlation for E-P-L correlator arms	17
Figure 12: Interpretation of the correlator outputs in phasor diagram.	18
Figure 13: Filtering effect related to the integration time.	19
Figure 14: The effect of carrier-phase misalignment.	19
Figure 15: Illustration of (a) Early, Prompt and Late correlation function with (b) the resulting zero-crossing.	23
Figure 16: The effect of the bandwidth size (Bn) of the loop filter.	25
Figure 17: Full implementation of the GPS tracking loop for single channel.	27
Figure 18: Input/Output relationship of the GPS tracking [13].	27
Figure 19: 1 st order FLL assisted 2 nd order PLL Loop Filter Architecture.	29
Figure 20: 1 st order DLL with carrier aiding.	30
Figure 21: Assessment of the tracking loop.	31
Figure 22: Correlator outputs of the In-phase (top) and Quadrature-phase (bottom).	32
Figure 23: Discriminator outputs for carrier tracking loop (top) and code tracking loop (bottom).	33
Figure 24: Frequency (top) and delay (bottom) of the signal vs. estimation by tracking loop.	33
Figure 25: Two path signals; (a) at the same frequencies and (b) at different frequency.	39
Figure 26: Illustration of (a) Constructive interference, and (b) Destructive interference [10].	41
Figure 27: S-Curve plot for direct path (green), multipath (red), and resulted composite signal (blue).	42
Figure 28: S-curve plots; (a) in case of constructive interference, and (b) in case of destructive interference.	42

Figure 29: Generic interpretation of MP error envelope.	43
Figure 30: Phasor diagram illustrating the relationship between the direct path and multipath.	44
Figure 31: Phasor Diagram illustrating the effect of the MP phase.	45
Figure 32: Phasor diagram of DP and MP associated with respective frequencies.	46
Figure 33: Synthetic receiver's trajectory.	46
Figure 34: Illustration for the range of LOS signal.	47
Figure 35: Illustration of DP and MP signals.	49
Figure 36: In-house Simulator for MP Channel model.	50
Figure 37: Output Samples of the Simulator.	51
Figure 38: Tracking Estimation using standard receiver configuration.	51
Figure 39: Statistical CIR of wideband channel model proposed by [18].	53
Figure 40: Overview block diagram of the DLR model implementation [21].	56
Figure 41: Sampled image of the artificial scenery [21].	56
Figure 42: DLR model for the isolated reflector [21].	56
Figure 43: Illustration on the integration of the DLR model in our simulator.	59
Figure 44: PSD of the DLR channel for urban environment.	60
Figure 45: PSD of the DLR channel for suburban environment.	61
Figure 46: Top-view of the PSD using the DLR model.	62
Figure 47: Snapshot of the MP delay during simulation.	63
Figure 48: MP delay distribution for the whole simulation for urban scenario.	63
Figure 49: MP delay distribution for the whole simulation for suburban scenario.	63
Figure 50: Illustration of generic GNSS receiver architecture.	66
Figure 51: Block architecture of the signal processing and navigation modules.	67
Figure 52: Illustration of signal acquisition in (a) strong signal presence and (b) signal absence.	68
Figure 53: NS Observations	69
Figure 54: GPS trilateration concept.	70
Figure 55: EKF Approach in a Navigation System.	76
Figure 56: Scalar tracking loop receiver architecture.	80
Figure 57: Centralized Architecture using Correlator's output.	86
Figure 58: Bank of Correlator outputs as Measurement in Single Step Approach.	87
Figure 59: Centralized Architecture using Discriminator's output.	87
Figure 60: Discriminator outputs as Measurement in Single Step Approach.	88
Figure 61: Decentralized Architecture using Correlator outputs.	90
Figure 62: Correlator outputs as Measurement in Two-Steps Approach.	91

Figure 63: Decentralized Architecture using Discriminator's outputs.	91
Figure 64: Discriminator outputs as Measurement in Two-Step Approach	92
Figure 65: Vector tracking implementation focusing only for single channel	94
Figure 66: (a) Satellite constellation and (b) the reference trajectory over map.	98
Figure 67: Estimated trajectory under nominal condition represented by (a) the trajectory and (b) the ENU positions.	98
Figure 68: Area indicated where MP were introduced inside the trajectory.	99
Figure 69: (a) Overall STL performances on positioning error and (b) the trajectory associated in the presence of MP.	100
Figure 70: (a) Overall delay error for STL mode for the whole trajectory with a (b) zoom-in at the MP presence.	101
Figure 71: Delay discriminator output in STL mode.	101
Figure 72: (a) Overall STL performance on positioning error and (b) the trajectory associated in the presence of MP.	102
Figure 73: (a) Overall delay error for VTL mode for the whole trajectory with a (b) zoom-in at the MP presence.	102
Figure 74: Delay discriminator output in VTL mode with (a) focusing on the contaminated channel and (b) focusing on the other channel.	103
Figure 75: Tracking performance of (a) STL and (b) VTL when contaminated channels are being discarded.	105
Figure 76: Comparison between both VTL approaches in the presence of MP when the contaminated channels are (a) used as measurements and (b) discarded.	106
Figure 77: (a) Short and (b) long masking area implemented over the trajectory.	107
Figure 78: Short masking effect on (a) delay and (b) frequency estimation for both STL and VTL.	107
Figure 79: Long masking effect on (a) delay and (b) frequency estimation for both STL and VTL.	108
Figure 80: Possible Scenario in Harsh environment – Alternating satellite masking and visibility.	109
Figure 81: Illustration of Diffuse and Specular MP.	109
Figure 82: Implementation of the frequency-domain detector in GNSS receiver.	117
Figure 83: FFT output for a given scenario.	118
Figure 84: Frequency spectrum of different MP conditions	119
Figure 85: FFT response for different values of C/N_0 .	121
Figure 86: Frequency spectrum with the presence of non-coherent MP.	122
Figure 87: Implementation for Multiple Delay Discriminator approach.	123
Figure 88: MEE of different discriminator functions and values of chip spacing.	125

Figure 89: Zoom for the MEE within short-MP ranges.	126
Figure 90: S-curve for different discriminator functions.	127
Figure 91: High-level description of the adaptive tracking architecture.	128
Figure 92: Proposed Adaptive Tracking Architecture.	129
Figure 93: NCO Control for adaptive tracking loop.	133
Figure 94: Correlators and discriminators for the proposed adaptive tracking loop.	134
Figure 95: PLL/FLL Architecture for adaptive tracking.	136
Figure 96: DLL Architecture for adaptive tracking.	136
Figure 97: Simplified receiver architecture for (a) STL mode and (b) VTL mode.	139
Figure 98: Frequency domain detector implementation.	146
Figure 99: Linear model of the adaptive delay estimator	149
Figure 100: Influence function β .	152
Figure 101: Weighting function.	153
Figure 102: Overview concept of STL/VTL mode.	154
Figure 103: Artificial reference trajectory.	155
Figure 104: Simulation configuration.	155
Figure 105: Satellite constellation.	155
Figure 106: Zoom on the MP scenarios	157
Figure 107: 2D global comparison of position estimation.	158
Figure 108: 3D global comparison of position estimation.	158
Figure 109: 2D - Positioning Error between STL, VTL and AVTL approaches.	159
Figure 110: 3D – True Error between STL, VTL and AVTL approaches.	159
Figure 111: Integrating the DLR to provide the channel profile.	161
Figure 112: Integrating the data-file generated by the DLR with the in-house simulator.	161
Figure 113: PSD of satellite #1.	162
Figure 114: Top view of DLR Simulated Trajectory for Car in Urban Environment (Sat #1)	162
Figure 115: 2D global comparison on position error using DLR Channel Model	163
Figure 116: 3D global comparison on true error using DLR Channel Model.	163
Figure 117: 2D - Positioning Error of STL, VTL and AVTL approaches using DLR channel model.	164
Figure 118: 3D - True Error of STL, VTL and AVTL approaches using DLR channel model.	164

List of Tables

Table 1: Common discriminator algorithm for PLL [1].	20
Table 2: Common discriminator algorithm for FLL [1].	22
Table 3: Common discriminator algorithm for DLL [1].	23
Table 4: Loop filter characteristics [1].	26
Table 5: Standard error model [15].	36
Table 6: Advantages and Disadvantages of Different VTL Architectures.	93
Table 7: Advantages and Disadvantages of Different Measurement Model	93
Table 8: Parameters of the MP introduce during simulation.	99
Table 9: Description of the controlled MP scenarios.	156
Table 10: Mean and maximum values of the positioning error.	160
Table 11: Mean and maximum values of the positioning error.	165

CHAPTER

1

CHAPTER 1 – Introduction

This chapter gives an overview of the project in general to set the baseline of the work and in what aspect it would explore. Moreover, the background history will enlighten the broader picture of the work. The motivations and objectives of this research are provided. Finally this introduction proposes an overview structure of every chapter of this PhD thesis.

1.2 History and background on GNSS

Global Navigation Satellite System (GNSS) is a common terminology for satellite navigation (SatNav) systems which provide autonomous geo-spatial positioning with global coverage. The Global Positioning System (GPS) operated by the United States (US) government is the only system that has been fully operational since 1995. This system has been followed by the Global Orbiting

Navigation Satellite System (GLONASS) operated by the Russian government which became operational in 2011 and satellites of the future, GLONASS-K2 are being launched. Others systems worth to be mentioned are the European Union's GALILEO positioning system and the expansion of China's regional Beidou navigation system to its global COMPASS navigation system. The first GPS satellite named Navstar 1 owned by the US was launched on 22nd February 1978 and the system was declared to have full global coverage since 1995. This full coverage can only be achieved with 24 GPS satellites that are also known as space vehicles (SV) in circular orbits around earth and distributed in 6 orbital planes.

Basically the system allows GNSS receivers to determine their location in the precision of a few meters using the propagation delay and Doppler frequency of the line-of-sight (LOS) signals transmitted by the satellites. The basic concept of this system is that each satellite continually transmits messages that include data transmission time, precise orbital information and its general system health. The receiver will use the transmitted message to determine the transit time of each message and compute the distances between the receiver and of each satellite. These distances are used in trilateration process to compute the absolute position of the receiver [1]. This approach needs to compute the satellite locations and to estimate accurately the range to each satellite. In open environment, these operations are neatly achieved by tracking the incoming signal in order to: 1) determine the transit time and the Doppler frequency and 2) extract the navigation message. This message is used for computing satellite locations and to perform ranging correction by taking into account satellite clock and propagation delay errors.

Since its beginning, many new GNSS-based applications emerge that push the boundary of the operational requirements beyond the capability offered by the conventional GNSS receivers. These phenomena have directly motivates advances in the receiver's algorithms to fit diverse application requirements including to overcome sources of errors that can affect the signals quality for optimum performance. Improvement due to GNSS augmentations and modernization can reduce many sources of errors. However multipath and shadowing effects are still significant and sometimes dominant contributors of errors [1]. Upon this realization, many researches have been carried out to provide better understanding on the characteristic of this error, its effects and best ways to mitigate their effects in order to have the optimum performance for any GNSS-based applications. We'll see that this study is part of this effort.

1.2 Motivation

The performance parameters of a GNSS system are predominantly measured in terms of accuracy and availability which are normally associated with the intended application. However, other performance parameters have been introduced to address sensitive applications such as localization for vehicle taxing, air navigation, safety-related applications. These applications need to increase the localization reliability and integrity: a precise accuracy specification associated with an interval of confidence is required. These applications need to offer a continuity of service, which demands for the navigation system to be available without interruption. Current activities in the field of GNSS aim at the enhancement of the overall navigation performance providing better navigation signals compared to those available today. Nevertheless these requirements cannot be satisfied without improving tracking algorithms inside the receiver.

This is particularly true in the case of interference and multipath dense scenarios and environments which severely degrade the performance of the GPS positioning as being illustrated in Figure 1. The GNSS signals propagating between the satellites and the receiver experience different kinds of propagation impairments such as reflection, refraction, diffraction and scattering of the emitted signal. These effects lead to fluctuations and changes in amplitude, phase and direction of the propagation waves, and sometimes to signals outages.

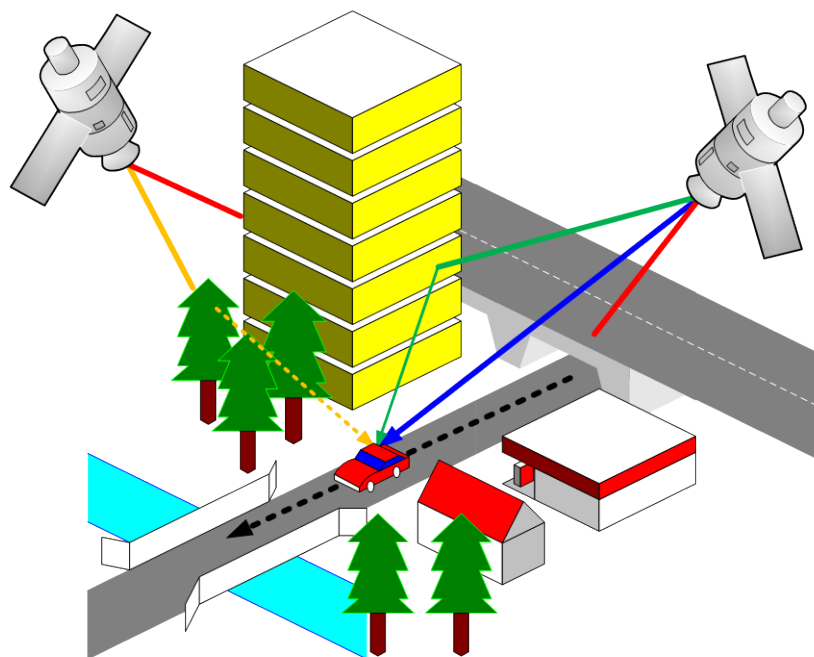


Figure 1: Scenario illustration of received path for a GNSS receiver.

Therefore, a better and more robust receiver design and implementation is crucial to ensure the performance of the GNSS system is met. A very promising approach is to optimize the modulation schemes of the present signals. Significant enhancement can be achieved in terms of code noise, tracking robustness and susceptibility to multipath. Present research activities in the field of GPS modernization or the development of European Galileo system aim to enhance the overall navigation performance by providing better and robust navigation signals compared to the ones available today. These GNSS signals are designed to provide better improved cross-correlation protection, lower tracking thresholds and reduced susceptibility to narrow band interference [2]. Moreover, when different systems such as GPS and GLONASS (Galileo in the future) are considered in multi-constellation receivers, availability can be improved.

Despite the many efforts of performance enhancement, multipath still remains as the dominant source of error and the limiting factor for many applications. Furthermore, short-delay multipath (approximately up to 30m) are considered the most difficult to tackle and do not depend on the signal design since they are the same for all modulations [3]. Therefore, this kind of multipath that are found in urban canyons, is considered as the major inevitable source of error contributing to the error budget, and it remains as the most difficult challenge to mitigate. That is why intensive research that has been conducted is focusing on how to improve the tracking sensitivity and robustness especially when dealing with strong multipath in urban environment.

Consequently improving the performance of a receiver in multipath environment is a great challenge and many studies are carried out to satisfy the above requirements: availability, reliability, integrity.

1.3 Research Objectives

The objectives of this PhD thesis represent a comprehensive and relevant approach for validating new receiver architectures which address the issue of localization in urban environment. In general, the objectives of this work can be well explained in 3 different perspectives.

The first objective is to analyse multipath phenomena, and to look at its impact on tracking loop performance. In depth coverage on multipath characteristics and behaviours, helps to give better understanding on how to mitigate it effectively by using certain signal processing techniques especially in the multipath dense scenarios such as urban environment. Therefore this investigation

aims to define a realistic simulation environment for assessing the performance of existing and future algorithm tracking loops in the presence of multipath.

The second objective is to review and re-evaluate the main architectures which are designed for multipath mitigation techniques. This involves in studying the different processing approaches in dealing with multipath scenarios, and their motivations. At the same time, the drawbacks of each technique will be also carefully studied in order to find better multipath mitigation techniques.

The final goal of this project is to propose a new tracking algorithm with improvement. Whereas the conventional techniques are implemented in a forward-only strategy which doesn't exploit the position, velocity and time (PVT) solution for tracking the incoming signal [4], [5], [6]. The algorithms that are proposed in the frame of this study are based on Vector Tracking Loop (VTL) architecture where the tracking loops take advantage of the state of the navigator. Improvement related to this approach will be assessed in the environment defined from the second objective.

1.4 Thesis Structure

This thesis will first cover the fundamentals in GNSS tracking loop architecture and its respective signal processing techniques before gradually discussing on major part of the research and its contributions. Therefore, besides the **Chapter 1** which is introducing new GNSS requirements and motivations behind this research, the rest of the chapters are organized as follows:

Chapter 2 describes the major state-of-the-art multipath mitigation techniques that are available in the literature. Before that, some background on the signal models and structures of the GPS signals is introduced. Furthermore, typical tracking loop architectures, their parameters and their typical behaviours in nominal situations are also discussed. The main purpose of this chapter is to summarize how the tracking loops behave in harsh environment.

Chapter 3 deals with the land mobile satellite channel. Two main channels are proposed for algorithm assessment. The first one is based on a simple deterministic model which allows a coarse characterization of the receiver. A more realistic model [7] is also analysed and used for simulating sub-urban and urban environment. Choosing the right channel model, especially the one closest to the real environment, is a fundamental issue that requires tracking techniques to be developed in realistic scenarios.

Different receiver architectures are described in **Chapter 4** and a VTL based architecture is proposed. The complete system architecture, implementation, strengths and weaknesses of each tracking loop implementation will be evaluated and discussed. Furthermore, performances of each tracking loop as well as the comparison are being carried out to further justify the adaptive tracking loop algorithm which is the main aim of this project.

Chapter 5 focuses on the implementation of an adaptive algorithm processing which allows the availability and the reliability of the receiver to be improved. The performance of this adaptive processing is evaluated first using a controlled multipath environment and later a more realistic channel models. This is considered as the heart of the thesis where all the contribution of this project is being described in detail.

This work is concluded in **Chapter 6** by giving the overall conclusion and perspectives of the project.

CHAPTER 2

CHAPTER 2 – GPS Fundamentals

This chapter examines the properties of GPS satellite signals and the receiver architecture considered in this PhD thesis. It can generally be divided into three parts. The first part discusses the signal components and structure, regarding the GPS system. It provides a good understanding on the principles and characteristics that make a GPS signal unique for positioning. The second part deals with signal processing operation inside the GPS receiver. This part presents conventional tracking loops that are commonly used for estimating signal parameters, are studied. A specific highlight is given on the analysis of the correlators and discriminators which strongly impact the quality of the estimators, as their outputs are usually used as observation of the signal parameters. The last part examines the behaviour of stand-alone tracking loops and the factors that affect its performances. These fundamental overviews are very important in order to proposed new tracking algorithm which is the main goal of this thesis work.

2.1 GNSS Signal

The GNSS system has its own unique way of transmitting and receiving signals to allow global navigation and position estimation. This GPS signal structure will be further explained, justifying the choices made in the navigation context. This system is composed of both civilian and military components even if most studies are focusing on the civilian segment. On the contrary, the military segment is used by secured users with some enhanced capability. Therefore, the study which is carried out here focuses mainly on the civilian segment of the GPS signals.

Basically, the GPS system is a code division multiple access (CDMA) scheme. It is also known as a direct sequence spread spectrum (DSSS) technique and used in many digital communication links. It is a form of multiplexing method where the transmitter encodes the signal using a unique pseudorandom sequence for each communication channel. This sequence is known by the receiver and can be used to decode the incoming signal.

Relative to the GPS system, each satellite's signal consists of a sinusoidal carrier, a unique wide pseudo-random noise (PRN) sequence and a digital navigation message as illustrated in Figure 2. The use of orthogonal PRN codes allows multiple satellites to operate at the same frequency without interfering with each other. Besides that, as regards to positioning, PRN code synchronisation enables ranging measurement, from each satellite to the user. Therefore the structure of the signal is well suited for a navigation system.

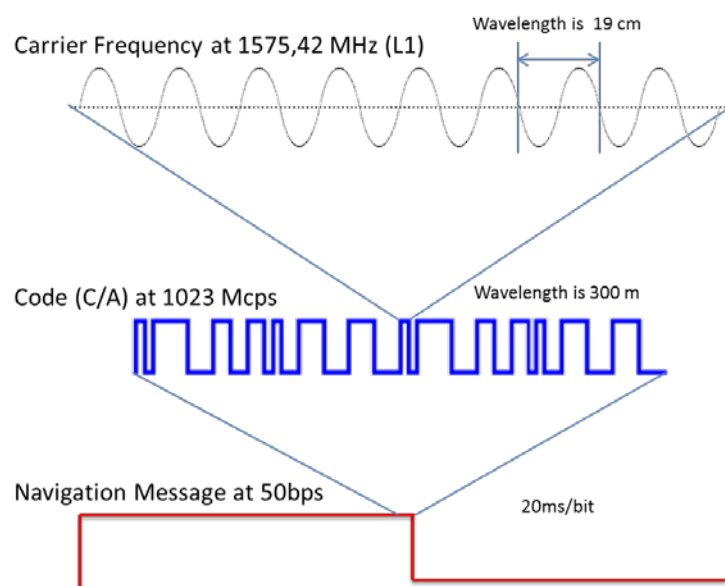


Figure 2: DSSS Modulation.

On one hand the *L*-band carrier frequency offers a good compromise as regards to antenna gain and ionospheric delay. In particular, this frequency offers accurate ranging measurement. On the other hand, the PRN sequence enables robust ranging measurement. Finally the data message which is broadcast by each satellite provides sufficient information to calculate the satellite positions, to date accurately the transmission time and to perform some correction such as the propagation error correction.

2.1.1 Signal Structure

As the GPS is a version of a spread spectrum system, all the signals in a single service use the same central frequency. In the case of the GPS system, the satellites broadcast the signals at different central frequencies:

$$L1, L1C = 154 \cdot 10.23 \text{ MHz} \approx 1575.42 \text{ MHz}$$

$$L2, L2C = 120 \cdot 10.23 \text{ MHz} \approx 1227.6 \text{ MHz} \quad (2.1)$$

$$L5 = 115 \cdot 10.23 \text{ MHz} \approx 1176.45 \text{ MHz}$$

where the link 1 (*L1*), the link 2 (*L2*) and the link 5 (*L5*) are multiples of the master clock frequency at 10.23 MHz . Both frequencies are very accurate as their reference is an atomic frequency standard which is slightly lower than 10.23 MHz to compensate a part of relativistic effect [8]. Besides that, multi-frequency receivers can compensate for errors induced by ionospheric effects by exploiting the frequency dependency of the ionospheric delay [9].

Considering the block IIR, launched in 1997-2004, the signal structure for the *L1* frequency contained both coarse/acquisition (C/A) code and precision (P(Y)) code signals whereas the *L2* frequency only contained the P(Y) code. Therefore, the transmitted signal by each satellite of the IIR block can be written as:

$$S_{L1,i}(t) = A_{P(Y)} \cdot D_i(t) \cdot P_i(t) \cdot \cos(2\pi f_{L1}t) + A_{C/A} \cdot D_i(t) \cdot C_i(t) \cdot \sin(2\pi f_{L1}t) \quad (2.2)$$

$$S_{L2,i}(t) = A_{P(Y)} \cdot D_i(t) \cdot P_i(t) \cdot \cos(2\pi f_{L2}t)$$

where $S_{L1,i}$ and $S_{L2,i}$ are the signals generated at the $L1$ frequency given by f_{L1} , and at the $L2$ frequency given by f_{L2} of the satellite i . The terms $A_{P(Y)}$ and $A_{C/A}$ denote the amplitude for the P(Y) code and the C/A code respectively. Note that $D(t)$ represents the data payload and that $P_i(t)$, $C_i(t)$ are the P(Y) and the C/A codes for the satellite i .

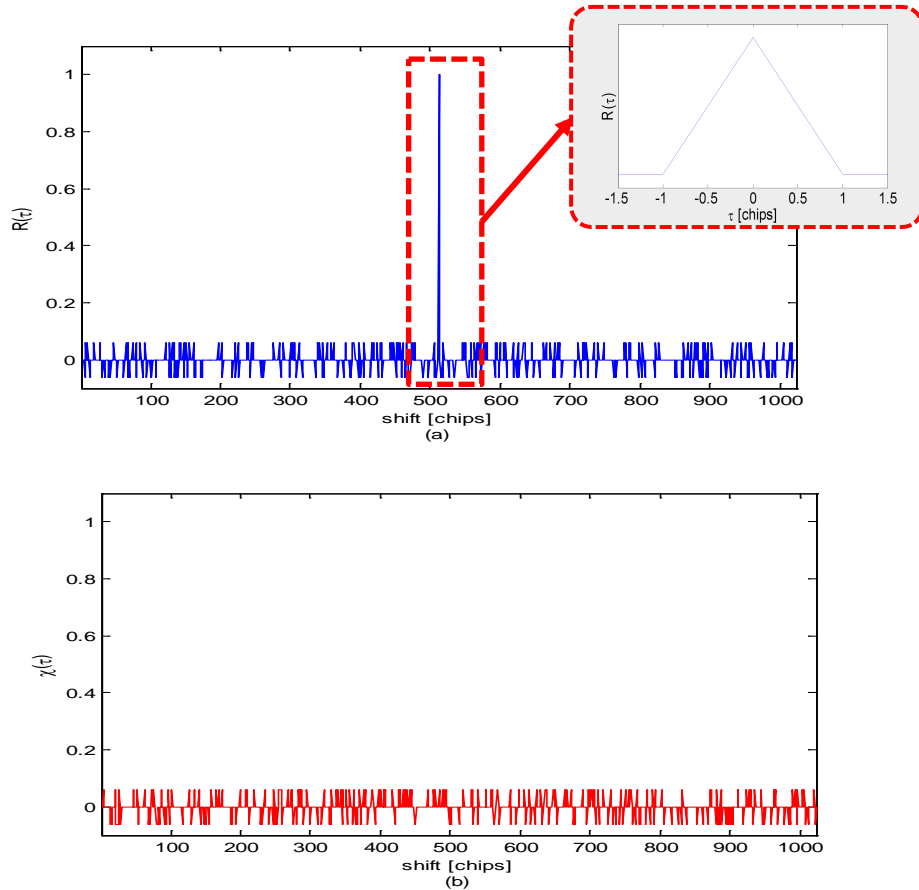


Figure 3: Example of (a) Auto-correlation and (b) Cross-correlation function of NRZ sequence based on Gold codes.

Another important aspect of the GPS signal concerns the pseudo-random noise (PRN) code properties and the signal representation. The PRN sequences used for GPS $L1$ -C/A system are based on Gold codes. These codes offer properties that are closer to those of ideal PN sequences. . In particular the autocorrelation of these code sequence denoted as $[c_i(1), \dots, c_i(L)]$ satisfies the following relation

$$\frac{1}{L} \sum_{n=1}^L c_i(n) c_i(n-k) = \delta(k) \quad (2.3)$$

In the case of C/A codes, the sequence length L is considered to be relatively short. These codes are obtained from a 10-bits shift register. The code is represented by a non-return-to-zero (NRZ) sequence which is transmitted at a chip rate of 1.023 Mbps with the code length is $L = 2^{10} - 1 = 1023$ bits. Orthogonality properties of these codes allow each satellite to be processed independently within the receiver. Moreover, as an NRZ representation of the sequence is used, the autocorrelation function is linear for $\tau < 1$ chip. Examples of simulated autocorrelation and cross-correlation functions of these codes are shown in Figure 3(a) and (b) respectively. The shape of the autocorrelation function will be further considered to define tracking loop discriminators.

Finally, the GPS signal structure includes a low rate waveform for representing a satellite message. This data message is used to provide information about the satellite's health, time and ephemeris, but also almanac data for the other satellites in constellation. This information is used by the receiver to synchronize the clock to the system time and to determine the position which is broadcast at 50 bps. Most discussion in this work will exclude the impact of the navigation message components as we only consider a data less signal or pilot channel.

2.1.2 Signal Model

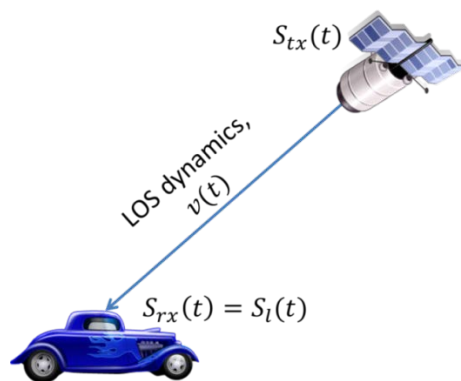


Figure 4: Illustration of received signal at the receiver.

Along the path from the satellite to the receiver, the signal is delayed, attenuated and affected by different propagation errors. Although the GNSS signal suffers from many sources of errors, the main point here is to consider the parameters that are relevant to define the suitable signal model for the received signal. In this thesis, only the GPS L1 signal is being considered as illustrated in Figure 4. The signal model at the input of the digital receiver, i.e., after the front-end

including filtering and down-conversion, is a complex signal that can be denoted in the absence of multipath (MP) as:

$$s(t) = A \cdot D(t - \tau(t))C(t - \tau(t)) \exp(j[2\pi(f_{IF})t + \varphi(t)]) + n(t) \quad (2.4)$$

where $\tau(t)$ represents the propagation delay, $\varphi(t)$ is the delay dependent carrier phase of the received signal. Note that the derivative of carrier phase depends on the LOS velocity. The frequency term (f_{IF}) which results from an intermediate frequency (IF) can be compensated inside the receiver. It will be considered as null in the framework of this study. The additive noise $n(t)$ is assumed to be a white Gaussian noise.

In the presence of MP, the received signal can further be characterized as a summation of different signals defined as in (2.4). The parameters (amplitude, delay, frequency and phase) of each MP are defined depending of the path that it has travelled. Since this study is focusing on the pilot channel, the received signal can be represented as follows

$$s_l(t) = \sum_{l=0}^{N-1} A_l \cdot D(t - \tau_l(t)) \cdot C(t - \tau_l(t)) \exp(j\varphi_l(t)) + n(t)$$

with (2.5)

$$\varphi_l = \varphi_l(0) + 2\pi \int_0^t f_l(u) du.$$

In this expression l denotes the l^{th} path, and the index $l = 0$ represents the direct path (DP) or LOS. In the frame of this project, the signal model is being represented after the acquisition phase, as the receiver is tracking the incoming signal. The phase variation results from the Doppler frequency offset which is related to the LOS velocity $v(t)$ as follows

$$f_l(t) = f_{L1} \frac{v(t)}{c}. \quad (2.6)$$

2.2 Tracking Loop Fundamentals

The main purpose of a tracking loop is to improve the estimation of the signal parameters provided during the acquisition stage. The function of the tracking loop is to refine these estimation

values and track its changes over time as well as to demodulate the navigation data. A general concept to demodulate the GPS signal is well explained in [10] and shown in Figure 5. The main idea is to implement a matched filter based on a correlator. This matched filter needs to generate a signal replica and to correlate it with the received signal. The replica is obtained by driving a local generator whose parameters are estimated. Tracking loops are usually used to perform signal parameter estimation.

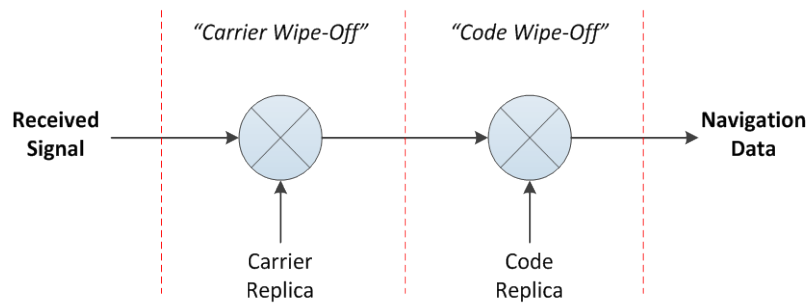


Figure 5: Basic demodulation scheme

Basically, the architecture of a tracking loop can be defined as shown in Figure 6. In this figure, the parameter θ_1 is the parameter of the incoming signal that has to be tracked (propagation delay, or carrier phase). The parameter θ_2 is the parameter of the signal replica that has been estimated. The parameter θ_e represents the estimator error. This error is provided by a discriminator which is designed depending on the parameter to track. The filter $F(s)$ has two main tasks; to filter the noise in the error measurement due to additive noise on the tracked signal and to shape the response of the tracking loop. The voltage controlled oscillator (VCO) is used to generate the replica of the tracked signal.

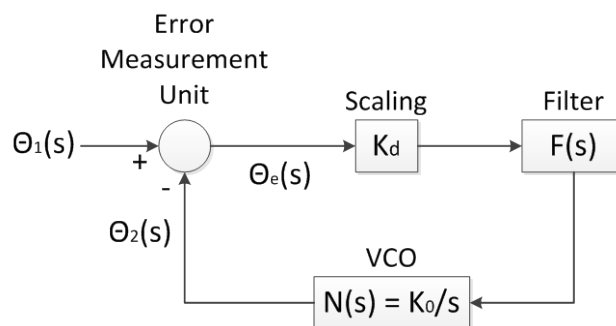


Figure 6: Generic model of tracking Loop.

Inside a GNSS receiver, in the conventional approach, a dedicated channel is assigned to each signal that is being tracked, which allows the received signals to be processed independently. For each processing channel, the receiver is continuously estimating and correcting important parameters (code delay, carrier phase and Doppler frequency). The code delay quantifies the distance from the satellite to the receiver antenna whereas the Doppler frequency reflects the relative LOS satellite-antenna velocity. The complete architecture for processing the incoming signal within tracking loops is given in Figure 7.

The signal input of this stage is a digital In-phase/Quadrature-phase (IQ) signal. This complex signal is correlated with a local replica by performing an 'Integrate & Dump' (I&D) operation (normally over a few code periods). In an ideal situation, when the carrier phase is being tracked, the in-phase (I) component should be as large as possible while keeping the quadrature-phase (Q) component as small as possible. The values from I and Q arms are then fed into discriminators for code and carrier phase error measurement. The frequency discriminator can also be used for aiding carrier phase tracking in high dynamic scenarios. Discriminator output are used as measurements for estimating the signal parameters and controlling the NCOs that deliver the signal replica.

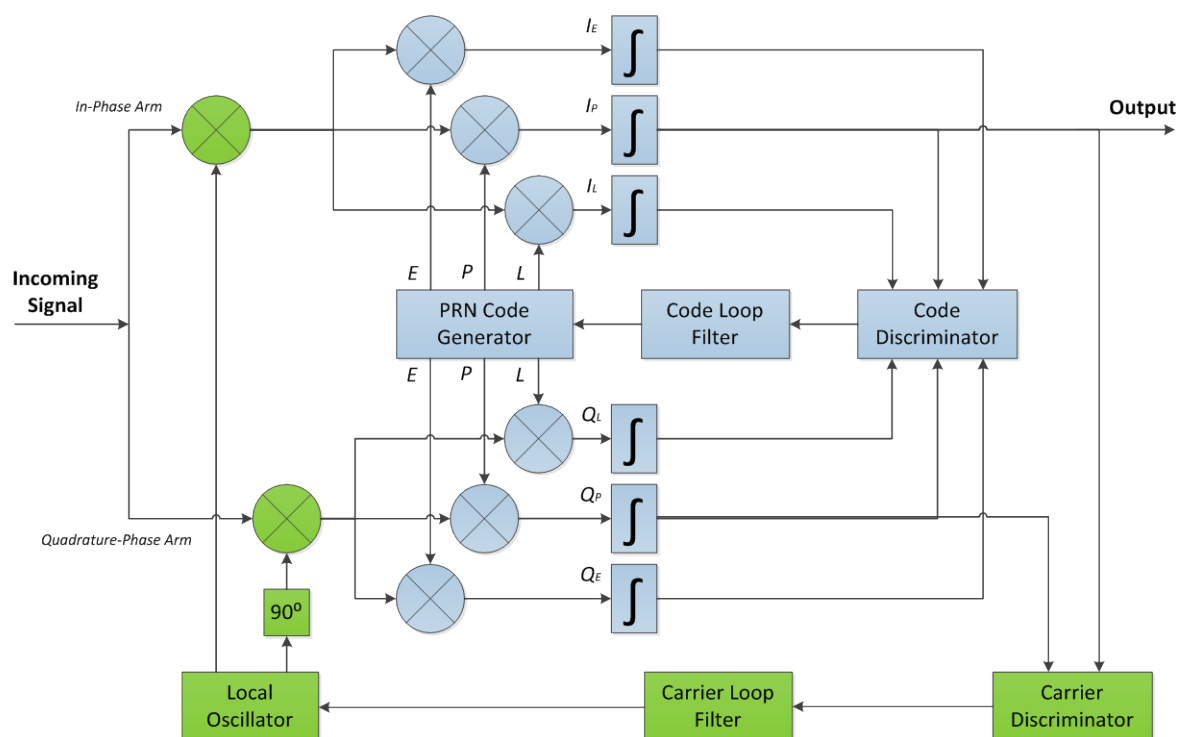


Figure 7: Complete Conventional Tracking Loop Architecture.

The complete conventional tracking loop architecture is shown in Figure 7. Here, the feedback loop for the carrier is referred as carrier tracking loop and can be designed to follow either the carrier phase by using a phase lock loop (PLL) architecture or a frequency lock loop (FLL). Some design combines both PLL and FLL for better tracking performance. On the other hand, the feedback loop for the code results in a delay lock loop (DLL) architecture. These tracking loops provide an estimation of the signal parameters that allows the navigation message to be decoded. At the same time, it provides an estimation of the pseudo-range (PR) and pseudorange-rate or delta-range (DR) measurements that are used to compute the user position, velocity and time (PVT) of the receiver. This particular process is carry out by the navigation system (NS) which will be discussed in Chapter 4.

2.2.1 Correlators

Correlations in GNSS receivers are basic operations, but are very much dependent on the synchronization between the incoming signal and the replicas. Typically the power of the received GPS signal is approximately 30 dB below the noise floor when the signal bandwidth is limited to 10 MHz. That means it is too weak for standard strong signal detection methods. Therefore, the way to retrieve it by using a correlator (which consists of a matched filter) is considered very important. The outputs of I and Q can give information about the instantaneous phase of the incoming signal, the amplitude as well as the delay. The architecture of this operation is given in Figure 8.

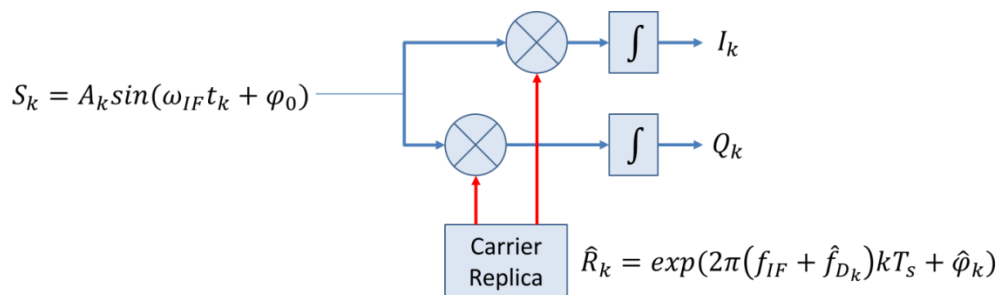


Figure 8: Complex correlator for ‘carrier wipe-off’.

In Figure 8, S_k represents the incoming signal that is correlated with the replica signal \hat{R}_k which is generated by the tracking loops. The intermediate frequency (IF) term is the result from the front-end operation and down-conversion of the signal. The interpretation of the correlation process

can be examined by looking at the phasor output which consists of the I and Q arms, as illustrated in Figure 9. From this simple illustration, it can be concluded that:

- i. In the case of perfect alignment between the local replica and the incoming signal (same frequency and phase) the output results in large positive I -correlation as in Figure 9 (a).
- ii. When the local replica and the incoming signal have the same frequency but 180° out of phase the output results in large negative I -correlation.
- iii. When the local replica and the incoming signal have the same frequency but 90° out-of-phase the output results in largest output at the Q -correlation as in Figure 9 (b).
- iv. When the local replica and the incoming signal have the same frequency but an arbitrary phase, the output is shown in Figure 9 (c). From this complex plane diagram, the magnitude and the phase of the signal can be determined.
- v. In the case of an incoming signal having a frequency offset which causes the phasor to rotate as in Figure 9 (d), the angle of the rotation is related to the frequency offset:

$$\Delta \hat{f}_m = \frac{\varphi_m - \varphi_{m-1}}{\Delta t} \quad (2.9)$$

- vi. Finally, if the correlation is performed with a zero-mean additive white Gaussian noise (AWGN), the output of the correlator results in I and Q magnitudes depending on the noise power. This output is affected by a circular complex Gaussian noise.

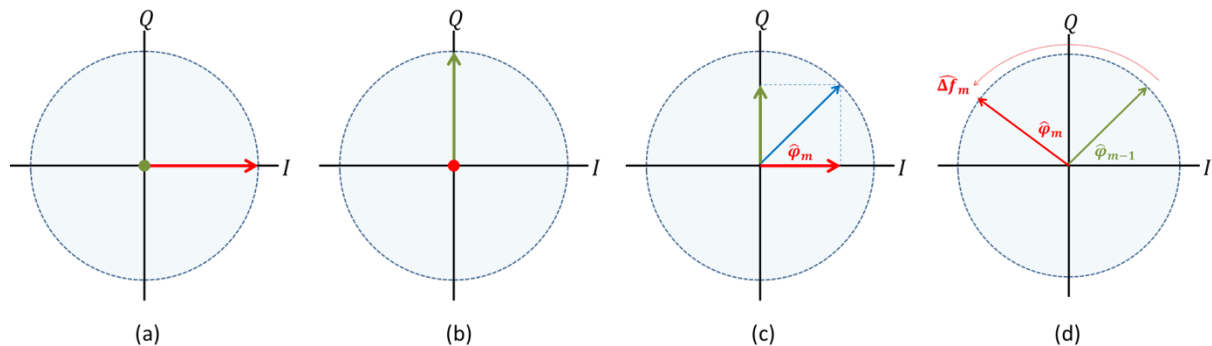


Figure 9: Phasor diagram of various conditions for I and Q components.

In order to provide a measurement of the code delay error, three replica signals are usually generated to produce the early (E), prompt (P) and late (L) correlator arms. Normally, the E and L replicas are generated by half-chip early and late with respect to the P correlator as shown in Figure 10.

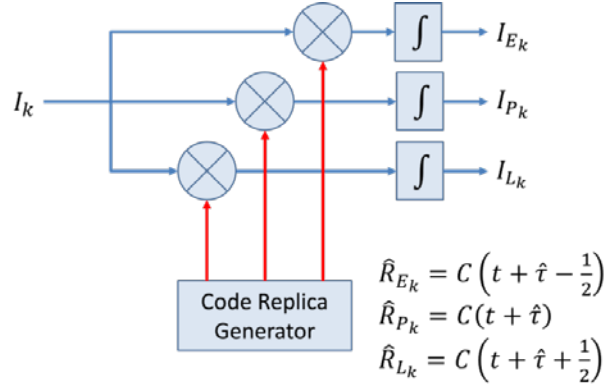


Figure 10: Early-Prompt-Late Correlation for I-arm.

The E/P/L autocorrelation function is depicted in Figure 11, when the magnitudes of the correlator outputs are considered. The E and L outputs are used in a DLL discriminator to enable the delay error to be measured. The P correlator output on the other hand, is processed for measuring the phase error and extracting the navigation message.

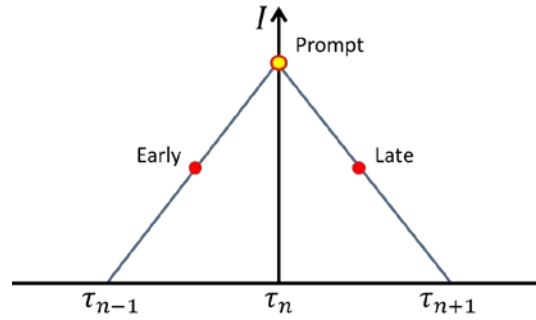


Figure 11: Code Correlation for E-P-L correlator arms

By considering only the LOS signal, the P correlator output can be expressed, at the time $t = \sum_{i=0}^k T_{int}(i)$, as:

$$I(k) \approx \sqrt{C_k} R(\Delta\tau_{0,k}) \cdot \frac{\sin(\pi\Delta f_{0,k} T_{int}(k))}{\sin(\pi\Delta f_{0,k} T_s)} \cdot \cos(\Delta\varphi_{0,k}) + n_i[k] \quad (2.10)$$

$$Q(k) \approx \sqrt{C_k} R(\Delta\tau_{0,k}) \cdot \frac{\sin(\pi\Delta f_{0,k} T_{int}(k))}{\sin(\pi\Delta f_{0,k} T_s)} \cdot \sin(\Delta\varphi_{0,k}) + n_q[k]$$

where C_k is the signal power, $R(\cdot) = \Lambda_{T_c}(\cdot)$ is the code autocorrelation function, $\Delta\tau_{0,k} = \tau_{0,k} - \hat{\tau}_k$ is the error between the LOS delay and the estimated local code delay, $\Delta f_{0,k} = f_{0,k} - \hat{f}_k$ is the error between the LOS frequency and the estimated local carrier frequency, and $\Delta\varphi_{0,k} = \varphi_{0,k} - \hat{\varphi}_k$ is the error between the LOS phase and the estimated local carrier phase. The additive noise $n(k) = n_i[k] + n_q[k]$ is a complex white Gaussian noise, whose power is related to the C/N_0 ratio:

$$\sigma_n^2(k) = C_k \cdot 10^{-\left(\frac{C}{N_0}\right)T_{int}} \quad (2.11)$$

where T_{int} is the integration time. The analysis of the signal power, whose complex representation in the absence of noise is shown in Figure 12, can be simplified as:

$$I(k) \approx A_k \cdot \cos(\Delta\varphi_{0,k}) \quad (2.12)$$

$$Q(k) \approx A_k \cdot \sin(\Delta\varphi_{0,k})$$

where

$$A_k = \sqrt{C_k} R(\Delta\tau_{0,k}) \cdot \frac{\sin(\pi\Delta f_{0,k} T_{int}(k))}{\sin(\pi\Delta f_{0,k} T_s)} \quad (2.13)$$

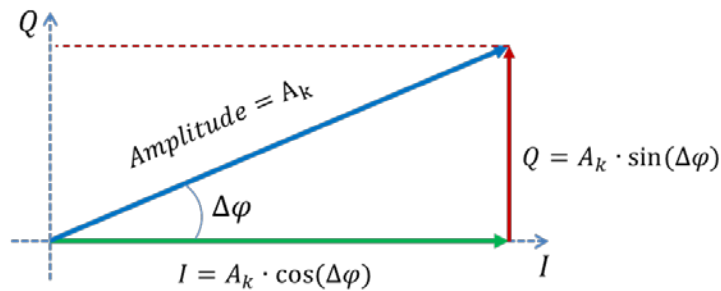


Figure 12: Interpretation of the correlator outputs in phasor diagram.

This means that the signal amplitude depends not only on the code alignment error, but also on the frequency error. The impact of the frequency error can be represented by the following function:

$$H_k(\Delta f) = \frac{\sin(\pi\Delta f T_{int})}{\sin(\pi\Delta f T_s)} \quad (2.14)$$

where T_{int} and T_s are the integration time and the signal sampling time, respectively. Under this circumstance, the signal amplitude can be further improved by increasing the integration time, T_{int} as depicted in Figure 13.

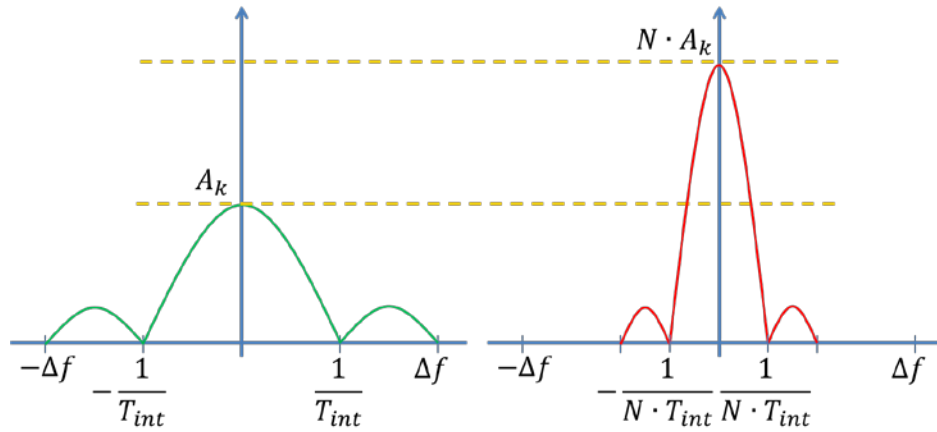


Figure 13: Filtering effect related to the integration time.

The effects of the instantaneous carrier phase are examined in Figure 14. First, we have considered a perfect carrier phase alignment which means $\Delta\varphi = 0$. In this condition, the signal correlation energy is in the I-channel which is depicted in Figure 14 (a). The Q-channel on the other hand is only affected by noise. Next we consider a phase misalignment $\Delta\varphi \neq 0$. In this condition, the signal energy is distributed between the I and Q channels. In both cases, the vector magnitude of the complex I and Q signal are the same.

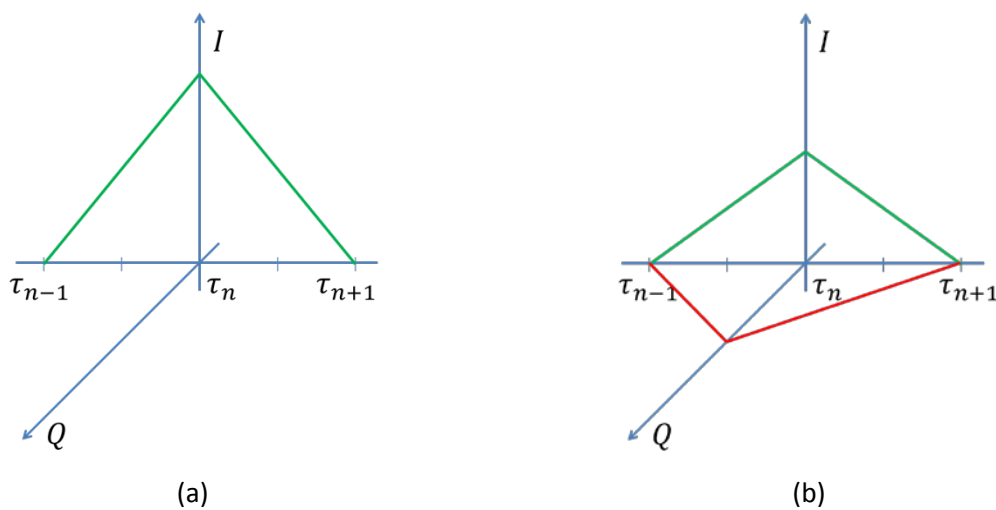


Figure 14: The effect of carrier-phase misalignment.

2.2.2 Discriminators

The main function of the discriminator is to provide measurable quantities such as phase, frequency and code delay information. There are three types of discriminator which correspond to the types of tracking loops (PLL, FLL and DLL) implemented. They are known as phase, frequency and delay discriminators depending on the measured parameter. Moreover, for each measurement, several architectures are proposed and the choice of the architecture impacts the performance and the complexity of the receiver.

a) Phase Locked Loop (PLL) Discriminators

Carrier phase discriminators or PLL discriminators estimate the residual phase error. This error is used to drive the frequency of the carrier replica in order to lock the phase of the replica on the incoming signal. However, PLL discriminators generally are sensitive to dynamic stress and can produce ambiguous range measurement with millimetre-level noise. Normally PLL discriminators are categorised as Pure PLL or Costas PLL as summarized in Table 1 [1]. The main difference is that pure PLL discriminator algorithms is sensitive to 180° phase change of BPSK modulation and uses four-quadrant arctangent. Costas PLL however is insensitive to BPSK modulation and can be used for GNSS carrier phase tracking.

Table 1: Common discriminator algorithm for PLL [1].

Discriminator Algorithm	Output Phase Error	Characteristics
$ATAN2(Q_P, I_P)$	$\Delta\varphi$	Pure PLL. Four-quadrant arctangent, optimal at high and low SNR, not signal amplitude dependent and high computational load.
$\frac{Q_P}{Ave \sqrt{I_P^2 + Q_P^2}}$	$\sin(\Delta\varphi)$	Pure PLL. Normalized by averaged prompt envelope that provides insensitivity at high and low SNR and low computational load.
$Q_P \times I_P$	$\sin 2\Delta\varphi$	Costas PLL. Classic analogue discriminator, near optimal at low SNR, slope proportional to signal amplitude squared, A^2 and moderate computational burden.

$Q_P \times \text{Sign}(I_P)$	$\sin \Delta\varphi$	Costas PLL. Decision directed discriminator, near optimal at low SNR, slope proportional to signal amplitude, A and least computational burden.
Q_P/I_P	$\tan\Delta\varphi$	Costas PLL. Suboptimal but good at high and low SNR, slope not dependent on signal amplitude, A, higher computational burden.
$\arctan(Q_P/I_P)$	$\Delta\varphi$	Costas PLL. Two-quadrant arctangent, optimal at high and low SNR, slope not dependent on signal amplitude, A and highest computational burden.

In the frame of this study the “arctan” based discriminator will be proposed to measure the innovation $\varphi - \varphi^{NCO}$, i.e., the difference between the signal phase and the replica phase which is estimated within the receiver. Therefore the discriminator output can be modelled as:

$$\Delta\varphi^{Disc} = \varphi - \varphi^{NCO} + w^\varphi. \quad (2.15)$$

If we consider that the NCO phase noise can be neglected, the power of the noise w^φ depends mainly on the signal to noise ratio of the incoming signal. As the aim of this research is to track the most relevant satellites, we consider only satellite signals with high $C/N_0 (\geq 40dBHz)$. For these values of C/N_0 , the noise power spectrum density is:

$$S_{v_\varphi}(f) = \frac{1}{4\pi^2 \left(\frac{C}{N_0}\right)}. \quad (\text{cycle}^2/\text{Hz}) \quad (2.16)$$

b) Frequency Locked-Loop (FLL) Discriminators

An FLL discriminator estimates the residual frequency error between the incoming signal and local replicas. The objective is to set the residual frequency to zero without forcing the phase of the controlled oscillator. FLL discriminators are considered more robust than PLL discriminators but can produce ambiguous range measurements with decimeter-level noise. The most common FLL discriminators are described in Table 2. The frequency is deduced from the phase variation between 2 successive integrations, performed at the epochs t_1 and t_2 , such as $t_2 = t_1 + T_{int}$.

Table 2: Common discriminator algorithm for FLL [1].

Discriminator Algorithm	Output Phase Error	Characteristics
$\frac{\mathbf{cross}}{(t_2 - t_1)}$	$\frac{\sin(\varphi_2 - \varphi_1)}{(t_2 - t_1)}$	Near optimal at SNR, slope proportional to signal A^2 and least computational burden
$\frac{\mathbf{cross} \times \mathbf{sign}(\mathbf{dot})}{(t_2 - t_1)}$	$\frac{\sin[2(\varphi_2 - \varphi_1)]}{(t_2 - t_1)}$	Decision directed, near optimal at high SNR, slope proportional to A and moderate computational burden
$\frac{\mathbf{ATAN2}(\mathbf{dot}, \mathbf{cross})}{(t_2 - t_1)}$	$\frac{(\varphi_2 - \varphi_1)}{(t_2 - t_1)}$	Four quadrant arctangent, optimal at high and low SNR, slope not signal amplitude dependent and highest computational burden.
where:		
$\mathbf{cross} = I_{P_{t1}} \times Q_{P_{t2}} - I_{P_{t2}} \times Q_{P_{t1}}$ $\mathbf{dot} = I_{P_{t1}} \times I_{P_{t2}} + Q_{P_{t1}} \times Q_{P_{t2}}$		

In the frame of this study the atan2 based discriminator will be proposed to measure the innovation $f - f^{NCO}$, i.e., the difference between the signal frequency and the replica frequency which is estimated within the receiver. Therefore the discriminator output can be modelled as:

$$\Delta f^{Disc} = f - f^{NCO} + w^f. \quad (2.17)$$

As the frequency is deduced from two phase measurements with uncorrelated noise we obtain, for high values of C/N_0 , the following noise power spectrum density:

$$S_{v_f}(f) = \frac{4S_{w_\varphi}}{t_2 - t_1} = \frac{1}{\pi^2 T_{int}^2 \left(\frac{C}{N_0} \right)}. \quad (\text{cycle}^2/\text{s}^2\text{Hz}) \quad (2.18)$$

c) Delay Locked Loop (DLL) Discriminators

The DLL discriminator is used to measure the incoming signal-local replica misalignment. Unlike PLL and FLL, it requires 2 additional correlators, as discussed earlier, which are the delayed and advanced version of the prompt correlator. The difference between early and late correlators

produces an S-curve. A perfect alignment between the incoming signal and the replica will result in zero-crossing of the S-curve. This principle is illustrated in Figure 15.

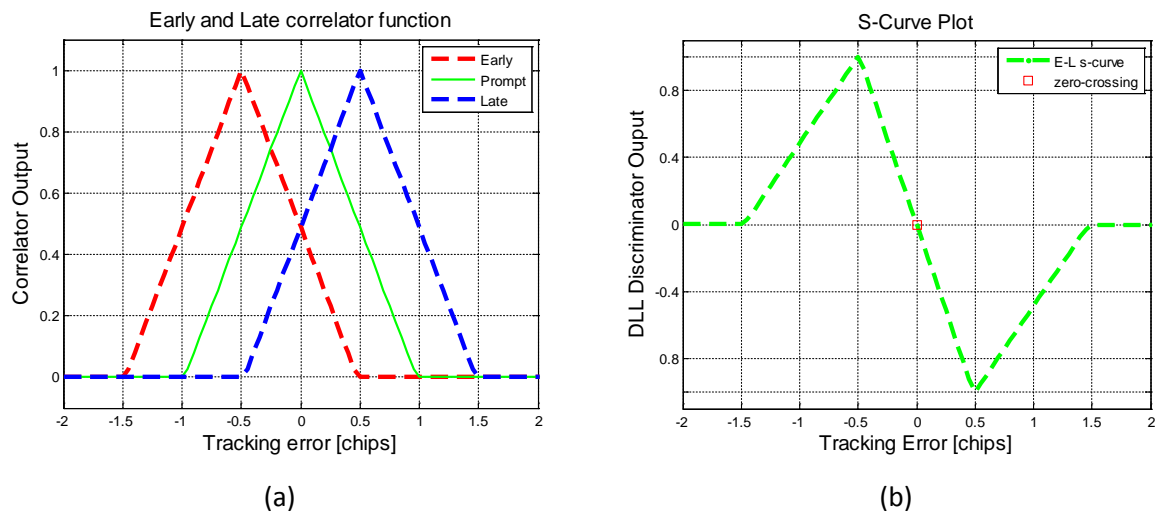


Figure 15: Illustration of (a) Early, Prompt and Late correlation function with (b) the resulting zero-crossing.

The performance of the DLL discriminator depends on the function used within the receiver. Generally, it can be divided into two types, non-coherent and coherent discriminators as presented in Table 3. Non-coherent DLL discriminators combine the signals from both I and Q channels to provide an output which is independent of the carrier phase, (i.e., of the carrier phase performance). The drawback of using the Q channel is that it will add extra noise in the computation. Alternatively, coherent discriminators provide better performance due to the fact that the squaring loss can be avoided but requires good carrier phase tracking as it becomes sensitive to carrier cycle slips. Moreover, all discriminators can be normalized to remove the amplitude sensitivity and work better during rapid signal fading conditions.

Table 3: Common discriminator algorithm for DLL [1].

Discriminator Algorithm	Characteristics
$\frac{1}{2} \frac{\sqrt{I_E^2 + Q_E^2} - \sqrt{I_L^2 + Q_L^2}}{\sqrt{I_E^2 + Q_E^2} + \sqrt{I_L^2 + Q_L^2}}$	Non-coherent early minus late envelope normalized to remove amplitude sensitivity and high computational load
$\frac{1}{2} ((I_E^2 + Q_E^2) - (I_L^2 + Q_L^2))$	Non-coherent early minus late power and moderate computational load.

$\frac{1}{2}[(I_E - I_L)I_P + (Q_E - Q_L)Q_P]$	Quasi-coherent dot product power uses all correlators and low computational load.
$\frac{1}{2}(I_E - I_L)I_P$	Coherent dot product uses only I-components and low computational load.

In the frame of this study the early-minus-late based discriminator will be proposed to measure the innovation $\tau - \tau^{NCO}$, i.e., the difference between the incoming signal code delay and the replica code delay which is estimated within the receiver. Therefore the discriminator output can be modelled as:

$$\Delta\tau^{DIS} = \tau - \tau^{NCO} + w^\tau. \quad (2.19)$$

If we consider that the NCO code delay error can be neglected, the power of the noise w^τ depends mainly on the signal to noise ratio of the incoming signal. For high C/N_0 , the power spectrum density of the noise is:

$$S_{v_\tau}(f) = \frac{d}{2 \left(\frac{C}{N_0} \right)} \quad (chips^2/Hz) \quad (2.20)$$

where d is the early-minus-late chip spacing, in chip. This expression is valid for $d \geq \pi/N_s$ [11], where N_s is the number of samples per chip.

2.2.3 Loop Filter

Loop filters are used to provide an estimate of the tracked parameters from noisy measurements provided by the discriminators that have just been characterized. Based on gain and integrators, a loop filter combines efficiently present and past values of these measurements, as a Kalman filter would do. However the gain matrix which weights the innovations is not determined recursively in order to optimize the estimate in a least-square sense. This gain matrix is computed to adapt the filter bandwidth depending on the dynamic of the estimated parameters. It produces the commands to the NCOs in a closed loop architecture. There are many design approaches for digital filters, which depend mainly on the filter order, only the fundamentals of the common digital loop filters [12] design will be discussed in this subsection. As being described in [1] and also suggested in

[10], the DLL can be modelled as a linear PLL and the performance of the loop can be predicted based on this model. This means that the filter design for both carrier tracking and code tracking are the same but with different parameter values. The design of the loop filters consists of dimensioning the filter order and bandwidth in order to determine its response depending on the incoming signal dynamics.

On the one hand, the choice of the filter noise bandwidth B_n is a trade-off between noise and dynamics. It needs to take into account the integration time, T_{int} with the general constraint

$$B_n \cdot T_{int} \ll 1. \quad (2.21)$$

If this condition is not fulfilled, the actual bandwidths will tend to be larger than the desired one which leads to filter instability. Parameter B_n controls the amount of noise allowed in the filter and can also control the settling time. These effects can be demonstrated by plotting the NCO outputs of the tracking loop which is illustrated in Figure 16. A large noise bandwidth implies that the tracking loop settles quickly (locked) to the real frequency but has relatively large frequency noise in the locked state. On the other hand, a smaller bandwidth impacts the time to lock but once locked, the frequency is more stable. Besides that, the loop noise bandwidth is able to determine maximum Doppler offset and rates tolerated by the loop.

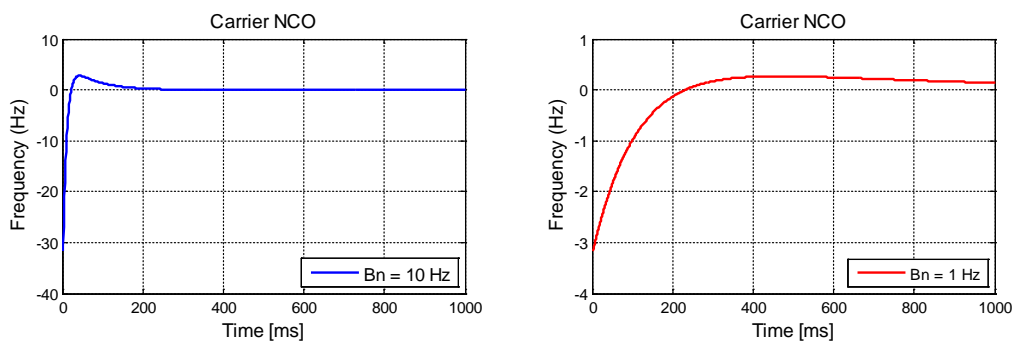


Figure 16: The effect of the bandwidth size (B_n) of the loop filter.

Table 4: Loop filter characteristics [1].

Loop Order	Typical Filter Coefficient Values	Characteristics
First	$c_1 = \omega_0$ $B_n = 0.25\omega_0$	Tracks phase (range), sensitive to velocity stress and unconditionally stable at all noise bandwidths.
Second	$c_1 = \omega_0^2$ $c_2 = 1.414\omega_0$ $B_n = 0.53\omega_0$	Tracks frequency (velocity), sensitive to acceleration stress and unconditionally stable at all noise bandwidths.
Third	$c_1 = \omega_0^3$ $c_2 = 1.1\omega_0^2$ $c_3 = 2.4\omega_0$ $B_n = 0.7845\omega_0$	Tracks acceleration, sensitive to jerk stress.

In the other hand the filter order is chosen depending on the dynamics of the parameter to be estimated as being described in Table 4 from [1] where c_1 , c_2 and c_3 represent the coefficient values which depends on the order of the loop. The zero order filters that leads to a first order tracking loop are sensitive to a velocity stress. A first order filter makes the tracking loop insensitive to the velocity, whereas a second order filter is necessary in case of acceleration. This means that a higher order filter is performing better in dealing with dynamic stress condition and provides less noisy output. The only drawback is the additional computational load of the filter as it is directly related to the amount of operation.

2.3 Tracking Loop Implementation

The full architecture of a receiver tracking loop implemented for a single channel is illustrated in **Figure 17**. In the context of this project, the GPS tracking loop is implemented using a Matlab® programming tool which allows the receiver to be designed on a software-defined platform. The design of the tracking loop requires a great deal of flexibility for future integration with other modules during the project. The specifications, for both carrier tracking and code tracking, are further discussed in detail, in the next subsections. The relationship between the input and output of each module in **Figure 17** is simplified in Figure 18, inspired by [13].

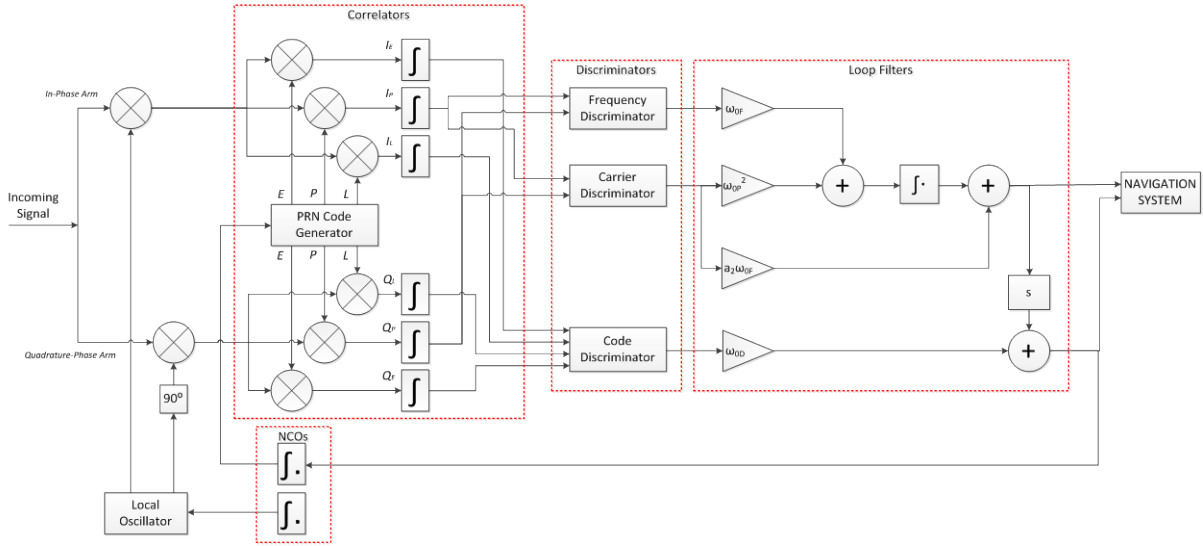


Figure 17: Full implementation of the GPS tracking loop for single channel.

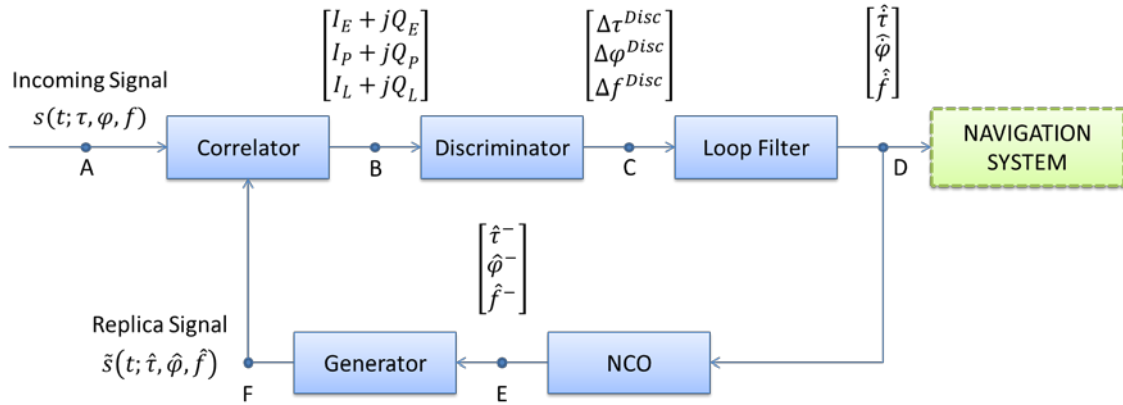


Figure 18: Input/Output relationship of the GPS tracking [13].

Based on Figure 18, the expression of each stage in the tracking loop can be represented. The outputs of the correlators consist of in-phase and quadrature-phase for Early, Late and Prompt arms respectively. The expressions of the outputs of the correlator are given by:

$$\begin{bmatrix} I_E + jQ_E \\ I_P + jQ_P \\ I_L + jQ_L \end{bmatrix}_k = \begin{bmatrix} A \cdot R(\Delta\tau - d) \cdot \text{sinc}(\Delta f T_{int}) \cdot \exp(j\Delta\phi) \\ A \cdot R(\Delta\tau) \cdot \text{sinc}(\Delta f T_{int}) \cdot \exp(j\Delta\phi) \\ A \cdot R(\Delta\tau + d) \cdot \text{sinc}(\Delta f T_{int}) \cdot \exp(j\Delta\phi) \end{bmatrix}_k + \begin{bmatrix} n_{I_E} + jn_{Q_E} \\ n_{I_P} + jn_{Q_P} \\ n_{I_L} + jn_{Q_L} \end{bmatrix}_k \quad (2.22)$$

when the function $\frac{\sin(\pi\Delta f T_{int})}{\sin(\pi\Delta f T_s)}$ is approximated by $\text{sinc}(\Delta f T_{int})$ since $\text{sinc}(x) = \frac{\sin(\pi x)}{\pi x}$.

These correlator outputs are used to provide a measurement of the signal code delay, carrier phase and frequency errors (see 2.2.2). These outputs allow signal parameters to be estimated (see 2.2.3). For both tracking loops the last stage, which is the NCO, can be modelled by using a 1st-order digital boxcar integrator. Therefore, the output of the NCO can generally be expressed as:

$$\tilde{\Theta}_k^- = \tilde{\Theta}_{k-1} + T_{int} \cdot \tilde{\dot{\Theta}}_{k-1} \quad (2.23)$$

where $\tilde{\Theta}^-$ denotes the a priori estimate of the parameter, $\tilde{\dot{\Theta}}$ is the rate of change of the estimated parameter and T is the time interval between each sample. In this case, Θ can either be the delay (τ), the carrier phase (φ) or the Doppler frequency (f_D).

2.3.1 Carrier Tracking Loop

The implementation of the carrier tracking loop is based on a 1st-order FLL assisted 2nd-order PLL architecture as in Figure 19. FLL and PLL discriminators are described in section 2.2.2 where the outputs of the discriminators are given by:

$$\Delta\varphi^{Disc} = \Delta\varphi + v^\varphi \quad (2.24)$$

and

$$\Delta f^{Disc} = \Delta f + v^f \quad (2.25)$$

for PLL and FLL discriminator respectively. The output of the discriminator $\Delta(\cdot)^{Disc}$ can be seen as a summation of the estimated residual error $\Delta(\cdot)$ determined by the discriminator functions taking into account the noise term $v^{(\cdot)}$ associated with it.

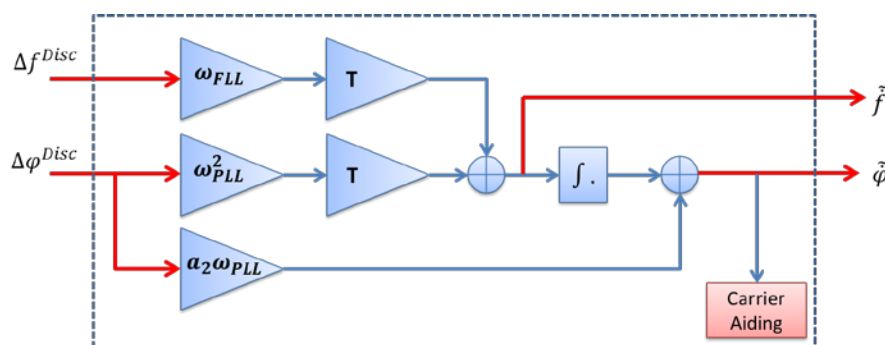


Figure 19: 1st order FLL assisted 2nd order PLL Loop Filter Architecture.

By implementing an FLL assisted PLL loop filter, the performance of the carrier tracking loop will benefit from both advantages provided by the FLL and PLL respectively. This means that it will be able to provide accurate velocity measurement and to track the signal phase at low C/N_0 , allowing coherent discriminators to be explored.. Besides that, it can also function as a pure FLL or a pure PLL in case the output of the FLL or PLL discriminators equals zero. The difficulty is to choose the right values for the noise bandwidth parameters for both FLL and PLL (these bandwidth parameters are denoted as B_n^{FLL} and B_n^{PLL} respectively). The output of the loop filter can be represented as:

$$\tilde{f}_k = \tilde{f}_{k-1} + T \cdot (\omega_{0_{PLL}}^2 \cdot \Delta\varphi^{Disc} + \omega_{0_{FLL}} \cdot \Delta\varphi^{Disc}) \quad (2.26)$$

$$\tilde{\varphi}_k = \tilde{f}_k + \sqrt{2} \cdot \omega_{0_{PLL}} \cdot \Delta\varphi^{Disc}. \quad (2.27)$$

The term ω_0 refers to the natural radian frequency which related to the noise loop bandwidth B_n . This relation depends on the order of the filter given in Table 4.

In a nominal condition (without interference), the dominant source of error for the carrier tracking loop is the phase jitter due to thermal noise [1] which is mainly produced by the additive noise which affects the incoming signal. Filter coefficients are computed based on the dynamic stress error (oscillator stress error, residual user dynamic) which determines filter bandwidths. By considering high C/N_0 ratio, the variance of the estimated phase is (see $S_{v_\varphi}(f)$):

$$\sigma_{\tilde{\varphi}}^2 \approx \frac{1}{4\pi^2 \left(\frac{C}{N_0}\right)}. \quad (\text{cycle}^2) \quad (2.28)$$

Note that B_n^{PLL} is the carrier phase loop noise bandwidth in Hz, C/N_0 is the carrier to noise ratio expressed as a ratio in Hz and T_{int} is the integration time in seconds. Therefore, the performance of the carrier tracking loop, for a given C/N_0 ratio depends mainly on the loop bandwidth. In the same way, if we neglect the impact of the FLL aiding we obtained for the implementation, the FLL thermal noise error is given by:

$$\sigma_{\tilde{f}}^2 \approx \frac{B_n^{PLL}}{\pi^2 T_{int}^2 \frac{C}{N_0}}. \quad (\text{Hz}^2) \quad (2.29)$$

Obviously the use of smaller bandwidths allows estimator performance to be improved. Nevertheless these bandwidths must be set depending on the dynamic stress error, which can be reduced by using a high quality oscillator. Velocity aiding, provided by the navigator for reducing the impact of the user dynamic, is also efficient, especially when the navigator integrates an inertial navigation system.

2.3.2 Code Tracking Loop

The code tracking loop is used to track the code delay of the incoming signal. When the PLL works properly, a 1st-order DLL with carrier aiding is implemented. The discriminator which is used to provide the delay innovation described in section 2.2.2 is given by:

$$\Delta\tau^{Disc} = \Delta\tau + v^\tau. \quad (2.30)$$

By looking at the loop filter order in Figure 20, a 1st order filter is considered to be sufficient because the aiding provided by the carrier loop filter takes out most of the code dynamics. This particular approach is called the carrier-aided code loop. The scale factor $K_{\phi\tau}$ is required because the Doppler effect on the signal is inversely proportional to the wavelength of the signal define as R_C/f_{L1} where R_C is spreading code chip rate (Hz) plus the Doppler effect and f_{L1} is L1-band carrier (Hz). Using the carrier aiding allows the DLL loop order as well as the DLL loop bandwidth to be reduced. The output of the code loop filter is given by:

$$\tilde{\tau}_k = K_{\phi\tau} \cdot \tilde{\varphi}_{k-1} + \omega_{0_{DLL}} \cdot \Delta\tau^{Disc} \quad (2.31)$$

where

$$K_{\phi\tau} = \frac{R_C}{f_{L1}} = \frac{1}{1540}. \quad (2.32)$$

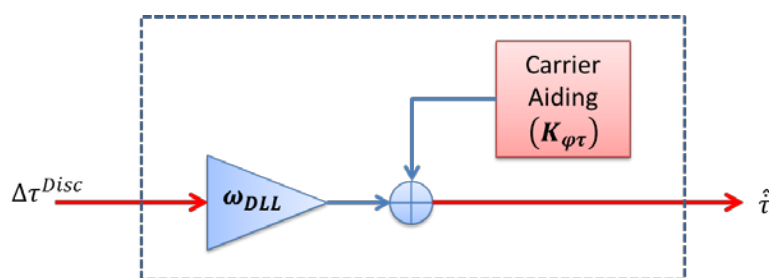


Figure 20: 1st order DLL with carrier aiding.

In optimal condition, the dominant sources of errors for the code tracking loop is the range jitter due to thermal noise and the dynamic stress error [1]. Thanks to carrier aiding, the dynamic stress error for DLL can be reduced significantly leaving the thermal noise as the main source of error. The thermal noise code tracking jitter for coherent dot power discriminator can be approximated, for high C/N_0 ratio defined in equation (2.20), by:

$$\sigma_{\tau}^2 = \frac{B_n^{DLL} \cdot d}{2 \left(C/N_0 \right)} \quad [chips^2] \quad (2.33)$$

where B_n^{PLL} is the code loop noise bandwidth in Hz and d is the early-minus-late chip spacing.

2.3.3 Tracking Loop Assessment

In order to evaluate the performance of the proposed tracking loop, we have designed a simulator with known parameters for the code delay, frequency and time for the whole simulation. Further details on the development of this simulator will be discussed in Chapter 3. The interest here is to see the behaviour of the tracking loop with respect to the actual receiver behaviour. The scenario is set to a static position in order to have very low dynamics for the receiver. The assessment set-up is presented in Figure 21.

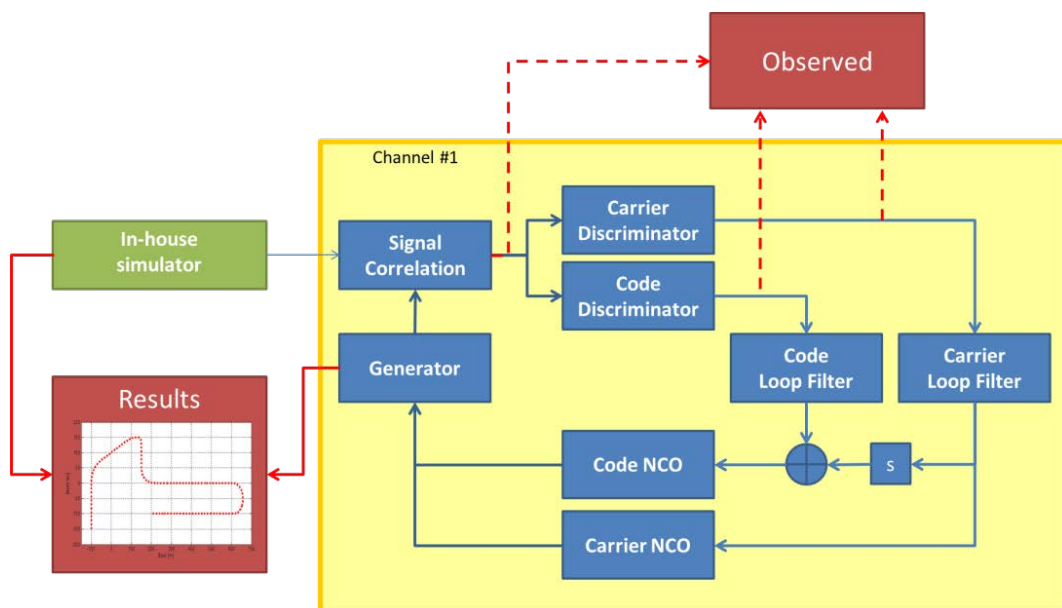


Figure 21: Assessment of the tracking loop.

The results provided by the tracking loop are presented in Figure 22, Figure 23 and Figure 24. Figure 22 shows the correlator outputs of the prompt, early and late arms. It is observed that the signal power is focused in the in-phase arm. In this case, the use of a coherent discriminator is highly favourable to further reduce the squaring loss introduced by using non-coherent discriminators. The behaviour of the discriminator outputs can be observed in Figure 23. As long as the carrier tracking is well locked, the code tracking is performed correctly. The response time of the tracking loop, which is here about $0.2s$, depends on the Loop noise bandwidth chosen for the implementation. Finally, Figure 24 compares the estimated values of the different parameters calculated by the tracking loop with their actual values. Note that once the carrier has been tracked, the code tracking performs well. The error introduced by the tracking loop is around 0.00015 chips ($\approx 0.045m$) which can simply be disregarded. The results presented here show that the tracking loop has been implemented correctly.

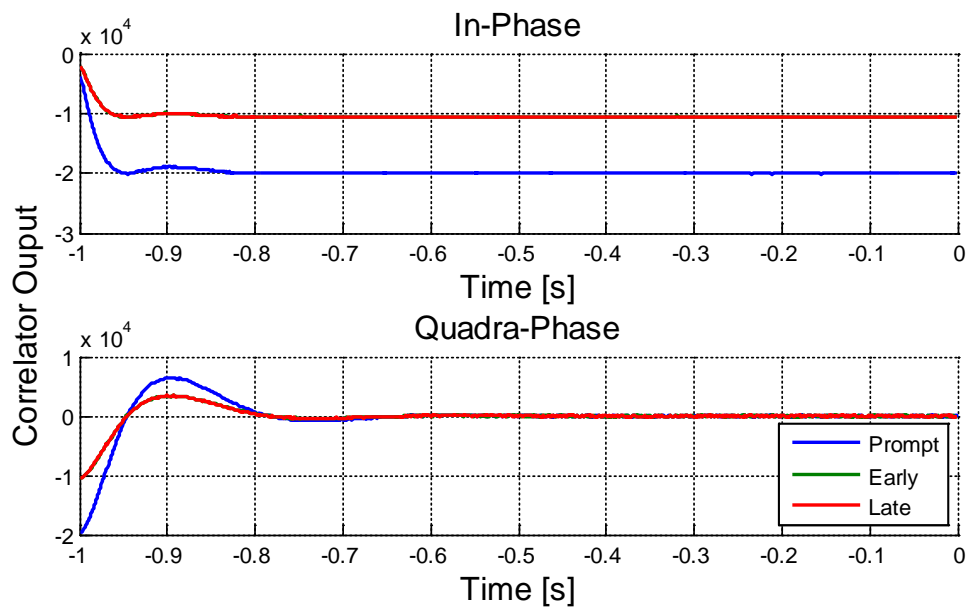


Figure 22: Correlator outputs of the In-phase (top) and Quadrature-phase (bottom).

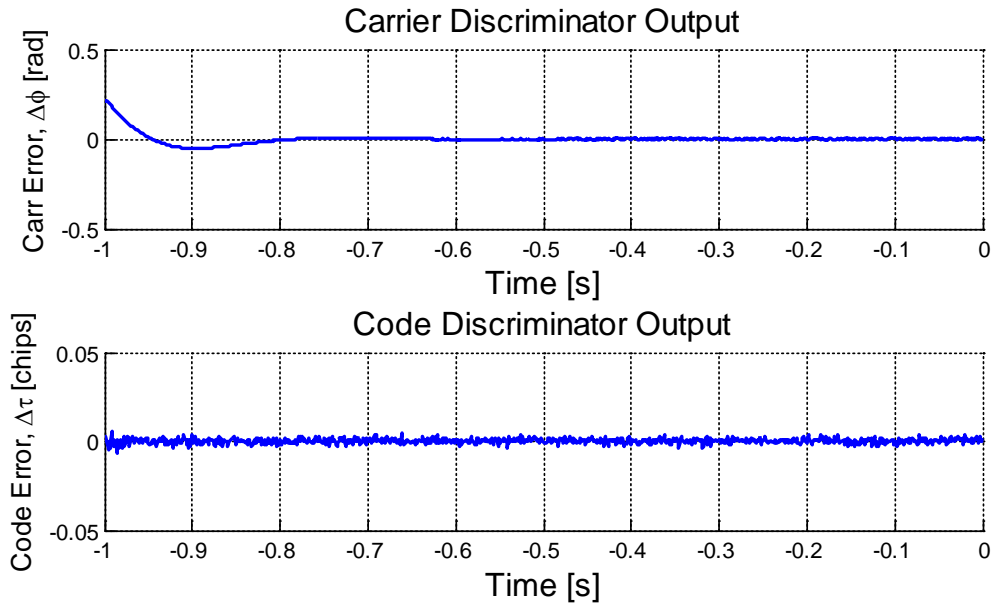


Figure 23: Discriminator outputs for carrier tracking loop (top) and code tracking loop (bottom).

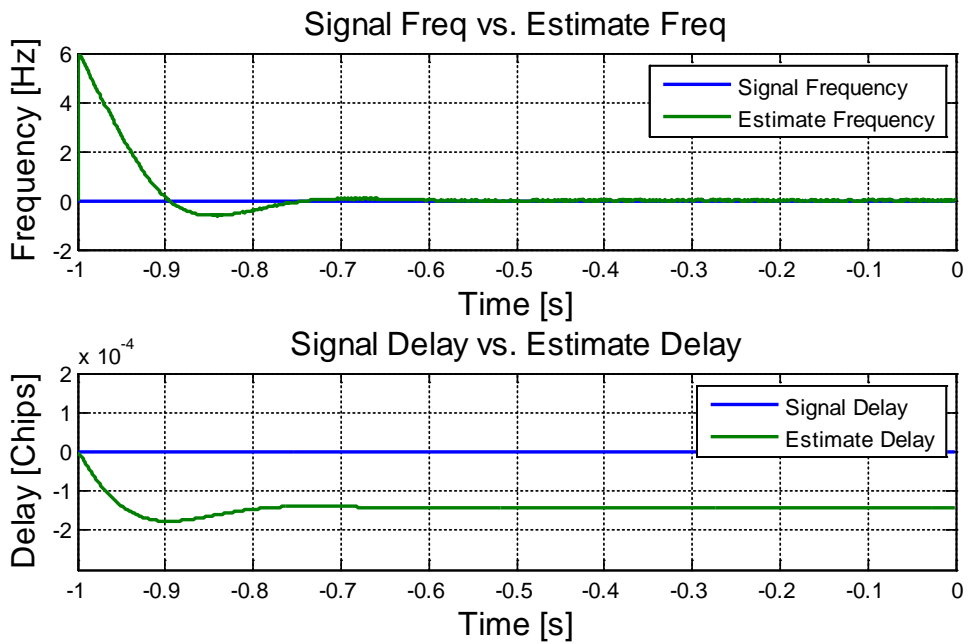


Figure 24: Frequency (top) and delay (bottom) of the signal vs. estimation by tracking loop.

2.4 Summary

This chapter focused on some fundamental principles related to the GPS, from the signal structure until the processing part inside the tracking loop. Every signal processing step that works inside the receiver architecture was discussed. The influence of each parameter involved inside the tracking was put into perspective in order to propose the most appropriate architecture for the targeted application. Discriminator outputs used as measurement for estimating the signal parameters were described. At the same time, tracking loops were implemented for processing the incoming signal. These loops will be integrated later in a conventional receiver for assessing its performance, especially in presence of interferences. The study focused on the impact of each parameter of interest on the filter order, tracking loop bandwidth and discriminator structure.

CHAPTER

3

CHAPTER 3 – Channel Analysis

The definition of an accurate model for propagation channels is crucial for testing and evaluating the performance of any satellite communication systems [14]. This is simply because the diverse nature of propagation environments has a great impact on the design consideration and rigorous testing before any implementation in real life applications. Furthermore, performance assessment using an appropriate channel model gives better understanding on the behaviour of the system and ensures the success for real implementation. Therefore, using the right modelling of the propagation channel is crucial to further study the performance of the proposed adaptive vector tracking loop (aVTL) algorithm, especially when dealing with real scenario.

3.1 Propagation Impairments

The signals propagating between a satellite and Earth (receiver) will experience different kinds of propagation impairments such as ionospheric and tropospheric propagation delays, as well as local fading effects such as shadowing, diffraction and finally, the most severe of all, additive interference in presence of the MP [1], [15]. The combination of these impairments during transmission can cause random fluctuations in amplitude, phase, angles of arrivals, de-polarisation of electromagnetics wave, degradation of the signal quality and ultimately increase the error rates of the communication links [16]. Ionosphere and troposphere both introduce various impairments that have an adverse impact on the performance of Earth-satellite radio propagation [16]. In ionosphere, impairment such as scintillation and polarization rotation effects is the foremost concern in satellite communication. On the other hand, troposphere introduces impairments such as dry air, water vapours, hydrometeors (moisture in atmosphere, gradient of temperature and sporadic structures of wind streams) that cause attenuation, refraction and absorption as well as scintillation and polarization of the radio signals [17]. Degradation caused by these effects varies depending on the geographic location, frequency and elevation angle. On top of the attenuation causes induced naturally by the atmosphere, radio waves also suffer from loss of energy due to complex and varying propagation environments on the terrain. Obstacles such as buildings, trees and objects (lamp posts, advertisement boards etc.) of different heights and surfaces cause shadowing and different MP propagation effects such as diffraction, scattering, reflection and absorption of the signals [1], [15], [16]. Moreover, the fact that users are constantly moving (car, pedestrians etc.) results in changes in signal strengths due to changes in phase (Doppler effect). According to [15], the standard deviations of the interferences affecting the C/A Code in normal situation are given in Table 5.

Table 5: Standard error model [15].

Error Source	Total 1σ -error [m]
Ephemeris data	2.1
Satellite clock	2.1
Ionosphere	4.0
Troposphere	0.7
Multipath	1.4
Receiver measurement	0.5

3.2 MP Channel Model

In the case of MP scenarios, GNSS receivers may receive the line of sight (LOS) signal (direct path) along with a number of reflected signals (MP). It is also worth mentioning that in more severe cases, the LOS signal is completely blocked especially in urban scenarios, which referred as to Non-Line-Of-Sight (NLOS) condition. In the presence of MP, the received signal depends on the amplitude, delay, frequency and phase of the LOS and MP signals. The complex representation of the composite baseband signal (without the data term), which is considered here by assuming a pilot channel, can be represented as follows:

$$s_l(t) = \sum_{l=0}^{N-1} A_l \cdot C(t - \tau_l(t)) \exp(j\varphi_l(t)) + n(t) \quad (3.1)$$

with

$$\varphi_l(t) = \varphi_l(0) + 2\pi \int_0^t f_l(u) du$$

where l represent the l^{th} path where ($l = 0$ represents the direct path (DP)), $A_l = \sqrt{P_l}$ is the amplitude of the l^{th} path signal which is related to its power P_l , $C(\cdot)$ is the PRN code and $n(t)$ is the complex white Gaussian noise. The parameters $\tau_l(t)$, $\varphi_l(t)$ and $f_l(t)$ are the code delay, carrier phase and signal frequency of the l^{th} path respectively and N is the number of received paths.

The first stage of a GNSS receiver consists of a matched filter which correlates the received signal, sampled at the frequency, $F_s = 1/T_s$ with a locally generated replica. A conventional integrate-and-dump (I&D) block is used to provide the matched filter output. The coherent k^{th} correlation, which is performed over the duration, $T_C(k)$ leads to the following in-phase (I) and quadrature-phase (Q) representation:

$$I(k) \approx \sum_{l=0}^{N-1} A_{l,k} R(\Delta\tau_{l,k}) \frac{\sin(\pi\Delta f_{l,k} T_C(k))}{\sin(\pi\Delta f_{l,k} T_s)} \cos(\Delta\varphi_{l,k}) + n_i[k] \quad (3.2)$$

$$Q(k) \approx \sum_{l=0}^{N-1} A_{l,k} R(\Delta\tau_{l,k}) \frac{\sin(\pi\Delta f_{l,k} T_C(k))}{\sin(\pi\Delta f_{l,k} T_s)} \sin(\Delta\varphi_{l,k}) + n_q[k]$$

where the parameters $\Delta\tau_{l,k}$, $\Delta f_{l,k}$ and $\Delta\varphi_{l,k}$ are the mean errors (i.e., the difference between the parameters of the received signal and the parameters of the locally generated replica) of the code delay, the signal frequency and the carrier phase, and $R(\cdot)$ denotes the spreading code autocorrelation function. The noises n_i and n_q are assumed to be independent white Gaussian sequences (with zero means). We will use the following expression for defining the correlator output:

$$u_z(k) = \sum_{l=0}^N A_{l,k}(\Delta f_{l,k}) R(\Delta\tau_{l,k}) \exp(j\Delta\varphi_{l,k}) + n_z(k) \quad (3.3)$$

with

$$u_z(k) = I(k) + jQ(k).$$

In this expression, $A_{l,k}$ is the amplitude of the l^{th} path signal. This amplitude depends on the power of the l^{th} path incoming signal, but also on its frequency error versus the coherent integration time ($\Delta f_{l,k} T_c$) given by:

$$A_{l,k} = \sqrt{2P_{l,k}} \frac{\sin(\pi\Delta f_{l,k} T_c(k))}{\sin(\pi\Delta f_{l,k} T_s)} \quad (3.4)$$

In the case of MP scenarios, there are many models proposed for modelling the channel [18], [19], [20] and [21] which was developed for communications and not specifically for GNSS. In this work, the following expression is used to define the impulse response of the channel in presence of MP:

$$h_c(k) = \sum_{l=0}^N a_{l,k} \delta(t - \tau_{l,k}) \exp(j\varphi_{l,k}) \quad (3.5)$$

where $a_{l,k}$, $\tau_{l,k}$, and $\varphi_{l,k}$ are the attenuation, the propagation delay and the carrier phase of the l^{th} path respectively ($l = 0$ for the DP). These parameters depend on the environment and on the vehicle dynamic.

In order to facilitate MP understanding in the framework of this study, we propose first to address very simple scenarios. These scenarios consider a LOS signal with one MP as illustrated in Figure 25 below.

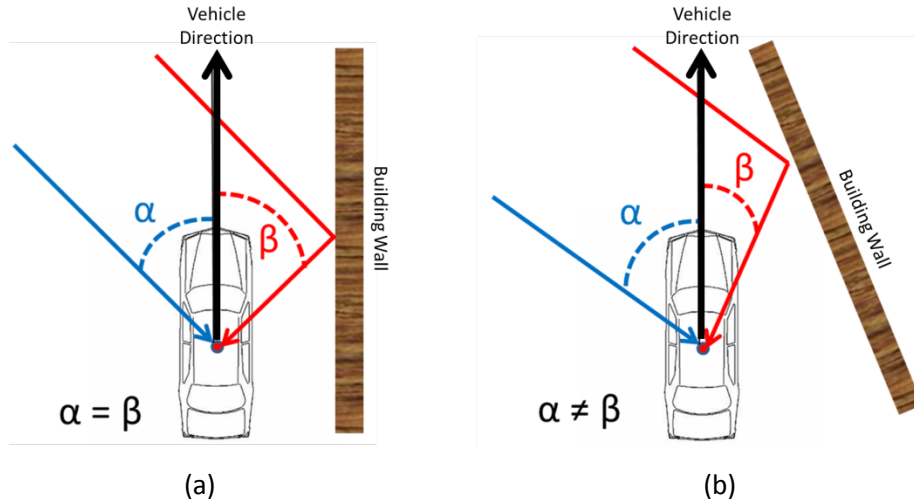


Figure 25: Two path signals; (a) at the same frequencies and (b) at different frequency.

Assuming a slow fading channel, MP can be classified in 2 categories depending on the value of the Doppler frequency of the direct path (DP) (f_0) and the MP (f_1). In case (a), when the vehicle is stationary or moves parallel to the reflecting surface, the DP and MP frequencies can be considered as equal. For any other motion, as shown in case (b), the DP and MP frequencies are different. The following expression is used to define the impulse response of the channel in presence of one MP:

$$h_c(k) = a_{0,k} \delta(t - \tau_{0,k}) \exp(j\varphi_{0,k}) + a_{1,k} \delta(t - \tau_{1,k}) \exp(j\varphi_{1,k}) \quad (3.6)$$

where a, τ and φ represent the attenuation, propagation delay and the carrier phase of the signals. Indices 0 and 1 represent the DP and MP respectively. This simple representation is justifiable because in the presence of several MP, the global contribution of the MP can be combined in a single component.

In this condition, two time domains can be defined depending on the vehicle environment described earlier. Domain \mathcal{D}_1 illustrated in Figure 25(a) corresponds to situations where when DP and MP Doppler frequencies are the same MP which will be referred to as coherent MP, as the MP is in phase relation with the DP over a short period of time. On the contrary, domain \mathcal{D}_2 illustrated in Figure 25(b) MP corresponds to different DP and MP frequencies, i.e., to a non-coherent MP scenario. Both domains can be represented as follows:

$$\begin{aligned} \mathcal{D}_1 : t \setminus f_1(t) &= f_0(t) \\ \mathcal{D}_2 : t \setminus f_1(t) &\neq f_0(t). \end{aligned} \quad (3.7)$$

In this context the expression of the coherent correlator output, which is deduced from equation (3.3), can be expressed as:

$$u_z(k) = A_{0,k}(\Delta f_{0,k}) R(\Delta \tau_{0,k}) \exp(j\Delta \delta \varphi_{0,k}) + A_{1,k}(\Delta f_{1,k}) R(\Delta \tau_{1,k}) \exp(j\Delta \delta \varphi_{1,k}) + n_k^f$$

with

$$\begin{aligned} \Delta \varphi_{0,k} - \Delta \varphi_{0,k-1} &\approx 2\pi \Delta f_{0,k} T_C(k) \\ \Delta \varphi_{1,k} - \Delta \varphi_{1,k-1} &\approx 2\pi \Delta f_{1,k} T_C(k). \end{aligned} \quad (3.8)$$

In this expression, $\Delta f_{0,k}$ and $\Delta f_{1,k}$ denote the DP and MP frequency errors that can be expressed as follows:

$$\begin{aligned} \Delta f_{0,k} &= \tilde{f}_{0,k} - \hat{f}_k \\ \Delta f_{1,k} &= \tilde{f}_{1,k} - \hat{f}_k \end{aligned} \quad (3.9)$$

where $\tilde{f}_{0,k}$, $\tilde{f}_{1,k}$ are the mean value of the incoming DP and MP signal frequencies for the k -th integration, \hat{f}_k is an estimation of the DP frequency provided inside the receiver by the considered tracking module.

In the domain \mathcal{D}_2 ($\tilde{f}_{0,k} \neq \tilde{f}_{1,k}$), correspond to a non-coherent MP condition, DP and MP decorrelation is possible in the frequency domain. On the contrary, in the domain \mathcal{D}_1 ($\tilde{f}_{0,k} = \tilde{f}_{1,k}$), DP and MP decorrelation requires a time domain representation. These two situations and the combinations of these two situations will be considered for performance evaluation. In order to propose specific MP mitigation techniques, we propose to study the MP effects on the performance of the tracking loop.

3.2.1 MP Effect on Tracking Loop

Similar to interference, MP is an external error source due to the environment that has a significant impact on the tracking loop performance. The primary MP parameters, which are all measured relatively to the direct signal, are the amplitude, delay, phase and phase-rate. Therefore, an analysis of the code and carrier tracking loops yields the relationship between the MP parameters and the resulting measurement errors. The relative MP strength is usually denoted as signal-to-MP

ratio (SMR). The MP effects yield errors in both code delay and carrier phase estimation of the tracking loop. The latter is much smaller than the former since it depends on the carrier frequency which is generally expressed in GHz . On the other hand, the code delay depends on the chipping rate which is expressed in $Mbps$. Note that, the carrier cycle error corresponds to the wavelength, $\lambda = c/f_{L1} \approx 19cm$ whereas the range error associated with the chip duration, typically $\delta\epsilon_\tau = c \cdot T_c \approx 293m$ [10].

Consider a simple case where the transmitted signal reaches the receiver via two paths: the line-of-sight (LOS) signal and a reflected MP signal which beats at the LOS frequency. Therefore, the received signal is composed of two components representing the DP and an MP that is a delayed, phase shifted and attenuated version of the LOS signal. Due to these changes, the two signal components interfere. Depending on the phase of the MP component, the composite received signal can be classified either to be a constructive or a destructive interference as illustrated in Figure 26. We consider here the two worst case scenarios. Constructive interference happens when the LOS and MP are in phase as in Figure 26(a) whereas destructive interference happens when they are out-of-phase as in Figure 26(b).

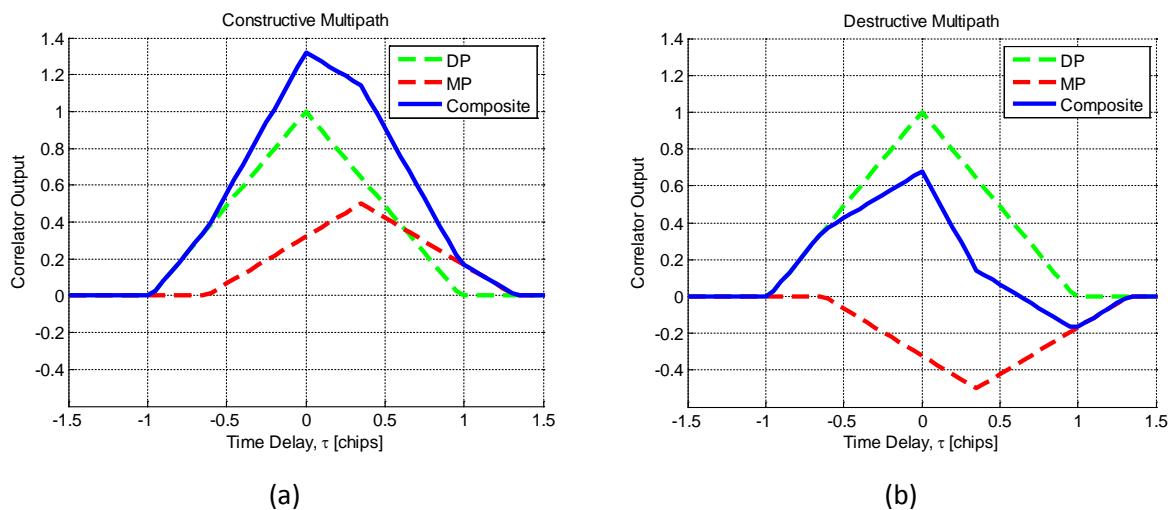


Figure 26: Illustration of (a) Constructive interference, and (b) Destructive interference [10].

In order to see the MP effect on the code range, we consider the output of a discriminator which is designed for measuring the code delay error in a delay tracking loop. Such a loop follows the zero-crossing of the discriminator response known as S-curve as illustrated in Figure 27. Analytically, the resulting discriminator output can be considered as the sum of the two discriminator components. One component is attributed to the direct path signal as shown in Figure

27 (green), while the other is associated with MP as displayed in Figure 27 (red). The zero crossing in an ideal case is obtained when the tracking error is zero. By looking at the composite signal in Figure 27 (blue), the zero-crossing is shifted from the correct position. This results in the local code to be lagging or leading depending on the MP phase, as illustrated in Figure 28. Therefore, the pseudorange MP error is given by the amount of lag or lead in the local code (i.e., the distance between the 2 red square markers illustrated in Figure 28).

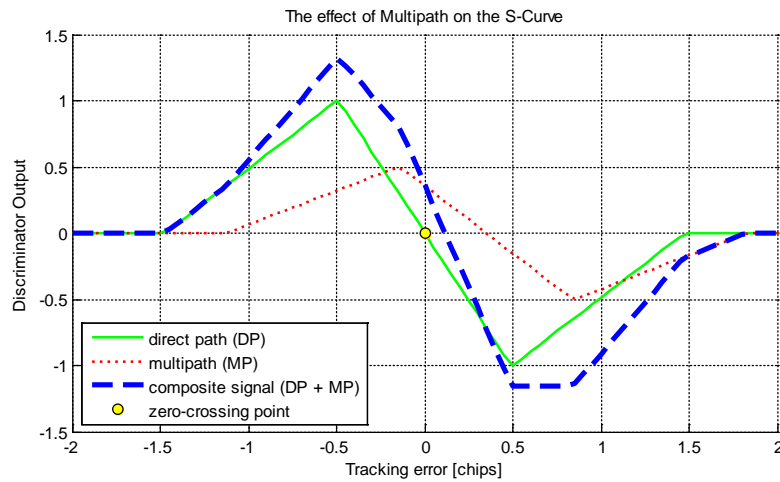


Figure 27: S-Curve plot for direct path (green), multipath (red), and resulted composite signal (blue).

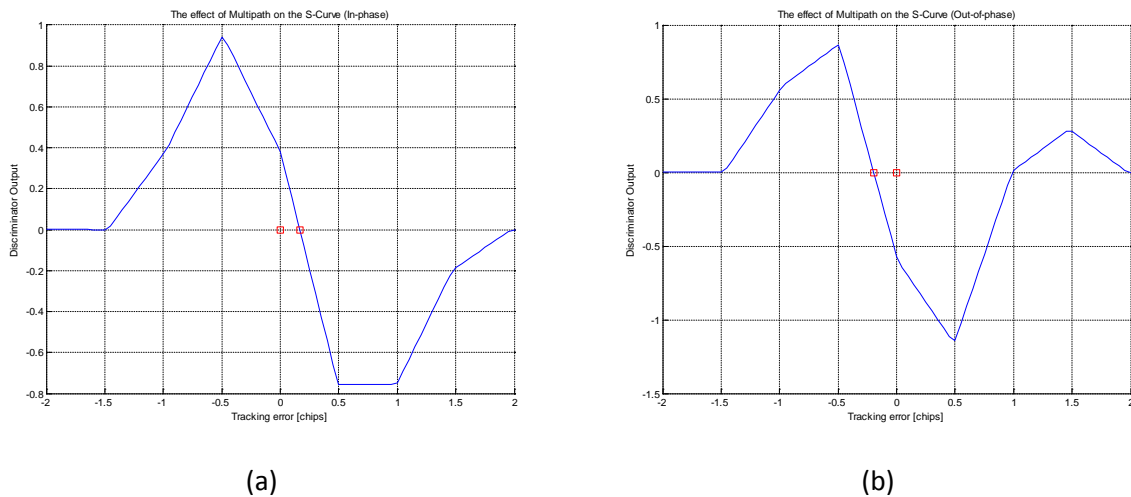


Figure 28: S-curve plots; (a) in case of constructive interference, and (b) in case of destructive interference.

Therefore, in the presence of single MP, an MP error envelope (MEE) can be plotted as in Figure 29. The slope of this envelope is a function of MP amplitude and delay. Typically, the MP

relative amplitude α is assumed to have a constant value. The upper bound (blue) of the MEE is the maximum range error when the MP is in-phase with direct path. The lower bound (red) of the envelope is when the MP is out-of-phase from the direct signal. In general, the MP error varies between these two extremes. For example, for a standard code discriminator with a chip spacing, $d = 1 \text{ chips}$ and relative multipath amplitude, $\alpha = 0.5$, the upper bound of the code MP tracking error is $\varepsilon_\tau \cong 0.25 \text{ chips} \approx 73.25 \text{ m}$.

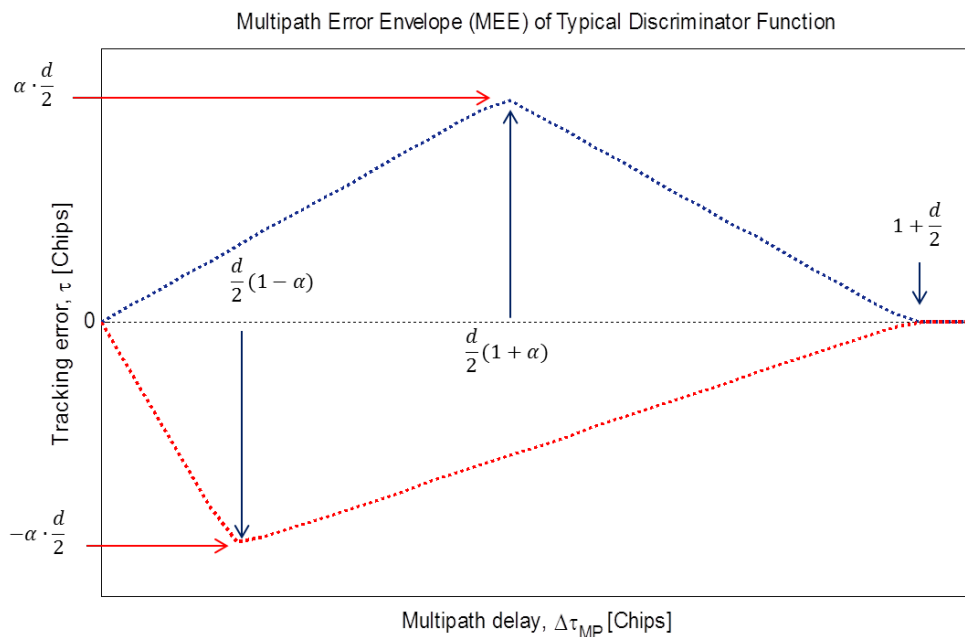


Figure 29: Generic interpretation of MP error envelope.

From these observations, it can be assumed that the MP will affect the performance of the code tracking depending of the discriminator spacing, d and the incoming signal strength of the MP, i. e. α . Furthermore, if the MP delay $\Delta\tau_{MP}$ is such as $\Delta\tau_{MP} > 1 + d/2$, then it no longer affects the code tracking. Therefore many studies related to MP mitigation suggest using small values of spacing, d . This strategy manages to mitigate effectively the medium and long MP delays. Unfortunately, this requires a trade-off in term of robustness as the tracking loop may lose the lock of the code in case of heavy short delay MP environment. Moreover this approach does not allow very near echoes that are hard to be detected and mitigated.

On the other hand, the impact of MP effects on the carrier phase should be studied. This effect may be viewed by using a phasor diagram which shows how this operation is being handled by a phase lock loop or the frequency lock loop depending on the receiver architecture. Here the

incoming carrier results from the LOS and a coherent MP, assuming that the frequency tracking is achieved. Here we assume that the phase lock loop (PLL) and the delay lock loop (DLL) are locked on the LOS signal ($\Delta\varphi_0 = 0, \Delta\tau_0 = 0$). We'll see later the relevance of the hypothesis $\Delta\tau_0 = 0$ in a vectorial tracking loop (VTL) configuration. The local carrier cannot distinguish the components of the distorted signal and therefore can track the composite signal. The phasor diagram depicting the relationship between the relative MP and the resulting carrier phase error is illustrated in Figure 30. Note that the relative phase between DP and MP signal is denoted by $\Delta\varphi_{MP}$. The phase difference between the direct and the composite signal, φ_C is the carrier phase MP error.

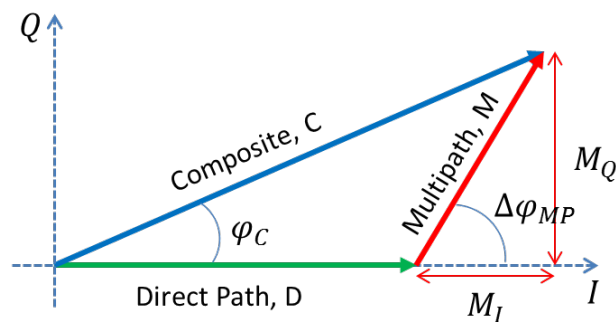


Figure 30: Phasor diagram illustrating the relationship between the direct path and multipath.

The magnitude of the DP and MP phasors is given by:

$$\begin{aligned} D &= R(\Delta\tau_0) = R(0) \\ M &= \alpha R(\Delta\tau_{MP}) \end{aligned} \quad (3.10)$$

where $R(\cdot)$ are the code autocorrelation function and $\Delta\tau_0, \Delta\tau_{MP}$ are the LOS and the MP delay errors and α in the multipath relative amplitude. In order to derive the equation for φ_C , the MP phasor is decomposed into its in-phase, M_I and quadrature-phase, M_Q as illustrated in Figure 30. Therefore, the expression for the phase of the composite signal is obtained as follows:

$$\varphi_C = \arctan\left(\frac{M_Q}{D + M_I}\right)$$

and can be re-written as:

$$\varphi_C = \arctan\left(\frac{\alpha \cdot R(\Delta\tau_{MP}) \cdot \sin(\varphi_M)}{R(0) + \alpha \cdot R(\Delta\tau_{MP}) \cdot \cos(\varphi_M)}\right) \quad (3.11)$$

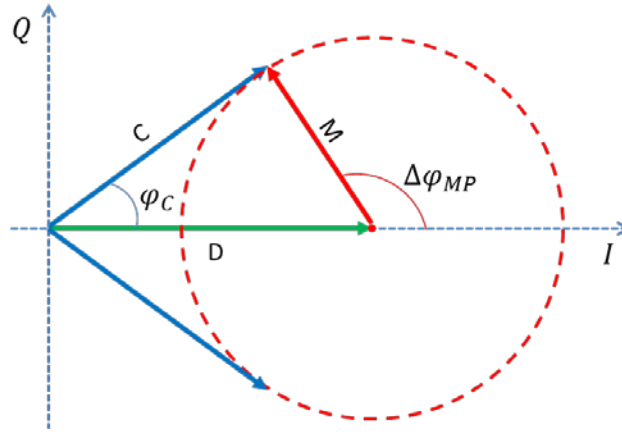


Figure 31: Phasor Diagram illustrating the effect of the MP phase.

Based on Figure 31, it is observed that for $\alpha < 1$ the maximum phase error, obtained for $\Delta\tau_{MP} = 0$, is:

$$\varphi_{c_{max}} = \arcsin(\alpha). \quad (3.12)$$

Hence, the maximum possible error is $\pi/2$ rad which corresponds to 1/4 of carrier wavelength. In the case of the GPS L1 frequency, this amounts to approximately 4.8cm.

The MP not only impacts the estimation of the code range and the carrier phase, but that of the measured signal power (which results not only from the LOS signal, but also from the MP). This can be seen clearly on the autocorrelation function displayed in Figure 26 as the constructive MP scenarios have higher amplitudes than in the destructive case.

Finally we have to consider the reflected signal whose relative phase varies with time. In the case of Figure 25 (b), the instantaneous MP frequency is:

$$f_l = \frac{\left[\omega_D + \frac{d\theta_l(t)}{dt} \right]}{2\pi} \quad (3.13)$$

where $\omega_D = 2\pi f_D$ is the angular frequency of the DP signal.

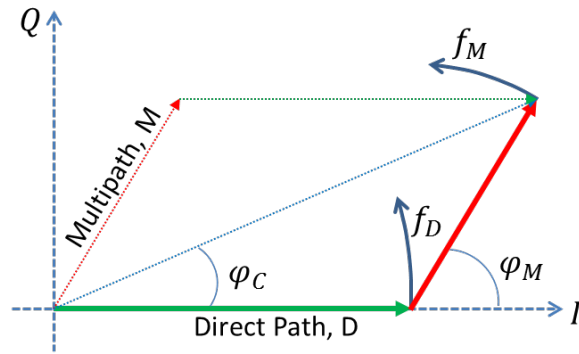


Figure 32: Phasor diagram of DP and MP associated with respective frequencies.

Consider the illustration in Figure 32. In this case, although the received signal is a composite signal between the LOS and MP signals, it can be viewed as separated components that have 2 different frequencies. Such a signal can be detected by using a Fast Fourier Transform (FFT) or any other suitable high resolution frequency estimators. In a simple approach this MP signal can be filtered and does not affect the receiver performance.

3.2.2 In-House Simulator

In order to assess our algorithms in a simple MP scenario (see Figure 25), an in-house signal simulator has been designed and used to evaluate the performance of the tracking loops. To recreate the MP channel model for which the existing true values of the receiver (delay, Doppler frequency, and position) are imposed, a synthetic receiver trajectory has been created as illustrated in Figure 33. The Absolute position and velocity of the receiver can be computed for different time instants when the vehicle is moving along this trajectory.

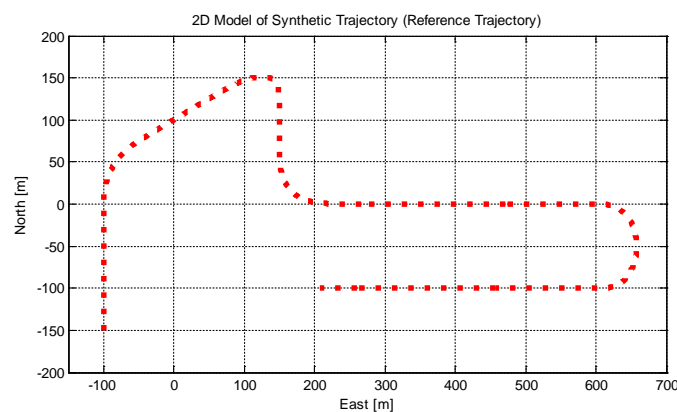


Figure 33: Synthetic receiver's trajectory.

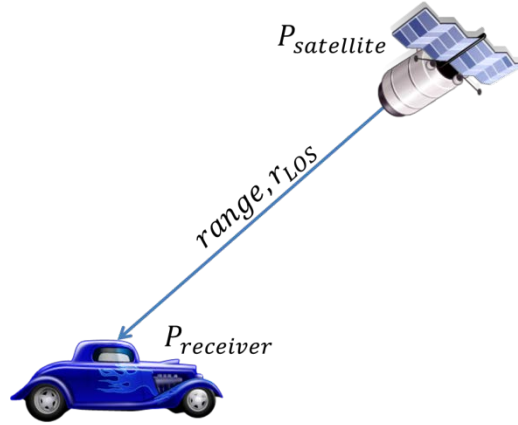


Figure 34: Illustration for the range of LOS signal.

The signal simulator generates the LOS and the MP signals separately before forming the composite signal associated with the MP channel model. First, the method producing the parameters of the LOS signal is considered. Assuming that the position of the satellite and the receiver are known, the range, r_{LOS} between the satellite and the receiver can be extracted geometrically and can be expressed as:

$$r_{LOS} = \|P_{sat} - P_{rec}\|. \quad (3.12)$$

By knowing the range, the delay of the LOS signal can be calculated by using this relationship:

$$\tau_k = \frac{r_{LOS}}{c} \quad (3.13)$$

where c is the speed of light. On the other hand the signal generated inside the satellite is considered:

$$s(t_{sat}) = A \cdot C(t_{sat}) \cdot \exp(j2\pi f_{L1} t_{sat}) \quad (3.14)$$

where t_{sat} is the time when the signal has been broadcast. When the signal arrives at the receiver, the relationship between reception time and propagation delay can be written:

$$t_{sat} = t_{rx} - \tau \quad (3.15)$$

where t_{rx} is the reception time at the receiver and τ is the propagation delay. Therefore, the received signal is:

$$s(t_{sat}) = A \cdot C(t_{rx} - \tau) \cdot \exp(j2\pi f_{L1}(t_{rx} - \tau)). \quad (3.16)$$

Then, by considering only the carrier components, the carrier wipe-off of the received signal can be expressed as:

$$\begin{aligned} u(t) &= \exp(j2\pi f_{L1}(t_{rx} - \tau)) \cdot \exp(-j2\pi f_{L1}t_{rx}) \\ u(t) &= \exp(-j2\pi f_{L1}\tau). \end{aligned} \quad (3.17)$$

Therefore, from this relationship, it is clear that the phase of the direct signal can be calculated at the time tT_s (T_s : sampling frequency) by:

$$\varphi_t = -2\pi f_{L1}\tau_t = -2\pi \frac{c}{\lambda_{L1}}\tau_t = -2\pi \frac{r_{LOS}(t)}{\lambda_{L1}}. \quad (3.18)$$

After defining all parameters, the signal component for the direct signal can be generated as follows:

$$S_t = A_t \cdot C(t - \tau_t) \cdot \exp(j\varphi_t). \quad (3.19)$$

In order to generate the MP component in the simulator, one can assume that the DP and MP signals are parallel to each other. Consider the illustration in Figure 35 for both conditions. One can assume that total r_{MP} is the extended range from the LOS signal assuming that at a certain point during transmission, the ranges of DP and MP signals are parallel and have the same length. Therefore, the 'extended range' of the MP is an extension of the length relative to the DP.

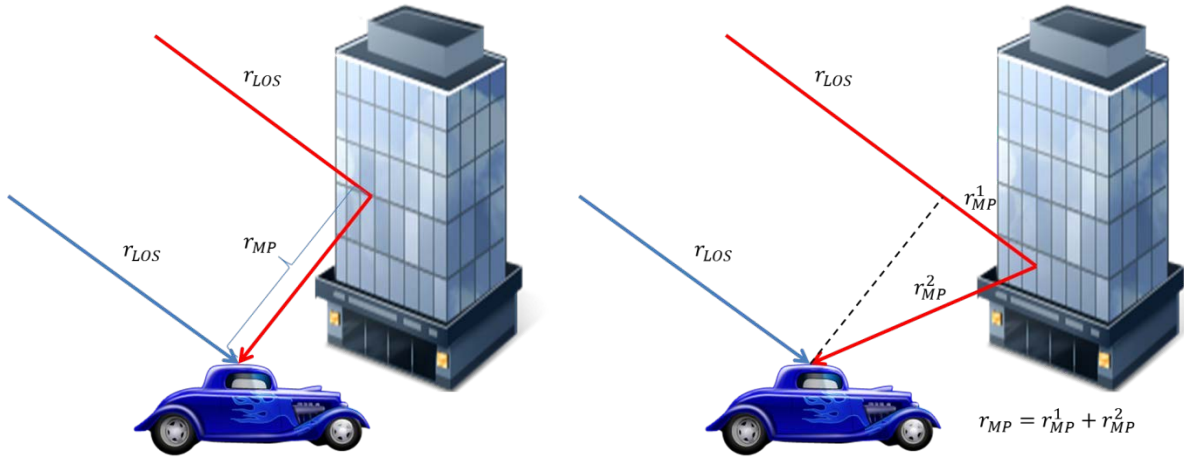


Figure 35: Illustration of DP and MP signals.

From this relationship, by considering only a single MP, the extra delay of this MP can be expressed as:

$$\Delta\tau_{MP} = \frac{r_{MP}}{c} \quad (3.20)$$

and the total delay is

$$\tau_{MP}(t) = \tau_t + \Delta\tau_{MP}(t). \quad (3.21)$$

Using the same relation for the LOS signal, the MP phase can be expressed as:

$$\Delta\varphi_{MP}(t) = -2\pi \frac{r_{MP}(t)}{\lambda_{L1}} \quad (3.22)$$

with the following total phase

$$\varphi_{MP}(t) = \varphi_k + \Delta\varphi_{MP}(t). \quad (3.23)$$

Therefore, the MP signal generated by the simulator is

$$S_{MP}(t) = A_{MP}(t) \cdot C(t - \tau_t - \Delta\tau_{MP}(t)) \cdot \exp\{j(\varphi_t + \Delta\varphi_{MP}(t))\} \quad (3.24)$$

The simulator was implemented by using a tap delay line approach as illustrated in Figure 36. The advantage of this simulator is the knowledge of the true parameters (delay, phase, frequency, velocity and time) at any point of the trajectory. It also allows the user to have full control of the following MP parameters

- the MP occurrences and disappearances,
- the MP number with the respective signal parameters,
- the relative MP amplitude, etc.

This simulator allows the performance evaluation of the designed tracking loops by comparing the signal parameters which are estimated by our algorithms to the actual parameter values considered at each time instant of the simulation.

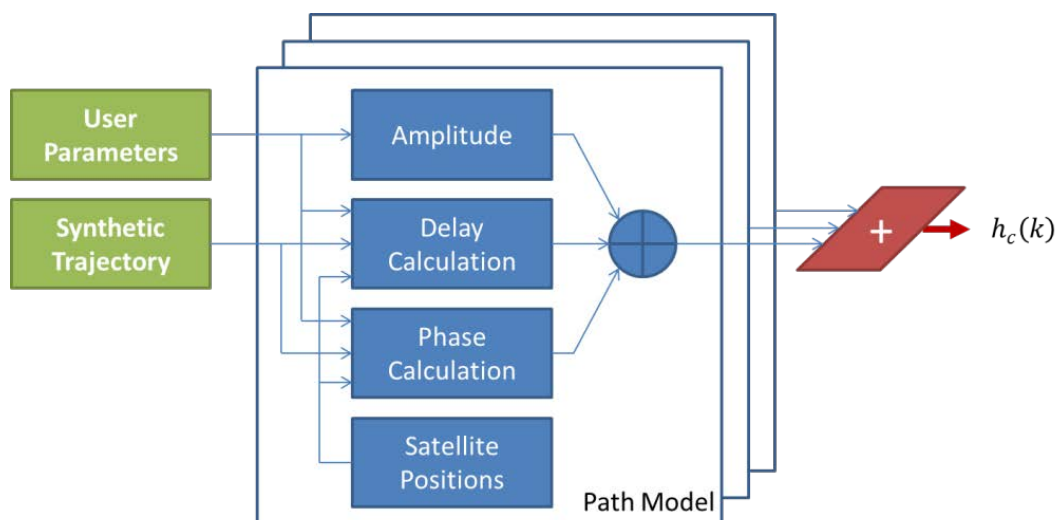


Figure 36: In-house Simulator for MP Channel model.

A typical example of the composite signal generated using the simulator is displayed in Figure 37, in the case of a DP and a single MP. In this example, the MP signal has a relative amplitude ratio of 0.3, a relative frequency of 1.5 kHz and a relative code phase of 0.5 chips with respect to the DP signal parameters.

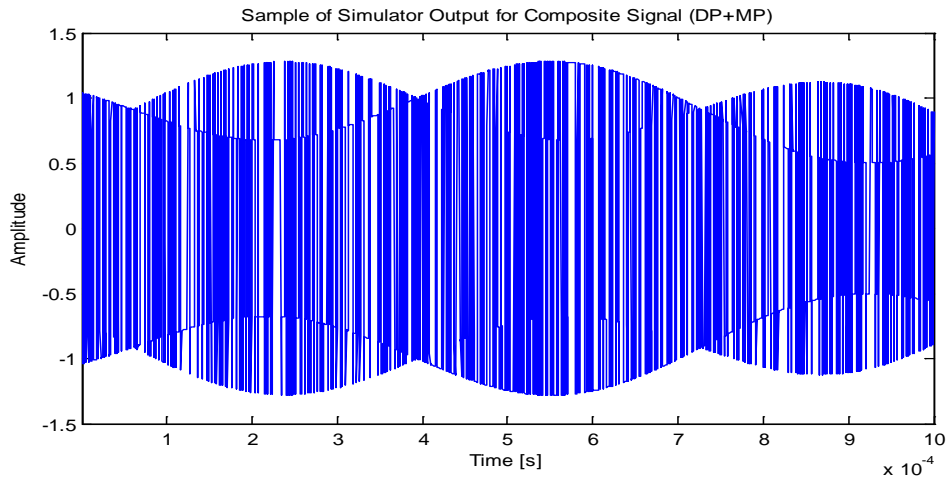


Figure 37: Output Samples of the Simulator.

A preliminary test was performed using our simulator in a standard receiver approach. 4 MP scenarios were introduced during the trajectories considered in the simulations. These scenarios take into account coherent, non-coherent and combination of both MP conditions. Scenario #1 considers the presence of non-coherent MP, scenario #2 is characterized by the presence of a non-coherent MP with LOS is lost for 3s, scenario #3 studies the presence of both coherent and non-coherent MP and lastly, in scenario #4, the vehicle is affected by the presence of coherent MP.

The estimation results obtained with the MP scenarios described above are presented in Figure 38. We can observe that for every MP scenario introduced, the resulted tracking estimation experienced a certain variations and biases in the position estimation. This simple test was done to validate the proposed simulator and to confirm its good behavior.

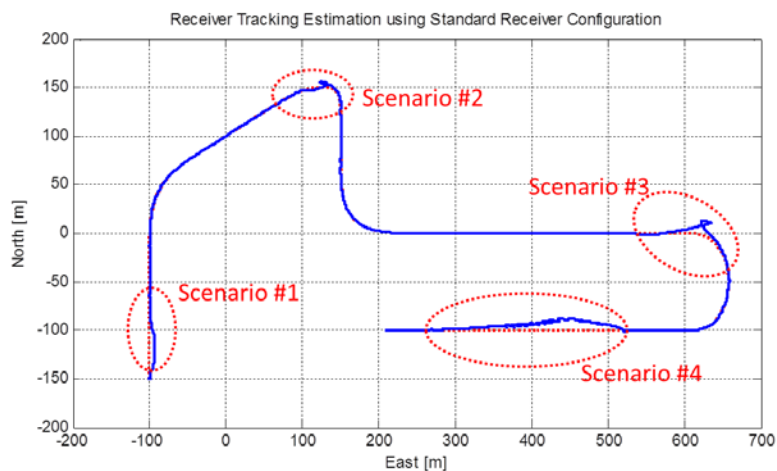


Figure 38: Tracking Estimation using standard receiver configuration.

3.3 Land-Mobile Satellite Channel

For modelling a land-mobile satellite (LMS) channel it is important to understand the propagation steps which dictate the behaviour of the channel and to derive the global rules and expressions of the channel. These will describe the dependence of the received signal with regard to some parameters such as frequency, elevation angle, antenna type, type of environment as well as the relative velocity between receiver and satellite. The received signal is modelled as the sum of three components associated with the DP, the reflection term (specular) and the MP (diffuse component) [22].

In order to study several receiver situations (corresponding to pedestrian or car users) we have to consider urban, suburban and rural scenarios. Therefore, the channel models can only be derived after extensive measurement campaigns and/or ray tracing simulations. Based on these measurements, a variety of statistical and/or combination of physical-statistical models have been developed where the probabilities are estimated and fitted by reasonable standard distribution functions which are briefly described in subsequent section.

3.3.1 Statistical Channel Model (SCM)

The statistical channel model (SCM) is formulated based on a number of statistical assumptions resulting from numerous measurement campaigns [23]. These statistical assumptions are then fitted so the resulted model can behave according to the real measurements with certain parameters which are associated with specific environments and vehicle dynamics. This makes it complex because the assessment of the signal combination is achieved by considering not only the signal characteristics and the receiver architecture, but also different MP propagation channels under various conditions [24].

We consider the DLR wideband channel model which was defined in [18]. It uses a tap delay line model that consists of 3 sub-models as illustrated in Figure 39. It decomposes the incoming signals into three kinds of signals: direct path, near echoes and far echoes. This model was defined from a general distribution for number of MP signals, their corresponding delays, and their relative amplitudes, as well as associated model parameters for different types of environment and elevation angles. Effects like shadowing are also taken into account by modelling the amplitude of the LOS component.

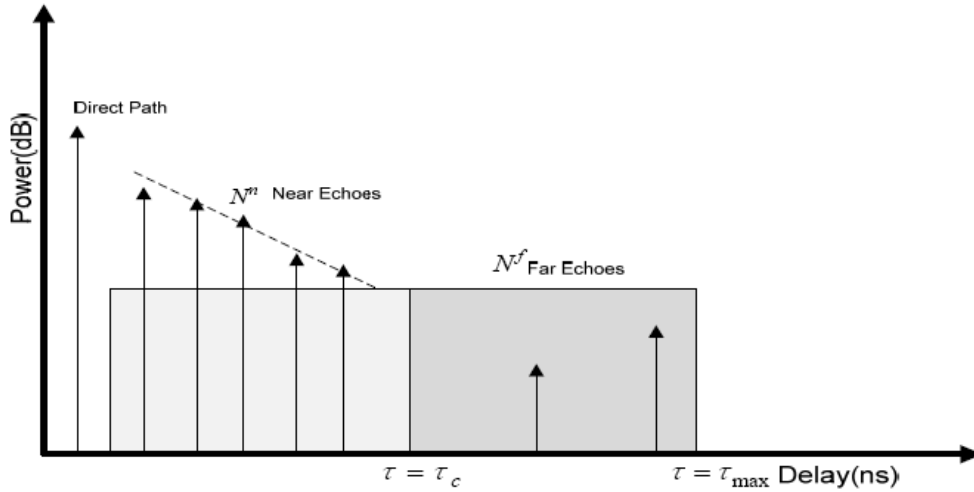


Figure 39: Statistical CIR of wideband channel model proposed by [18].

Based from [18], the DP amplitude has to be modelled based on shadowing characteristics. It is expected that this distribution depends on LOS signal quality. In an open sky environment a Rice distribution is used to describe the probability density function (pdf) of the LOS signal amplitude (a_1):

$$pdf_{Rice}(a_1) = \frac{a_1}{\sigma^2} I_0 \left(\frac{a_1}{\sigma^2} \right) \exp \left(-\frac{a_1^2 + 1}{2\sigma^2} \right), \quad a_1 > 0 \quad (3.35)$$

where the standard deviation σ is set depending on the environment. Conversely, in the presence of shadowing, the pdf of the LOS amplitude is a the Rayleigh distribution whose pdf is

$$pdf_{Rayl}(a_1) = \frac{a_1}{\sigma^2} \exp \left(-\frac{a_1^2}{2\sigma^2} \right), \quad a_1 > 0 \quad (3.36)$$

with a lognormal-distribution for the mean power $2\sigma^2 = P_0$:

$$pdf_{ln}(P_0) = \frac{10}{\sqrt{2\pi} \sigma \ln 10} \cdot \frac{1}{P_0} \exp \left\{ -\frac{[10 \log P_0 - \mu]^2}{2\sigma^2} \right\} \quad (3.36)$$

Consider now the MP echoes. The near echoes (near MP), that appear in the close vicinity of the receivers (with delays $0 < \Delta\tau_k^{(n)} < \tau_e$ where $\tau_e \approx 200m \approx 0.7 \text{ chips}$), are considered in priority. The number of near echoes N is Poisson distributed:

$$P[N = n] = \frac{\lambda^n}{n!} e^{-\lambda} \quad (3.37)$$

The delay distribution $\tau^{(n)}$ of the MP signals associated with these echoes is an exponential distribution whose pdf is

$$P_{exp}(\tau^{(n)}) = \frac{1}{b} e^{-\frac{\tau^{(n)}}{b}}, \quad \tau^{(n)} > 0 \quad (3.38)$$

where b is the unique model parameter that represents the typical path delay in a specific environment. The mean power of the near echoes $S(\tau) = \varepsilon(a_1^2)$ is exponentially decreasing with $\tau^{(n)}$:

$$S(\tau^{(n)}) = S_0 e^{-\delta\tau^{(n)}} \quad (3.39)$$

Given, for a fixed delay, a mean echo power $S(\tau^{(n)})$, the amplitude $a_k^{(n)}$ will vary around this mean value according to a Rayleigh distribution with $2\sigma^2 = S(\tau^{(n)})$.

Consider now the case for far echoes. The number of far echoes $N^{(f)}$ is also distributed according to a Poisson distribution with the following relationship

$$N^{(f)} = N - N^{(n)} - 1 \quad (3.40)$$

The far echoes appear with delays $\tau_e < \Delta\tau_k^{(f)} < \tau_{max}$, with only a few echoes with long delays. The delay distribution, $\tau_k^{(f)}$ of the far MP signals on the other hand are uniformly distributed in $[\tau_e, \tau_{max}]$. More details about the numerical values of the model parameters for each path are given in [18]. Note that the far echoes can be easily mitigated.

3.3.2 Physical-statistical Channel Model (PSCM)

The physical-statistical channel model (PSCM) can be viewed as a hybrid channel model which combines the physical geometric theory and the statistical data from measurement campaigns. These types of models are trying to get the advantages of both modelling techniques in providing better channel models. The physical models known as deterministic models are strongly related to the physical parameters but require a precise description of the environment and high computation load [22] such as the model based on ray tracing [25]. Therefore, physical models alone are not able to cope with the heterogeneous nature of the environments. However, the physical models have shown some advantages with respect to a pure statistical model [14].

The channel model proposed by DLR [26] is one of the most realistic channel models where it considers and approximates the parameters of every single reflection of specular MP. This channel model combines data obtained from a measurement campaign with deterministic scenario. It separates the incoming signal into a DP and a reflected path. The direct path is modelled by taking into account the vehicle motion, under the proposed scenario, whereas the reflected paths are generated with statistical properties depending on the geometry of the simulated environment.

With regard to the direct path, the LOS signal can be blocked or degraded in the case of urban environment. If the LOS is obstructed by house fronts, the attenuation is modelled as a diffracting “knife-edge”. For modelling the influence of trees, a model which merges an attenuating cylinder to represent the trunk of the trees and a statistical fading process to describe the branches and leaves is considered. The last major obstacles which are taken into account in urban scenario are lamp-posts which are modelled as a “Double Knife Edge Model”.

On the other hand, the reflected signals are assumed to be statistically distributed by considering the echo distribution obtained from the measurement data. These signals are generated according to a complex model which takes into account the influence of the reflector’s geometric occurrence, specular MP lifespan, relative angle, mean power and time series characteristics. The number of the echoes that are generated at each epoch is also an important parameter. It is interesting to note that the number of rays can be more than 50 paths per epoch.

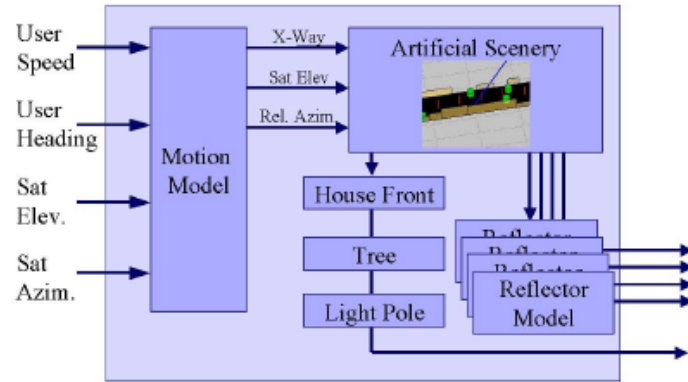


Figure 40: Overview block diagram of the DLR model implementation [21].

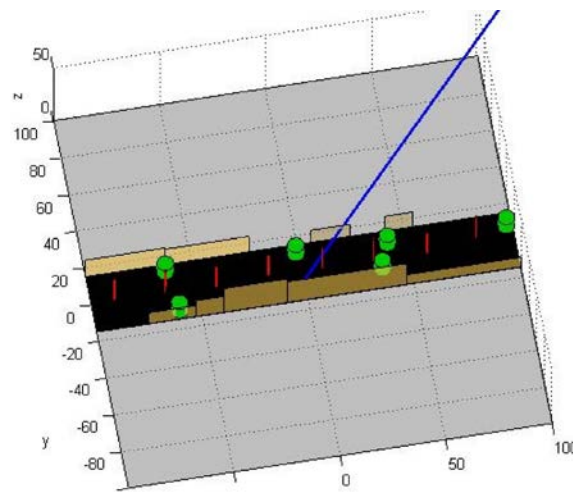


Figure 41: Sampled image of the artificial scenery [21].

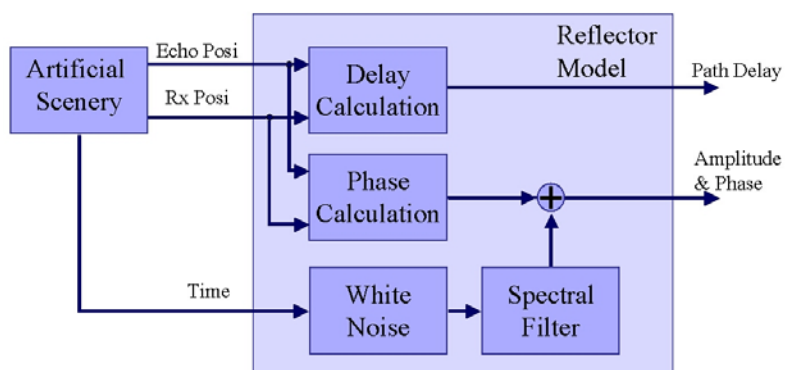


Figure 42: DLR model for the isolated reflector [21].

The block diagram in Figure 40 gives an overview implementation of the DLR model proposed in [21]. The x-coordinate and the relative satellite azimuth are derived from the user speed

and heading which drives the artificial scenery illustrated in Figure 41. The artificial scenery is used to generate continuous series of receiver positions according to the actual speed and created the characteristics of the reflected signal as illustrated in Figure 42. As a result, the output of the DLR model implementation is a complex time-variant channel impulse response given by:

$$h(t, \tau) = \sum_{l=0}^{N(t)} a_l \cdot \delta(\tau - \tau_l(t)) \quad (3.42)$$

where a_l is the complex parameter which depend on the l^{th} path amplitude and phase. These output argument vectors which describe the channel, whose size increases or decreases over time, are provided with the history of user position. Since the impulse response is calculated for every new time step where for each time step, the echoes is then generated for every time instances. This allow each impulse to be identified in order to build the output vectors to mirror the history of the time and also the travelled user way [7].

3.3.3 Weakness of existing models

Both statistical and physical-statistical channel models that are being presented here have their own strength and weaknesses accordingly. Without pitting one against another, these weaknesses will be discussed in very broad and general terms. Some of the existing channel models are based on measurement campaigns that are limited in bandwidth due to the equipment's capability. Besides, there is no information about the angle of arrival of reflected signals related to these data. On the other hand, models that are based on ray-tracing suffer from a high computational load to provide the channel impulse response sequences and needs an accurate 3D model of the vehicle environment. Moreover, the information regarding the order of reflections, refraction and diffraction are considered insufficient.

3.3.4 Integrating LMS channel model in our Simulator

The DLR channel model proposed a different approach for channel modelling which makes it attractive for practical applications. Thanks to the DLR, this channel model has been made available online (with some restriction) and thus it gives a good general idea on how it works. Upon request, the free version of the DLR model is available from the DRL website [26]. The technical note [7] gives

detailed descriptions explaining how to use this model. As mentioned earlier, this model is based on both deterministic and stochastic processes within artificial scenery that has to be parameterized by the user. It is implemented in Matlab® using object oriented programming language.

The obstacles created in the artificial scenery consist of house fronts, trees and lamp posts, (that are shaped and placed by statistical processes) are assumed to follow truncated normal Gaussian distributions. The following distribution, which is characterized by the mean, the variance σ^2 , and the specified interval $[x_{min}, x_{max}]$, is defined as:

$$p(x|x \in [x_{min}, x_{max}]) = \tilde{p}(x) = \begin{cases} 0 & x < x_{min} \\ \frac{1}{C} \cdot \frac{1}{\sqrt{2\pi\sigma^2}} e^{-\frac{(x-\mu)^2}{2\sigma^2}} & x_{max} \geq x \geq x_{min} \\ 0 & x > x_{max} \end{cases} \text{ with } C = \int_{x_{min}}^{x_{max}} p(x)dx \quad (3.41)$$

For example, for shaping the house fronts and placement processes, the values of the house mean, maximum, minimum and standard deviation are set by the user, along with the mean, maximum, minimum and standard deviation values of the house width. This concept is applied to all physical obstacles to create the artificial scenery. The technical note provided in [7] provides further details about the model.

In order to integrate the DLR model with our simulator, the DLR model has been handled in a separate simulation to generate a data file independently. The delicate part has been to integrate our synthetic trajectory with the DLR model generator data which is illustrated in Figure 43. Since the trajectory is also associated with a certain velocity for the whole pathway, it is important to ensure this velocity is fed into the DLR channel model. Besides that, a real constellation is used to give the DLR model its azimuth and elevation angle. All the other generic parameters are kept as close as the DLR model default configuration.

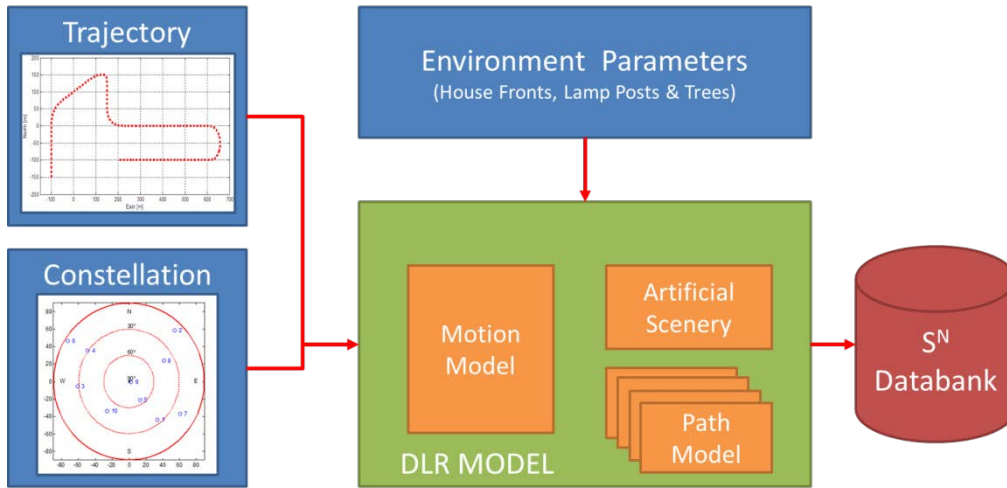


Figure 43: Illustration on the integration of the DLR model in our simulator.

The data file which is provided according to the DLR model is used to evaluate the performance of the algorithms that have been developed in the frame of this study. This is very important for this project because of the following reason.

1. The true ECEF position is known thanks to the generated synthetic trajectory (Figure 33) to allow the measurement produced by the tracking simulation to be evaluated precisely.
2. The behaviour of the tracking loop can be further understood as DLR model is claiming to provide close to real-life scenarios in the selected scenarios.
3. The resulted reaction of the tracking loop is a good indicator to further improve the adaptive vector tracking loop algorithm introduced in our work [27], [28] and [29].

3.3.5 Simulation Environment of the DLR Channel

As mentioned earlier, the performance of our algorithms will be assessed by using a simple model based on a few specular paths, and the more realistic DLR channel model. When the DLR model is used, the data file generated from the model is used as the input for the in-house simulator to evaluate our receiver performance. While the DLR model is able to generate more than 50 paths (including paths with very small power attenuation), only the 15 strongest (and closest) MP are considered for evaluation. Besides that, the generated data available are limited to the following scenarios: (i) Car moving in urban environment and (ii) Car moving in sub-urban environment. Moreover, the parameters and setups for urban and sub-urban environments are set by using the default values suggested by DLR model in their demo files.

To characterize the propagation channel we represent the power spectrum density (PSD) of the correlator output of the receiver when it is tracking the LOS signal. According to the expression of this output is:

$$I(k) + jQ(k) \approx A_{0,k} + \sum_{l=1}^{N-1} A_{l,k} R(\delta\tau_{l,k}) \frac{\sin(\pi\delta f_{l,k} T_C(k))}{\sin(\pi\delta f_{l,k} T_s)} \exp(j\delta\varphi_{l,k}) + n_c[k] \quad (3.42)$$

where $A_{0,k}$ is the LOS amplitude, $A_{l,k}$, $f_{l,k}$, $\varphi_{l,k}$ represent the k^{th} path amplitude, frequency and phase shift, $\delta\tau_{l,k}$ represent the k^{th} path delay, related to the LOS delay.

The PSD is obtained from a set of 1024 samples while the correlation time is 1msec. This PSD is represented by considering car which moves in both urban (Figure 44) and in sub-urban environment is given in (Figure 45).

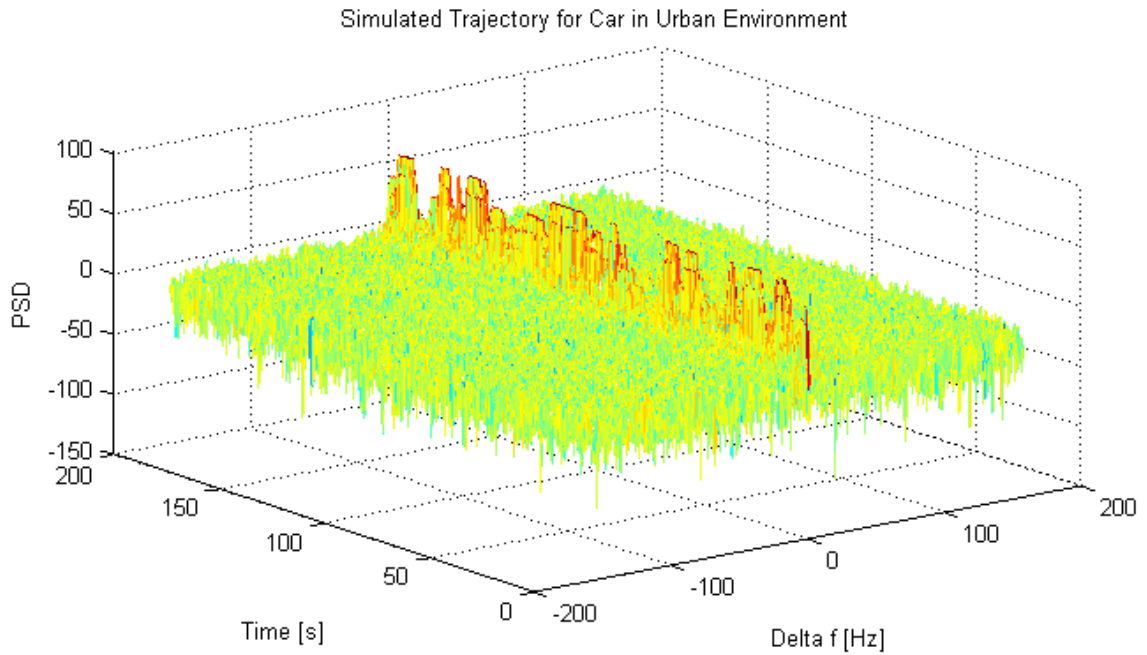


Figure 44: PSD of the DLR channel for urban environment.

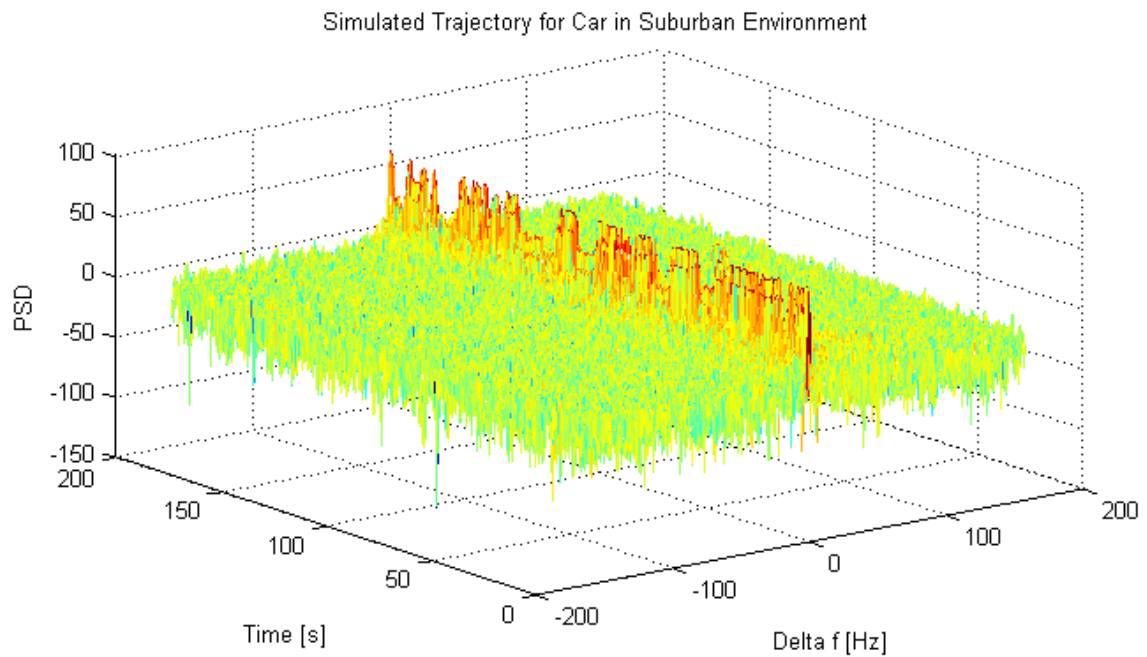


Figure 45: PSD of the DLR channel for suburban environment.

A top view of the PSD is also illustrated in Figure 46. The simulations for both cases are compared. It is observed that masking effect happens more frequently and longer in the urban environment compares to the suburban scenario. This is expected as the urban environments have more obstacles to block the incoming signals. Besides that, the receiver is assumed mostly parallel to the buildings as the urban is a more constricted environment that results in less dispersion in frequency. On the contrary, the MP occurs in wider range of frequencies in suburban environment, as this less constricted than in urban environment. In that case the receiver can be assumed to move in directions that are not necessarily parallel with the buildings and obstacles.

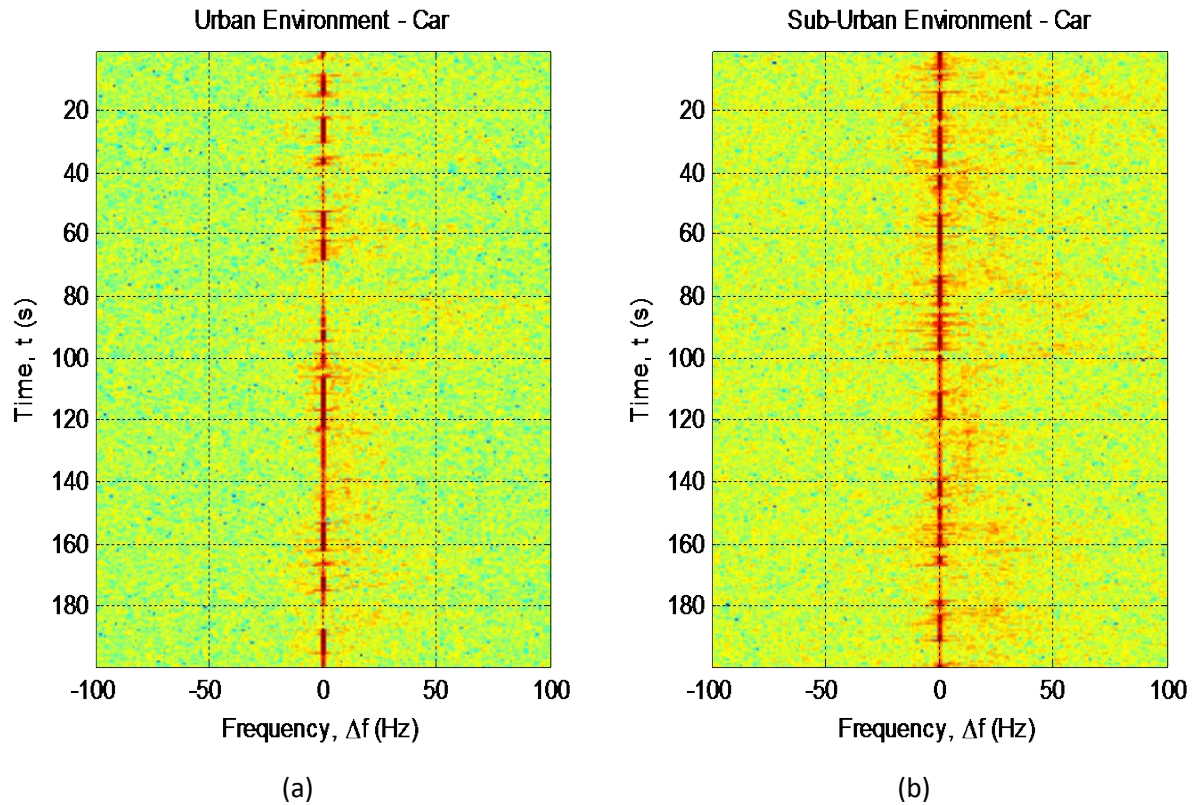


Figure 46: Top-view of the PSD using the DLR model.

Now consider looking the distribution of the MP in terms of the delays. The snapshot of the MP delay for the urban environment for 1s simulation is given in Figure 47. This figure shows that the MP delay is spread over a range from 0 to 450 meters (1.5 chips). But most of the delays are very short. The complete distribution of the MP delay for the whole simulation is plotted in Figure 48 for urban scenario and in Figure 49 for the suburban scenario. Comparing both distributions, the short delay MP occurs twice more in urban scenarios than in suburban scenarios. Based on Figure 48, nearly 50% of the MP is less than 0.05 chips. One can conclude that in urban scenario, as the building is assumed to be much closer to the road, shorter MP are generated. But, both urban and suburban environment suffers from the short delay MP which remains as a major error contributor as they are hard to detect.

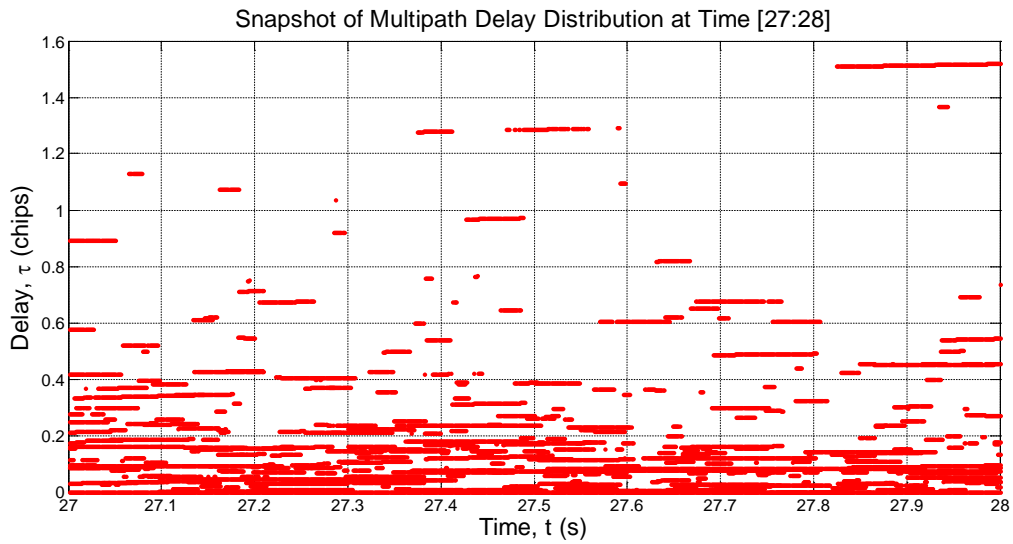


Figure 47: Snapshot of the MP delay during simulation.

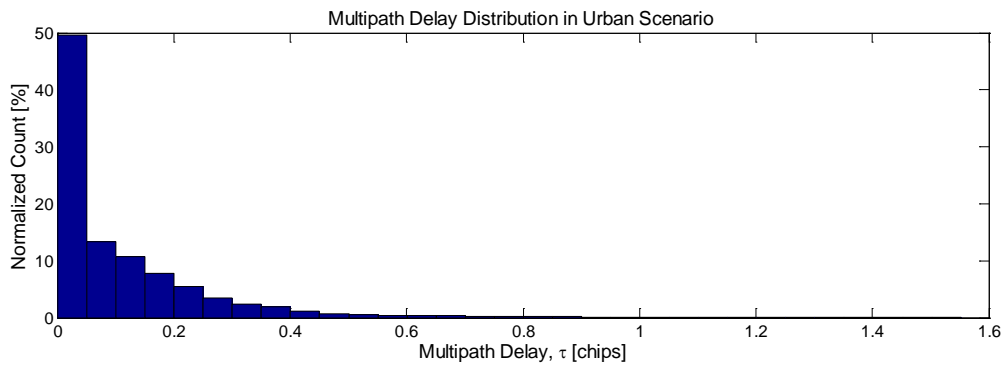


Figure 48: MP delay distribution for the whole simulation for urban scenario.

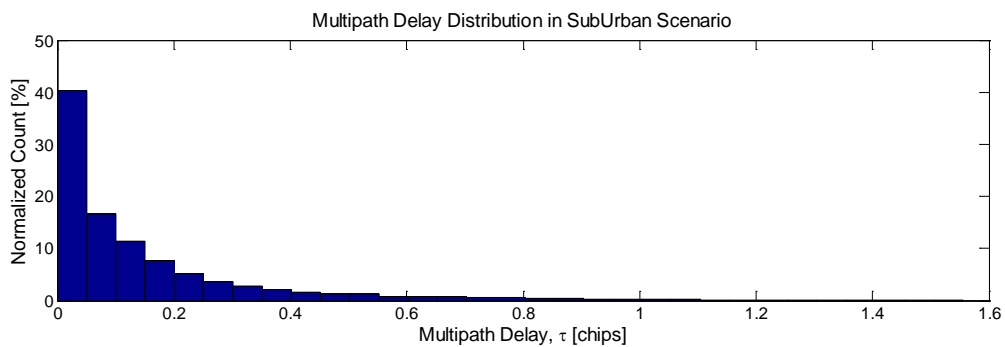


Figure 49: MP delay distribution for the whole simulation for suburban scenario.

3.4 Summary

This chapter focuses on the GNSS incoming signal in degraded environment such as urban environment. In this kind of environment the signal representation is strongly affected by the presence of MP. This kind of interference impacts the tracking loop behaviour resulting in bias in propagation delay and Doppler frequency estimation. Improvement of tracking loops has to be made. For assessing new algorithms two Land-mobile satellite channels have been described. First we propose an In-house simulator which allows MP number, parameters, occurrences and disappearances to be easily controlled by the user. Then a more realistic channel simulator was presented. These two channel models have been used during this study for characterizing different tracking loop architecture, and different MP mitigation algorithms.

CHAPTER

4

CHAPTER 4 – Signal tracking in GNSS Receivers

This chapter discusses different architectures used for tracking the incoming signals in a GNSS receiver to provide the position, velocity and time (PVT) solution. First, it addresses the traditional receiver which is based on a scalar tracking loop (STL) implementation. Then, a vectorial architecture known as vector tracking loop (VTL) is analysed considering diverse implementations. Emphasizes are given on the structure and the formulation of the state models that are proposed for the various tracking loop architectures. In this context classical receivers based on delay-locked loop (DLL), phase-locked loop (PLL) or/and frequency-locked loop (FLL) are implemented, resulting in a two-step Bayesian approach for estimating the navigation solution. These studies in tracking architectures motivates a lot of effort to further improve the signal tracking algorithms for better accuracy, availability and integrity of the received signals. These improvements are very crucial especially in the case of harsh environments.

4.1 GNSS receiver architecture

In general, the receiver architectures are tailored to different GNSS systems and applications. However, the basic building blocks of a generic GNSS receiver can be simplified as shown in Figure 50. As illustrated, the receiver can be regarded as four processing steps:

1. **Antenna** – the GNSS signals are captured by the L-band antenna, along with noise and possible interference depending on the dynamics of the receiver and its environment.
2. **Front-end** – the task is to provide a digital representation of the received signal via frequency down conversion, filtering, signal amplifying and digitizing. This module includes a low-noise amplifier (LNA), mixers, local oscillators (LO), analog-to-digital (ADC) and automatic gain control (AGC) to perform these operations. It results in a sampled, quantized and encoded signal which is processed within customized integrated circuits.
3. **Baseband signal processing** – the main task is to acquire and track the different signals by performing several signal processing routines. The first element of this block is the matched filter which needs to elaborate the replica of the tracked signals. Other elements include correlators, discriminators, local estimators and numerical control oscillators (NCO). This stage provides observables such as pseudo-ranges (PR) and pseudo-range rates (also known as delta-ranges (DR)) to the navigation stage. Additional information, such as Carrier-to-Noise (C/N_0) ratio or lock indicators, can also be provided.
4. **Navigation** – the observables provided will be used to estimate the antenna's position and velocity. This process needs to align the receiver time to the satellite time which is the GPS time. In other words, this stage provides the GPS time and meaningful results to the users.

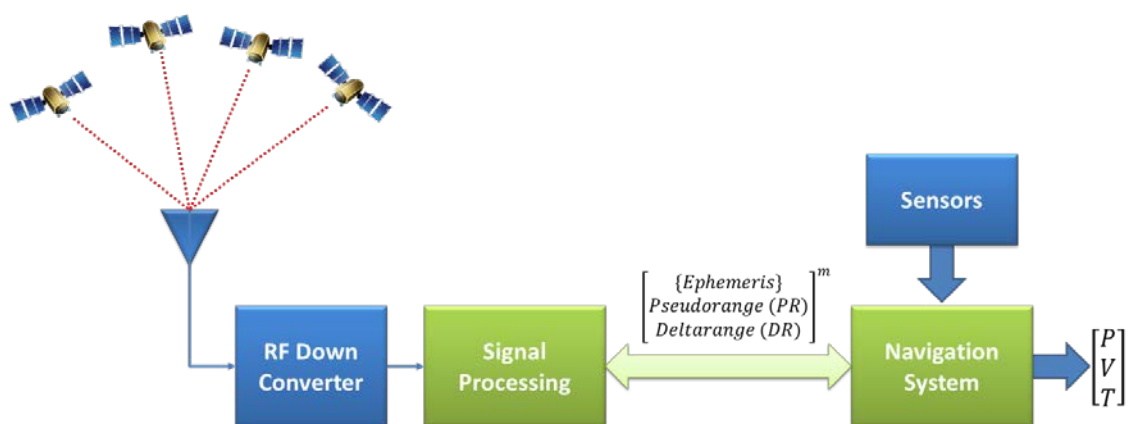


Figure 50: Illustration of generic GNSS receiver architecture.

In the framework of this study, only the two last stages are investigated. The “signal processing” stage consists of estimating the parameters of the incoming signal, what is commonly called “signal tracking”. The last stage benefits from signal parameters to estimate the user location. These two stages lead to a distributed architecture [30] and are often tightly coupled as the navigator can contribute to a better estimation of signal parameters by 1) providing a frequency aid which allows the local estimator bandwidths to be reduced and (more rarely) 2) by controlling the different NCOs in a VTL architecture. These two stages are detailed in Figure 51.

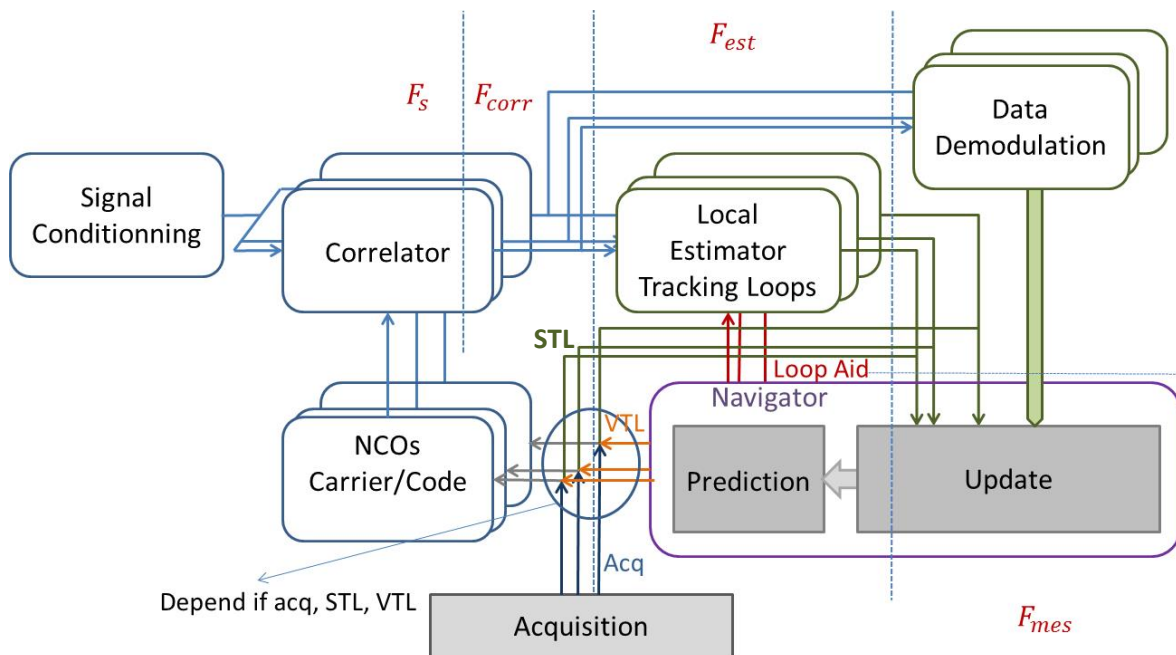


Figure 51: Block architecture of the signal processing and navigation modules.

Before extracting measurements by tracking satellite signals, the receiver first needs to know which satellites are in view. This process is called acquisition where several correlations between the incoming signal and multiple replicas of the possible expected signal are generated for different code delays and Doppler frequencies. This process will give an initial value of “good” code delay and Doppler frequencies for further tracking purposes. These good values are further improved in the tracking mode. This tracking loop will provide the pseudorange (PR) and Doppler frequency values that are used to provide the PVT solution of the receiver. The way the receiver improves and updates these values depends on the configuration of the architecture, generally using STL approach or a more sophisticated VTL approach.

Signal Acquisition

Acquisition is a coarse estimation and synchronization process which gives the estimates of the PRN code delay offset and the carrier Doppler frequency which is later used to initialize the tracking mode. The goals of the acquisition are 1) to detect the presence of useful signals and 2) to give a rough estimate of the main signal parameters. Signal acquisition is a two dimensional (2D) delay-frequency search which is performed for each satellite. It is based on a correlation principle to identify the satellites in view before extracting any measurement. It provides a coarse estimation of the propagation delay and of the Doppler frequency which are related to the satellite-user range and the velocity.

For signal search, different local replicas are generated that correspond to different combinations of code delay and Doppler frequency pairs. These replicas are correlated with the input signals. When the local replicas and the incoming signal are aligned, their correlation generates a peak as illustrated in Figure 52 (a). The code delay and Doppler frequency pair corresponding to this peak is considered as the good estimate to start the tracking process, if this pair has an amplitude above a certain threshold. In fact, the threshold for handing over to tracking mode is calculated based on the probability of false alarm (PFA) and determine the probability of detection (PD) of the incoming signal. If the signal is lower than this threshold, the satellite is assume to be absent as illustrated in Figure 52 (b).

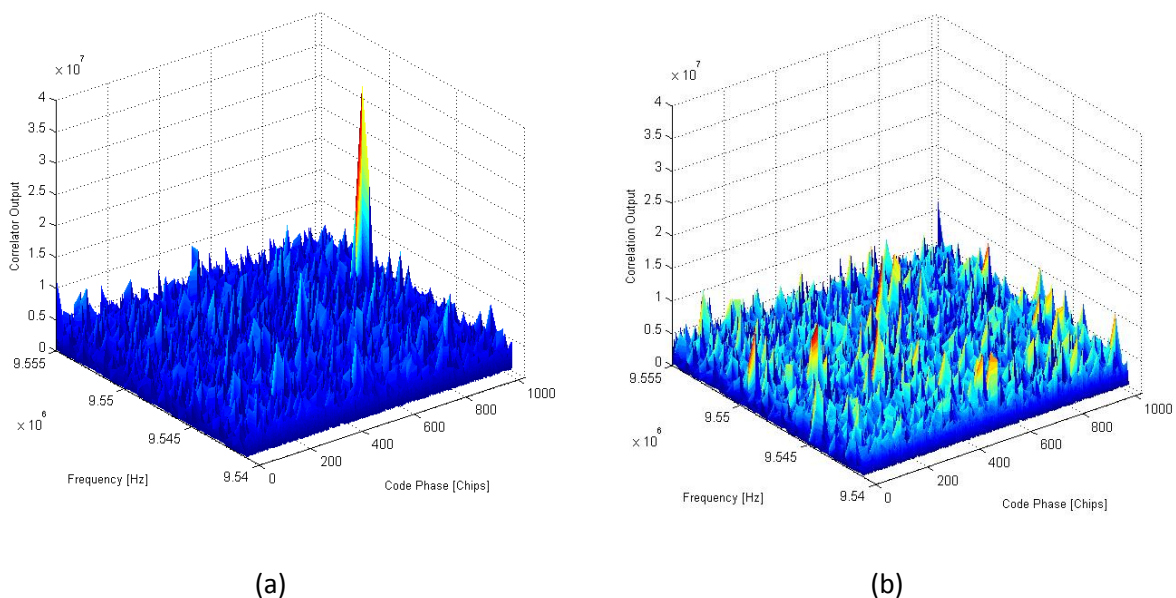


Figure 52: Illustration of signal acquisition in (a) strong signal presence and (b) signal absence.

4.2 Navigation Solution (NS)

Fundamentally, the navigation solution (NS) is an estimate of the user position and other required parameters where the term 'state' is used to describe all the parameters to be determined [31]. Generally, the NS will estimate the position, velocity and time (PVT) based on the measurements of the PRs and Doppler frequencies provided by the tracking loops. The NS is typically an implementation of an iterative least mean squares (LMS) algorithm or of a Kalman filter (KF). Today, there are many applications for which the GPS receiver is integrated with one or more sensors such as an inertial navigation system (INS) which will expand the 'state' to include the specific sensors error states. But in this thesis, it is restricted to a stand-alone GPS navigation estimation approach.

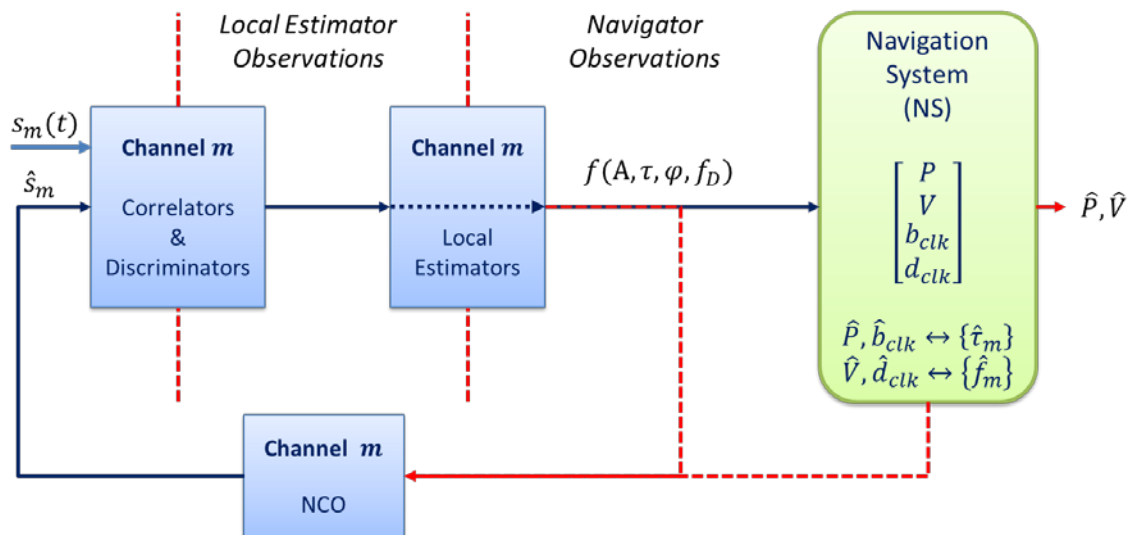


Figure 53: NS Observations

In Figure 53, the navigator observations are based on the inputs from the tracking loop which is a function of the signal power (amplitude), delay (τ), instantaneous phase (φ) and also the signal Doppler frequency (f_D). These parameters can be translated into more meaningful GPS measurements. The exact algorithm and implementations for the NS differ depending on the application. However, in each case, the most basic measurements are the same and include user-to-satellite LOS propagation delay and Doppler frequency. In most receivers a DLL is generally used for estimating the propagation delay and a PLL, which can be combined with an FLL, is used to estimate the carrier Doppler. Moreover, in order to calculate the PVT of the user, information describing the satellite position, velocity and error models (to correct the satellite clock offset and atmospheric

delay) are required. These parameters are contained in the navigation data message transmitted by the satellite to the receiver.

4.2.1 Least Mean Square (LMS) PVT Estimation

Each channel inside the receiver will provide some estimates which will be used to estimate the user's PVT. Consider the received signal model from equation (2.4):

$$s(t) = A.D(t - \tau(t))C(t - \tau(t)) \exp(j[2\pi(f_{IF})t + \varphi(t)]) + n(t). \quad (4.1)$$

The received signal includes relevant parameters for navigation. By using the concept of trilateration illustrated in Figure 54, the GPS receiver determines its position by measuring the time delays τ , from at least 4 different visible satellites. The phase can also be used for smoothing delay measurements in order to improve the positioning accuracy. Besides that, the Doppler frequency f_D which is related to the derivative of the phase can be used to determine the velocity. This fundamental concept of PVT estimation will be used throughout this work.

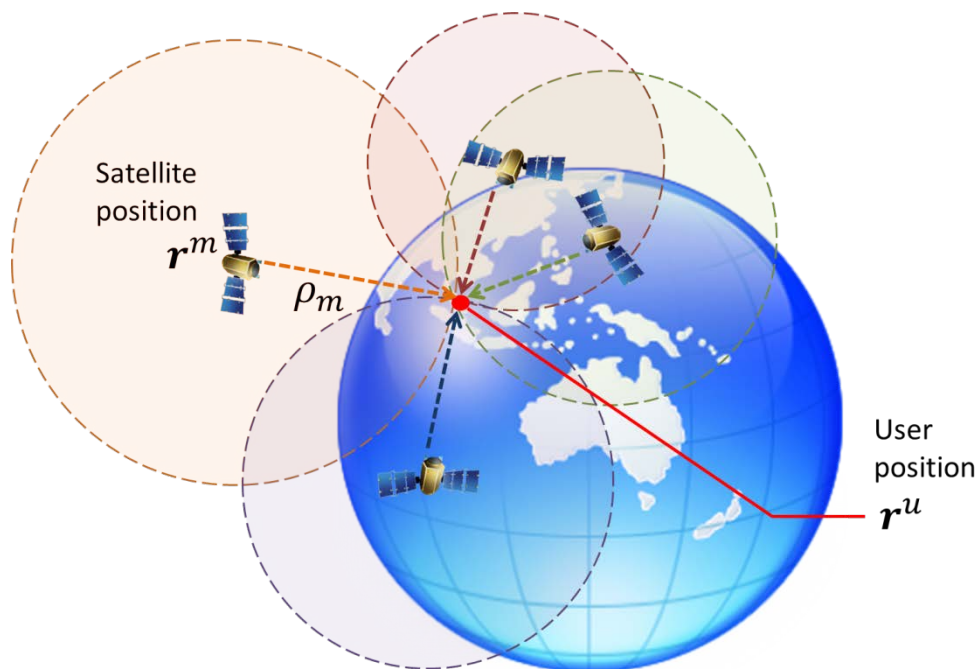


Figure 54: GPS trilateration concept.

a) Position Estimation

Since the satellites transmit their signals synchronously at different distances from the user, the signals arrive at the receiver with different time delays. The propagation delay τ can be represented as the difference between the transmit time (t_{tx}) of the satellite and the received time (t_{rx}) at the receiver. This delay can be related to the satellite-receiver distance. The PR observable is merely a time interval scaled by the speed of light:

$$\rho = c \cdot \tau = c(t_{rx} - t_{tx}). \quad (4.1)$$

Therefore, the raw PR observation of satellite index- m is related to the position of the user u by taking into account various transmission delays and can be written:

$$\rho_m^{raw} = \|\mathbf{r}^m - \mathbf{r}^u\| + c \cdot \delta t_u + \epsilon_{\rho_m} \quad (4.2)$$

with

$$\mathbf{r}^m = \begin{bmatrix} x \\ y \\ z \end{bmatrix}^m \text{ and } \mathbf{r}^u = \begin{bmatrix} x \\ y \\ z \end{bmatrix}^u$$

where

$$\|\mathbf{r}^m - \mathbf{r}^u\| = \sqrt{(x_m - x_u)^2 + (y_m - y_u)^2 + (z_m - z_u)^2} = d_m \quad (4.3)$$

and

$$\epsilon_{\rho_m} = c(\delta t_{iono} + \delta t_{tropo} + \delta t_m) + n. \quad (4.4)$$

In this representation, \mathbf{r}^m is the location of the satellite # m , whereas \mathbf{r}^u is the user location and δt_u is the user clock bias with respect to satellite # m . The term d_m is used to define the geometrical distance between the satellite and the user. In this work, the term ϵ_{ρ_m} which represents different error sources (ionospheric delay (δt_{iono}), tropospheric delay (δt_{tropo}), satellite clock and various error (δt_m) and thermal noise (n)) is ignored. The term ‘‘pseudo’’ in PR is used to indicate the measured range taking into account the range error due to the clock synchronization between the satellite and the user. Once the propagation delay and the various satellite errors have been corrected, the PR can be written as:

$$\rho_m = \|\mathbf{r}^m - \mathbf{r}^u\| + c \cdot \delta t_u + n_{\rho_m} \quad (4.5)$$

where n_{ρ_m} is contains as the thermal noise contribution and the residual errors which remaining after correction.

By having at least four visible satellites, the receiver can determine the position and clock bias using the PR measurements. This is typically being implemented by using the iterative least squares method or Kalman filtering [12]. For both methods, the PR equations are linearized around the initial known receiver position. This initial PR measured from the m -th satellite can be expressed as:

$$\rho_m = f(x_u, y_u, z_u, t_u) + n_{\rho_m} \quad (4.6)$$

with

$$\begin{aligned} x_u &= \hat{x}_u + \Delta x_u \\ y_u &= \hat{y}_u + \Delta y_u \\ z_u &= \hat{z}_u + \Delta z_u \\ c\delta t_u &= c\delta \hat{t}_u + \Delta c\delta t_u \end{aligned}$$

where the true user position and clock bias are expressed as the estimates plus corrections. Based on these relations, the function $f(\dots)$ can be rewritten as a function of the nominal trajectory and the error terms and can therefore be expressed as:

$$f(x_u, y_u, z_u, b_{clk}) = f(\hat{x}_u + \Delta x_u, \hat{y}_u + \Delta y_u, \hat{z}_u + \Delta z_u, c\delta \hat{t}_u + \Delta c\delta t_u) + n_{\rho_m}. \quad (4.7)$$

As the ranges to the satellites are very large with respect to the user position error, the PR equation can be linearized by expanding the equation using a first-order Taylor approximation. Therefore, the function which determines the approximate position can be expressed as a linear system detailed below:

$$\Delta \rho_m = \hat{\rho}_m - \rho_m \approx \frac{x_m - \hat{x}_u}{d_m} \Delta x_u + \frac{y_m - \hat{y}_u}{d_m} \Delta y_u + \frac{z_m - \hat{z}_u}{d_m} \Delta z_u + \Delta c\delta t_u$$

Equivalently

$$\Delta \rho_m \approx LOS_{x,m} \Delta x_u - LOS_{y,m} \Delta y_u - LOS_{z,m} \Delta z_u + \Delta c\delta t_u$$

$$\Delta \rho_m \approx LOS_m^T [\Delta x_u \quad \Delta y_u \quad \Delta z_u] + b_{clk} \quad (4.8)$$

where

$$\hat{\rho}_m = \sqrt{(\hat{x}_m - x_u)^2 + (\hat{y}_m - y_u)^2 + (\hat{z}_m - z_u)^2} + \Delta c \delta t_u \quad (4.9)$$

and

$$LOS_m = \frac{\mathbf{r}^m - \hat{\mathbf{r}}^u}{d_m}. \quad (4.10)$$

The term LOS_m can be seen as the unit line-of-sight (LOS) vector from the user to the satellite and b_{clk} is the clock bias due to the synchronization between the satellite and the user.

In absence of noise, the linearized PR equations can be written in concise matrix form as shown below:

$$\begin{bmatrix} \Delta \rho_1 \\ \Delta \rho_2 \\ \vdots \\ \Delta \rho_m \end{bmatrix} = \begin{bmatrix} LOS_{x,1} & LOS_{y,1} & LOS_{z,1} & 1 \\ LOS_{x,2} & LOS_{y,2} & LOS_{z,2} & 1 \\ \vdots & \vdots & \vdots & \vdots \\ LOS_{x,m} & LOS_{y,m} & LOS_{z,m} & 1 \end{bmatrix} \begin{bmatrix} \Delta x_u \\ \Delta y_u \\ \Delta z_u \\ b_{clk} \end{bmatrix} \quad (4.11)$$

with

$$\Delta \rho_m = H \cdot \Delta u.$$

Based from this relationship, the vector of corrections Δu can be calculated easily. When there are four PR measurements, this system of equations can be solved by inverting the matrix H :

$$\Delta u = H^{-1} \cdot \Delta \rho_m. \quad (4.12)$$

However, when the system is overdetermined with more than four PR measurements available, Δu can be calculated by using the Moore-Penrose pseudo inverse as shown below:

$$\Delta u = (H^T H)^{-1} H^T \Delta \rho. \quad (4.13)$$

The vector of corrections is then added to the estimated vector $(\hat{x}_u, \hat{y}_u, \hat{z}_u, \delta \hat{t}_u)$ to get the next refined estimates of the user position and clock bias.

b) Velocity Estimation

The velocity estimation can be conducted similarly to the position estimation by taking advantage of the PR rate. As mentioned earlier, the Doppler frequencies of the received signals can

be used to determine the receiver velocity. The use of the Doppler frequencies are commonly known as the delta-range rate (DR) measurements because they are functions of the user velocity relative to the satellite and of the clock drift of the receiver oscillator. The observed frequency shift is due to the Doppler shift produced by the satellite and user motion, as well as the frequency error drift of the satellite and user clocks. This frequency Doppler shift is the projection of the relative satellite-user velocity onto the LOS, scaled by the transmitted frequency $L_1 (\approx 1575.42 \text{ MHz})$ and is given by [31]:

$$f_D = - \left[LOS_m^T \cdot \frac{(\mathbf{v}^m - \mathbf{v}^u)}{c} \right] f_{L1}. \quad (4.14)$$

The term \mathbf{v}^m and \mathbf{v}^u are the satellite and user velocity vectors whereas LOS_m is the LOS unit vector from the user to the satellite # m . At the same time, the satellite velocity is calculated from the ephemeris data of the navigation message. The Doppler can be converted into a DR observation given by expanding equation (4.12):

$$\dot{\rho}_m = LOS_m^T \cdot (\mathbf{v}^m - \mathbf{v}^u) + d_{clk} + n_{\dot{\rho}_m} \quad (4.15)$$

with

$$\mathbf{v}^m = \begin{bmatrix} \dot{x} \\ \dot{y} \\ \dot{z} \end{bmatrix}^m \text{ and } \mathbf{v}^u = \begin{bmatrix} \dot{x} \\ \dot{y} \\ \dot{z} \end{bmatrix}^u$$

where d_{clk} is the user's clock drift and $\mathbf{v}^m, \mathbf{v}^u$ are the individual unit velocity vector of satellite # m and user u . Similarly to position estimation, the error in the observation $n_{\dot{\rho}_m}$ is ignored. In practice, this $n_{\dot{\rho}_m}$ is used to weight the quality of the signal for example in the EKF or weighted LMS approaches. Therefore, the predicted DR based upon the current estimates of the user velocity $\hat{\mathbf{v}}^u$ is given by:

$$\hat{\rho}_m = LOS_m^T \cdot (\mathbf{v}^m - \hat{\mathbf{v}}^u) + d_{clk} \quad (4.16)$$

Therefore,

$$\Delta \dot{\rho} = \hat{\rho}_m - \dot{\rho}_m = LOS_{x,m} \Delta v_x^u - LOS_{y,m} \Delta v_y^u - LOS_{z,m} \Delta v_z^u + d_{clk} \quad (4.17)$$

where the equations resulting from different satellites can be arranged into a set of linear equations given by:

$$\begin{bmatrix} \Delta\dot{\rho}_1 \\ \Delta\dot{\rho}_2 \\ \vdots \\ \Delta\dot{\rho}_m \end{bmatrix} = \begin{bmatrix} LOS_{x,1} & LOS_{y,1} & LOS_{z,1} & 1 \\ LOS_{x,2} & LOS_{y,2} & LOS_{z,1} & 1 \\ \vdots & \vdots & \vdots & \vdots \\ LOS_{x,m} & LOS_{y,m} & LOS_{z,m} & 1 \end{bmatrix} \begin{bmatrix} \Delta\dot{x} \\ \Delta\dot{y} \\ \Delta\dot{z} \\ d_{clk} \end{bmatrix} \quad (4.18)$$

$$\Delta\dot{\rho}_m = H \cdot \Delta v^u.$$

Therefore, the receiver is able to calculate the correction vector for the user velocity and the clock drift by using the same method as the one used for the position calculation.

The estimation techniques describe above allows the position and the velocity of the receiver to be estimated.. Besides that, this method also shows that the propagation delay and the Doppler frequency can be related to the user location and velocity respectively. The propagation delay and the Doppler frequency provide relevant information about the position and velocity when the number of satellites is higher than three. We'll see later that this information can also be used, even if the number of satellites is lower than 4, when a dynamic model is exploited. Moreover, from the equations (4.10) and (4.16) used for position and velocity estimation, the LOS unit vectors are intimately related to the estimation of the position, velocity and states of the clock (clock bias and clock drift). This relationship will be fully exploited in the vector tracking algorithm.

In this section we have recalled the use of the LMS algorithm which exploits the orthogonality properties of the pseudo inverse to minimize the quadratic error which represents the difference between the estimated solution and the true solution. This approach showed the interest of using PR and DR measurements for estimating the user location and velocity. Using this algorithm, the error is directly related to the power of the measurement error and to the geometry matrix.

4.2.2 Extended Kalman Filter (EKF)

As indicated above, the NS filter can be implemented by using an extended Kalman filter (EKF) to provide the solution for the user PVT. This method provides a recursive solution to the linear optimal filtering problem that can be applied to both stationary and non-stationary environments. It can incorporate the knowledge of the previous measurements into current estimation and is computationally efficient. Besides that, it needs the user clock and dynamics to be modelled in this algorithm which makes it perfect for GPS applications.

In practice, the dynamic of the vehicle is often taken into account for filtering measurement error by implementing an EKF technique. In that case a system model has to be defined. In a standalone configuration, the acceleration of the vehicle is used to define the system noise covariance matrix depending on the dynamic of the user. This system noise can be reduced in an INS/GNSS integrated system, as much as the quality of inertial sensors is good.

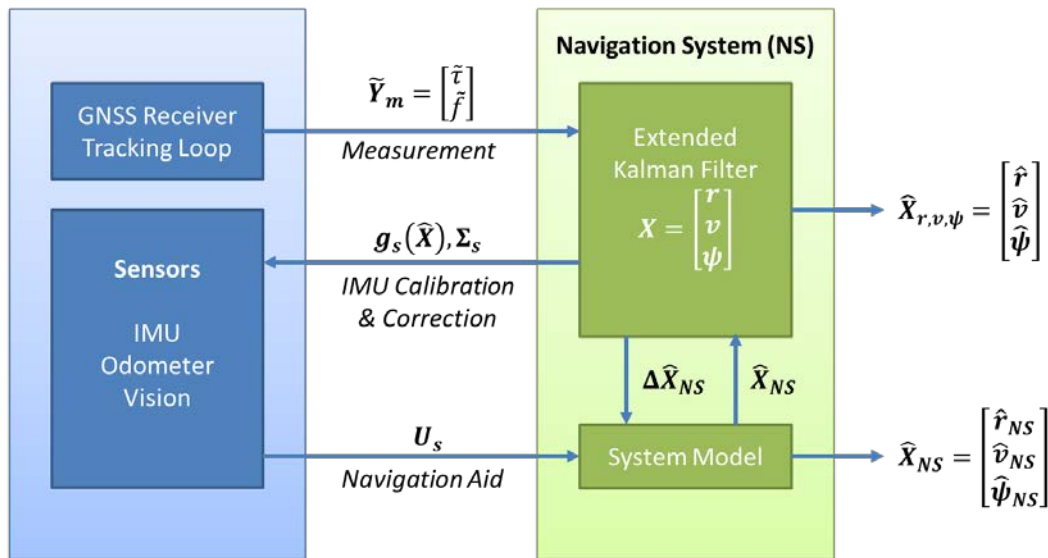


Figure 55: EKF Approach in a Navigation System.

Consider the diagram in Figure 55, where the EKF is used to incorporate the knowledge of the current measurement into current estimates (which results in better estimation). We propose to use the propagation delay and the Doppler frequency as the observation model given by:

$$Y = \begin{bmatrix} \tau \\ f \end{bmatrix}. \quad (4.19)$$

Here, only GNSS measurements are considered whereas the proposed system model is defined in what follows.

a) System Model

The system model required for the EKF algorithm describes how the state vector can be estimated and also how the error covariance propagates with time. Therefore it is crucial to define

the state model carefully which includes in this case, the position, \mathbf{r} and velocity, \mathbf{v} in the ENU frame and the clock states, ψ that as represented below:

$$\begin{aligned}\mathbf{r} &= [r_E \quad r_N \quad r_U]^T \\ \mathbf{v} &= [v_E \quad v_N \quad v_U]^T \\ \psi &= [b_{clk} \quad d_{clk}]^T\end{aligned}\tag{4.20}$$

where b_{clk} and d_{clk} are the user clock bias and drift respectively. We define the NS state vector in the ENU frame as follows:

$$X^{NS} = [r_E \quad v_E \quad r_N \quad v_N \quad r_U \quad v_U \quad b_{clk} \quad d_{clk}]^T\tag{4.21}$$

where the NS state transition matrix is given by:

$$\Phi^{NS} = \begin{bmatrix} A & 0 & 0 & 0 \\ 0 & A & 0 & 0 \\ 0 & 0 & A & 0 \\ 0 & 0 & 0 & A \end{bmatrix}\tag{4.22}$$

and where

$$A = \begin{bmatrix} 1 & T_{NS} \\ 0 & 1 \end{bmatrix}\tag{4.23}$$

T_{NS} being the NS filter update rate. The state transition matrix defines how the state vector changes with time as a function of the system dynamics. Finally, the following state equation will be considered in this chapter

$$\hat{X}_{k+1}^{NS} = \Phi^{NS} \hat{X}_k^{NS} + w_k\tag{4.24}$$

where \hat{X} is the estimated state vector, Φ^{NS} is the state transition matrix and w_k is the system noise vector. Note that this system noise vector w_k depends on the vehicle dynamic and on the receiver clock noise representation.

The covariance matrix Q is the system noise covariance matrix which defines how the uncertainties of the state estimates increase with time due to noise source in the system [32]. In our work, the NS process noise covariance matrix, Q^{NS} is given by:

$$E\{ww^T\} = Q^{NS} = \begin{bmatrix} Q_{dyn} & 0 \\ 0 & Q_{clk} \end{bmatrix} \quad (4.25)$$

with

$$Q_{dyn} = \begin{bmatrix} Q_A & 0 & 0 \\ 0 & Q_A & 0 \\ 0 & 0 & Q_A \end{bmatrix}$$

where

$$Q_A = \begin{bmatrix} \sigma_a^2 \cdot \frac{T_{NS}^4}{4} & \sigma_a^2 \cdot \frac{T_{NS}^3}{2} \\ \sigma_a^2 \cdot \frac{T_{NS}^3}{2} & \sigma_a^2 \cdot T_{NS}^2 \end{bmatrix} \quad (4.26)$$

and

$$Q_{clk} = \begin{bmatrix} \sigma_b^2 \cdot T_{NS}^2 + \sigma_d^2 \frac{T_{NS}^4}{4} & \sigma_d^2 \cdot \frac{T_{NS}^3}{2} \\ \sigma_d^2 \cdot \frac{T_{NS}^3}{2} & \sigma_d^2 \cdot T_{NS}^2 \end{bmatrix}. \quad (4.27)$$

b) Measurement Model

For implementing an EKF algorithm, a measurement model has to be defined. The measurement model is used to link the state vector with a set of measurements. First, we define the measurement vector Y based on the observation provided to the NS. In this case, the measurement vector Y is given by:

$$\hat{Y}_k^{NS} = \begin{bmatrix} \hat{t}^1 \\ \hat{f}^1 \\ \vdots \\ \hat{t}^m \\ \hat{f}^m \\ \vdots \\ \hat{t}^{N_{sat}} \\ \hat{f}^{N_{sat}} \end{bmatrix} \quad \text{with } 1 \leq m \leq N_{sat} \quad (4.28)$$

where the elements in Y are the observation provided by the satellites, m is the channel index of the receiver and N_{sat} visible satellites. Therefore, the associated measurement equation is given by:

$$\hat{Y}_k^{NS} = H_k \hat{X}_k + v_k. \quad (4.29)$$

In this relationship, matrix H is the measurement matrix given by:

$$H_k^{NS} = \begin{bmatrix} \frac{LOS_x^1}{\lambda_C} & 0 & \frac{LOS_y^1}{\lambda_C} & 0 & \frac{LOS_z^1}{\lambda_C} & 0 & \frac{1}{\lambda_C} & 0 \\ 0 & \frac{LOS_x^1}{\lambda_{f_{L1}}} & 0 & \frac{LOS_y^1}{\lambda_{f_{L1}}} & 0 & \frac{LOS_z^1}{\lambda_{f_{L1}}} & 0 & \frac{1}{\lambda_{f_{L1}}} \\ \vdots & \vdots \\ \frac{LOS_x^m}{\lambda_C} & 0 & \frac{LOS_y^m}{\lambda_C} & 0 & \frac{LOS_z^m}{\lambda_C} & 0 & \frac{1}{\lambda_C} & 0 \\ 0 & \frac{LOS_x^m}{\lambda_{f_{L1}}} & 0 & \frac{LOS_y^m}{\lambda_{f_{L1}}} & 0 & \frac{LOS_z^m}{\lambda_{f_{L1}}} & 0 & \frac{1}{\lambda_{f_{L1}}} \\ \vdots & \vdots \\ \frac{LOS_x^{N_{sat}}}{\lambda_C} & 0 & \frac{LOS_y^{N_{sat}}}{\lambda_C} & 0 & \frac{LOS_z^{N_{sat}}}{\lambda_C} & 0 & \frac{1}{\lambda_C} & 0 \\ 0 & \frac{LOS_x^{N_{sat}}}{\lambda_{f_{L1}}} & 0 & \frac{LOS_y^{N_{sat}}}{\lambda_{f_{L1}}} & 0 & \frac{LOS_z^{N_{sat}}}{\lambda_{f_{L1}}} & 0 & \frac{1}{\lambda_{f_{L1}}} \end{bmatrix} \quad (4.30)$$

where

$$\lambda_C = \frac{c}{R_C} \quad \text{and} \quad \lambda_{f_{L1}} = \frac{c}{f_{L1}}.$$

The measurement model is associated with a certain measurement noise covariance matrix R^{NS} , which is defined from the variances of each measurement provided to the NS:

$$E[vv^T] = R_{Y_k}^{NS} = \text{diag} \left(\sigma_{\tilde{r}_1}^2, \sigma_{\tilde{f}_1}^2, \dots, \sigma_{\tilde{r}_m}^2, \sigma_{\tilde{f}_m}^2, \dots, \sigma_{\tilde{r}_{N_{sat}}}^2, \sigma_{\tilde{f}_{N_{sat}}}^2 \right)_k. \quad (4.31)$$

Note that $R_{Y_k}^{NS}$ is a diagonal matrix because measurements coming from different channels are assumed to be independent and that the variances are different in the different channels since they depend on the performance of the individual tracking loop and C/N_0 .

4.3 Scalar Tracking Loop (STL) Configuration

The previous section showed the relevance of the propagation delay and of the Doppler frequency for estimating the user location and velocity. In a conventional receiver, a traditional scalar tracking loop (STL) is used for refining these parameters. It works by tracking the satellites in view independently. Therefore, each channel uses its own tracking loop to track a satellite signal by itself. Furthermore, the NS also works independently from the tracking loop, which means there is no interaction from the NS to the individual tracking loop channels. The raw GPS data is first

processed to provide measurement estimates thanks to the tracking loops. These estimates are then fed forward to the navigation processor. The PVT estimates of the navigation processor are then formed using the estimates of the tracking loops. A basic scalar-tracking architecture is shown in Figure 56.

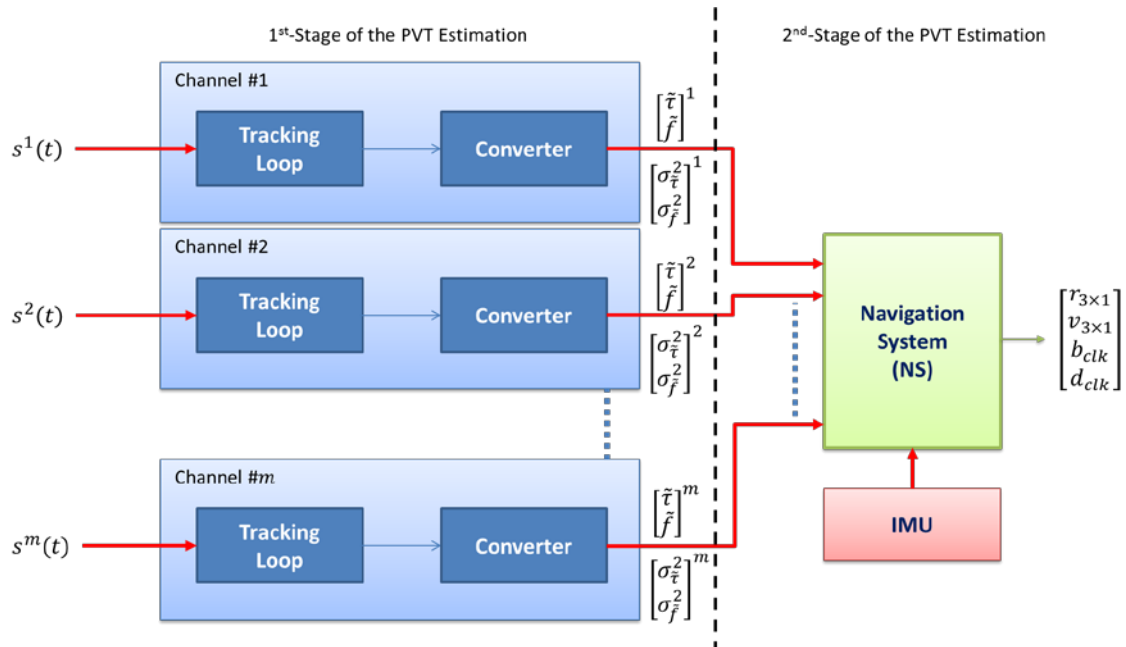


Figure 56: Scalar tracking loop receiver architecture.

From the illustration above, the flow of information is strictly in one direction that can be viewed as a two-stage approach. Tracking loops for each channel are used for estimating the propagation delay and Doppler frequency independently. The estimated propagation delay and Doppler frequency are fed forward to the navigation processor. The navigation processor uses the estimated propagation delay and Doppler frequency to estimate the receiver position, velocity, and clock states [33]. The user position, velocity, clock bias and drift are commonly referred to as user navigation states [34] as specified by equation (4.21). Therefore, one can assume that STL operates like an open loop system in providing the PVT solution. In an STL, we can separate the estimation process into 2 parts; (1) the estimation of the local replica of each channel (tracking loop) and (2) the estimation of the receiver's PVT by the NS.

4.3.1 Local Estimator

The goal of the local estimator is to estimate and replicate the incoming code phase and carrier frequency as being discussed in Chapter 2. The idea here is to illustrate how the estimation is being carried out for the STL architecture. Recall that in this project, the STL is designed by using a 1st-order DLL with carrier aiding for code-delay estimation and 1st-order FLL assisted 2nd-order PLL for carrier phase estimation. The update of the local estimator can also be represented in a Kalman filter (KF) form where the state vector X is:

$$X_k = [\tau \quad \varphi \quad f]_k^T \quad (4.32)$$

where τ is the code delay, φ is the carrier phase and f is the carrier frequency. The NCO update rule for each channel can be represented as:

$$\hat{X}_{k+1} = X_{k+1}^- + K \cdot \Delta Y_k \quad (4.33)$$

with

$$X_{k+1}^- = \Phi^{\text{LE}} \cdot X_k. \quad (4.34)$$

In this representation, the matrices Φ , K and ΔY are given by:

$$\Phi^{\text{LE}} = \begin{bmatrix} 1 & 0 & K_{\varphi\tau} T_{\text{int}} \\ 0 & 1 & T_{\text{int}} \\ 0 & 0 & 1 \end{bmatrix} \quad (4.35)$$

$$K = T_{\text{int}} \begin{bmatrix} \omega_{\text{DLL}} & 0 & 0 \\ 0 & \sqrt{2}\omega_{\text{PLL}} & 0 \\ 0 & \omega_{\text{PLL}}^2 & \omega_{\text{FLL}} \end{bmatrix} \quad (4.36)$$

$$\Delta Y_k^{m^{\text{Disc}}} = \begin{bmatrix} \Delta\tau \\ \Delta\varphi \\ \Delta f \end{bmatrix}_k^{m^{\text{Disc}}} = \begin{bmatrix} \overline{\tau_k - X_{k-1}(1)} \\ \overline{\varphi_k - X_{k-1}(2)} \\ \overline{f_k - X_{k-1}(3)} \end{bmatrix} \quad (4.37)$$

where $\overline{\tau_k - X_{k-1}(1)}$, $\overline{\varphi_k - X_{k-1}(2)}$ and $\overline{f_k - X_{k-1}(3)}$ represents the mean error over the integration time for the delay, the phase and the frequency of the loop respectively. From this relationship, the state transition matrix F is related to the NCO current states, as the NCOs are used to propagate the code delay and the carrier phase.

The filter gain K providing weight to measurements is time-invariant, and depends on the loop order and on the loop bandwidths. Indeed the ω term is the natural radian frequency for DLL, PLL and FLL respectively and is calculated based on the selected loop filter order and noise loop bandwidth B_n [1]. ΔY is based on the respective discriminator outputs, T_{int} is the integration time and $K_{\phi\tau} = R_c/f_{L1} = 1/1540$ is a scale factor related to the carrier aiding, R_c is the spreading code chip rate and f_{L1} is the carrier frequency. The parameter of the noise bandwidth, B_n for each DLL, PLL and FLL will determine the gain values of the matrix K of the filter. In practice, the NCO will try to match the frequency of the local replica to the frequency of the incoming signal for both PLL and DLL which is given by:

$$\begin{bmatrix} \hat{f}_{DLL} \\ \hat{f}_{PLL} \end{bmatrix}_{k+1}^+ = \begin{bmatrix} K_{\phi\tau} & K_{11} & 0 \\ 1 & 0 & K_{22} \end{bmatrix} \begin{bmatrix} X(3) \\ \Delta Y(1) \\ \Delta Y(2) \end{bmatrix}_{k+1}. \quad (4.38)$$

The resulted frequencies will be used to control the local oscillators that produce the replica signal to be matched with the incoming signal.

4.3.2 Parameters affecting STL Performance

The parameters that affect the performance of the STL based navigator are related to the quality of the system model, (i.e., to the dynamic model), and to the quality of the measurement model which depends on the STL performance. In a stand-alone GNSS navigator, the dynamic model depends on the application. On the contrary, the measurement model depends on the quality of the incoming signal, but also on tracking loop management. Note that these performance principles for the tracking loop have been discussed in detail in Chapter 2.

Here, these STL design parameters are being reiterated for discussion. First, the choice of the discriminator will determine the thermal noise variance and computational load of the tracking loop. Specifically for DLL, the selection Early-Late spacing and the choice of a coherent/non-coherent approach also affects the performance of the tracking loop. Secondly, the choice of the filter order and the noise bandwidth is crucial to the overall performance of the tracking loop. There are trade-off issues that need to be considered when considering the acceptable dynamic performances against the tolerable noise of the receiver. Finally, it is important to note that integration time of the

correlation process highly depends on the type of environment. For example, in the presence of weak signals, increasing the integration time improves the performance of the tracking loop but it is not true in the presence of strong signals.

Most of the parameters discussed above are based on the tracking loop components rather than on the implementation of the STL architecture. Granting that STL is relatively easy to be implemented and at the same time, having independent channels gives some level of robustness to the architecture. However, on the downside, the fact that the signals are inherently related via LOS vectors for the receiver position and velocity is completely ignored, which makes impossible for the channels to aid each other which can be advantageous. This means STL does not exploit the inherent coupling between the receiver dynamics and the dynamics seen by the tracking loops. Besides that, this architecture leads to a distributed estimator which requires to define properly the covariance matrices at the output of the first stage of the estimator.

In addition, the STL architecture does not work well when dealing with constraint environment when scintillation, interference, multipath or signal attenuation or outages occur [35]. Therefore, in this situation, channel contamination is very likely to impact the STL architecture. Indeed the STL architecture will use the contaminated measurement to provide the PVT estimation at the second stage as illustrated in Figure 56. There have been many efforts to provide an equivalent error model for the PR in harsh scenario especially when dealing with MP such as the works investigated in [36], [37] and [38]. In [36], the author considered the worst case of MP scenario, i.e., when there is no relative Doppler between the direct signal and the reflected signal which results in a bias on the PR estimation. In [37], the MP appearance and disappearance is supposed to yield mean value jumps in the measurement equation thus introducing biases whereas in [38], the PR distribution is unknown and modelled as a mixture of Gaussian distribution. Unfortunately, none of the models used in these studies are able to address the contamination issue affecting the NS.

4.4 Vector Tracking Loop (VTL) Architecture

The VTL architecture was previously studied in [34] where the conceptual idea of vector-based tracking was introduced. Later, many studies regarding vector tracking use [39] as a main reference for developing the vector-based architecture. The first vector based approach is called Vector Delay Locked Loop (VDLL) which was proposed in [39] to utilize the receiver position and

clock bias results to control the code NCO for each channel in parallel. Presently, variations of this approach are being explored because of the fact that a VTL provides a deep level of integration between signal tracking (of each channel) and NS. Here, the main principle of vector architecture is discussed and a study highlighting the advantages and disadvantages of such approach is conducted. In the context of this thesis which proposes a receiver based on a reconfigurable architecture, this study will be very useful to adapt efficiently this architecture to the receiver situation.

4.4.1 Principal of Vector Tracking Architecture

A VTL takes advantage of the fact that the user states estimated by the NS are determined from the propagation delay and the Doppler frequency of signals broadcast by a set of m satellites which is the main difference between the STL and VTL implementation. This means that the receiver position and velocity is being determined based on the code delay and the carrier Doppler frequency of the received signals. A VTL takes this concept and reverse it by using the receiver position and velocity to predict, for each satellite, the code delay and the Doppler frequency of the received signal. This information is used in the process which produces signal replicas for tracking the signals by using the following relations:

$$\hat{\tau}^m = \frac{1}{\lambda_c} [LOS_m^T \cdot (\hat{\mathbf{r}}^u - \mathbf{r}^m) + b_{clk}] \quad (4.39)$$

$$\hat{f}^m = \frac{1}{\lambda_{L1}} [LOS_m^T \cdot (\hat{\mathbf{v}}^u - \mathbf{v}^m) + d_{clk}]. \quad (4.40)$$

The estimated delay and Doppler frequency provided by the NS will then be used to command the NCO in each channel for generating the replicas.

Residuals are formed in each channel by taking the difference between the predicted and received signals. These residuals are then used to update the estimates of the receiver position and velocity. In other words, in a vector architecture, the PVT estimation provided by the NS is used to drive the NCO of each channel to track and lock the incoming signal. Therefore, the channels are no longer tracked on a satellite-by-satellite basis. Since the NCO are controlled by the NS, aiding between channels are now possible. Moreover in the context of multi-sensor navigation system,

each tracking channel takes advantages of the available measurements, allowing for example poor GNSS signals to be tracked.

Many studies have concluded that VTL outperforms STL for tracking signals at the receiver. The most notable advantage of the VTL is the increased interference immunity including jamming, robust dynamic performance, the ability to operate at low signal power or weak signals and to bridge short-time signal outages and to rapidly reacquire blocked signals [39], [34], [40]. Although the current VTL architectures provide several important advantages, they suffer from some fundamental drawbacks. The most significant drawback is that the failure of tracking in one channel may affect the entire system and lead to loss of lock of all satellites. When contamination occurs, the error in each channel will accumulate in time and further affect the NS accuracy which will then degrade the tracking loop performance [35]. Besides that, another primary drawback of implementing VTL is in the processing load and complexity. This is because the central EKF used must be iterated on a time scale commensurate with the tracking process that can be very high for dynamic applications [41]. This means that every new measurement provided at certain time instance has to be synchronized between the tracking level and the NS. It should be noted that this constraint can be removed by integrating an INS to interpolate the NS state between measurements.

Consequently, a great deal of study has been done for vector-based algorithms to be integrated with inertial sensors which results in a hybrid navigation system. This hybrid approach is generally referred to as ultra-tight or deeply integrated (DI) GPS/INS architecture [42], [43]. The details on the design, implementation and performance of DI algorithms have been discussed vastly in a lot of publications such as [13], [34], [44], [45] and [46] among others. There are several VTL architectures that have been described in the literature.. The various architectures of VTL are classified into four groups based on two criteria: 1) the degree of centralization required for the estimation and 2) the presence or absence of discriminators inside the architecture. The degree of centralization refers to the presence or absence of the local estimator inside the tracking loop. Therefore the architecture impacts the way to form the measurement vector used as observation to update the NS.

4.4.2 Centralized Architecture

This variation of vector architecture can be regarded as a single step approach where the local estimator is being discarded in the design. The NS for this type uses directly the correlators or

discriminator outputs as measurement. Therefore, the solutions described in this section belong to this group of architectures and differ by the source of measurements provided to the NS.

a) Centralized Architecture using Correlator outputs (Single-step Approach)

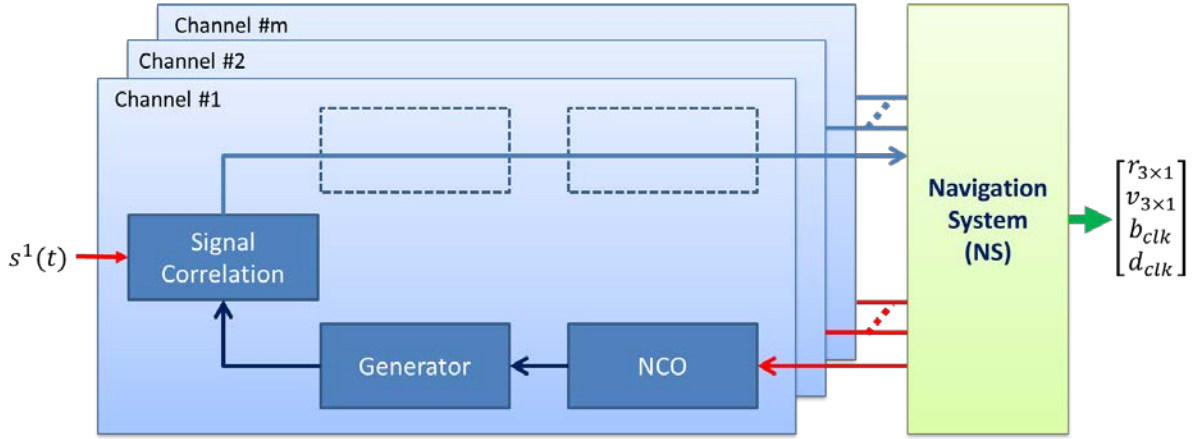


Figure 57: Centralized Architecture using Correlator's output.

This architecture uses the states of NS to predict the code delay and carrier Doppler frequency of the available satellites based on [45], i.e., to control the channel NCOs. The control is made possible by correlating the predicted signals with the received signal which are then used to generate code delay and carrier Doppler frequency residuals. The residuals are then used to update the NS states. The closed loop for aligning the replica and the received signals is performed through the EKF. This approach removes the use of both discriminators and local estimator inside the local tracking loop as shown in Figure 57.

In this approach, the NS uses the outputs of the correlators directly as the measurement model such that:

$$\tilde{Y}_m = [u_z(m, k, l)] \quad \text{with} \quad \begin{cases} 1 \leq m \leq N_{sat} \\ 3 \leq l \leq N_{corr} \end{cases} \quad (4.41)$$

and

$$u_z(m, k, l) = A_k(\Delta f_{m,k}) R_c(\Delta \tau_{m,k} + \delta_l) \exp(j\Delta \phi_{m,k}) + w_u(m, k, l) \quad (4.42)$$

In this representation, $\Delta f = f - \hat{f}$, $\Delta \tau = \tau - \hat{\tau}$ and $\Delta \phi = \phi - \hat{\phi}$ where the symbol ' $\hat{\cdot}$ ' represents the estimation provided by the NS. This approach requires N_{corr} correlators per satellite, delayed in

time (bank-of-correlators) where l is the index of the correlators. This means that each channel will provide a large measurement vector ($\approx 2 \times N_{sat} \times N_{corr}$) to the NS for PVT estimation as illustrated in Figure 58.

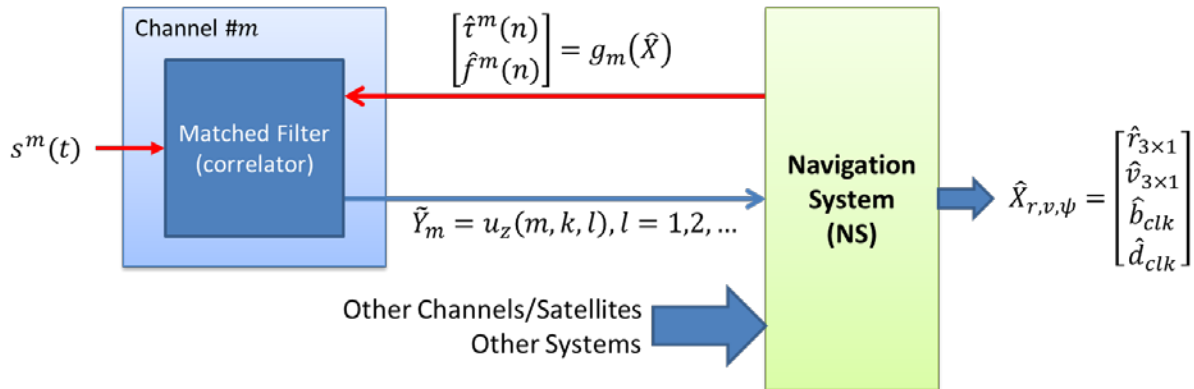


Figure 58: Bank of Correlator outputs as Measurement in Single Step Approach.

The benefits of this approach are that allows tracking signals with poor C/N_0 and can effectively address harsh environment condition thanks to the use of the bank of correlators. On the other hand, this approach is not able to track the carrier phase easily. Furthermore, for high dynamic applications, high-rate positioning must be achieved. The main problem with this approach is due to the fact that a bank of correlators is used as measurement (one-bank per channel) [29]. This leads to a large dimension of the measurement model and of course, increases the computational load.

b) Centralized Architecture using Discriminator outputs (Single-step Approach)

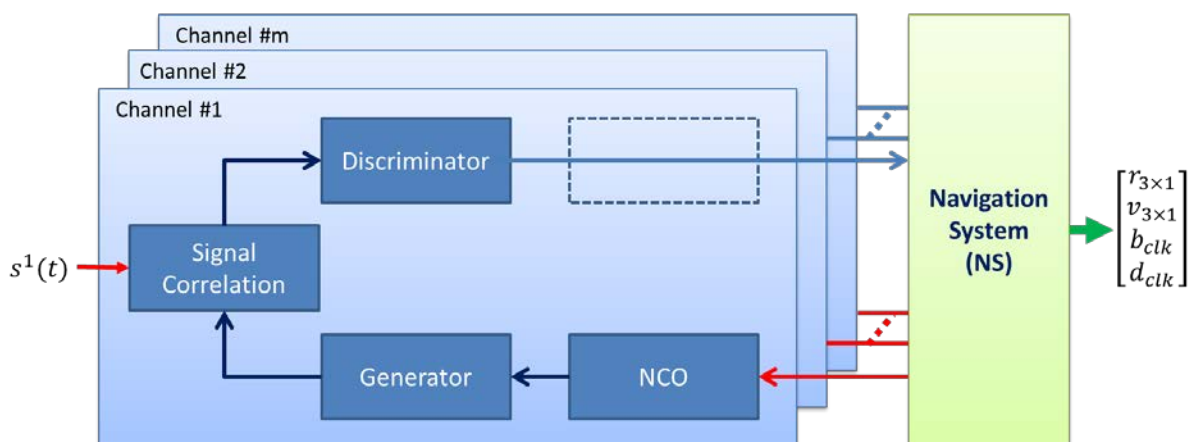


Figure 59: Centralized Architecture using Discriminator's output.

The implementation of this architecture is shown in Figure 59. This approach is very close to the previous one but discriminators are used to provide a simple measurement model as it delivers the innovation based on delay and frequency measurements. It results in a significant simplification of the measurement model since the measurement vector reduces to

$$Y = \Delta \tilde{Y}_m^{Disc} = \begin{bmatrix} \tilde{\tau}_m - \tau_m \\ \tilde{\varphi}_m - \varphi_m \\ \tilde{f}_m - f_m \end{bmatrix}. \quad (4.43)$$

This approach was explored in [44] , [46] and [47] to name a few. As in the case with the traditional STL, a typical code discriminator can be used but a normalized version is generally preferred to eliminate the data bit sensitivity. On the other hand, a frequency discriminator is used instead of a PLL discriminator as being suggested in [46] and [48]. The motivations behind the use of frequency discriminator include the fact that carrier phase is harder to track on the basis of this architecture, as this operation would require centimetres accuracy. Besides that, for VTL implementation, the carrier phase difference is no longer of interest (except for smooth delay error measurement and to perform coherent integration). The use of propagation delay error and frequency Doppler error, i.e., of delay and frequency discriminators as location and velocity observation satisfies for the requirements of the navigation system [48]. On other aspects this solution is similar to the previous one as displayed in Figure 60.

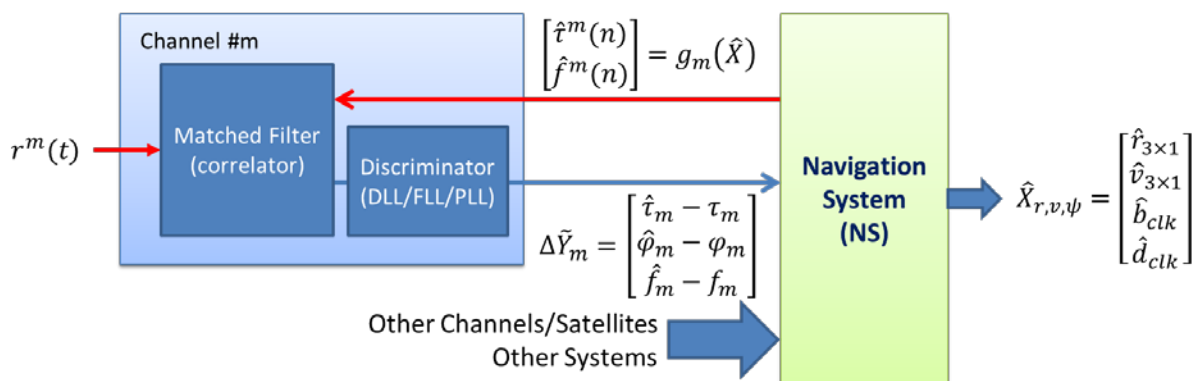


Figure 60: Discriminator outputs as Measurement in Single Step Approach.

This architecture was proposed by [49] and later resumed by [13]. These studies agree and have successfully shown the superiority of vector tracking compared to traditional tracking architecture. Other studies such as [48] confirm the ability for this approach to estimate occasionally position with less than four satellites and to make possible the tracking of signal with low C/N0.

Besides the improvements, the carrier phase of the signals remains an issue. As for the previous architecture, tracking the phase, which allows coherent integrator to be implemented, is difficult on the basis of this architecture.

4.4.3 Decentralized Architecture

This architecture can be considered as a two-step estimation approach where the local estimator (LE) outputs are being exploited by the NS. This approach differs from an STL approach as the NCOs which provide signal replicas are controlled by the navigator, taking advantage of the navigation solution which is estimated from available measurements (satellite measurements in a standalone GNSS system). Compare to the centralized approach, this architecture allows the receiver to be easily switched to the STL architecture. Moreover it allows phase tracking. Finally, for low rate of the NS, this solution allows local estimates to be propagated at a higher rate, and consequently to provides more accurate measurements.

By using the local estimators, [42] [50] have highlighted that it is possible to reduce the order and the update frequency of the NS filter. Besides that, the use of KF as local estimators allows for the measurements to be weighted according to the received signal power by using an estimator of C/N_0 . Moreover, the work of [33] and [11] have highlighted that it is possible to decouple the channels in NS in order to operate in scalar mode.

The decentralized approach is considered as one of the most studied in the literature where the observation model is rigorously exploited by a Bayesian estimator. The observation model can be adapted to any shape of GNSS signal and also takes into account the presence of multipath [36]. This will be beneficial when multi-constellations are considered. Besides all the variation of the implementation either on the measurement model or the choice of local filter, all of these studies assess the effectiveness of vector tracking in degraded environment. Similar to the centralized approach, the decentralized approach can exploit the outputs of the correlator or discriminator as measurement.

a) Decentralized Architecture using Correlator output (Two-step Approach)

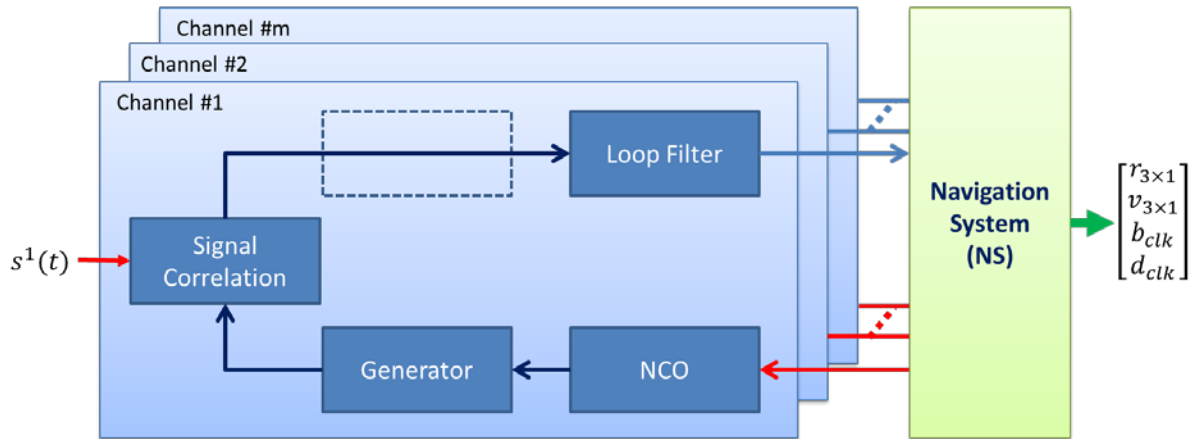


Figure 61: Decentralized Architecture using Correlator outputs.

This solution is based on a local estimator which uses a bank of correlators to form the observation model in order to provide an estimate of the propagation delay and of the Doppler frequency. This local estimator can be defined by the following state equation (similar to equation 4.37):

$$\tilde{X}_{k+1} = \begin{bmatrix} \tilde{\tau} \\ \tilde{\varphi} \\ \tilde{f} \end{bmatrix}_{k+1} = \Phi^{\text{LE}} \cdot \tilde{X}_k + w_k \quad (4.44)$$

but is completed by the following measurement innovation:

$$\Delta Y_k = \begin{bmatrix} u_z(m, k, l) \\ \cdot \\ \cdot \end{bmatrix} \quad (4.45)$$

where

$$u_z(m, k, l) = A_k(\Delta f_{m,k}) R_c(\Delta \tau_{m,k} + \delta_l) \exp(j\Delta \varphi_{m,k}) + w_u(m, k, l) \quad (4.46)$$

with $\Delta \tau_{m,k} = \tau - \hat{\tau}_{m,k}$, $\Delta \varphi_{m,k} = \varphi - \hat{\varphi}_{m,k}$ and $\Delta f_{m,k} = f - \hat{f}_{m,k}$. Compare to the STL, this approach differs from the innovation which is obtained here from the estimates provided by the navigator. Here, only the phase is locally estimated as the navigator accuracy does not provide a precise phase estimate.

Many of these studies, such as in [33], [50] and [51] among others, replace the conventional tracking loop by a single EKF to solve this estimation issue. The studies in [51] and [52] highlighted that a better statistical measurement model was obtained without the use of discriminators. Besides that, studies addressing the best estimation approach are also of interest. For example [53] proposed to use sequential Monte Carlo methods such as particle filter (PF) for performing estimation. This approach is depicted in Figure 62. A local estimator delivers measurements to the navigator which controls the NCOs that deliver signal replicas. Each local estimator exploits correlator outputs which provide an innovation related to the navigator estimates.

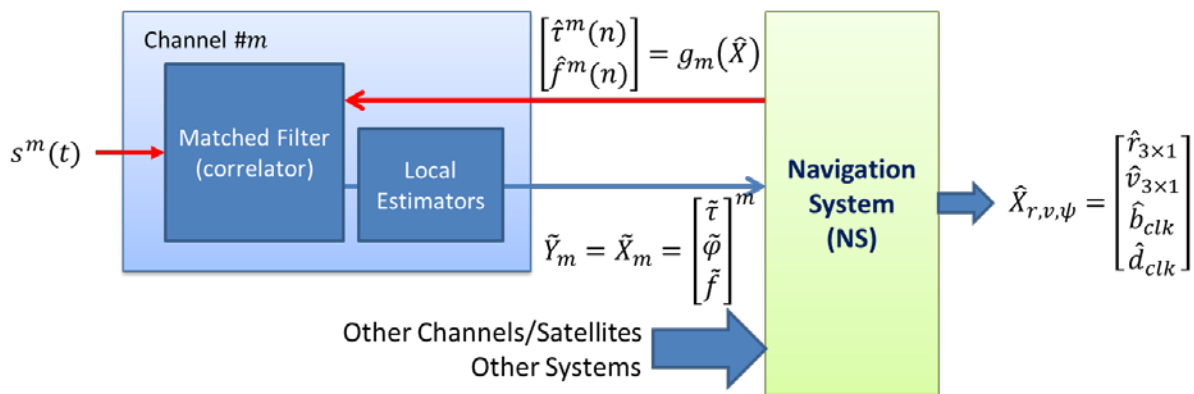


Figure 62: Correlator outputs as Measurement in Two-Steps Approach.

b) Decentralized Architecture using Discriminator outputs (Two-step Approach)

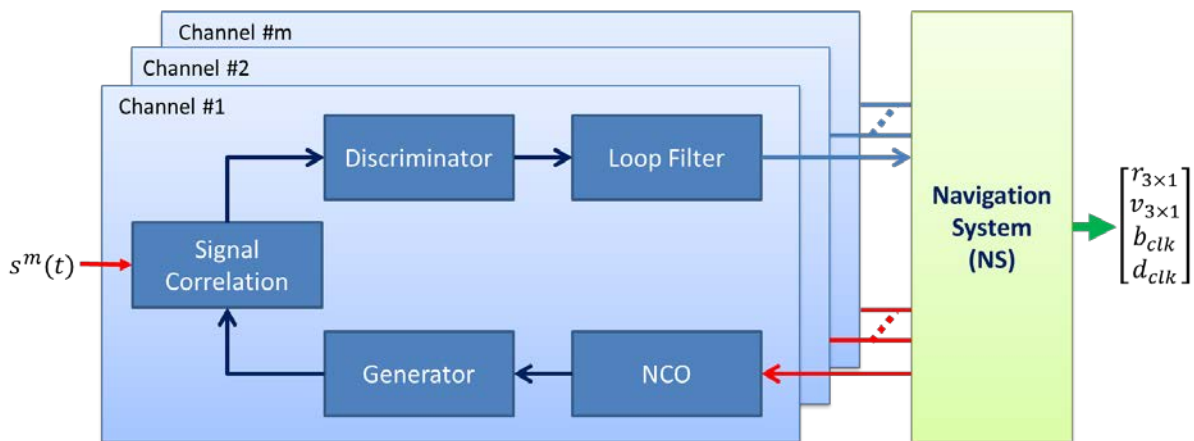


Figure 63: Decentralized Architecture using Discriminator's outputs.

This configuration displayed in Figure 63 is considered to be the closest implementation to the STL architecture based on a conventional tracking loop. This architecture differs from the

previous one as the measurement model exploited by local estimators is based on discriminator outputs given by:

$$\Delta\tilde{Y}_m = \begin{bmatrix} \hat{t}_m - \tau_m \\ \tilde{\varphi}_m - \varphi_m \\ \hat{f}_m - f_m \end{bmatrix}. \quad (4.47)$$

Several studies have explored this type of configuration including the one introducing the concept of vector based tracking algorithm for GPS signals [54]. It introduced the concept of feedback from the navigation filter to the tracking loop in each channel. This solution offers nearly the same benefits and performances as the previous architecture. The fact that the discriminator is used allows for a less complex architecture with smaller matrix size for the measurement vector.

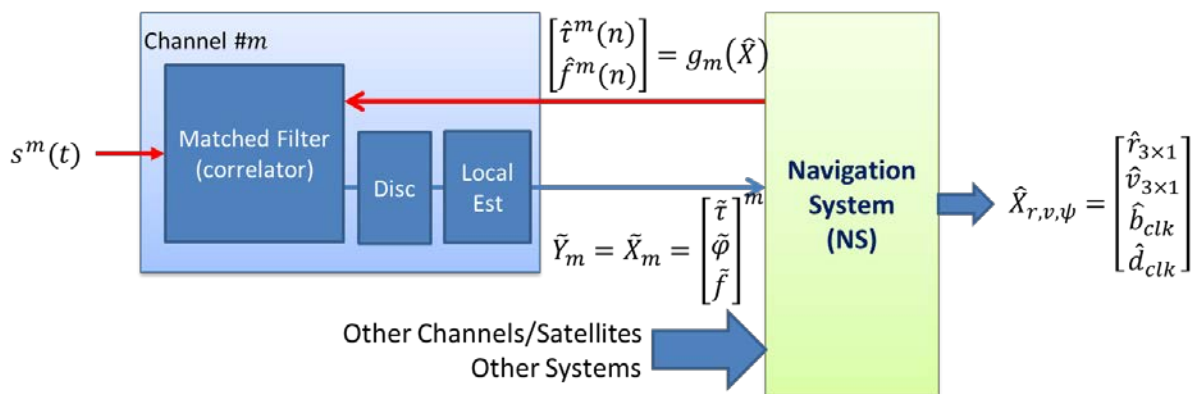


Figure 64: Discriminator outputs as Measurement in Two-Step Approach

The work from [55] further explored the local estimator by integrating it with an FLL-assisted PLL filter in a vector based approach. This enables code and carrier tracking even during outages of a single channel as long as there are four available channels to calculate the PVT parameter solutions. This work further concludes that this architecture extends and stabilizes the range for carrier phase tracking.

Studies in [56] prove that this type of architecture is able to perform better than an STL under bad signal conditions especially when dealing with large and fast signal power variations if no clear LOS signal is available. Besides that, it also demonstrates that the signal can still be tracked even in very low GPS signal power. A variation of this implementation is proposed in [57] that uses two PLL. In this approach, the first PLL is used to monitor the dynamics of the receiver for all channels and the other one is use to monitor the individual channel.

4.4.4 Summary of the VTL Approach

In the frame of this project we propose to implement only one type of VTL architecture for assessing the performance obtained with this approach and to compare its performance with a conventional STL based receiver. The current studies about VTL architectures, never mentions which type of vector tracking architecture should be preferred to the other. Many papers compare the VTL approach to that of the traditional receiver, without providing a comparison between the different VTL approaches. The different VTL approaches with their advantages and disadvantages are summarized in Table 6 and Table 7 inspired by [29].

Table 6: Advantages and Disadvantages of Different VTL Architectures.

	Architecture	
	Centralized	Decentralized
Advantages	<ul style="list-style-type: none"> • Good covariance management • NS is the only estimator 	<ul style="list-style-type: none"> • Easier channel synchronization. • Reduced NS filter order. • Independent Tracking and Navigation rate.
Disadvantages	<ul style="list-style-type: none"> • Easily contaminated (compared to decentralized) as each channel does not improved the estimation locally to the absent of local estimator. 	<ul style="list-style-type: none"> • Covariance matrix management as the output of each local estimator defines the observation of the global estimator.

Table 7: Advantages and Disadvantages of Different Measurement Model

	Measurement Model	
	Bank-Of-Correlators	Discriminators
Advantages	<ul style="list-style-type: none"> • More accurate statistical model. • More accurate MP modelling (i.e., MEDLL). 	<ul style="list-style-type: none"> • Simpler measurement model. • Lower dimension of measurement model. • MP mitigation is easier.
Disadvantages	<ul style="list-style-type: none"> • Large dimension of the measurement vector used by the NS (in case of centralized). 	<ul style="list-style-type: none"> • Unable to provide an accurate measurement model in the presence of MP.

In the context of this thesis, we have proposed to implement a vectorial approach based on a decentralized architecture with discriminators. This approach allows the receiver to be easily switched from an STL to a VTL approach, and vice versa. Using this approach offers the possibility to choose the tracking loop rate and the navigator rate independently. Moreover the use of discriminators facilitates the implementation of tests for monitoring each channel in order to adapt it efficiently to the incoming signal. Finally, by estimating locally the carrier phase, it allows coherent integrations to be used. An adaptive VTL/STL algorithm based on this configuration will be investigated in the next chapter.

4.5 VTL Implementation

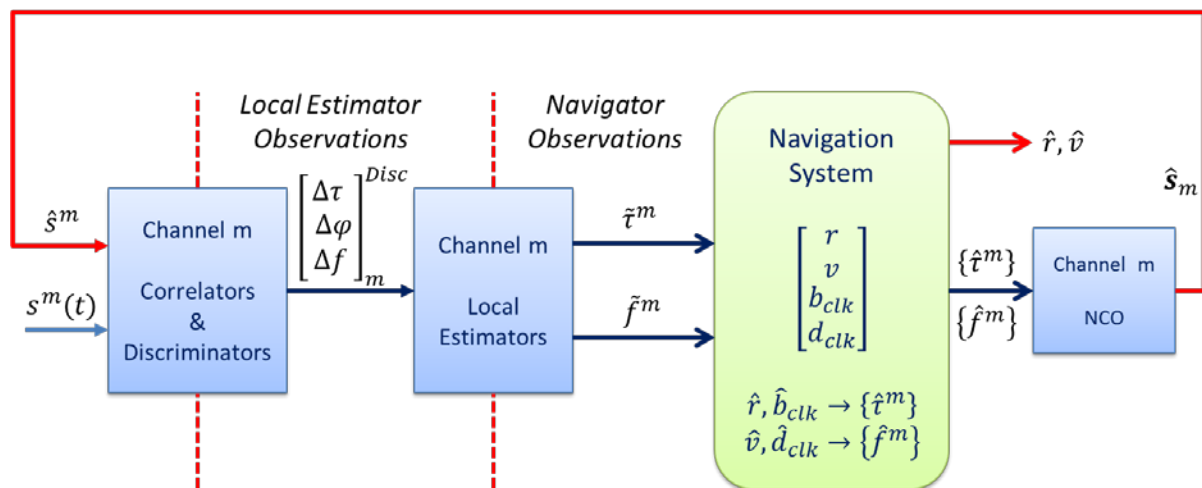


Figure 65: Vector tracking implementation focusing only for single channel

The distributed VTL architecture with discriminator outputs is studied in the framework of this thesis work. This architecture is analysed in detail and illustrated in Figure 65. The main stages of this architecture are the following:

- A matched filter based on a correlator is used to process the incoming signal. In the same way Early Late correlators are implemented. Signal replicas are controlled by the NS. Therefore a discriminator based on the correlator provides an innovation related to the NS estimates.
- These discriminator outputs are combined to the local estimator output to provide observations of the local estimates, which represent an estimation of the propagation delay,

and of the Doppler frequency. These estimates are sent to the NS. Local estimators are based on TL.

- The last stage is the NS which is based on an EKF. The measurement model is built from local estimator outputs. This navigator provides not only the position and velocity, but also NCO commands. This information can also be used for performing statistical tests at discriminator outputs.

The navigation system estimates the vehicle position and velocity as well as receiver clock bias and drift based on the information provided by each channel. In our VTL implementation, these values are also used for controlling the numerically controlled oscillators (NCOs) that will be used to provide the replica signals for each satellite in visibility. The navigation filter used in this case is based on an EKF that is proved to be efficient for real time implementation and easy to implement in an iterative-in-time nature.

Therefore, the system model implemented in this thesis has been described earlier in section 4.3.2. The NS uses the outputs of local estimators of all visible satellites as measurements. It provides the position and velocity of the user, as well as an estimation of the code propagation delay and carrier Doppler frequency to each channel. Besides that, it delivers noise covariance matrices for these outputs. The local tracking loop implementation associated with the VTL implementation has been clearly described in section 2.3 with the local estimator described in 4.3.1. The objective of purposing this type of VTL is to ensure that closest similarity with the STL architecture.

4.5.1 Measurement Model

Local estimator outputs are used as the measurement model in order to update the NS. These outputs concern the propagation delay and the Doppler frequency:

$$Y^{NS} = [Y_1, Y_2, \dots, Y_m]^T + v_k \quad (4.48)$$

where

$$\tilde{Y}_m = \begin{bmatrix} \tilde{\tau} \\ \tilde{f} \end{bmatrix}_m$$

and where $\tilde{\tau}^m$ and \tilde{f}^m are the estimated code delay and Doppler frequency, associated with the m^{th} channel (satellite). The noise term v_k is the measurement noise with covariance matrix R_k , i.e.,

$$\mathbf{v}_k \sim N(0, R_k) \quad (4.49)$$

where R_k is constructed from the variances of the estimates provided by each channel, depending on the incoming C/N_0 ratio, but also depending on the tracking loop implementation (integration time of the correlator, chip-spacing of the discriminator and the filter-order/bandwidth of the local estimator). The propagation delay error of the navigator is related to the error of the estimated position and clock bias whereas the frequency error is related to the error of the estimated velocity and clock drift. The measurement model can be defined as follows:

$$\tau^m = \frac{1}{\lambda_c} [LOS_m^T \cdot (\mathbf{r}^{NS} - \mathbf{r}^m) + b_{clk}] + v_\tau \quad (4.50)$$

$$f^m = -\frac{1}{\lambda_{fL1}} [LOS_m^T \cdot (\mathbf{v}^{NS} - \mathbf{v}^m) + d_{clk}] + v_f \quad (4.51)$$

As tracking loops work independently, the measurement noise covariance matrix can be represented in a diagonal matrix as follows

$$E[\mathbf{v}\mathbf{v}^T] = R_Y^{NS} = \text{diag} \left(\sigma_{\tau^1}^2, \sigma_{\tau^2}^2, \dots, \sigma_{\tau^m}^2, \sigma_{f^1}^2, \sigma_{f^2}^2, \dots, \sigma_{f^m}^2 \right). \quad (4.52)$$

The diagonal elements of this covariance matrix are obtained on the basis of the implemented tracking loops [1]. The power of these errors, for the DLL and the PLL aided FLL are respectively given by (see (2.26) and (2.31));

$$\sigma_{\tau^i}^2 = \frac{B_n^{DLL} \cdot d}{2 \cdot C/N_0} \quad (4.53)$$

$$\sigma_{f^i}^2 = \frac{1}{\pi^2 \cdot T_{int}^2} \left(\frac{B_n^{FLL}}{C/N_0} \right) \quad (4.54)$$

where T_{int} is the integration time, d is the early-late spacing of the DLL discriminator and B_n is the noise bandwidth loop for DLL and FLL respectively. The integration time can be defined as the number of accumulated correlation time performed by the tracking loop.

4.5.2 NS Outputs

The NS computes the estimates of the state vector \hat{X}_{k+1}^{NS} and the corresponding covariance matrix \hat{Q}_k^{NS} by using the conventional EKF. It also delivers the parameters used for generating the replicas of the received signal that are being tracked for each channel. The estimated propagation delay and Doppler frequency for each satellite can be obtained by these relationships;

$$\hat{t}_m = \frac{R_C}{c} [LOS_m^T \cdot (\mathbf{r}^{NS} - \mathbf{r}^m) + b_{clk}] \quad (4.55)$$

$$\hat{f}_m = -\frac{f_L}{c} [LOS_m^T \cdot (\mathbf{v}^{NS} - \mathbf{v}^m) + d_{clk}] \quad (4.56)$$

The new estimated values of \hat{t}_m and \hat{f}_m are used to command the local NCO. Moreover, under the assumption of a Gaussian distribution for the state vector, the standard deviation estimates (\hat{t}^m, \hat{f}^m) can be computed as follows

$$\sigma_m^t = \sqrt{H_{2m-1} P^{NS} H_{2m-1}^T} \quad (4.57)$$

$$\sigma_m^f = \sqrt{H_{2m} P^{NS} H_{2m}^T} \quad (4.58)$$

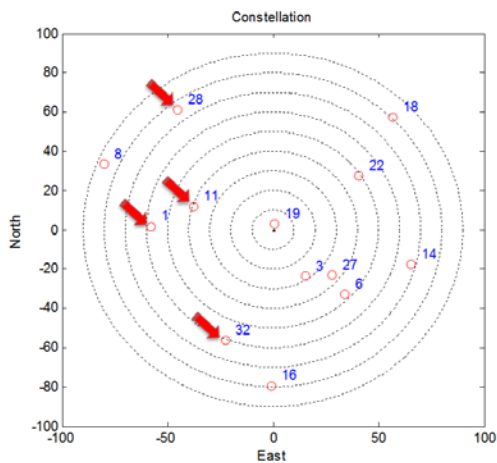
where P^{NS} is the error covariance matrix associated with the state vector and H_{2m-1} and H_{2m} are the $(2m-1)^{th}$ and $(2m)^{th}$ lines of the observation matrix H^{NS} respectively.

4.6 Performance Evaluation for STL vs. VTL

The performance evaluation for both STL and VTL is carried out to ensure that the implementations of STL and VTL in this project are corresponding to those of actual receivers. The simulator discussed in Chapter 3 is used to generate the signal related to different simple environments allowing the performance of STL and VTL to be compared.

4.6.1 Simulation Methodology

In order to demonstrate the performance of both STL and VTL architectures, the simulation has been carried out based on the same trajectory. The trajectory is defined from data collected during a measurement campaign around the ISAE campus Supaero. The incoming signal corresponding to this trajectory is obtained from our simulator, whereas the trajectory is used as a reference trajectory in order to compare STL and VTL architectures. The satellite constellation and reference trajectory superimposed on a map are presented in Figure 66 (a) and (b) respectively. Therefore, under nominal conditions, the estimation of the receiver over the trajectory is presented in Figure 67 (a) and the corresponding ENU position is presented in Figure 67 (b).

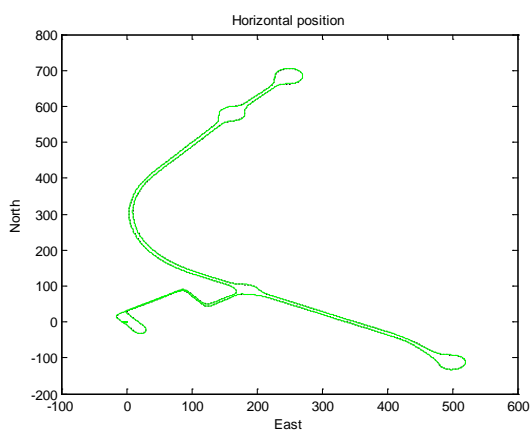


(a)

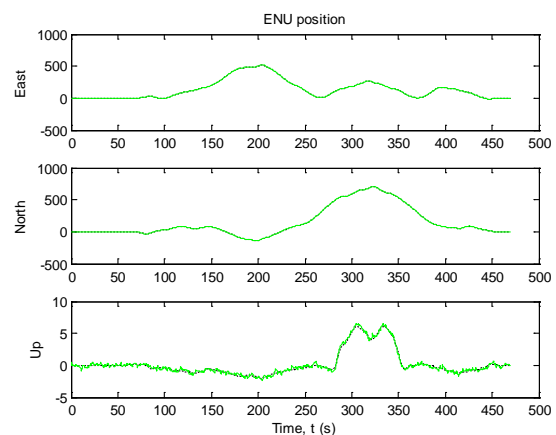


(b)

Figure 66: (a) Satellite constellation and (b) the reference trajectory over map.



(a)



(b)

Figure 67: Estimated trajectory under nominal condition represented by (a) the trajectory and (b) the ENU positions.

4.6.2 Impact of MP

In order to evaluate the performance of the receiver in presence of MP, the in-house simulator allows for MP to be introduced with a certain degree of SMR, delay, instantaneous phase and Doppler frequency that are relative to LOS signal at any period along the trajectory. As for the LOS, all satellites are considered to have strong signal with $C/N_0 = 40dBHz$. Here, four satellites will be contaminated by MP and the performance will be observed through the delay, phase and frequency errors of the tracking loop for both STL and VTL approaches. The MP parameter values are presented in Table 8 and are also indicated with arrows in Figure 66. These MP were introduced for 10s between the periods of 215s and 225s of the trajectory as shown in Figure 68.

Table 8: Parameters of the MP introduce during simulation.

Sat ID	1	3	6	8	11	14	16	18	19	22	27	28	32
MP	SMR (dB)	-3	-	-	-	-3	-	-	-	-	-	-3	-3
	Delay (chip)	0.3	-	-	-	-0.2	-	-	-	-	-	0.1	0.2
	Phase (cycle)	0.05	-	-	-	0.03	-	-	-	-	-	0.02	0.02
	Frequency (Hz)	0.1	-	-	-	0.1	-	-	-	-	-	0.1	0.1

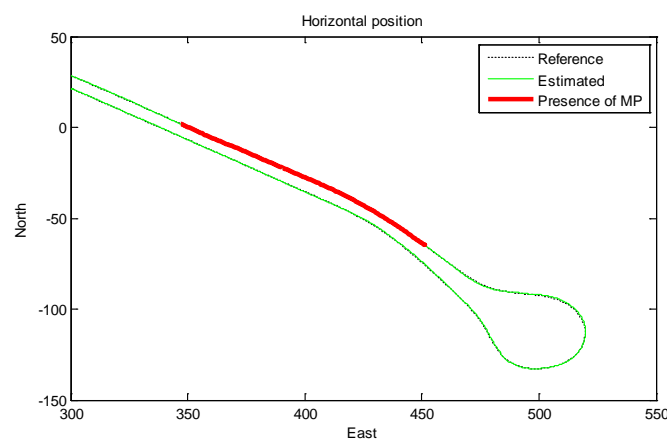


Figure 68: Area indicated where MP were introduced inside the trajectory.

The purpose of the comparison is to observe the effect of MP for both STL and VTL architectures where the focus is given to the local tracking parameters. The effects of the MP are analyzed in order to compare the two architectures and to propose a new strategy for mitigating the effect of the MP. In order to do this, we consider two conditions: 1) all channels including the contaminated one are considered as measurements and 2) contaminated channels are being discarded.

a) Considering all visible channels (including contaminated channels)

First, we consider the performance for both STL and VTL in the presence of MP when all channels are providing measurements to the NS. The MP presences which degrade the delay measurement used by the navigator are illustrated in i) for STL and ii) for VTL.

i. STL in the presence of MP

The overall performance of the STL architecture on positioning error is presented in Figure 69 (a) and the associated trajectory focusing on the area where MP has been introduced inside the simulation is presented in Figure 69 (b).

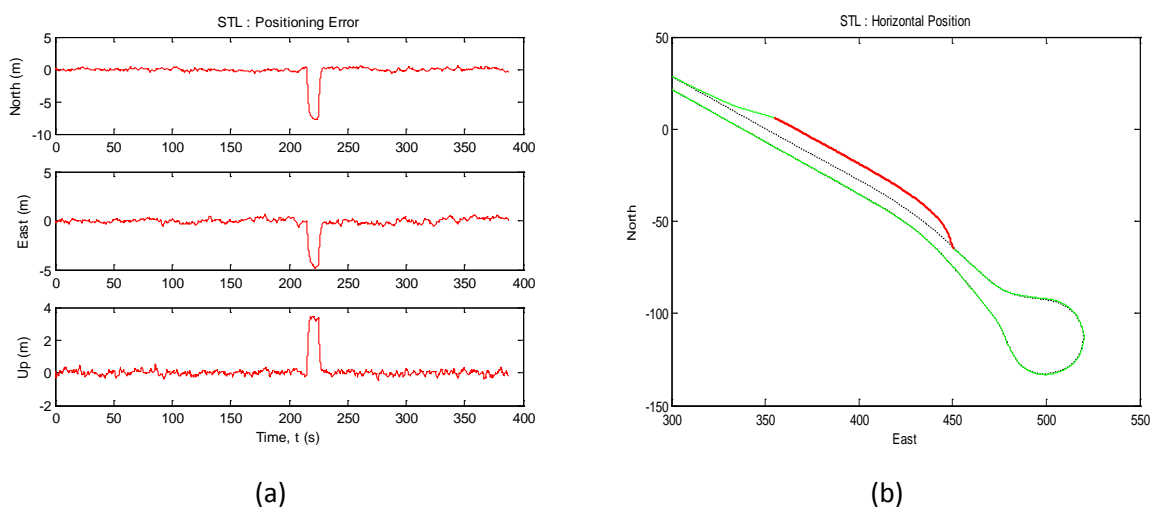


Figure 69: (a) Overall STL performances on positioning error and (b) the trajectory associated in the presence of MP.

The positioning error is observed during the period [215s – 225s], when MP are introduced in accordance with Table 8. During this period, it is interesting to observe the delay error for each satellite that is used for estimating the vehicle position. Here, we can observe in Figure 70 that the delay measurements produced by the satellites that are affected by MP, are showing a significant amount of error, depending on MP delay parameters.

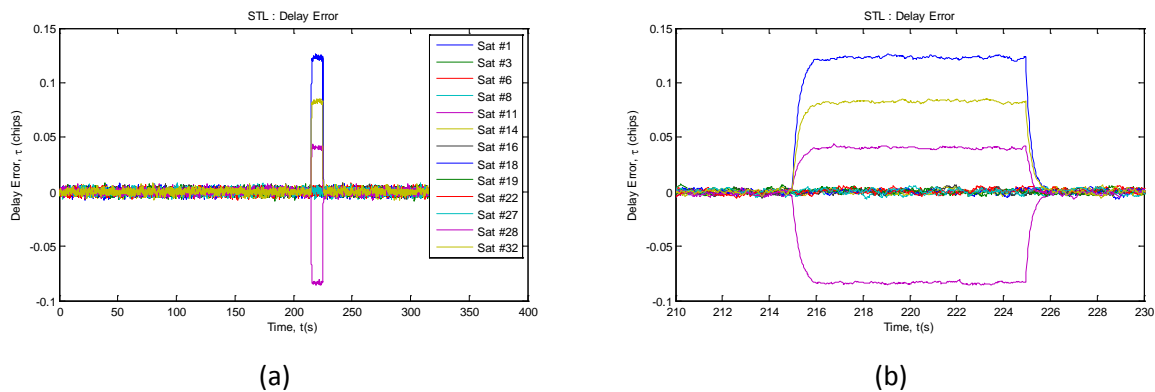


Figure 70: (a) Overall delay error for STL mode for the whole trajectory with a (b) zoom-in at the MP presence.

It is interesting to observe the output of the delay discriminators in the STL mode. These outputs are presented in Figure 71. We can see that the DLL of all contaminated satellites quickly converge to correct the delay discriminator error. These convergences occur when the MP is starting to appear inside the channel, introducing a bias in delay measurement; and when the MP is disappearing from the channel, removing the error in delay measurement.

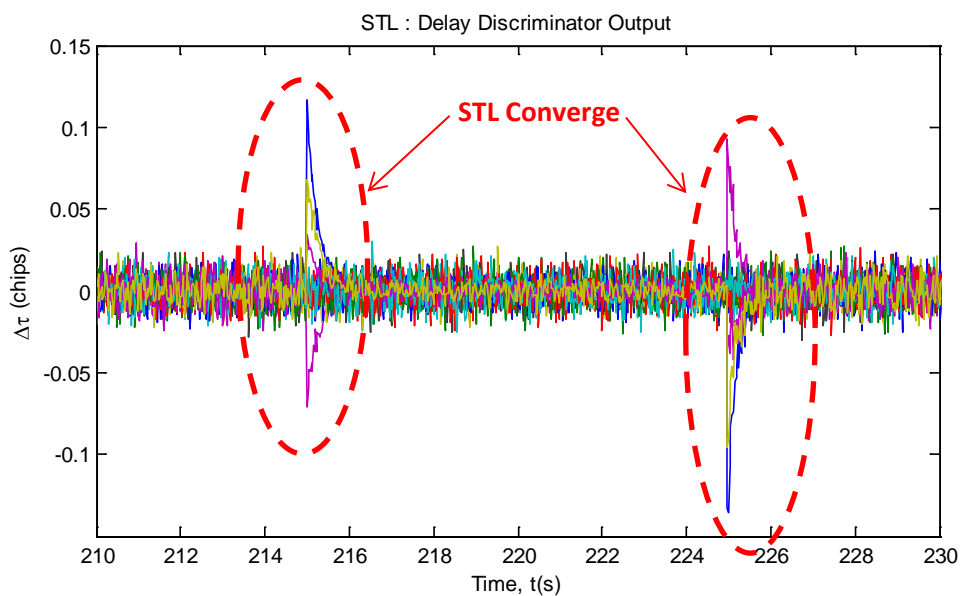


Figure 71: Delay discriminator output in STL mode.

ii. VTL in the presence of MP

The overall performance of the VTL mode for the whole trajectory is presented in Figure 72 with a zoom on a region where MP has been introduced in Figure 72 (b). Here, the performance of the VTL seems to be similar to the STL mode. However, when we observe closely the ENU positioning error presented in Figure 72 for the VTL mode, we can conclude that in the case of MP, STL works slightly better than the VTL mode. The reason for this can be further explained when we look closely at the delay discriminators outputs associated with the VTL mode.

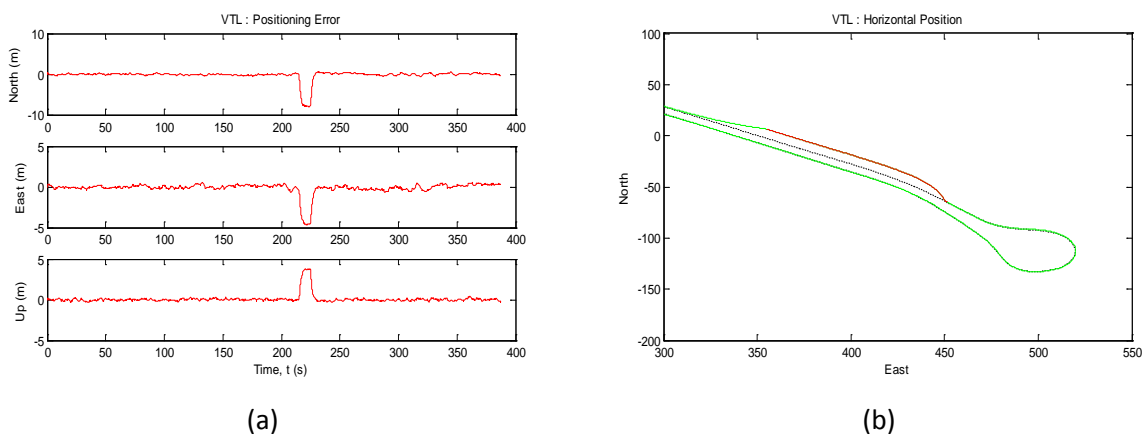


Figure 72: (a) Overall STL performance on positioning error and (b) the trajectory associated in the presence of MP.

Similarly, the errors on delay measurements that are presented in Figure 73 for the VTL mode look very similar to what was presented in STL mode. A more accurate analysis shows that delay errors are slightly larger in VTL mode than in STL mode.

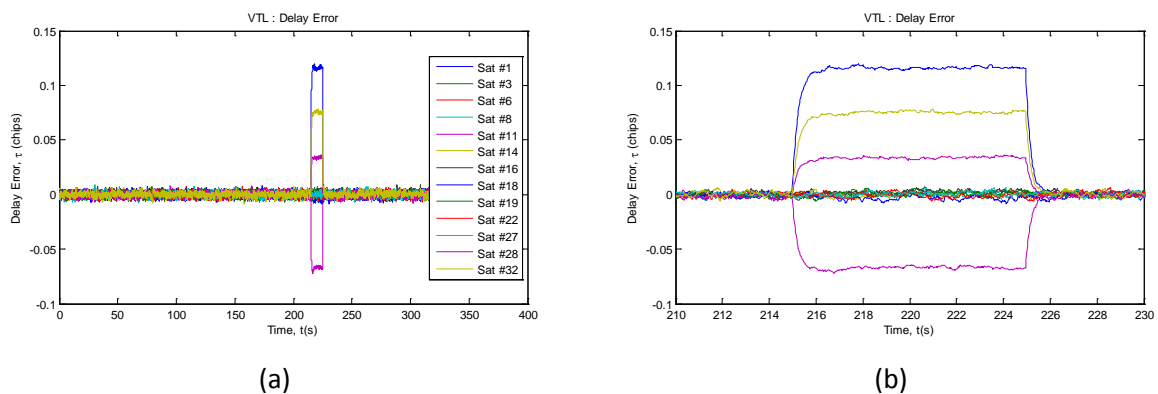
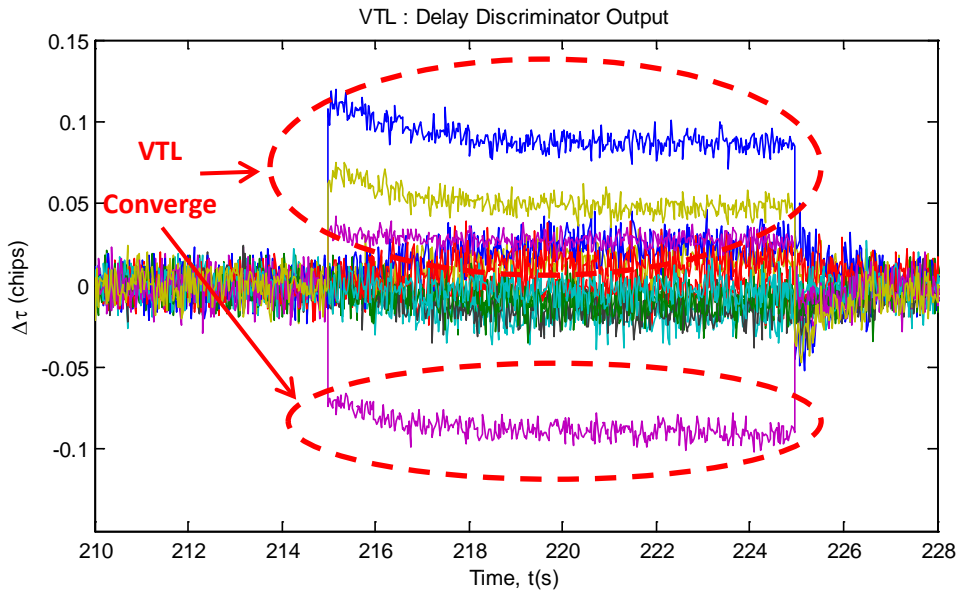
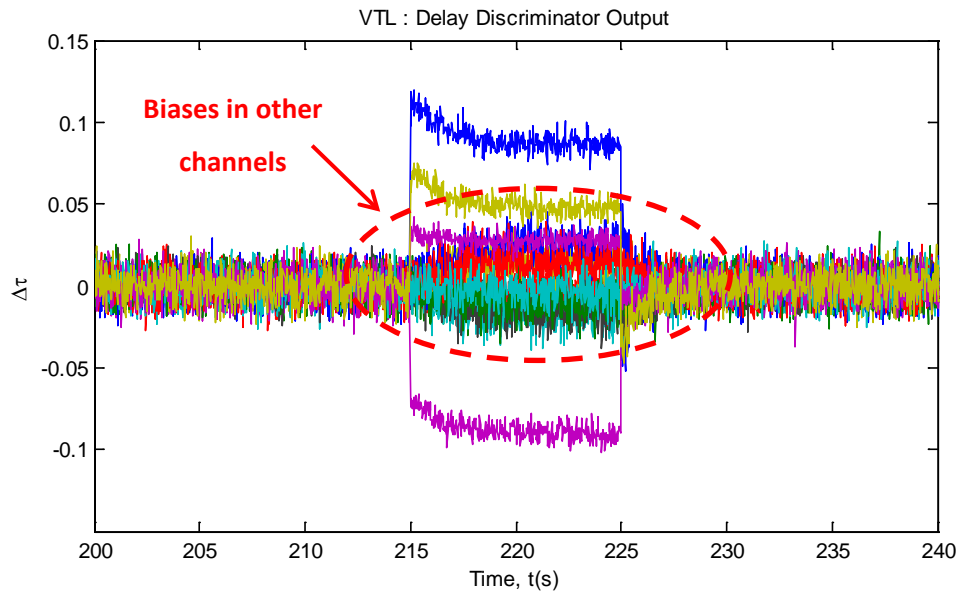


Figure 73: (a) Overall delay error for VTL mode for the whole trajectory with a (b) zoom-in at the MP presence.



(a)



(b)

Figure 74: Delay discriminator output in VTL mode with (a) focusing on the contaminated channel and (b) focusing on the other channel.

Regarding the positioning error, this behaviour can be explained by analysing the delay discriminator outputs which are presented in Figure 74. In a VTL mode, as NCOs are controlled by the navigator, any positioning error impacts all the satellites. In this situation, a delay discriminator experiences not only the error due to the presence of MP, but also the error on the estimated delay, as it is estimated by the navigator. On the Figure 74 (a), we observe that, contrary to the STL, delay discriminators are able to measure the extra delay due to MP. At the MP appearance, this delay is

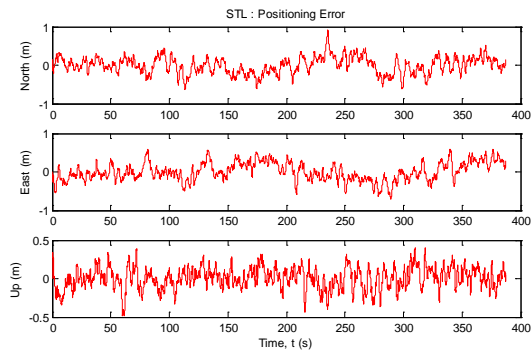
correctly measured. As this delay error results in a bias in the measurement used by the navigator, the navigator converges to a wrong position, shifting the operating point of the NCO. Consequently the delay error of the contaminated channel is not exactly measured. Moreover, the discriminator of the healthy channel exhibits an error which is discernible for the channel 27 in Figure 74 (b). This behaviour further proves that in VTL mode, good channels are vulnerable to contaminated channels and cause higher degree of error in the estimations.

b) Considering only healthy channels (discarding contaminated channels)

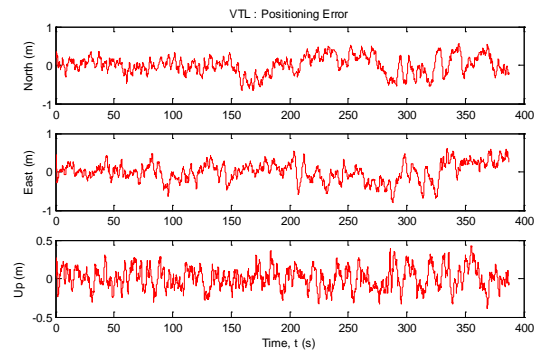
Next, the same scenarios are used but this time, only the healthy channels are used as measurements by the navigator. When the contaminated channels are being discarded, the tracking performance in presence of MP does not degrade the delay measurements used by the navigator. Here, the comparison between STL and VTL are presented side by side as presented in Figure 75 (a) for STL and Figure 75 (b) for VTL.

In this approach, the channels/satellites that are contaminated are discarded. In this situation the channels whose tracking loops are affected by MP are not used by the navigator for computing the vehicle location. The performance of STL and VTL approaches are then compared side by side. We can see that, for both approaches, the receiver performs better. The mean errors on the estimated location, which are represented in Figure 75 (a-1) and Figure 75 (b-1), respectively for the STL and the VTL approach, remains close to zero.

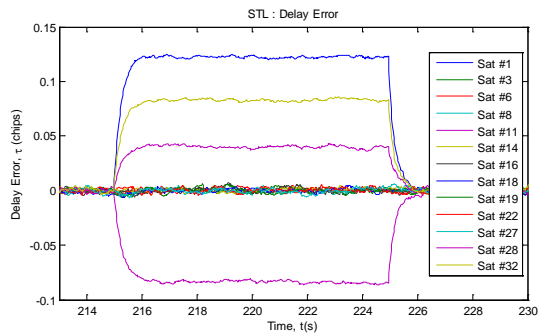
The delay errors for STL and VTL are presented in Figure 75 (a-2) and Figure 75 (b-2) respectively. By analysing closely the results, we can conclude that if the contaminated channels are being discarded, the VTL method performs slightly better than the STL approach. This can also explain why the biases that affected the healthy channels (when these contaminated channels are used for estimation) are no longer visible in Figure 75 (b-3). Regarding the STL, the convergence of the contaminated channels is presented in Figure 75 (a-3). What is interesting to observe is that when the navigator is not contaminated, the delay discriminator outputs can be used in a VTL mode for detecting contaminated channel. The impact of MP on the discriminator outputs can also be observed. On the contrary, the STL tracking loop converges in order to minimize the delay discriminator outputs, making impossible to detect the presence of MP.



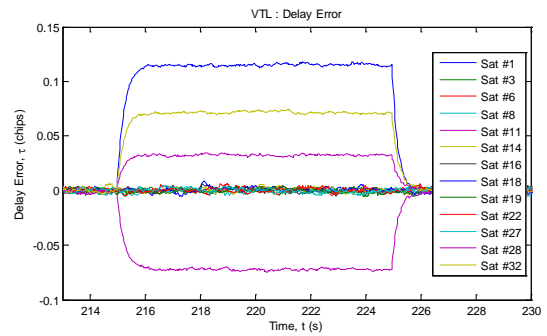
(a-1)



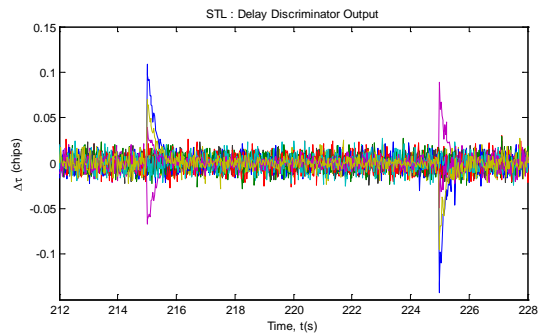
(b-1)



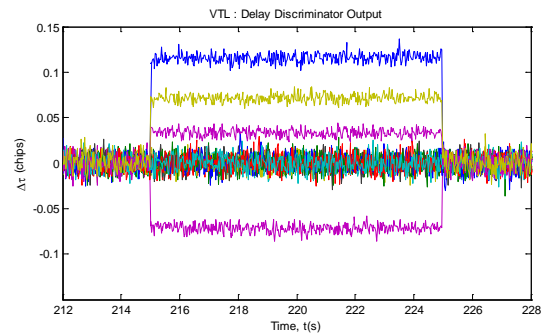
(a-2)



(b-2)



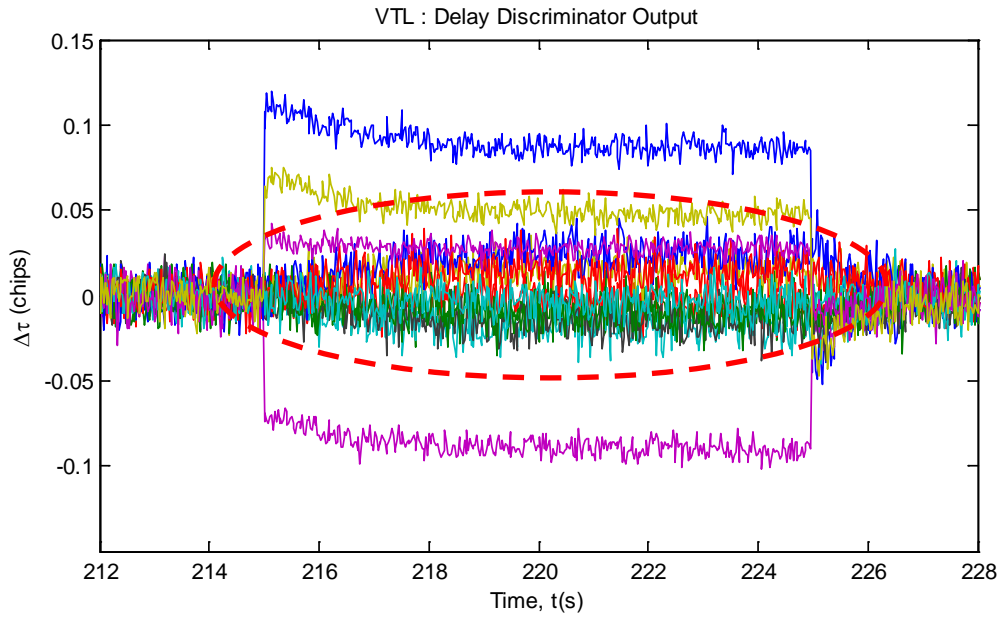
(a-3)



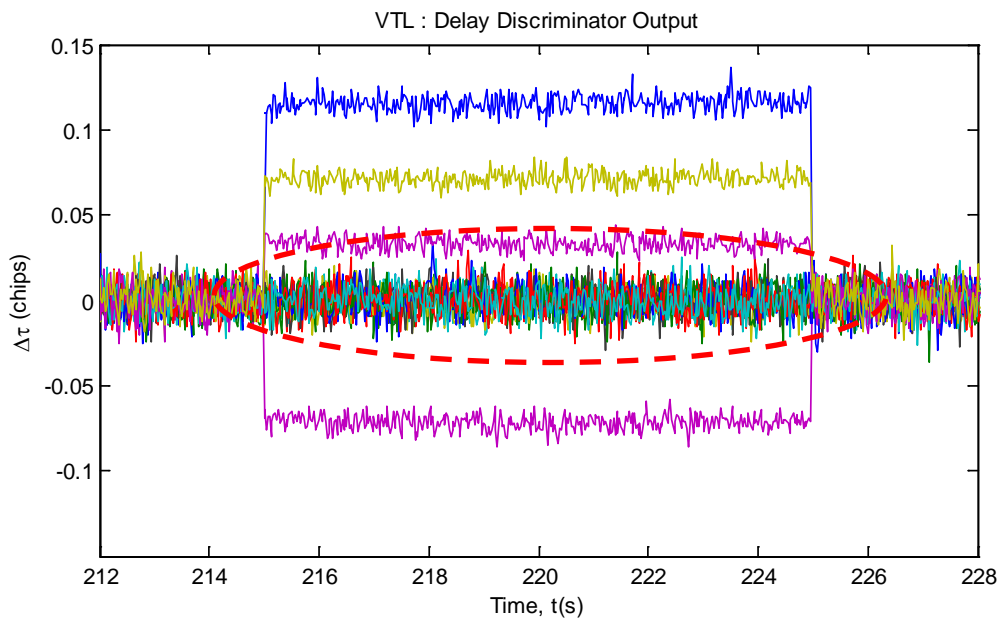
(b-3)

Figure 75: Tracking performance of (a) STL and (b) VTL when contaminated channels are being discarded.

In addition to the comparison between the performance obtained with the STL and VTL architectures, we have proved that the VTL are sensible to channel contamination. These observations are illustrated in Figure 76 (a) and (b) where we can observe the effect of the contaminated channels have to the healthier channels which results in poor performance when compare to the STL approach.



(a)



(b)

Figure 76: Comparison between both VTL approaches in the presence of MP when the contaminated channels are (a) used as measurements and (b) discarded.

4.6.3 Impact of Masking

The aim of this analysis is to assess the receiver performance in case of LOS masking. For emulating the masking effect, the LOS signal associated with one of the satellite is forced to zero.

This masking scenario will be assessed under 2 conditions referred to as short masking and long masking. Both scenarios are evaluated under the STL and VTL approach for better understanding on how masking affects the performance of the tracking loop in both architectures. The masking areas in the trajectory for short and long masking are presented in Figure 77 (a) and (b) respectively.

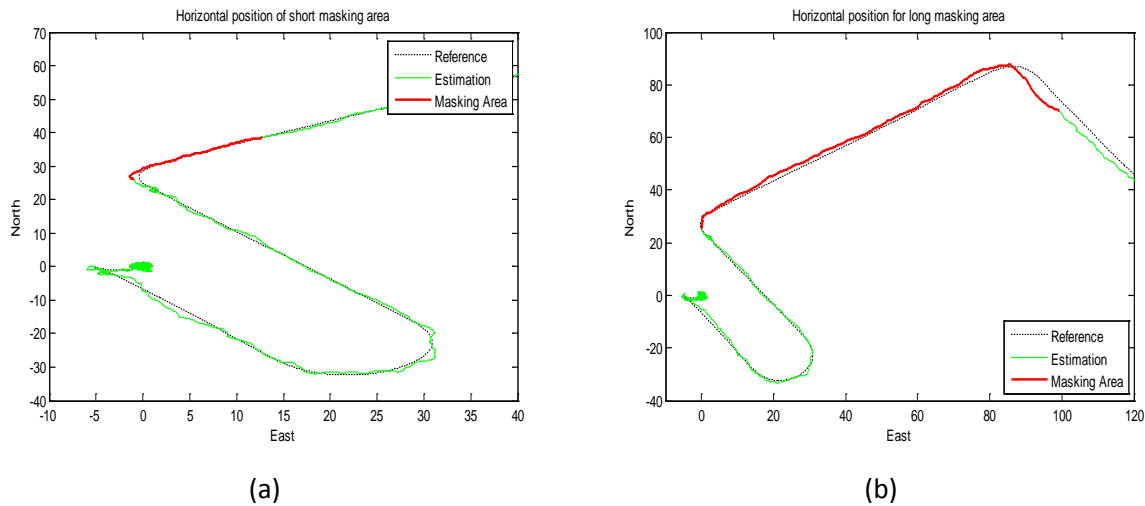


Figure 77: (a) Short and (b) long masking area implemented over the trajectory.

Both short masking and long masking effects are presented in Figure 78 and Figure 79 respectively. In the case of short masking, we can see that both STL and VTL manage to estimate the vehicle position as opposed to STL which suffers more severely than the VTL approach. This can be clearly observed for the delay in Figure 78 (a) and for the frequency in Figure 78 (b).

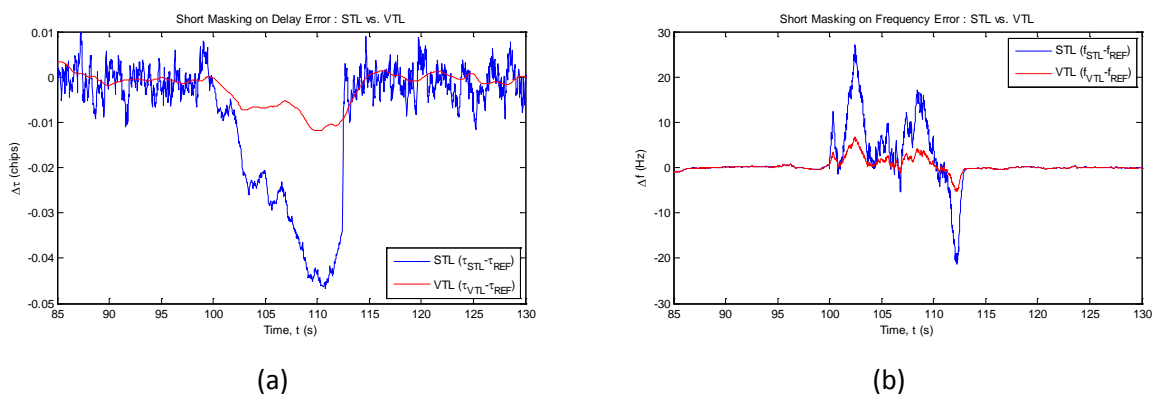


Figure 78: Short masking effect on (a) delay and (b) frequency estimation for both STL and VTL.

On the contrary, in the case of long masking as presented in Figure 79 (a) for the delay and Figure 79 (b) for the frequency, although both approaches suffer from severe performance

degradation, the results obtained with the STL approach are strongly deteriorated. On the other hand, although the performance of the VTL method decreases, the method is still able to estimate the vehicle position with reasonable accuracy. Indeed VTL tracking takes advantage of the other ‘good’ satellites which still provide reliable measurements to the navigator controlling the local NCOs.

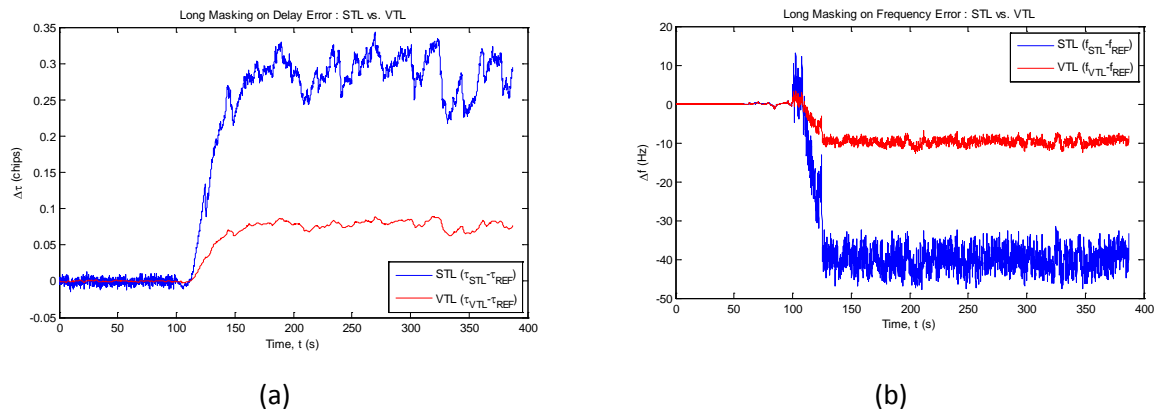


Figure 79: Long masking effect on (a) delay and (b) frequency estimation for both STL and VTL.

Therefore, we can postulate that in the case of masking, the main advantage of the VTL approach, with respect to STL approach is its ability to maintain the tracking loop to be in the operating mode. Furthermore, for long masking scenario, it is also possible for a satellite to be blindly tracked as soon as it appears. Moreover, it is also proved that such architecture allows signals with small C/N_0 to be tracked.

4.6.4 Possible Enhancement of the Current Tracking Architecture

Based on the literature review and on our simulations, we have proposed improved tracking architectures. For both STL and VTL methods, the proposed improvement will address the issues of masking, channel contamination and the benefits of MP detection for improving measurement reliability of the receiver.

a) Satellite availability improvement

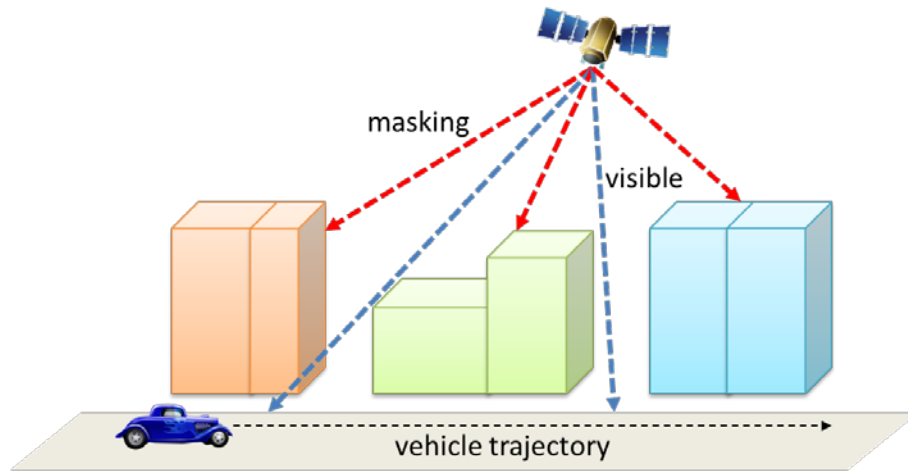


Figure 80: Possible Scenario in Harsh environment – Alternating satellite masking and visibility.

Satellite availability can be further improved by taking advantage of the VTL architecture. Consider a harsh environment scenario depicted in Figure 80. In this scenario, it is possible for the vehicle to experience quick variant of signal masking and visibility for the same satellite. The fact that the NCO is controlled by the NS in the VTL architecture can be exploited in case of signal masking. In this case, the channel that experience outages can blindly track the satellite thanks to the global NS that allow for the local NCO to ‘follow’ the signal based on the global navigation solution. When the same signal is made available again, faster acquisition and tracking can be resumed quickly.

b) MP Detection

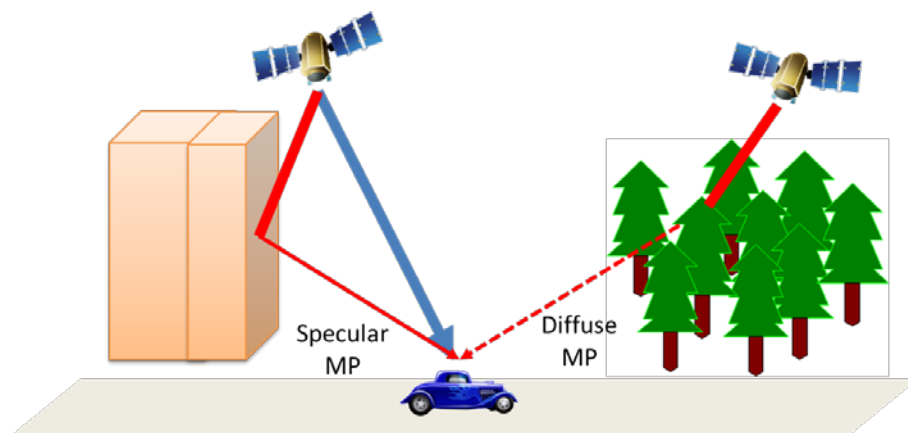


Figure 81: Illustration of Diffuse and Specular MP.

In general, MP can be classified in two different categories referred to as diffuse and specular MP. Both types of MP affect the received signal parameters in different aspects. Therefore, we strongly believe that if the presence and absence of a MP can be detected, a better tracking approach can be implemented. Furthermore, if the type of MP can be efficiently classified, then specific strategies can be proposed to efficiently mitigate their impact with respect to the received signal. As a result, reliable measurements can be provided by the channels to the NS, thus improving the overall tracking performance. This MP characterization will be further discussed in Chapter 5 along with the proposed strategies to address issues caused by these MP.

c) Mitigating measurement contamination

Although VTL improves the performance of tracking thanks to the global navigation solution, they are also significantly subject to the errors affecting each channel. This is the main problem of a VTL architecture where any tracking error in one channel can potentially adversely affect the other channels and lead to an increased degradation in the navigation performance. This is particularly the case in constraint environment where the combined effect of satellite outage and MP causes a lack of integrity in providing reliable measurement to the NS. Therefore, this specific issue on channel contamination will be addressed and discussed in Chapter 5.

4.7 Summary

This chapter was dedicated to formulate various tracking architectures for providing the user PVT. The first architecture discussed was the traditional architecture known as STL. This is the foundation of all tracking algorithm based on a forward only strategy where the channels track the incoming signals independently. Besides that, a vectorial tracking approach was described to further improve the performance of the tracking loop. Various ways on how to implement the VTL architecture were discussed and the advantages and disadvantages of each approach were highlighted. The approach allowing us to take advantage of the navigator solution seems to be of high interest for monitoring the quality of the incoming signal and improving tracking loop performance. On the one hand any navigator aiding bring improvement in terms of availability, as this technique enables low power signal to be tracked. On the other hand, statistical tests can be implemented by considering a priori information on the measurements delivered by the navigator.

The chapter concluded with a performance evaluation of STL and VTL architectures in a controlled environment. VTL based receivers outperform STL based receivers, especially in case of masking or attenuation of the incoming signal. However, VTL approaches are sensitive to measurement contamination, as one channel can adversely affect the other channels. This chapter concluded with the necessity of defining strategy for detecting the presence of MP affecting measurements, mitigating MP effect, or discarding any contaminated channel. This detection is made easier for a VTL based architecture as the test takes advantage of the knowledge of the navigation solution which is elaborated by the navigator.

The contribution of this chapter is the assessment of STL and VTL tracking performances for current architectures. This assessment leads to a proposition for implementing specific VTL architectures that are compatible with the traditional STL architecture allowing a dynamic reconfiguration of the receiver. The specificities of the proposed adaptive tracking algorithm and its implementation will be discussed in Chapter 5.

CHAPTER

5

CHAPTER 5 – Adaptive Vector Tracking Loop (AVTL)

The adaptive vector tracking loop (AVTL) approach is proposed after having thoroughly investigated signal processing characteristics and relevant tracking loop parameters (Chapter 2), the behavior of the signal propagating on the basis of different channel models, especially in the presence of MP (Chapter 3) and different architectures of the receiver tracking stage (Chapter 4). In this chapter related to AVTL, some processing techniques or approaches inside the tracking loops are introduced in order to improve the estimation of the received LOS signal parameters. The main objective is to propose specific processing to enhance tracking loop performance in MP dense environment, in order to provide reliable measurements to the navigator. The major contribution of this work is to show that an adaptive vector tracking scheme (associated with the specific processing to take advantage of the global navigation solution) allows the robustness, the availability and the reliability of the designed receiver to be improved. The improvements resulting from this approach are

analyzed and discussed, focusing on the robustness and the reliability of tracking loops, and of the receiver integrity.

5.1 Urban Environment – Perspective for Adaptive MP Scenarios

MP propagation remains a dominant source of errors in GNSS where it introduces noises and biases which can lead to large errors in position estimates, especially in challenging environments such as urban canyons. Different techniques have been proposed to mitigate MP effects within the receiver tracking loops. The most efficient methods exploit high resolution time-frequency decomposition [58], or channel deconvolution [59]. However, these blind techniques have a high computation complexity.

In general, MP can be classified in 2 different classes: diffuse or specular. In one hand, diffuse MP is the result from physical scattering phenomena and sources of diffraction. Consequently, in a rich scattering scenario, the number of MP components is considered too large to be individually resolved. The diffuse MP will cause the signal to be spread in the frequency domain, degrading the C/N_0 ratio. In practice, the estimation of the C/N_0 ratio allows for this degradation to be taken into consideration. On the other hand, specular MP is the effect of discrete, coherent reflections from smooth surfaces. This phenomenon can be observed when the vehicle remains at the same location, or moves along a building which is parallel to the vehicle motion. The specular MP however is concentrated in the delay-frequency domain. Such MP introduced bias on the PR estimates when the MP frequency is within the carrier tracking loop bandwidth.

In the context of AVTL, the integrated navigation solution (which can also benefit from the use of other complementary sensors) can be harnessed to improve GNSS signal tracking in the presence of MP. This study considers slow fading channels for which MP effects can be classified in two main categories depending on the value of the MP frequency with respect to the LOS signal. When the vehicle moves with an inclination with respect to the reflecting surfaces, we can observe that the support of the Doppler spectrum is broadened. In this case, signal decorrelation can be performed in the frequency domain. On the contrary, when the vehicle is stationary or moves in the direction of the reflecting surfaces, the MP and direct path (DP) frequencies have the same value. Thus the signal decorrelation must be addressed in the time domain.

In this study, we propose two (2) different MP mitigation approaches which both involve the detection of MP presence. The first approach consists of detecting and discarding any channel in the context of multi GNSS constellation. However, in urban canyon this technique can strongly affect the geometry dilution of precision (GDOP). The other approach aims at mitigating MP effect within the AVTL in order to reduce the impact of the MP on PR measurements, allowing this measurement to be used in a robust Kalman filter (KF). Besides that, we also propose a blind tracking approach that allows the signal to be tracked in case of signal masking. This method allows a signal to be acquired as soon as the satellite returns visible, improving satellite availability.

5.2 Time-Frequency Processing

The basic stage of the receiver is the matched filter which performs the correlation of the incoming signal with a local replica to provide the in-phase (I) and the quadrature-phase (Q) samples, which has been elaborated in Chapter 2. The output of this stage was described in Chapter 2 in nominal conditions and in the Chapter 3 in presence of MP. In particular the expression of the correlator output was defined in (3.3) as:

$$u_z(k) = I(k) + jQ(k) = \sum_{l=0}^L A_{l,k}(\Delta f_{l,k}) R(\Delta\tau_{l,k}) \exp(j\Delta\varphi_{l,k}) + n_k \quad (5.1)$$

where $l = 0$ is representing the DP. Except for specific applications where the system is able to use some information about the environment, MP acts as an interference affecting the LOS signal yielding the following correlator output:

$$u_z(k) = A_{0,k}(\Delta f_{0,k}) R(\Delta\tau_{0,k}) \exp(j\Delta\varphi_{0,k}) + \sum_{l=1}^L A_{l,k}(\Delta f_{l,k}) R(\Delta\tau_{l,k}) \exp(j\Delta\varphi_{l,k}) + n_k \quad (5.2)$$

where the parameters $\Delta\tau_{l,k}$, $\Delta f_{l,k}$ and $\Delta\varphi_{l,k}$ are the mean errors (i.e., the difference between the parameters of the received signal and the parameters of the locally generated replica) of the code delay, the signal frequency and the carrier phase. Note that $A_{l,k}$ is the amplitude of the l^{th} path signal and $R(\cdot)$ denotes the spreading code autocorrelation function.

The aim of the approach presented in this chapter is to reduce the impact of MP. The solutions that are explored here are based on a channel analysis that was carried out in Chapter 3. This chapter points out that some MP that are spread in frequency domain, can be mitigated using filtering techniques. On the other hand MP that are concentrated in the frequency domain around the LOS frequency impact strongly the receiver. We propose here different approaches to mitigate MP errors in the frequency domain and in the time domain, in the framework of a VTL based receiver.

5.2.2 Frequency Analysis

Frequency analysis is performed in a VTL context, i.e., when the NCO that is used to generate the local replica is controlled by the navigator. The parameters describing the LOS components ($\Delta f_0, \Delta \tau_0$) in equation (5.2) are defined from the navigator outputs. For the satellite with the index m we obtain:

$$\Delta \tau_0 = \tau_0 - \hat{\tau}_0 \quad \text{with} \quad \hat{\tau}_0 = \frac{LOS_m^T|_{r=r^{NS}}}{\lambda_c} (\mathbf{r}^{NS} - \mathbf{r}_m) + \frac{b}{\lambda_c} \quad [\text{chips}] \quad (5.3)$$

$$\Delta f_0 = f_0 - \hat{f}_0 \quad \text{with} \quad \hat{f}_0 = -\frac{LOS_m^T|_{r=r^{NS}}}{\lambda_{L_1}} (\mathbf{v}^{NS} - \mathbf{v}_m) - \frac{d}{\lambda_{L_1}} \quad [\text{cycles/s}] \quad (5.4)$$

where $\hat{\tau}_0$ and \hat{f}_0 are the estimated delay and frequency of the navigators. Under the assumption that the integrity of the receiver is ensured, we can admit that $E\{\Delta \tau_0\} = 0$ and $E\{\Delta f_0\} = 0$. Furthermore, since the tracking loops and the navigator behave as a low pass filters, the variance of these parameters depends not only on the quality of the incoming signal, but also on the tracking loop and navigator description.

It is important to note that the assumption $E\{\Delta \tau_0\} = 0$ and $E\{\Delta f_0\} = 0$ can be done if the navigator order copes with the receiver dynamic. Indeed a position velocity based model will be appropriate to low dynamic models. Higher dynamic will need a larger order or the use of an Inertial Model Unit (IMU). Similarly, the features of the local oscillator must be considered, as the oscillator can affect the frequency observation over the 1s observation duration. An FFT is performed, under this assumption, at the prompt correlator output. The FFT exhibits a peak about the zero frequency

whose amplitude depends on the LOS power. The implementation for frequency-domain detector of this stage is represented in Figure 82.

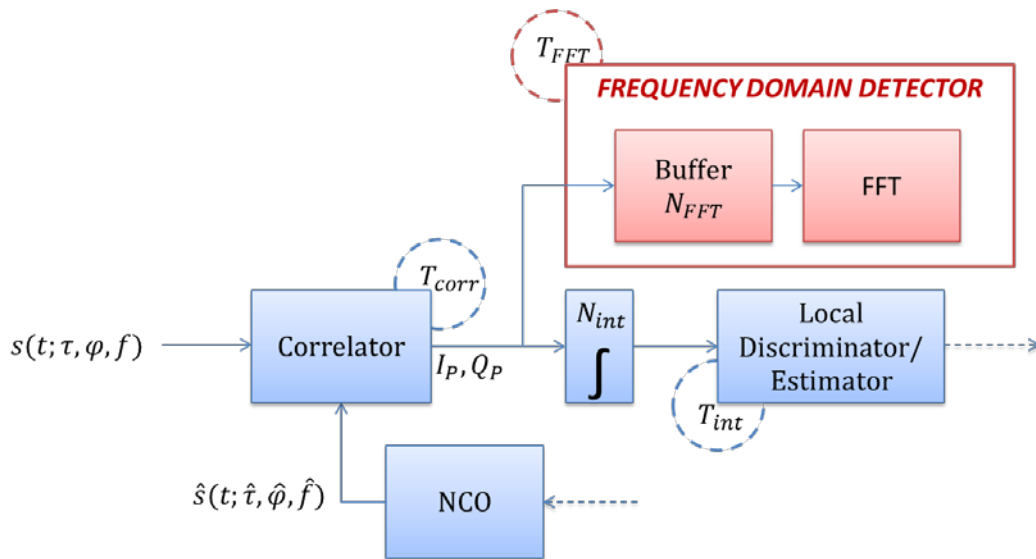


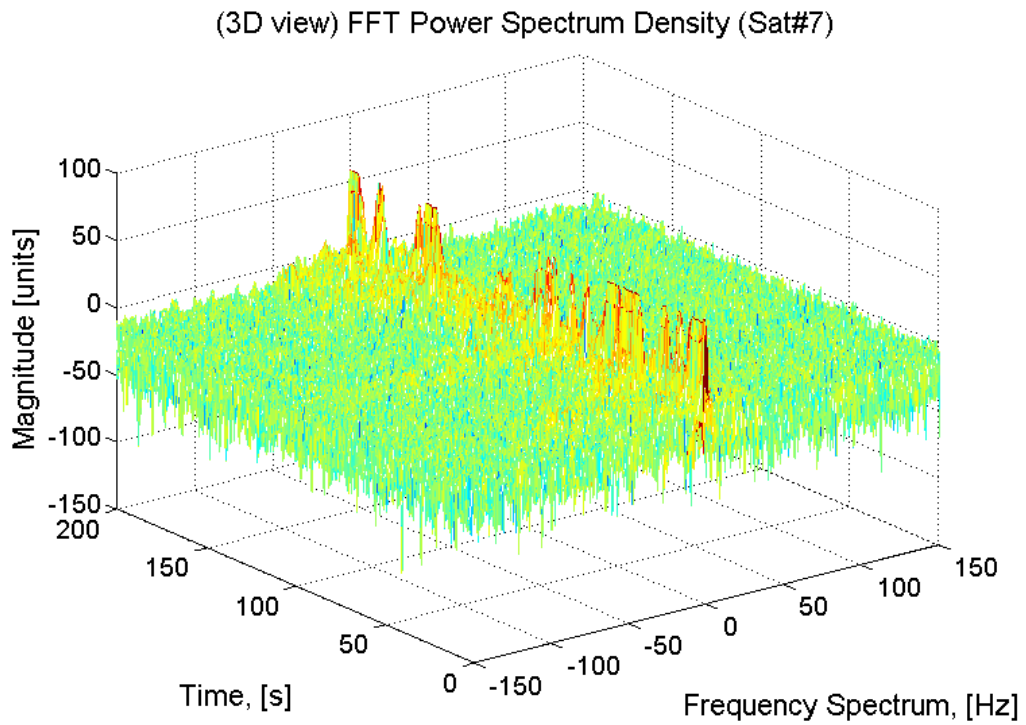
Figure 82: Implementation of the frequency-domain detector in GNSS receiver.

a) Spectral resolution

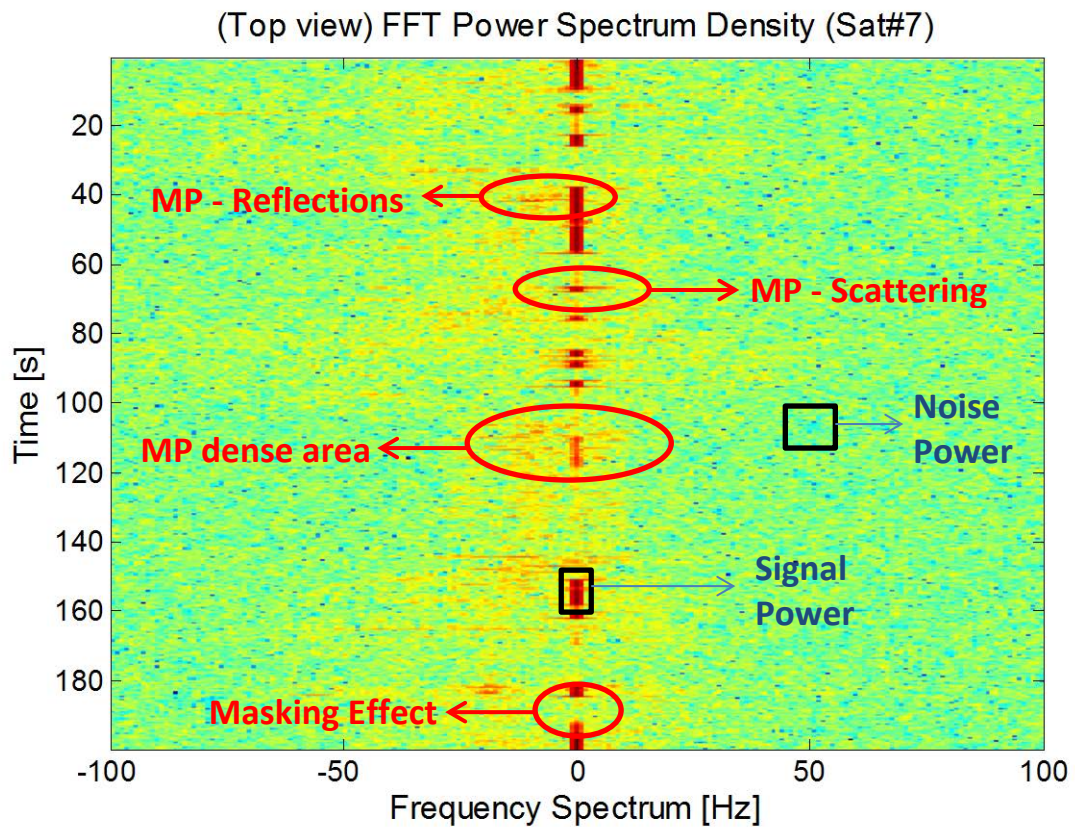
In the context of this receiver the basic correlation of the incoming signal with the local replica is performed over a correlation time, T_{corr} . A longer integration time will be obtained by cumulating coherently these basic correlations in order to obtain an integration time, $T_{int} = N_{int} \cdot T_{corr}$. For performing the FFT the basic correlator output is considered. The choice of the length of the FFT is made in order to obtain a frequency resolution of $1Hz$. As the basic correlation time is $10ms$, the FFT is set to $N_{FFT} = 128$ points. Moreover zero padding is performed to extrapolate the FFT output in the frequency domain, i.e.,

$$\Delta f_{step} = \frac{1}{T_{FFT}} = \frac{1}{N_{FFT} \cdot T_{corr}} \sim 1Hz. \quad [Hz] \quad (5.5)$$

For a given scenario which is considered experiencing harsh condition, the FFT of the prompt correlator output is represented in Figure 83. Figure 83 (a) is a 3D representation of the FFT power spectrum density and Figure 83 (b) is the top view of the same simulation where different MP conditions have being considered.



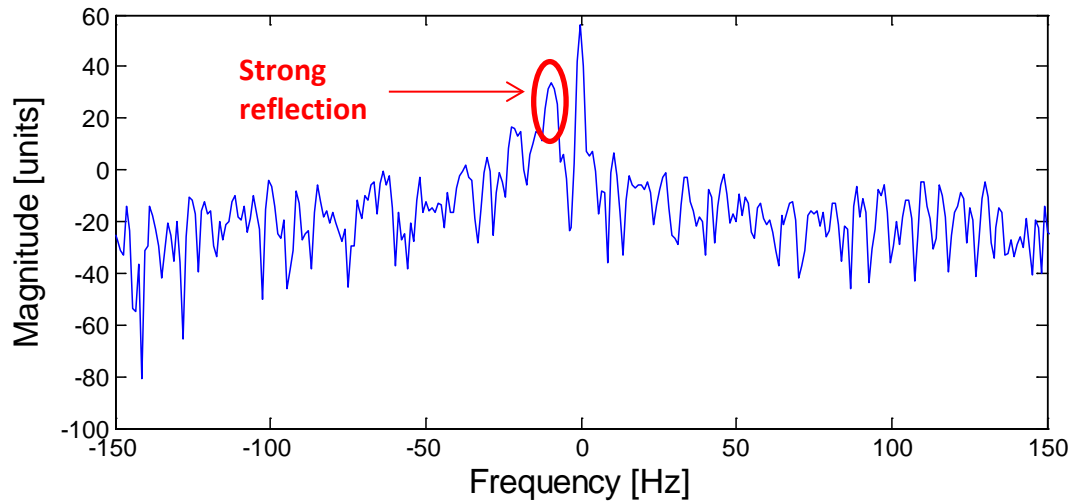
(a)



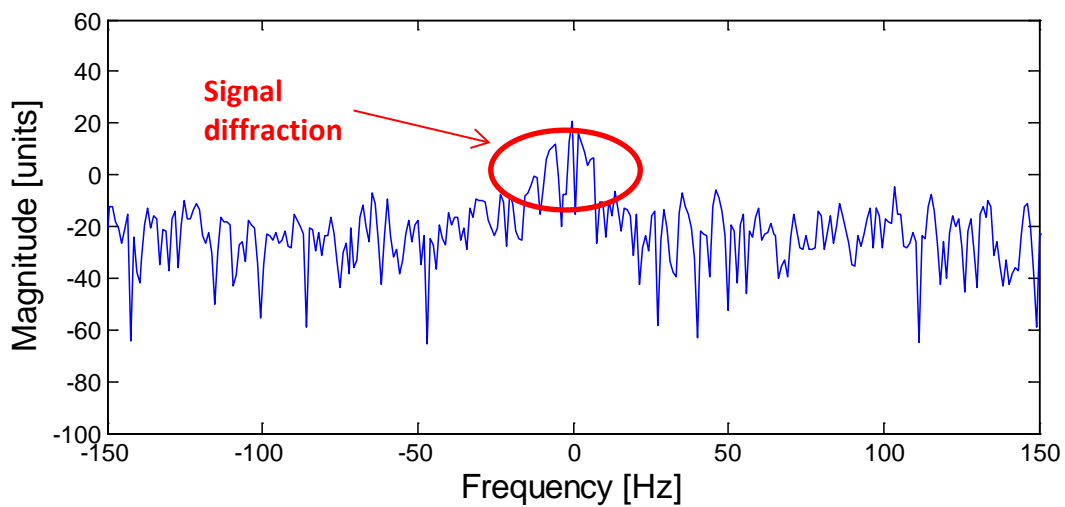
(b)

Figure 83: FFT output for a given scenario.

Figure 84 shows that under strong MP reflection ($f_1(t) \neq f_0(t)$), peaks can be observed in the frequency domain. These peaks are represented in Figure 84 (a) and (b) for strong MP reflections and scattering conditions respectively.



(a) Strong MP reflections



(b) Scattering MP condition

Figure 84: Frequency spectrum of different MP conditions

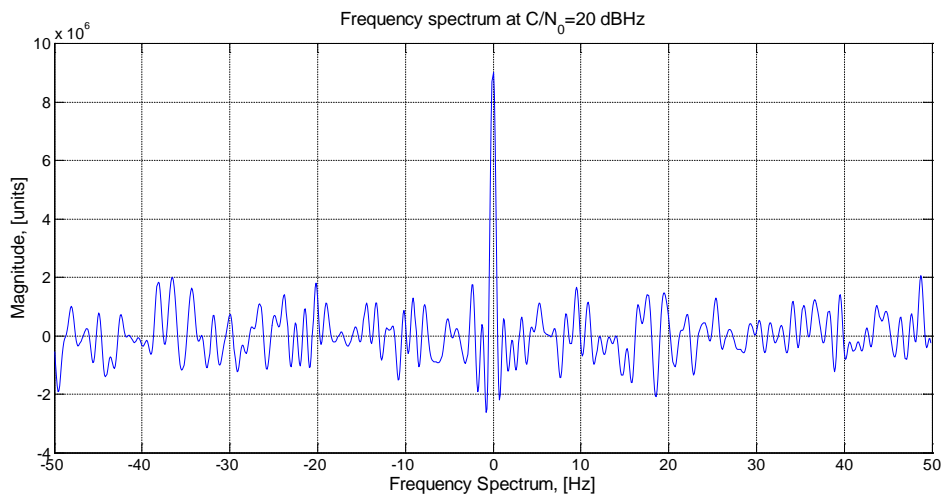
This representation can easily be used to detect masking effect, as the presence of LOS influences the PSD shape around the zero frequency. Compared to a simple C/N_0 estimator, this approach allows an NLOS signal which is not at the LOS frequency to be discarded. Moreover this representation allows the C/N_0 and $C/(N_0 + I)$ to be estimated (where N_0 represents the white noise power and I the interference power) as a function of the bandwidth [29]. This knowledge of

the ratio $C/(N_0 + I)$ expressed as a function of the receiver bandwidth will be used to set the integration time ($T_{int} = N_{int} \cdot T_{corr}$) and tracking loop bandwidths in order to reduce MP effects. In that case, the main limitations are the vehicle and the oscillator stress.

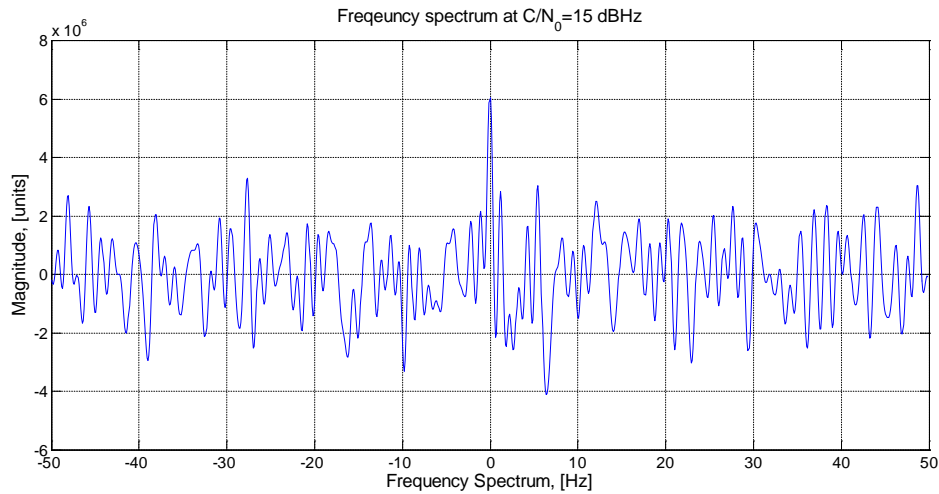
b) DP signal power

An important use of the FFT representation is to detect signal masking. Many studies have suggested that a value of 40dBHz for C/N_0 is considered nominal for GNSS signal. In practice signal with lower C/N_0 ratio can be tracked. For example the tracking threshold of a conventional DLL is 11dBHz . At this level the standard deviation of the delay error is about 100 meters when the integration time and the DLL bandwidth are respectively set to 20ms and 2Hz . In the same way, the phase can be tracked for a C/N_0 ratio higher than 25dBHz , when the PLL bandwidth is set to 20Hz .

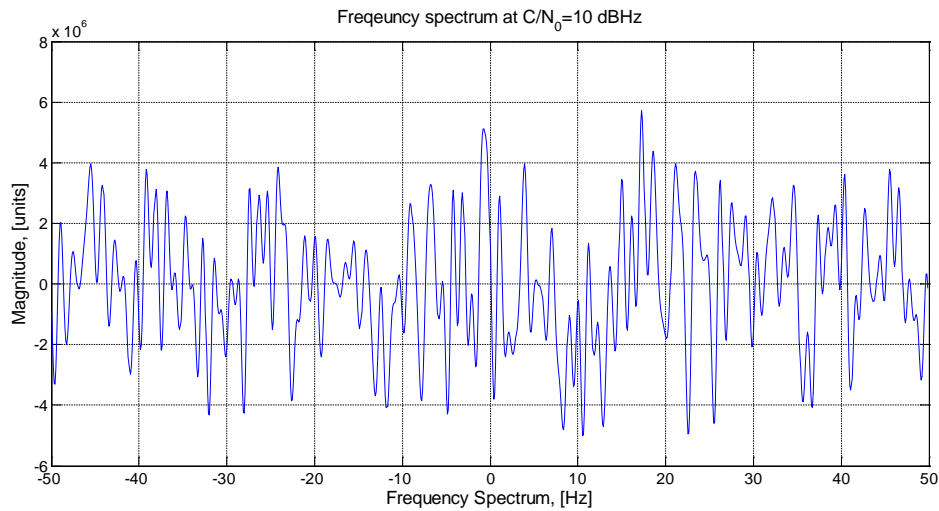
Here we propose to look at the impact of C/N_0 ratio on the FFT representation. A simple analysis as presented in Figure 85 shows that this technique allows LOS signal with a C/N_0 ratio higher than 15dBHz to be detected. Signals with lower C/N_0 ratio will be considered as masked. The expected outcome of this test is to provide values of C/N_0 that can be considered for monitoring purposes by the frequency-domain detector. When the C/N_0 of the incoming signal is reduced, we can see that the noise floor is higher. As a result, it is very difficult to identify the LOS signal.



(a) $C/N_0 = 20\text{dBHz}$



(b) $C/N_0 = 15\text{dBHz}$



(c) $C/N_0 = 10\text{dBHz}$

Figure 85: FFT response for different values of C/N_0 .

c) Non-coherent multipath frequencies

Another use of this representation could be to track NLOS signals whose frequencies differ from the LOS frequency, as demonstrated in Figure 86. However, tracking this signal could be of interest only if a 3D representation of the environment is available. In that case the NLOS could be used if this 3D representation allows the NLOS path to be constructed. It is not the purpose of this study.

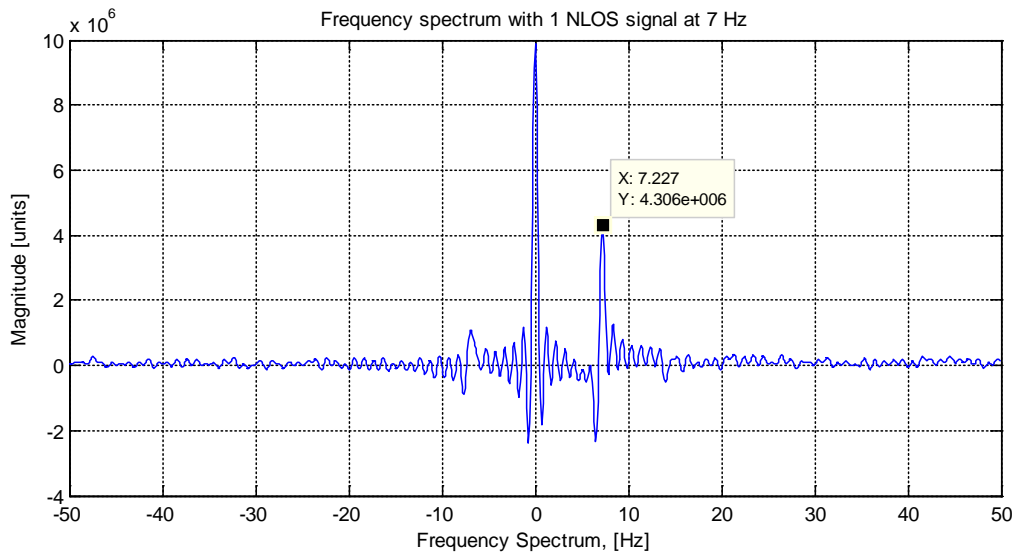


Figure 86: Frequency spectrum with the presence of non-coherent MP.

5.2.3 Time-Delay Analysis

The previous frequency analysis has shown that a MP located out of the LOS band can be mitigated by configuring the coherent integration time and by using as appropriate tracking loop bandwidth to obtain the required $C/(N_0 + I)$ ratio. This approach allows the receiver robustness to be improved, by making the tracking of the LOS signal easier in the absence of interference and by reducing the impact of this interference if necessary. By using a vector DLL architecture, only the vehicle stress and the local tracking loop stress have to be considered. Improvement can result from the use of an inertial Navigation System, and of a stable oscillator based on an OCXO technology.

In the frame of this study we propose two approaches to address the issue of coherent MP. The basic one supposes that the number of available satellite should increase in a near future. Using a multi-constellation receiver, enable GPS, Glonass, Beidou Compass, and Galileo to be tracked, and should guarantee a good GDOP by selecting the most relevant satellites, i.e. the satellites are not contaminated. However, in deep urban canyon, the number of visible satellites can significantly decrease. In that case decorrelating in the time domain is necessary. However, it is not an easy task since MP relative delays are very small in this kind of environment. In order to address this issue, two main classes of techniques were explored. The first uses a Bayesian in which a dynamic model of the parameter is available [36]. This approach is not efficient for fast time varying environment. The other approach considers samples of a stationary interval. The most efficient methods use high

resolution time-frequency decomposition [58] or channel deconvolution [59]. Techniques based on a MP estimating delay locked loop have also been considered. These methods have high computational load and their robustness has not been always clearly proved.

In the present study we propose to use a narrow correlator in the context of a VDLL tracking loop. From the MP error envelope (MEE) provided in Chapter 3, we acknowledge that the early (E) and late (L) spacing of the DLL discriminator provide a significant improvement in the code delay tracking performances. By reducing the E and L spacing, the coherent MP can be easily mitigated to the detriment of the robustness in comparison with discriminators based on larger spacing. Here we propose to switch dynamically between 3 discriminators that can be designed from a set of 6 correlators as illustrated in Figure 87. The appropriate discriminator will be chosen depending on the presence or the absence of MP.

In case of MP, the value of the chip spacing (CS), represents the delay in chips between two correlators, will be deduced, in a VTL complex, from the state of the navigator. The other parameters which impact the choice of the chip spacing that are the oscillator stress and the vehicle stress that are considered as constants. The main advantage of the VTL architecture in this context is to reduce the stress on the estimated delay, especially for a low C/N_0 ratio. Indeed, while the error on the estimated delay is strongly related to this ratio in an STL approach, this error can be reduced in a VTL approach which takes advantage of other measurements.

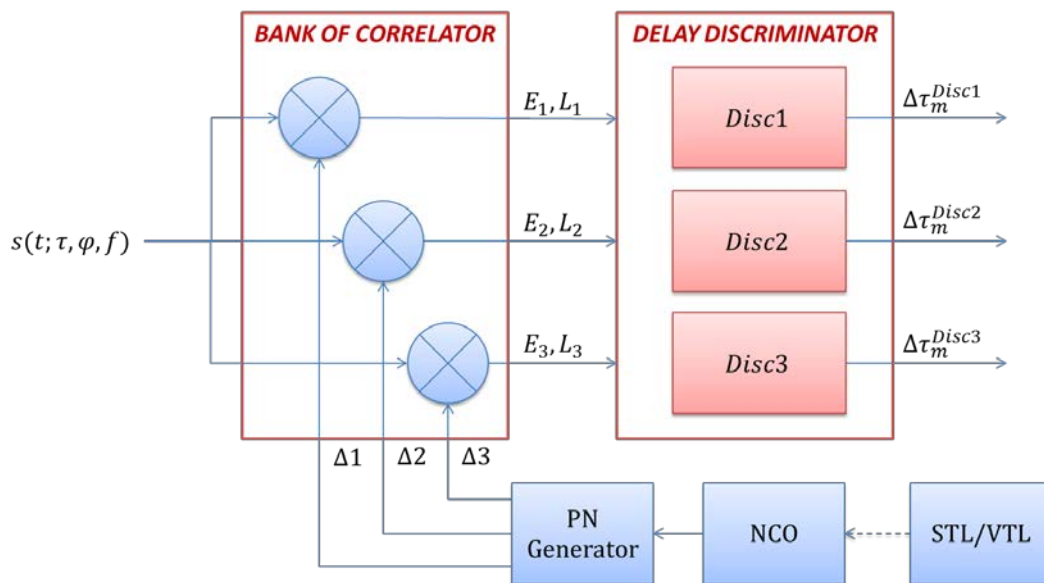


Figure 87: Implementation for Multiple Delay Discriminator approach.

a) Discriminator function responses

By using a bank-of-correlators with different spacing values between Early and Late correlators, we can perform different types of discriminator function such as the early-minus-late (*EML*), and Double Delta ($\Delta\Delta$) discriminators. This multiple discriminator approach was introduced in [28] where it is used to estimate accurately the presence of coherent MP. Here we propose to perform four different discrimination functions from the correlator outputs. Indeed a conventional *EML* discriminator can be obtained, as well as two $\Delta\Delta$ which differ from the chip spacing value. A $\Delta\Delta$ discriminator is used because of the good MP rejection performance as presented in [60]. Moreover, the use of a bank-of-correlators allows for $\Delta\Delta$ to be easily implemented.

The *EML* discriminator function is based on the non-coherent *EML* normalized envelope [1] which has been presented in Chapter 2, Table 3. The main difference is in the choice of the chip spacing where instead of using traditional 1-chip spacing, 0.4 chip spacing is being used instead. The $\Delta\Delta$ discriminator used five correlators arms (Very Early (*E2*), Early (*E1*), Prompt (*P*), Late (*L*) and Very Late (*L2*)) instead of the traditional *E,P,L* correlators. Here, we proposed to use 7 correlators arm to construct two $\Delta\Delta$ discriminators. Under ideal condition, the expression of each arm for the autocorrelation can be defined as:

$$\begin{aligned}
 P(\Delta\tau) &= R(\Delta\tau) \\
 E3(\Delta\tau) &= R(\Delta\tau + 2\Delta) \\
 E2(\Delta\tau) &= R(\Delta\tau + \Delta) \\
 E1(\Delta\tau) &= R\left(\Delta\tau + \frac{\Delta}{2}\right) \\
 L1(\Delta\tau) &= R\left(\Delta\tau - \frac{\Delta}{2}\right) \\
 L2(\Delta\tau) &= R(\Delta\tau - \Delta) \\
 L3(\Delta\tau) &= R(\Delta\tau - 2\Delta).
 \end{aligned} \tag{5.6}$$

The *EML* discriminator output is defined as:

$$S^{EML}(\Delta\tau) = E3(\Delta\tau) - L3(\Delta\tau). \tag{5.7}$$

The $\Delta\Delta$ expressions which are based on High Resolution Correlator (HRC) presented in [60] can be expressed in the form of *EML* discriminator functions, whose detector functions $S^{\Delta\Delta 1}$ and $S^{\Delta\Delta 2}$ are given by:

$$S^{\Delta\Delta 1}(\Delta\tau) = E1(\Delta\tau) - L1(\Delta\tau) - \frac{1}{2}(E2(\Delta\tau) - L2(\Delta\tau)) \quad (5.7)$$

$$S^{\Delta\Delta 2}(\Delta\tau) = E2(\Delta\tau) - L2(\Delta\tau) - \frac{1}{2}(E3(\Delta\tau) - L3(\Delta\tau)). \quad (5.8)$$

In practice the value of Δ is chosen depending on the sampling frequency of the incoming signal. Here we choose $\Delta = 1/10$, by considering high sampling frequencies ($\geq 20\text{MHz}$).

The performance of the discriminators can be evaluated by using the MEE approach which has been elaborated in sub-chapter 3.2.1. The MEE for delay discriminator proposed in this work is presented in Figure 88 with a zoom view for short delay MP for the chosen MEE is presented in Figure 89. This simple analysis of the MEE shows that the error can be reduced to approximately 30m, 15m, 5m depending on the CS value used for the discriminator functions.

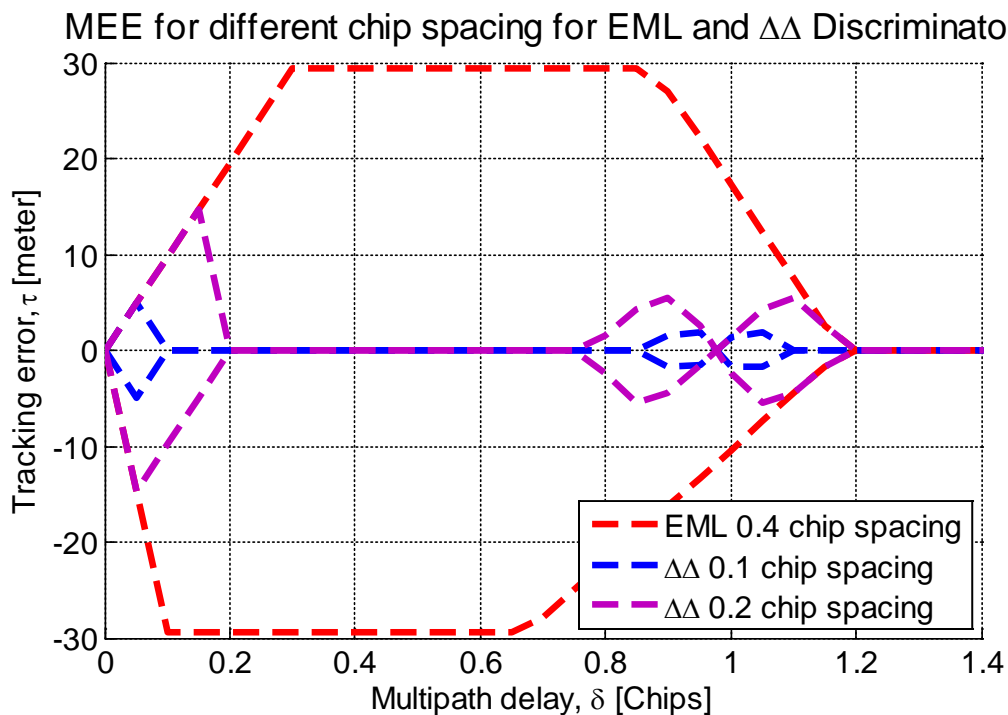


Figure 88: MEE of different discriminator functions and values of chip spacing.

(Zoom) MEE for different chip spacing for EML and $\Delta\Delta$ Discriminator

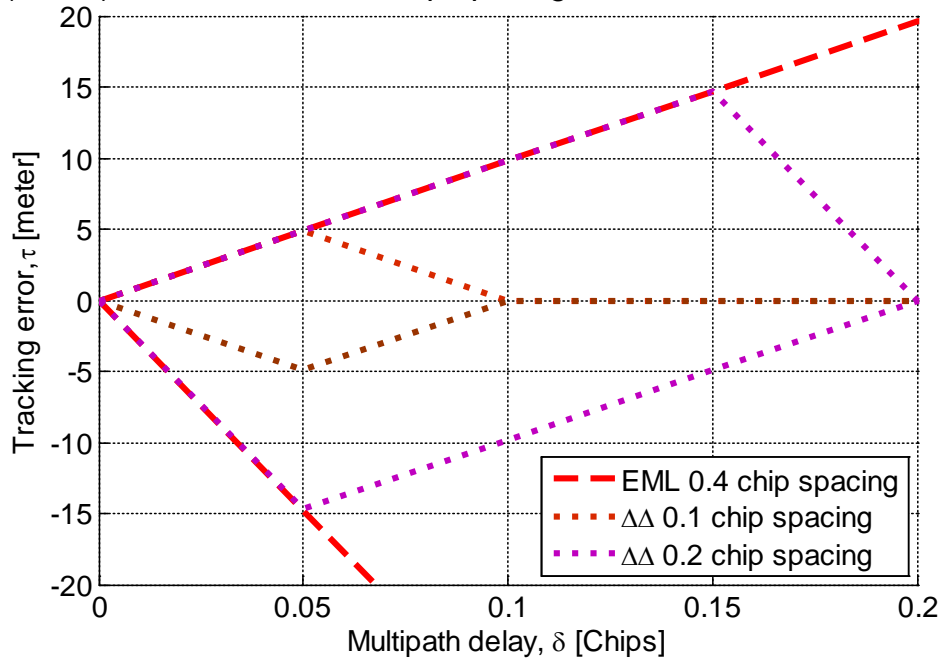


Figure 89: Zoom for the MEE within short-MP ranges.

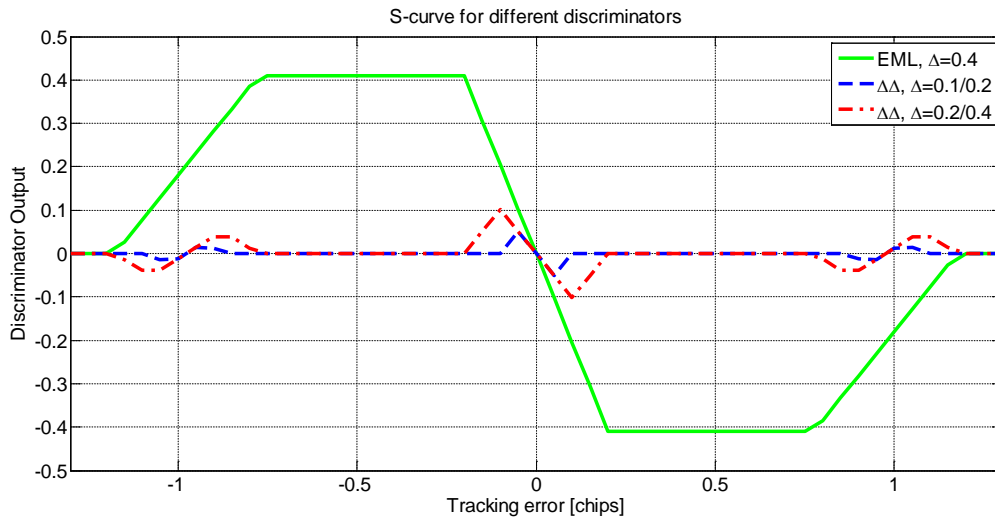
Finally we have to consider the impact of the discriminator on the tracking threshold. In practice this threshold depends on the operating range of the discriminator which is related to the value of the chip spacing of the correlators. In [1] a rule-of-thumb threshold is given:

$$3\sigma_{\tau} + R_e \leq \frac{D}{2}. \quad (5.9)$$

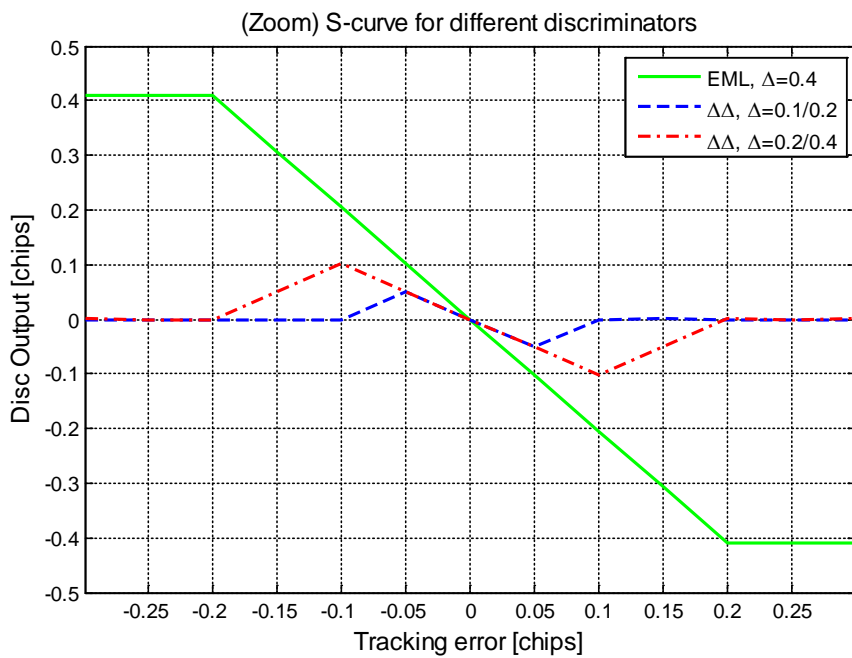
In this expression σ_{τ} is the 1-sigma code tracking error, R_e is the dynamic stress error, and D is the discriminator operating range.

Here we consider that the estimator order allows the dynamic stress error to be neglected. In that case the operating mode must be adapted to the 1-sigma code tracking error. This error depends on the performance of the local estimator local in an STL architecture. It depends on the navigator performance in a VTL architecture. An analysis of the code tracking error will be provided further.

b) S-curve for the different discriminators



(a)



(b)

Figure 90: S-curve for different discriminator functions.

The representation in Figure 90 (a) shows the discriminator output as a function of the delay error $\Delta\tau_0$, by considering only the LOS signal for the 3 different discriminators where the zoom around the zero-crossing is depicted in Figure 90 (b). As expected the range of the discriminator is related to the CS value, showing that the use of a narrow discriminator requires the NCO stress to be reduced.

5.3 Adaptive Tracking Architecture and Implementation

The proposed adaptive tracking is mainly focused on the improvement of the local tracking loop in order to ensure reliable measurements to the NS. The high-level architecture is illustrated in Figure 91 and the detailed description is shown in Figure 92. Note that the estimated parameters provided by each channel in Figure 91 are identified by (\sim) whereas the estimated parameters provided by the NS are identified by (\wedge).

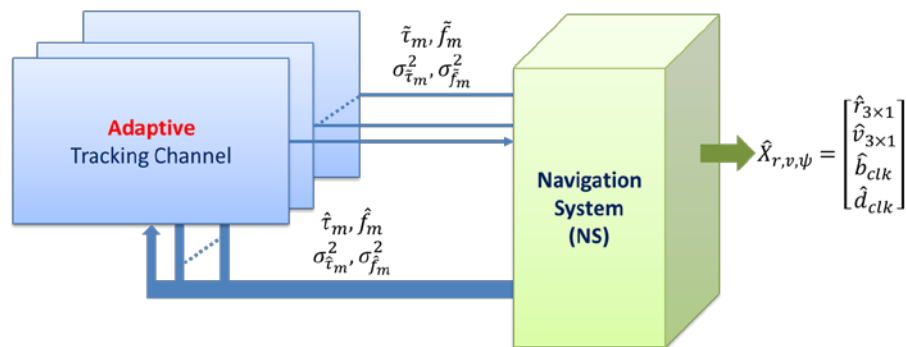


Figure 91: High-level description of the adaptive tracking architecture.

Based on Figure 92, there are four additional elements compared to a conventional tracking loop which offers performance enhancement for signal tracking. The monitoring module which monitors the health of the measurements is on the basis of two MP detectors. A frequency-domain detector is used for detecting the presence of the direct path. It is based on a frequency analysis which allows the integration time to be computed for guaranteeing a minimum ratio signal power over noise+interference power ($C/(N_0 + I)$). As the frequency detector is not able to detect and decorrelate an NLOS signal at the direct path frequency, a time domain detector is used to detect any MP interference that occurs at the DP frequency. The output of these detectors are analysed and used by the control module for managing the tracking parameters and the loop configuration.

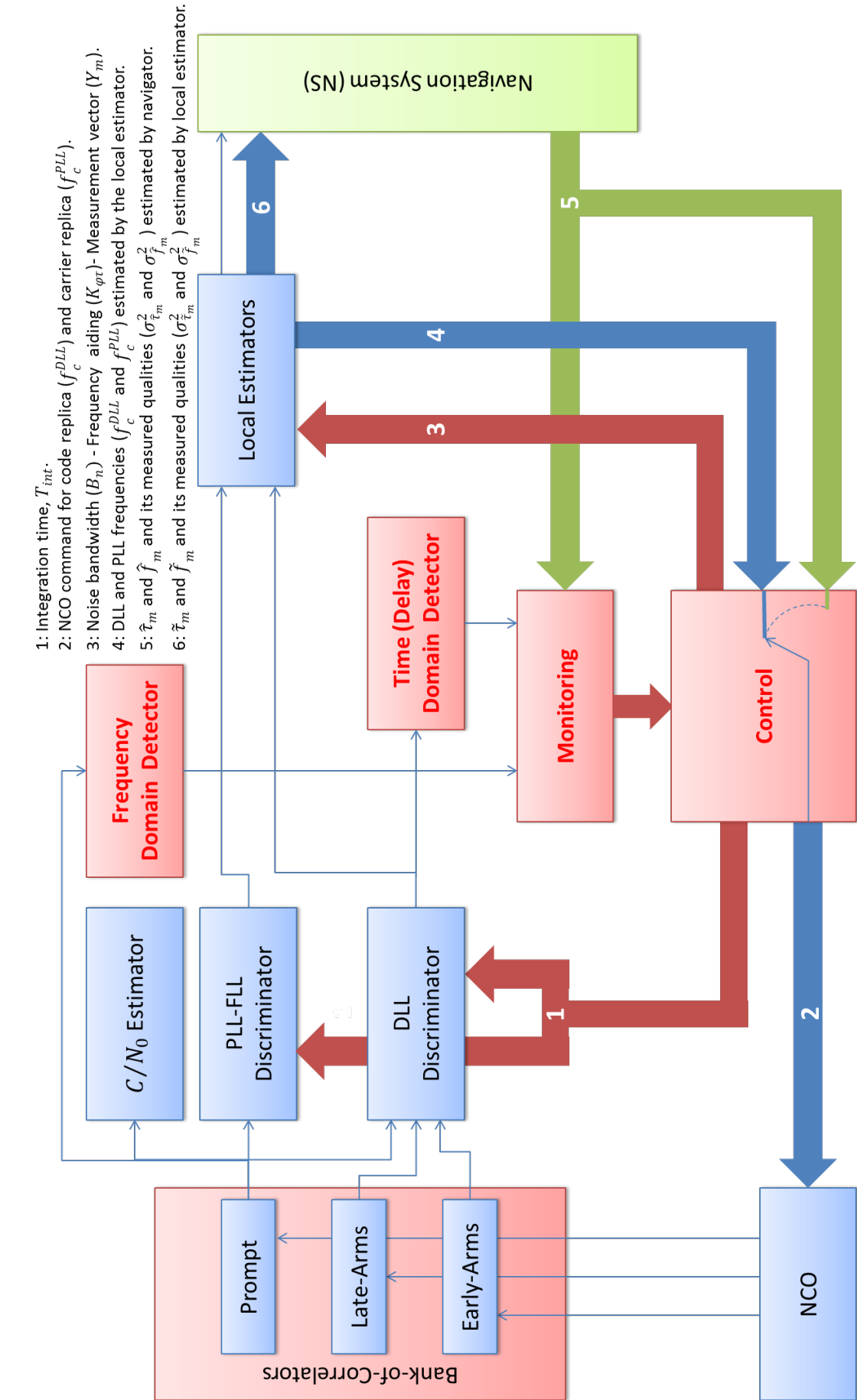


Figure 92: Proposed Adaptive Tracking Architecture.

The core of the architecture is the NS. Here a simple model is used and the state vector includes the position and the velocity of the vehicle. The navigator rate is set to $1/T_{NS}$. For high dynamic of the receiver, the “dynamic stress” can be reduced by increasing the navigator rate, or the navigator order. Especially a position, velocity, acceleration model will allow the impact of an acceleration stress to be reduced. A significant improvement can also be obtained by integrating an inertial navigation system to the receiver. The state vector which includes the vehicle position and velocity is estimated based on EKF that uses observations provided by each tracking channel. The main change compared with a conventional receiver is that adaptive tracking loops are proposed here to provide the observations used by the receiver. When a channel is switched in an STL mode, local estimators perform PR and DR estimation in a standalone mode (i.e., without using the navigator). In a VTL configuration, the navigator is used in a navigator-assisted tracking approach.

In a VTL approach, in comparison with a conventional receiver, the navigator, when it operates properly, provides complementary outputs that are used to control the NCO which delivers a replica of the incoming signal for each of the available channels. Configurable discriminators allow the receiver to measure the phase errors of the different channel carriers, and to compare the frequency and the propagation delay of the incoming signal to those computed from the velocity and the position estimated by the NS. Finally, these observations are used inside the local estimators. In this cascade approach, reliability enhancement comes from the statistical tests that are used to ensure the integrity of the measurements that are delivered at the NS input. Compared to a conventional forward approach that uses PR and DR measurements delivered by the STL, this approach allows higher rate processing. Whereas a conventional receivers performs statistical test at the navigator rate, this approach allows tests to be achieved at the tracking loop rate. It should be noted that a vehicle, whose velocity is $36km/h$, moves over $10m$ during $1s$. Consequently MP interference is a non-stationary effect.

5.3.1 Navigation System

The NS estimates the vehicle position and velocity and the receiver clock bias and drift. The simple system model investigated in this study assumes weak dynamics for the vehicle and negligible receiver clock stress. Applications involving higher dynamics would require the use of an inertial navigation system for increasing NCO input rates and an error-state “cascaded filtered integration” architecture as in [61].

a) System model

The system model is adopted from the one that has been defined in 4.3.2, equations (4.20) through (4.27). Here, the state equation \hat{X}^{NS} is recalled

$$\hat{X}_{k+1}^{NS} = \Phi^{NS} \hat{X}_k^{NS} + w_k \quad (5.10)$$

where $X^{NS} = [r_E \ v_E \ r_N \ v_N \ r_U \ v_U \ b_{clk} \ d_{clk}]^T$, Φ^{NS} is the state transition matrix and w_k is the process noise vector depending on the vehicle dynamic and on the receiver clock noise representation. Besides that, it is interesting to note that for the NS, the navigator rate ($1/T_{NS}$) is adapted to the vehicle dynamic.

b) Observation model

Local estimator outputs are used as measurements in order to update the NS as illustrated in Figure 92. These outputs include the frequency and propagation delay which are related to the velocity and the position that are parts of the NS state vector. Thus the measurement vector is defined as

$$Y^{NS} = [Y_1^{NS} \ \dots \ Y_m^{NS} \ \dots \ Y_{N_{sat}}^{NS}]^T + v \quad \text{with } 1 \leq m \leq N_{sat} \quad (5.11)$$

where $Y_m^{NS} = \begin{bmatrix} \tilde{\tau}_m \\ \tilde{f}_m \end{bmatrix}$ is constructed from the local estimator outputs, and v is the observation noise which is defined from the variance of the local estimator outputs ($\sigma_{\tilde{\tau}_m}^2, \sigma_{\tilde{f}_m}^2$). The propagation delay (expressed in chips) is related to the estimated location as follows

$$\tilde{\tau}_m = \frac{1}{\lambda_c} [LOS_m^T \cdot (\mathbf{r} - \mathbf{r}^{NS}) + b_{clk}] + v_\tau \quad (5.12)$$

where $\lambda_c = c/R_c$ (c is the speed of light and R_c is the chip rate) represents the code wavelength and LOS_m is the LOS vector associated with the m^{th} satellite defined by equation (4.10). On the other hand, the frequency error (expressed in cycle/sec) is similarly related to the error of the estimated velocity via the following relation

$$\tilde{f}_m = -\frac{1}{\lambda_{L_1}} [LOS_m^T \cdot (\mathbf{v} - \mathbf{v}^{NS}) + d_{clk}] + v_f \quad (5.13)$$

where $\lambda_{L_1} = c/f_{L_1}$ is the carrier wavelength. As stated in the previous chapter, the measurement noise vector depends on the parameters of the local estimators. For each channel, the error variance of Y_m^{NS} is computed by considering the signal power to noise power spectrum density (C/N_0) ratio of the m^{th} incoming signal, the estimator bandwidth, the discriminator function and its output rate as described by (2.26) and (2.31) for the frequency and delay respectively.

c) Navigation System outputs

The NS computes estimates of the state vector \hat{X}_k^{NS} (containing the vehicle state and the receiver clock bias and drift) and of the corresponding covariance matrix \hat{P}_k^{NS} by using a conventional EKF. It also delivers the parameters used for generating replicas of the received signals that are being tracked. The required parameters, which are the estimated propagation delay and the Doppler frequency of each satellite, have been defined in Section 4.5.2 by equation (4.55) through (4.58) when we proposed to use the NS solution presented in Chapter 4. The estimated propagation delay and Doppler frequency for each satellite can be obtained from the estimated vehicle location and velocity by these relationships:

$$\hat{t}_m = \frac{1}{\lambda_C} [LOS_m^T \cdot (\mathbf{r}^{NS} - \mathbf{r}^m) + b_{clk}] \quad (5.14)$$

$$\hat{f}_m = -\frac{1}{f_{L_1}} [LOS_m^T \cdot (\mathbf{v}^{NS} - \mathbf{v}^m) + d_{clk}] \quad (5.15)$$

Moreover, under the assumption of a Gaussian distribution for the state vector, the standard deviations of the estimates (\hat{t}_m, \hat{f}_m) are also computed and are used to build statistical tests inside the local estimators. These standard deviations are defined as

$$\sigma_{\hat{t}_m} = \sqrt{H_{2m-1} P^{NS} H_{2m-1}^T} \quad (5.16)$$

$$\sigma_{\hat{f}_m} = \sqrt{H_{2m} P^{NS} H_{2m}^T} \quad (5.17)$$

where P^{NS} is the error covariance matrix associated with the NS state vector, and H_{2m-1} , H_{2m} are respectively the $(2m - 1)^{th}$ and the $(2m)^{th}$ lines of the observation matrix H^{NS} . The matrix H^{NS} , which is constructed from the equations (5.10), (5.11) and (5.12), is defined as:

$$H^{NS} = \begin{bmatrix} \frac{LOS_1^T}{\lambda_c} & 0 & \dots & \frac{1}{\lambda_c} & 0 \\ 0 & -\frac{LOS_1^T}{\lambda_{L_1}} & \dots & 0 & -\frac{1}{\lambda_{L_1}} \\ \vdots & \vdots & \dots & \vdots & \vdots \\ \frac{LOS_m^T}{\lambda_c} & 0 & \dots & \frac{1}{\lambda_c} & 0 \\ 0 & -\frac{LOS_m^T}{\lambda_{L_1}} & \dots & 0 & -\frac{1}{\lambda_{L_1}} \\ \vdots & \vdots & \dots & \vdots & \vdots \end{bmatrix}. \quad (5.18)$$

It is important to note that the covariance of the delay and frequency estimates, which are used for controlling the local oscillators, depends not only on the quality of the tracked signal but also on other channels and, possibly, from other measurements.

5.3.2 NCO Control

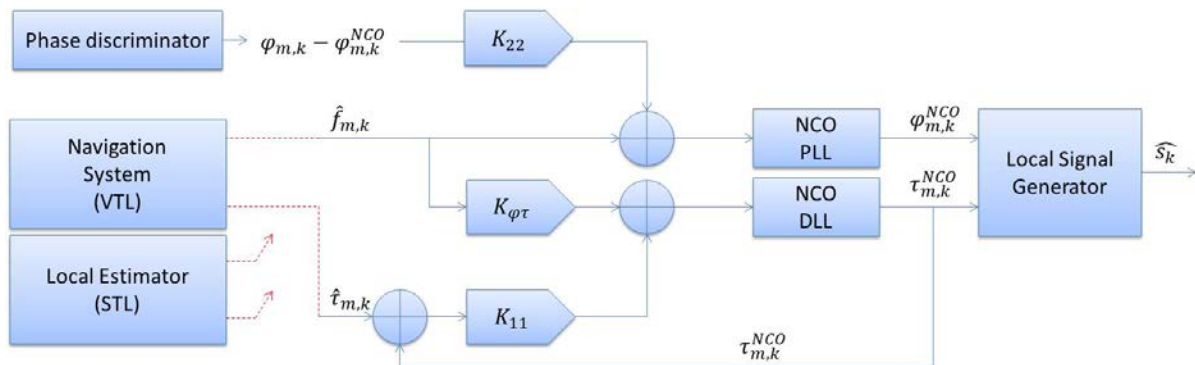


Figure 93: NCO Control for adaptive tracking loop.

We describe here the block which is called “Control” in Figure 92. In an STL architecture the NCO are controlled from the local estimators. We describe here a vector-loop architecture in which the outputs of the NS are used for controlling the NCOs. Moreover, as the NS is not accurate enough to estimate the signal carrier phase error, the output of the phase discriminator is also used to remove any *static-phase-error* accumulation [42]. The description of this block is given in Figure 93. It can be noted that this stage can be easily switched into a scalar mode to track a valid satellite when the NS is not operating satisfactorily.

5.3.3 Correlators and Discriminators

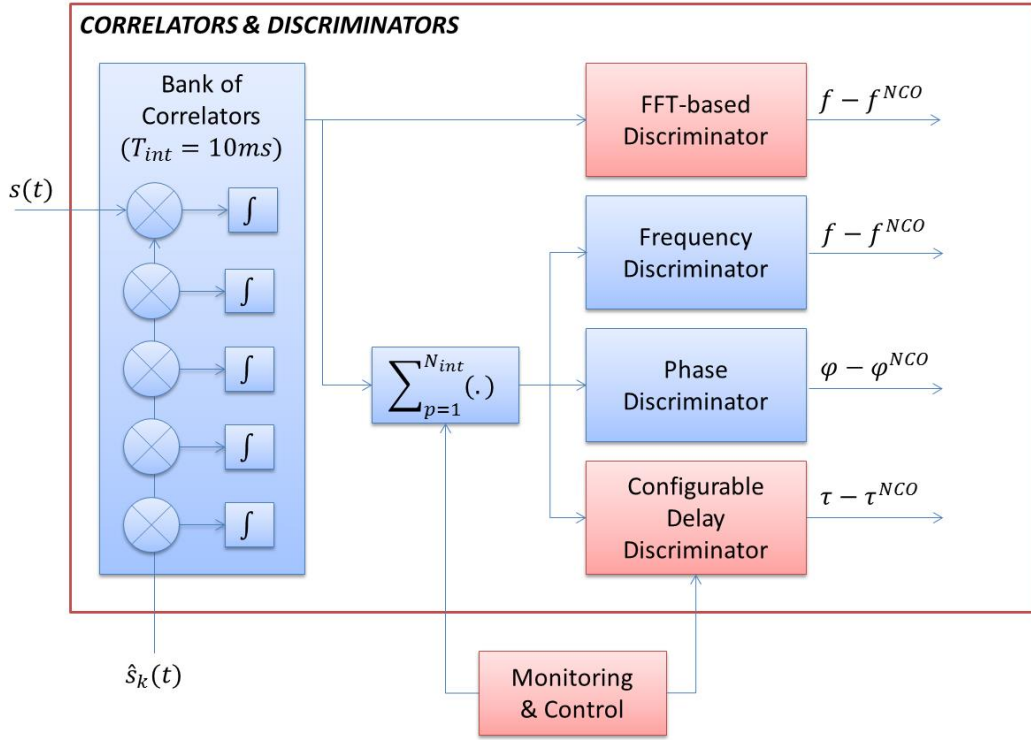


Figure 94: Correlators and discriminators for the proposed adaptive tracking loop.

The architecture of the stage which integrates the correlators and the adaptive discriminators is presented in Figure 94. As described above, a set of discriminators is available in order to adapt the discriminator range depending on the MP environment. Discriminators are used to determine, for each available satellite, the carrier phase and frequency errors, and the code propagation delay error that are exploited by the local estimators. These discriminators process the bank-of-correlators outputs to provide these measurements as expressed in (5.6). Their operating rate depends on the integration time, T_{int} given by:

$$T_{int} = N_{int} T_{corr} \quad (5.19)$$

where T_{corr} is the length of the coherent correlation in seconds (s) and N_{int} is the programmable number of coherent correlations.

These discriminators provide the propagation delay error ($\Delta\tau_m = \tau_m - \tau_m^{NCO}$) and the Doppler frequency error ($\Delta f_m = f_m - f_m^{NCO}$) that are related to the NS position and velocity errors through the equations (5.13) and (5.14), as well as the phase error ($\Delta\varphi_m = \varphi_m - \varphi_m^{NCO}$) which

represents the phase error of the local carrier. In an STL architecture, these outputs represent the parameter errors that are estimated locally. In that case, these observations are used as measurements by the local estimators. When a VTL is used, the delay and the frequency errors are exploited to provide the errors to the navigator, respectively for the estimated position and velocity. It may be noted that the phase error is used in both architectures to correct the current phase value of the carrier generator [42] as presented earlier in Figure 93. Finally the conventional FLL discriminator is used to provide Δf_m to verify that the PLL is operating properly [28].

5.3.4 Local Estimator

The local estimator stage is of crucial importance in an STL. Since the goal of the proposed approach is to favour LOS signals in nominal reception conditions (i. e., for good C/N_0 ratios), a simple estimator can be used to provide an estimation of the GNSS signal parameters. Contrary to a local estimator based on a KF (that adapts optimally the Kalman gain matrix over time and can use correlator outputs as observations), the proposed estimator uses a time-invariant gain weighting the measurements that are provided by a set of relevant discriminators. This approach degrades the estimation performance for low C/N_0 ratio. However it provides performance similar to the one obtained with the EKF for high C/N_0 ratio [13].

One advantage of an estimator based on a time-invariant gain is that it can be easily reconfigured by adapting its bandwidth to the system dynamic. This adaptation can be performed when the frequency uncertainty of the incoming signal is known. The frequency uncertainty depends on the power of the vehicle velocity error (i.e., on the statistic of the NS state vector), on the vehicle acceleration and on the receiver clock stability. Here we consider that the order of the navigator, and the receiver clock stability, allow the “dynamic stress” (i.e., the impact of the acceleration) and the “lock stress” to be neglected.

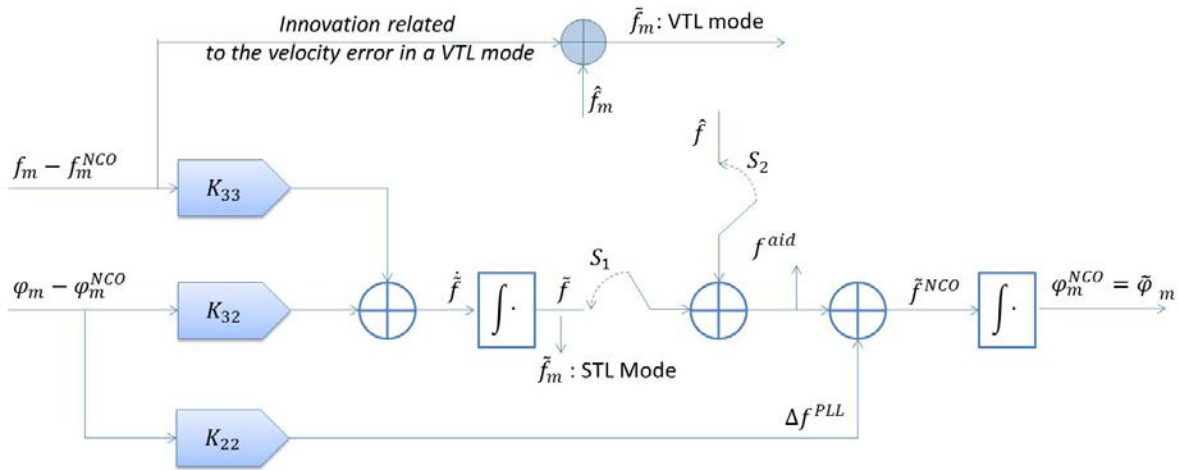


Figure 95: PLL/FLL Architecture for adaptive tracking.

The estimator investigated in this paper is based on a second order PLL assisted by a first order FLL as presented in Figure 95 (S_1 on, S_2 off). In a VTL mode, under the assumption that the velocity is known, a first order PLL is used (S_2 on, S_1 off). In this mode the frequency discriminator output is used as measurement by the navigator as an observation of the velocity error.

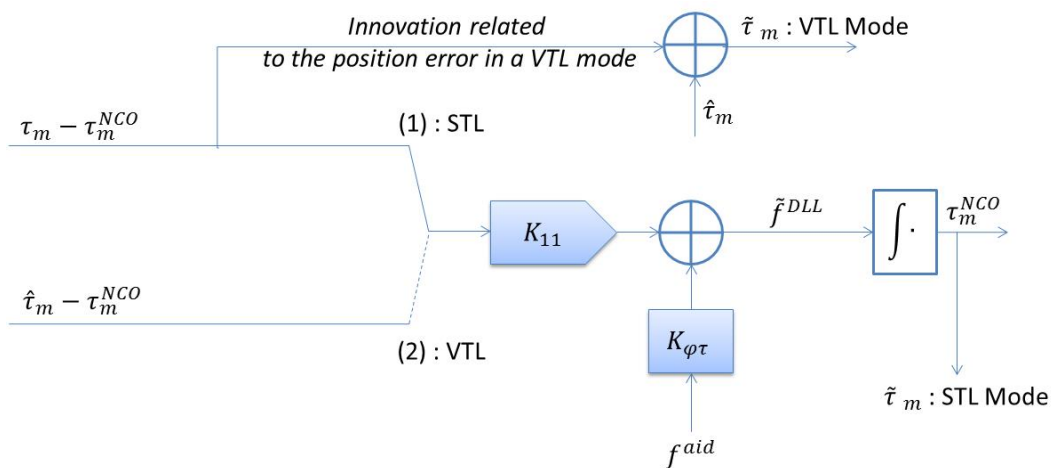


Figure 96: DLL Architecture for adaptive tracking.

With regard to the DLL, a first-order DLL with carrier aiding is adopted as presented in Figure 96. In a VTL mode the discriminator output is used as an observation of the delay error within the navigator.

a) State space model

The local estimator is based on tracking loops that are equivalent to a sequential filter using discriminator outputs as measurements. The weights of this filter are not optimally adapted. Instead, they are adjusted depending on the selected loop bandwidths. The state space system is given here without taking into account the process noise. The system model is described by the following equation

$$\tilde{X}_{m,l} = \begin{bmatrix} \tilde{\varphi}_m \\ \tilde{f}_m \\ \tilde{\tau}_m \end{bmatrix}_{m,l} = \begin{bmatrix} 1 & T_{int} & 0 \\ 0 & 1 & 0 \\ 0 & K_{\varphi\tau}^m T_{int} & 1 \end{bmatrix} \begin{bmatrix} \tilde{\varphi}_m \\ \tilde{f}_m \\ \tilde{\tau}_m \end{bmatrix}_{m,l-1}. \quad (5.20)$$

The observation model relating the state vector to the discriminator outputs is defined depending on the tracking loop configuration. In the STL mode, the following model is used:

$$Y_m^{STL} = \begin{bmatrix} \Delta\varphi_m^{DISCRI} \\ \Delta f_m^{DISCRI} \\ \Delta\tau_m^{DISCRI} \end{bmatrix}. \quad (5.21)$$

In a VTL mode this model is:

$$Y_m^{VTL} = \begin{bmatrix} \Delta\varphi_m^{DISCRI} \\ \hat{\tau}_m - \tilde{\tau}_m \end{bmatrix} \quad (5.22)$$

where $\hat{\tau}_m$ is deduced from the current location. It is important to note that, in the STL mode, the propagation rate is the integration time which represents the discriminator outputs rate. In a VTL mode, the local estimator works with respect to the delay estimation at the navigation rate.

b) Recursive implementation of the local estimator

In the STL mode, the local estimator can be defined by the following recursive equations

$$\begin{aligned} \tilde{f}_{m,l}^- &= \tilde{f}_{m,l-1}^+ \\ \tilde{\varphi}_{m,l}^- &= \tilde{\varphi}_{m,l-1} + T^{EL} \tilde{f}_{m,l-1}^+ \\ \tilde{\tau}_{m,l}^- &= \tilde{\tau}_{m,l-1}^+ + K_{\varphi\tau}^m T^{EL} \tilde{f}_{m,l-1}^+ \end{aligned}$$

$$\begin{aligned}\delta f_{m,l} &= f_{m,l} - \tilde{f}_{m,l-1}^+ \\ \delta \tau_{m,l} &= \tau_{m,l} - \tilde{\tau}_{m,l-1}^+ \\ \delta \varphi_{m,l} &= \varphi_{m,l} - \tilde{\varphi}_{m,l-1}^+\end{aligned}$$

$$\begin{aligned}\tilde{f}_{m,l}^+ &= \tilde{f}_{m,l}^- + K_{33}^m T^{EL} \delta f_{m,l} + K_{32}^m T^{EL} \Delta \varphi_{m,l} \\ \tilde{\tau}_{m,l}^+ &= \tilde{\tau}_{m,l}^- + K_{11}^m T^{EL} \delta \tau_{m,l} \\ \tilde{\varphi}_{m,l}^+ &= \tilde{\varphi}_{m,l}^- + K_{22}^m T^{EL} \delta \varphi_{m,l}\end{aligned}$$

In this mode, $\tilde{\tau}_{m,l}^+$ and $\tilde{f}_{m,l}^+$, which are respectively related to the position and the velocity, are used as observations by the navigator. In the case of a VTL configuration, the equations are defined as:

$$\begin{aligned}\tilde{f}_{m,l}^- &= \hat{f}_{m,l} \\ \tilde{\varphi}_{m,l}^- &= \tilde{\varphi}_{m,l-1} + T^{EL} \hat{f}_{m,l-1} \\ \tilde{\tau}_{m,l}^- &= \tilde{\tau}_{m,l-1}^+ + K_{\varphi\tau}^m T^{EL} \hat{f}_{m,l-1}\end{aligned}$$

$$\begin{aligned}\delta \varphi_{m,l} &= \varphi_{m,l} - \tilde{\varphi}_{m,l-1}^+ \\ \tilde{\varphi}_{m,l}^+ &= \tilde{\varphi}_{m,l}^- + K_{22}^m T^{EL} \delta \varphi_{m,l}\end{aligned}$$

$$\begin{aligned}\tilde{f}_{m,l}^+ &= \tilde{f}_{m,l}^- \\ \tilde{\tau}_{m,l}^+ &= \tilde{\tau}_{m,l}^- + K_{11}^m T^{EL} (\hat{t}_m - \tilde{\tau}_{m,l-1}^+)\end{aligned}$$

In the VTL mode, the discriminators are used to provide the observation to the navigator. By considering that the discriminator outputs are updated at the navigator rate, we have:

$$\begin{aligned}\delta \tau_{m,l} &= \tau_{m,l} - \tilde{\tau}_{m,l-1}^+ \\ \tilde{\tau}_{m,l} &= \tilde{\tau}_{m,l}^+ + \delta \tau_{m,l} \\ \delta f_{m,l} &= f_{m,l} - \tilde{f}_{m,l-1}^+ \\ \tilde{f}_{m,l} &= \tilde{f}_{m,l}^+ + \delta f_{m,l}\end{aligned}$$

where $\delta \tau_{m,l}$ and $\delta f_{m,l}$ are the discriminator outputs, $\tilde{\tau}_{m,l}$ and $\tilde{f}_{m,l}$ represent the local estimator outputs which are used as measurement by the navigator. Moreover, for each mode, the different gains are adjusted, when it is required, to impose adequate channel loop bandwidths.

c) Noise variance analysis

The aim of this analysis is to compare the 2 architectures, whose basic representations are given in Figure 97. In this figure, θ denotes the parameter to be estimated (f or τ).

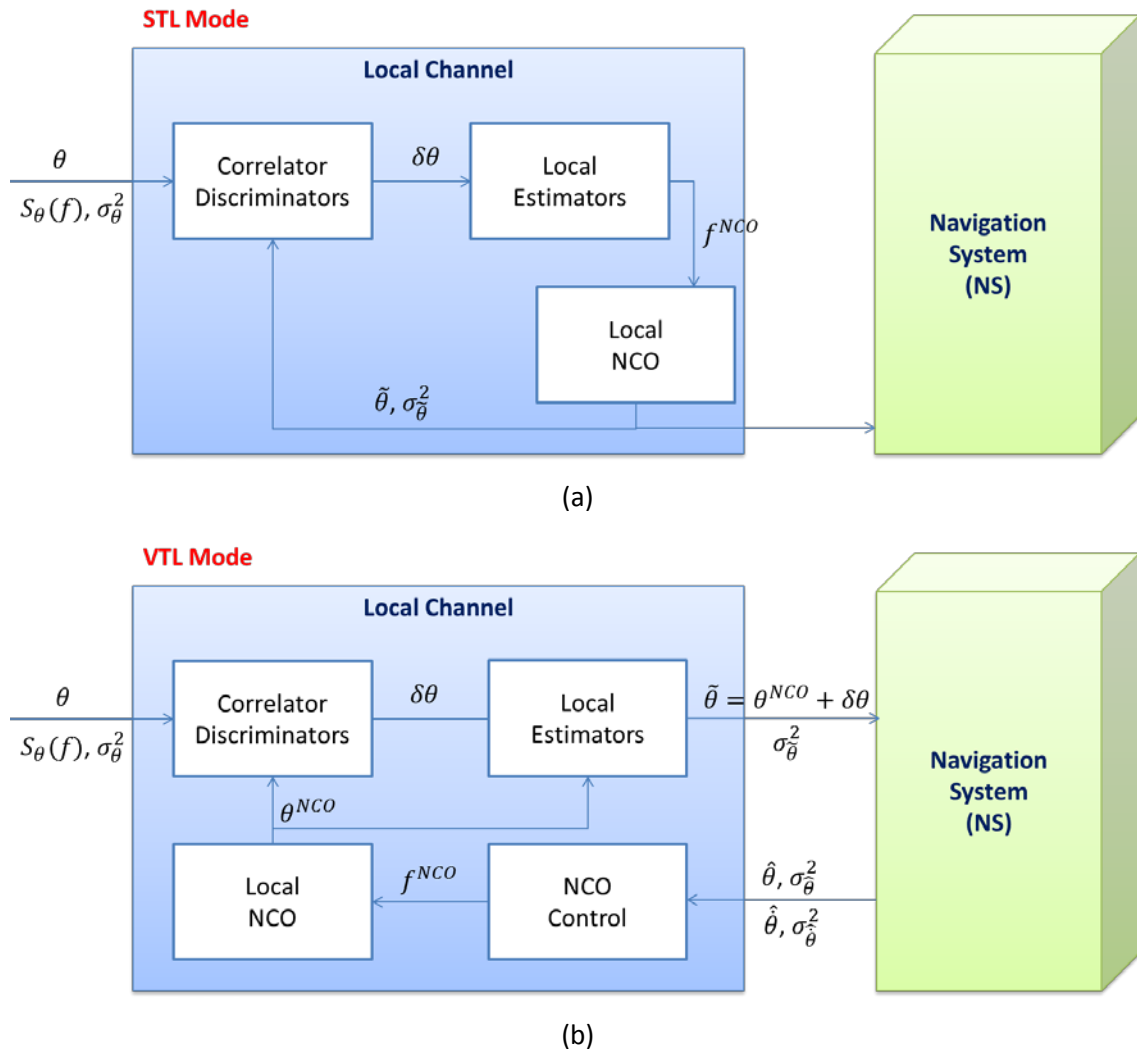


Figure 97: Simplified receiver architecture for (a) STL mode and (b) VTL mode.

i. STL approach

When a conventional approach, based on the STL architecture is used, the estimator outputs and the NCO parameters (τ, f) are strongly linked. Especially the NCO delay is the one that is estimated by the local estimator. In this case, the discriminators measuring the NCO propagation delay error and the NCO frequency error provide the innovation for the local estimator.

The behaviour of the NCO, as well as the performance of the local estimator, depends on the quality of the incoming signal. For high CT_{int}/N_0 ratio, the variances of the estimator outputs are given by the following relations [12], given by the equations (2.26) for the frequency, or (2.31) for the delay where

$$\sigma_{\tilde{f}}^2 \approx \frac{B_n^{PLL}}{\pi^2 T_{int}^2 C/N_0} \quad (5.23)$$

$$\sigma_{\tilde{d}}^2 \approx \frac{B_n^{PLL}}{\pi^2 T_{int}^2 C/N_0} \quad (5.24)$$

with $d = 4\Delta$ when EML discriminator is used.

In these expressions B_n^{PLL} and B_n^{DLL} , which are respectively the bandwidth of the DLL, and the bandwidth of the PLL, characterize the local estimator. Consequently, in this type of architecture, the variance of the estimated parameter $\tilde{\theta}$, and the stress on the related NCO parameter, are strongly dependent on the incoming signal C/N_0 ratio, and on the local estimator bandwidth. With regard to the stress of the NCO, we obtain:

$$(\sigma_{\tilde{\theta}}^{NCO})^2 = (\sigma_{\tilde{\theta}}^{DYN})^2 + (\sigma_{\tilde{\theta}}^{Oscillator})^2 + \sigma_{\tilde{\theta}}^2 \quad (5.25)$$

where $\sigma_{\tilde{\theta}}^2$ is the variance of the local estimator output, $(\sigma_{\tilde{\theta}}^{DYN})^2$ represents the dynamic error (acceleration stress for a second order estimator) which is close to zero if the local estimator order is suitable for the particular application, and $(\sigma_{\tilde{\theta}}^{Oscillator})^2$ depends on the quality of the oscillator.

ii. VTL approach

On the contrary, when a VTL architecture is used, the parameter to be considered for characterizing the NCO stress is the parameter whose estimate is provided by the navigator. Its variance is defined as:

$$(\sigma_{\tilde{\theta}}^{NCO})^2 = (\sigma_{\tilde{\theta}}^{NAV})^2 + (\sigma_{\tilde{\theta}}^{Oscillator})^2 + \sigma_{\tilde{\theta}}^2 \quad (5.26)$$

where $(\sigma_{\theta}^{NAV})^2$ is the dynamic stress which depends here on the navigator order, σ_{θ}^2 is the variance of the parameter which is deduced from the navigator state. Consequently, the variance of this parameter depends not only on the quality of the tracked signal, but also on the other measurements (other satellites or other complementary sensors). The impact of the C/N_0 ratio is only visible on the measurement which is provided to the navigator.

A simple analysis is conducted here to characterize the variance σ_{θ}^2 , by considering the frequency and the delay that are estimated by the navigator. The estimation is performed for different steps:

- The a priori position and velocity are computed by the navigator.
- The position and the velocity are updated by using the available measurements, including the discriminator outputs of the GNSS receiver channels.
- The new position and velocity are used for computing the parameters which are used for controlling the NCO which provide the signal replica of each channel (equations 5-13 and 5.16).

We can translate this estimation issue by considering a classical state-space model. The process model $\hat{X}_{k+1}^{NS} = \Phi^{NS} \hat{X}_k^{NS} + w_k$ is described by the equations (4.20) to (4.27). With regard to the measurement model, all the measurements must be taken into account and the observation model is defined by the equations (5.10) to (5.12) and (5.17) for GNSS measurements. Characterizing the estimator from the posterior Cramer Rao Bound (CRB) which allows a lower limit of the estimation mean square error to be defined [62] is not easy here as the measurement model is not linear. In practice, as an EKF is used for estimating the navigator state, the mean square error of the estimated parameters will be deduced from the state covariance matrix which is propagated under the assumption of Gaussian systems. Note that the variance $\sigma_{\hat{f}}^2$ and $\sigma_{\hat{\tau}}^2$ are defined by the equations (5.15) and (5.16).

It is important to note that, even if the VTL approach allows the NCO stress to be reduced, this approach does not improve necessarily the quality of the measurements which are provided to the navigator. Indeed, the impact of the quality of the tracked signal is visible at the discriminator outputs. Considering the measurement related to the channel which is studied, an analysis of the discriminator outputs must be performed.

1. Frequency discriminator variance analysis

When the FFT output is used for measuring the frequency error ($f - f^{NCO}$), a good accuracy is obtained by considering the prompt correlator output over 1s. In practice, a conventional discriminator is exploited [1] and the observation duration is adapted to the receiver dynamic. For high C/N_0 ratio ($C/N_0 > 35dBHz$), a basic analysis can be achieved. The signal considered is the correlator output where in nominal condition, the expression of this signal is:

$$u_z(k) = A(\Delta f_k) R(\Delta \tau_k) \exp(j\Delta \varphi_k) + n_k. \quad (5.27)$$

It is admitted that the additive noise leads to a phase noise whose power spectrum density is:

$$S_\varphi(f) = \frac{2}{C/N_0} \text{ rad}^2/\text{Hz}. \quad (5.28)$$

Considering a coherent integration time, T_{int} , the power of the phase noise, in the correlator bandwidth, is:

$$\sigma_\varphi^2 = \frac{2}{C/N_0 T_{int}}. \quad (5.29)$$

The frequency is obtained by considering the phase variation during the integration time:

$$f_k = \frac{\varphi_k - \varphi_{k-1}}{2\pi T_{int}}. \quad (5.30)$$

The power of the frequency noise is deduced from the 2 above equations:

$$\sigma_f^2 = \frac{2\sigma_\varphi^2}{4\pi^2 T_{int}^2} = \frac{2}{\frac{4\pi^2 C T_{int}^3}{N_0}}. \quad (5.31)$$

The frequency discriminator is used to measure the frequency innovation ($\delta f = f^{NCO} - f \sim \hat{f} - f$).

$$(\sigma_f^{DISCRI})^2 = \sigma_{\delta f}^2 = \sigma_{\hat{f}}^2 + \sigma_f^2. \quad (5.32)$$

When the measurement model defined by the equations (5.10) to (5.12) is used, the variance of the discriminator output represents the innovation variance which is associated with the frequency measurement of the satellite # m . This is defined as:

$$(\sigma_f^{DISCRI})^2 = \sigma_{\delta f}^2 = H_{2m} P^{NS} H_{2m}^T + \sigma_f^2 \quad (5.33)$$

where $H_{2m} P^{NS} H_{2m}^T$ represents the variance of the a priori frequency which is deduced from the state vector covariance matrix, and σ_f^2 is the measurement noise defined as

$$\sigma_f^2 = \frac{1}{\frac{2\pi^2 C T_{int}^3}{N_0}} \quad (5.34)$$

Therefore, the measurement model, which is provided to the navigator as an observation of the user velocity, is:

$$\begin{cases} \tilde{f}_k = \hat{f}_{k-1} + \delta f_k \\ \sigma_{\tilde{f}}^2 = \frac{1}{\frac{2\pi^2 C T_{int}^3}{N_0}} \end{cases} \quad (5.35)$$

2. Delay discriminator variance

The most classical approach consists of comparing the early and late correlator outputs. In a nominal condition, the expression of this signal is:

$$S(\Delta\tau_k) = A(\Delta f_k) \cdot R\left(\Delta\tau_k + \frac{d}{2}\right) \exp(j\Delta\varphi_k) - A(\Delta f_k) R\left(\Delta\tau_k - \frac{d}{2}\right) \exp(j\Delta\varphi_k) + n_k\left(\frac{d}{2}\right) - n_k\left(-\frac{d}{2}\right) \quad (5.36)$$

where $R(\cdot)$ is the autocorrelation function of the spreading code, $A = \sqrt{C}$ where C is the signal power. The noise term is expressed as:

$$n_k(u) = \frac{1}{M} \sum_{l=1}^M n_{in}(kT_{int} + lT_s) C_m(kT_{int} lT_s - \hat{t} - u). \quad (5.37)$$

In this expression, C_m represents the spreading code for the satellite # m , M is the number of samples of the incoming signal in the coherent integration time, and n_{in} is the noise which affects the incoming signal. Using 2 correlators, respectively shifted with the delays u and v , we have :

$$E\{n(u)n^*(v)\} = \sigma_n^2 R(u - v) \quad (5.38)$$

where, $\sigma_n^2 = N_0/T_{int}$ is the noise power in the correlator bandwidth. By neglecting filtering effects in the RF front end, the discriminator output becomes

$$\frac{S(\Delta\tau_k)}{\sqrt{C}} = \left[1 - \left| \Delta\tau_k + \frac{d}{2} \right| - 1 + \left| \Delta\tau_k - \frac{d}{2} \right| \right] + n_k^{EmL}/\sqrt{C} \quad (5.39)$$

$$\frac{S(\Delta\tau_k)}{2\sqrt{C}} = -\Delta\tau_k + \frac{n_k^{EmL}}{2\sqrt{C}} \approx -\hat{\tau} + \tau + \frac{n_k^{EmL}}{2\sqrt{C}}. \quad (5.40)$$

For $d < 1$, the variance of the measurement noise is

$$\sigma_\tau^2 = E \left\{ \frac{1}{4C} (n_k^{EmL})^2 \right\} = \frac{1}{4C} E \left\{ n_k \left(\frac{d}{2} \right) - n_k \left(-\frac{d}{2} \right) \right\} = \frac{\sigma_n^2}{2C} (1 - d) \quad (5.41)$$

where the parameter d , which is the early-late chip spacing, is set to 4Δ when the conventional delay discriminator is used.

An analysis such as the one conducted for the frequency observation can be performed. The delay discriminator measures the error of the NCO delay ($\delta\tau = \tau^{NCO} - \tau \sim \hat{\tau} - \tau$) is used. The variance of the discriminator output is:

$$(\sigma_\tau^{DISCRI})^2 = \sigma_{\delta\tau}^2 = \sigma_{\hat{\tau}}^2 + \sigma_\tau^2. \quad (5.42)$$

For the measurement model defined by the equations (5.10) to (5.12), the variance of the discriminator output represents the innovation variance which is associated with the delay measurement of the satellite # m

$$(\sigma_\tau^{DISCRI})^2 = \sigma_{\delta\tau}^2 = H_{2m-1} P^{NS} H_{2m-1}^T + \sigma_\tau^2 = H_{2m-1} P^{NS} H_{2m-1}^T + \sigma_\tau^2 \quad (5.43)$$

where $H_{2m-1} P^{NS} H_{2m-1}^T$ represents the variance of the a priori delay, which is deduced from the state vector covariance matrix, and σ_{τ}^2 is the measurement noise defined by:

$$\sigma_{\tau}^2 = \frac{\sigma_n^2}{2C} (1 - d). \quad (5.44)$$

This measurement noise is deduced from the C/N_0 through the relation:

$$\sigma_{\tau}^2 = \frac{1}{2 C/N_0 T_{int}} (1 - d). \quad (5.45)$$

The measurement model provided to the navigator as an observation of the user position, is:

$$\left\{ \begin{array}{l} \tilde{\tau}_k = \hat{\tau}_{k-1} + \delta\tau_k \\ \sigma_{\tilde{\tau}}^2 = \frac{1}{2 C/N_0 T_{int}} (1 - d). \end{array} \right. \quad (5.46)$$

3. VTL performance

The VTL approach can be used to elaborate measurements that are defined by equation (5.35) for the Doppler frequency and equation (5.46) for the propagation delay. The measurement noise covariance matrix, related to the measurement vector which is defined by the equations (5.10) to (5.12) and (5.17), is:

$$R = \begin{bmatrix} \frac{1}{\gamma_1} \begin{bmatrix} \frac{1-d}{2} & 0 \\ 0 & \frac{1}{2\pi^2 (T_{int}(1))^2} \end{bmatrix} & 0 & 0 \\ 0 & \frac{1}{\gamma_2} \begin{bmatrix} \frac{1-d}{2} & 0 \\ 0 & \frac{1}{2\pi^2 (T_{int}(2))^2} \end{bmatrix} & 0 & 0 \\ 0 & 0 & 0 & 0 \end{bmatrix} \quad (5.47)$$

where $\gamma_m = \frac{1}{\left(\frac{C}{N_0}\right)_m T_{int}(m)}$ is the inverse of the power over noise ratio with regard to the output of the prompt correlator of the channel # m .

This measurement model does not outperform the one which is obtained by using a conventional STL approach. The main interest of the VTL approach is to reduce the NCO stress, allowing narrow discriminator to be used to track the delay error [63].

5.3.5 Monitoring and Control

The aim of the “monitoring” and “control” modules are to ensure the integrity of the measurement provided by the local channels to the NS. It can be implemented by using statistical tests to decide whether the null hypothesis (no interference) is accepted or rejected. This statistical analysis is performed to validate the measurements of the satellite under test. In that case the satellite which does not satisfy the test can be discarded, degrading the GDOP. Another approach aims at reducing the impact of the interference. Mitigating MP effects allows a reliable measurement to be provided. Moreover the control is able to address the following issues [27]:

- Efficient coherent integration time by the number of cumulated correlations.
- Optimum delay discriminator chip spacing in case of coherent NLOS.
- Computing the variance of the local estimator outputs (estimated delay and frequency) as seen in 5.5.4 (c).
- Weighting the estimated parameters depending on their likelihood.

This control is achieved by monitoring the outputs of the frequency domain detector and the delay domain detector.

a) Monitoring the FFT output

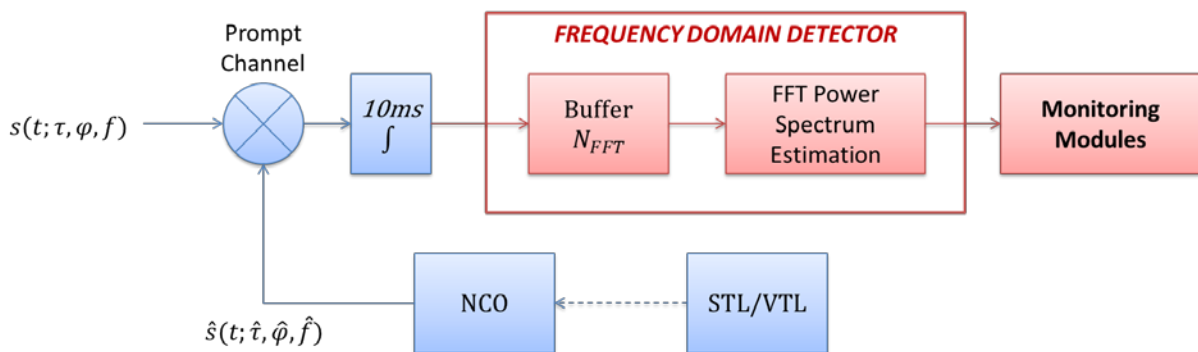


Figure 98: Frequency domain detector implementation.

The FFT-based approach is used as a frequency domain detector that allows the issue of non-coherent MP and DP masking condition to be addressed (see 5.2.2). The approach is described in [29]. The analysis is performed in a VTL context. This analysis concerns the prompt correlator output when the oscillators are controlled by the navigator. This output is defined as:

$$u_z(k) = \sum_{n=0}^N A_{n,k}(\Delta f_{n,k}) R(\Delta \tau_{n,k}) \exp(j\Delta \varphi_{n,k}) + w_k^f. \quad (5.48)$$

An FFT is performed considering 128 samples of the incoming signal:

$$x(i) = \begin{cases} u_z(k+i-N_f), & \text{for } 1 < i \leq N_f, N_f = 128 \\ 0, & \text{for } 128 < i \leq N, N = 1024 \end{cases} \quad (5.49)$$

The discrete Fourier transform of the signal is defined as:

$$U_z(l, k) = G_w \cdot \sum_{i=k-N+1}^k x(i) w(i) \exp\left\{-j2\pi \frac{i(l-\frac{N}{2})}{N}\right\} \quad (5.50)$$

where $w(\cdot)$ is a Hamming weighting function whose attenuation is compensated by the gain G_w .

The analysis is performed from the power spectrum density (PSD):

$$S_{uz}(l, k) = \frac{\|U_z(l, k)\|^2}{N_f}. \quad (5.51)$$

The LOS detection is performed by integrating the PSD around the zero frequency in a band $[-k_\sigma \sigma_{\hat{f}_m}, k_\sigma \sigma_{\hat{f}_m}]$ where $\sigma_{\hat{f}_m}$ is defined by the equation 5.15, and k_σ is a scaling factor which is set to 2.5. The result of this integration is

$$C(k) = C(k, L) - P_n(L) \text{ with } C(k, L) = \frac{1}{N} \sum_{p=N/2-2-L}^{N/2+2+L} [S_{uz}(p, k)] \quad (5.52)$$

where $L = \left\lceil \frac{k_\sigma \sigma_{\tilde{f}_m}}{NT_{corr}} \right\rceil$. In this expression $P_n(L)$ represents the power of the white Gaussian noise in the considered band, which is estimated in an interference-free band.

The following duo hypotheses are considered for detecting the presence of the LOS:

$$\begin{cases} H_0(\text{LOS absence}): u_z(k) = \sum_{n=1}^N A_{n,k}(\Delta f_{n,k}) R(\Delta \tau_{n,k}) \exp(j\Delta \varphi_{n,k}) + w_k^f \\ H_1(\text{LOS presence}): u_z(k) = \sum_{n=0}^N A_{n,k}(\Delta f_{n,k}) R(\Delta \tau_{n,k}) \exp(j\Delta \varphi_{n,k}) + w_k^f \end{cases} \quad (5.53)$$

The hypothesis H_1 is chosen if $C(k) > \eta_C$.

Moreover, the integration time is chosen from the following ratio:

$$\Gamma_C(M) = \frac{C(k)}{C(k, M) - C(k)}, M > L \quad (5.54)$$

which represents the ratio signal power over noise+interference power. The value M, and thus the integration time is chosen for guaranteeing an appropriate value for this ratio.

$$\begin{cases} \mathbb{I}(M) = \begin{cases} 1 & \text{if } \Gamma(k, M) > \Gamma_{min} \\ 0 & \text{otherwise} \end{cases} \\ M^o = \arg \max_M \mathbb{I}(M) \\ T_{int}(k) = \frac{NT_{corr}}{M^o} \end{cases} \quad (5.55)$$

b) Monitoring the delay estimator output

The purpose of monitoring the delay estimator output is to detect the presence of coherent MP. Such a MP which is at the LOS frequency cannot be mitigated in the frequency domain. Consequently it affects the delay estimator, resulting in a bias in the estimate. The test which is proposed addresses the output of the delay discriminator as presented in Figure 99.

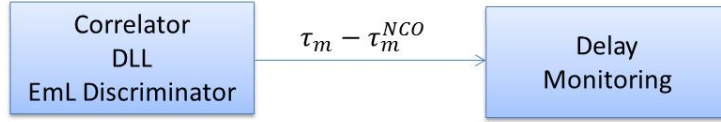


Figure 99: Linear model of the adaptive delay estimator

As it was shown Figure 18 of Chapter 2, when a single NLOS signal is considered, this NLOS induces a signal in the quadrature branch, whose power depends on the NLOS phase and amplitude. When a conventional STL architecture is used, tracking loops will converge in order to cancel the phase and delay error. When a test is performed at the delay and phase discriminators outputs, it allows the appearance or the disappearance of an MP to be detected, i.e., which correspond to any variation of the NLOS signal.

Here we propose to perform a statistical test when a VTL architecture is considered. The main advantage of this architecture is the VTL converges to the LOS delay. Consequently, the delay measurement is obtained at the output of an EML discriminator. In presence of an NLOS signal, a test performed at this discriminator output allows this NLOS signal to be detected. In [28], the test is performed using the In-phase output of the early minus late discriminator. This discriminator is described by the equation (5.7) recalled below

$$I_{EML}(\Delta\tau) = R_I(\Delta\tau + 2\Delta) - R_I(\Delta\tau - 2\Delta) + n_{EML}^I \quad (5.56)$$

where R_I represents the in-phase correlator output. In this case, the test is very sensitive to the phase of the NLOS that can vary very quickly over time. In [64] it is proposed to perform the test on the module of the EML discriminator given by:

$$|EmL(\Delta\tau)| = |R(\Delta\tau + 2\Delta) - R(\Delta\tau - 2\Delta) + n_{EML}|. \quad (5.57)$$

For this approach, the following test statistic is considered:

$$\begin{cases} H_0 \text{ (absence of NLOS): } EmL(l) = n_{EmL}(l) \\ H_1 \text{ (presence of NLOS): } EmL(l) = \delta\tau_{MP}(k) + n_{EmL}(l) \end{cases} \quad \text{for } l \in \{-L + 1, \dots, 0\} + k \quad (5.58)$$

where $\delta\tau_{MP}$ is the delay error, due to the presence of NLOS signal.

The power of the additive noise is estimated from a frequency analysis. And the likelihood ratio is obtained, considering that the NLOS amplitude is unknown yielding the following test:

$$\begin{array}{c} H_1 \\ |EmL|^2 \geq \eta \\ H_0 \end{array} \quad (5.58)$$

where $\overline{EmL} = \frac{1}{L} \sum_{l=0}^{L-1} EmL(l+k)$ and η is the test threshold.

Here we consider that the oscillator and the navigator stresses can be neglected. In this case, the delay discriminator output represents the innovation of the delay measurement, which is used for updating the navigator (see the section 5.5.4(a-ii)). The threshold is obtained from the Mahalanobis distance which is defined from the power of this innovation. This distance is defined here depending on the power of the measurement error, and on the accuracy of the delay estimated by the navigator ($\sigma_{\tau_m}^2$), which is defined by the equation (5.15) and the discriminator which is defined in equation (5.43). Therefore, the threshold η can be defined as:

$$\eta = \frac{k}{\sqrt{L}} \sqrt{\sigma_{\hat{\tau}_m}^2 + \sigma_{\tau_m}^2} = \frac{k}{\sqrt{L}} \sqrt{H_{2m-1} P^{NS} H_{2m-1}^T + \sigma_{\tau}^2} \quad (5.59)$$

where k is set to 2.5, and $\sigma_{\tau_m}^2$ is the variance of the measurement error which depends on the C/N_0 ratio. This variance is defined by equation (5.45).

c) Controlling the delay discriminator

In presence of NLOS, two approaches were studied in the literature. The first one assumes that the number of satellites is high enough and that any contaminated channel has been discarded. The second one consists of mitigating MP effects in order to exploit any measurement, especially when dealing with a low number of reliable satellites. This processing is performed using of two operations. First, the discriminator is selected optimally and second, the measurement is marked as contaminated to be processed in a robust KF.

i) Delay Discriminator management

In practice wide range discriminators are sensitive to MP. Reducing the discriminator chip spacing improves the behaviour of the discriminator in presence of MP. Nevertheless a too small chip spacing can result in a loss of lock for the DLL. The main idea of this approach is to adapt the discriminator range to the NCO stress. Using the rule (5.9), the chip spacing can be chosen from the following parameters:

- i. The oscillator stress which depends on its technology, which can be neglected for OCXO technology and normal rate measurement.
- ii. The navigator stress, which can be neglected if the navigator suits for the application.
- iii. The error related to the navigator accuracy ($\sigma_{\hat{\tau}_m} = \sqrt{H_{2m-1} P^{NS} H_{2m-1}^T}$), instead of the error on the delay measurement in a STL architecture ($\frac{B_n^{DLL} \cdot d}{2(C/N_0)}$).

By considering that the first two sources of errors can be neglected, the following rule is adopted for switching the most appropriate discriminator:

$$d = 2\Delta = 2.5 \sigma_{\hat{\tau}_m} = \sqrt{H_{2m-1} P^{NS} H_{2m-1}^T}. \quad (5.60)$$

ii) Measurement model management

In presence of an NLOS signal, i.e., when the delay detector reports the presence of MP, the delay measurement which is provided to the navigator is marked as contaminated. Such a measurement is used in a robust KF [65] which consists of weighting the Kalman gain matrix depending on the power of the innovation related to each measurement. Here, we propose to use a similar approach. First a gain is defined, depending on the power of the innovation, by using an influence function β define as:

$$\beta_{m,k}^{\Delta\tau} = \beta(\tilde{\tau}_{m,k} - \hat{\tau}_{m,k}^-) \quad (5.61)$$

where $\tilde{\tau}_{m,k}$ and $\hat{\tau}_{m,k}^-$ represents respectively the delay measurement and the a priori delay measurement obtained in the navigator after the prediction stage. We note that $\sigma_{\Delta\tau} = \sqrt{H_{2m-1} P^{NS} H_{2m-1}^T + \sigma_{\tau}^2}$ is the 1-sigma innovation error. Here, the influence function is defined as:

$$\beta(e) = \begin{cases} e, & |e| \leq k_{\Delta\tau,1}\sigma_{\Delta\tau} \\ e + k_{\Delta\tau,1}\sigma_{\Delta\tau} \left(1 - \exp\left\{ \frac{(e + k_{\Delta\tau,1}\sigma_{\Delta\tau})^2}{2(k_{\Delta\tau,2}\sigma_{\Delta\tau})^2} \right\} \right), & k_{\Delta\tau,1}\sigma_{\Delta\tau} < e < 3\sigma_{\Delta\tau} \\ e - k_{\Delta\tau,1}\sigma_{\Delta\tau} \left(1 - \exp\left\{ \frac{(e - k_{\Delta\tau,1}\sigma_{\Delta\tau})^2}{2(k_{\Delta\tau,2}\sigma_{\Delta\tau})^2} \right\} \right), & -3\sigma_{\Delta\tau} < e < -k_{\Delta\tau,1}\sigma_{\Delta\tau} \\ 0, & \text{elsewhere} \end{cases} \quad (5.62)$$

This function is represented by Figure 100, for $\sigma_{\Delta\tau} = 1$, $k_{\Delta\tau,1}=1.5$, $k_{\Delta\tau,2}=1$.

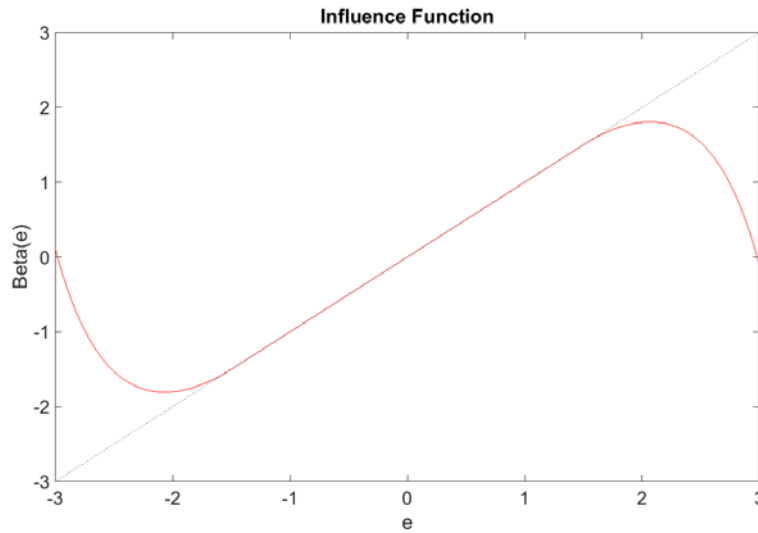


Figure 100: Influence function β .

This function is used for weighting the observation matrix, depending on the innovation amplitude, i.e., depending on

$$\gamma_{m,k}^{\Delta\tau} = \frac{\beta(\tilde{\tau}_{m,k} - \hat{\tau}_{m,k}^-)}{\tilde{\tau}_{m,k} - \hat{\tau}_{m,k}^-} = \frac{\beta_{m,k}^{\Delta\tau}}{\tilde{\tau}_{m,k} - \hat{\tau}_{m,k}^-}. \quad (5.63)$$

The gain is plotted in Figure 101 as a function of the Innovation amplitude, for $\sigma_{\Delta\tau} = 1$, $k_{\Delta\tau,1}=1.5$, $k_{\Delta\tau,2}=1$.

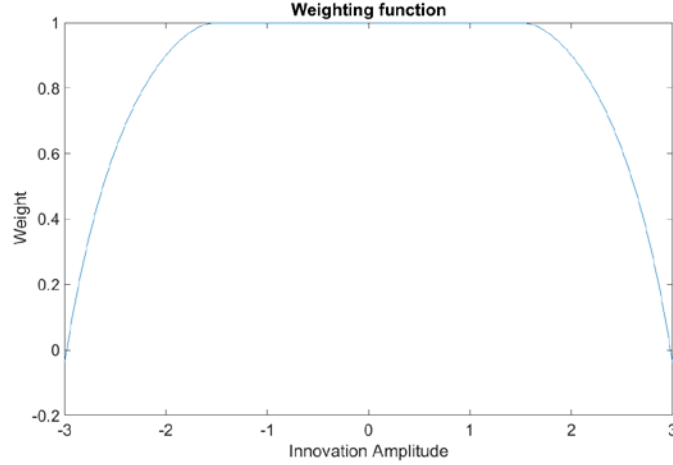


Figure 101: Weighting function.

The new measurement model based on the observation vector ΔY_m^{NS} and the matrix H^{NS} , which are described by (5.10) and (5.17) respectively is defined by:

$$\Delta Y_{m,k}^{NS} = \begin{bmatrix} \tilde{t}_{m,k} - \hat{t}_{m,k}^- \\ \tilde{f}_{m,k} - \hat{f}_{m,k}^- \end{bmatrix} \quad (5.64)$$

$$H_k^{NS} = \Gamma_k^{\Delta\tau} H_k^{NS} \quad (5.65)$$

where $\Gamma_k^{\Delta\tau}$ is a diagonal matrix whose diagonal elements are $(\gamma_{1,k}^{\Delta\tau}, 1, \dots, \gamma_{m,k}^{\Delta\tau}, 1, \dots)$.

d) Controlling the STL/VTL mode

The proposed architecture allows the receiver to be easily switched in the STL mode or in the VTL mode (see the Figure 95 and Figure 96). A reconfigurable architecture is synthesized Figure 99. The main objective is to avoid a channel to be contaminated by any other channel. This objective can be achieved by detecting any contamination for the navigator. This issue is not addressed here. But the mechanism which is implemented for controlling the tracking mode is very simple. A channel is switched in the STL mode when the navigator is marked as contaminated and when the C/N_0 ratio of the received signal allows this signal to be tracked. In the other situations the channel is configured in a VTL tracking mode. When the C/N_0 ratio is too low, the VTL allows the signal to be tracked (in a blind mode in case of satellite masking) without using the measurement provided by the channel.

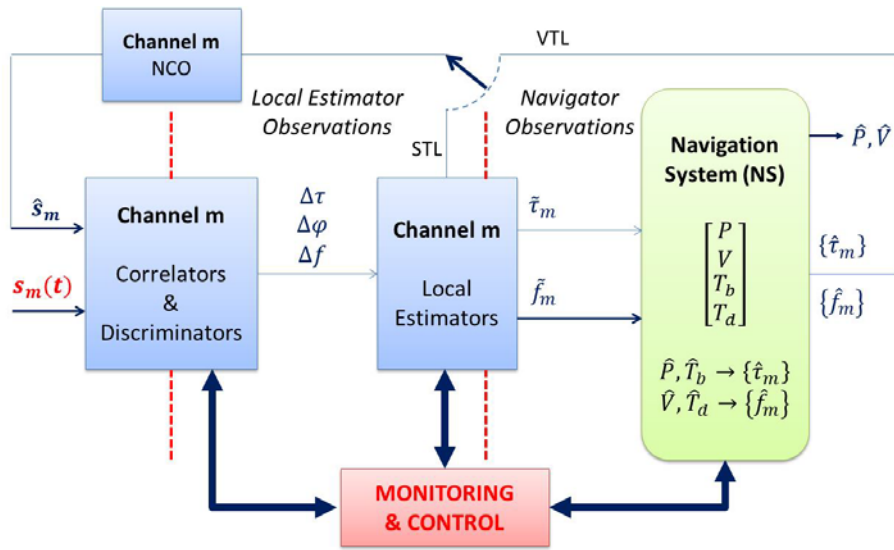


Figure 102: Overview concept of STL/VTL mode.

5.4 Adaptive Tracking Performance Analysis

The proposed adaptive tracking approach is being implemented under the similar simulation framework as the conventional STL and VTL architectures. These three architectures are then tested, first with a controlled MP scenarios using the in-house simulator developed for this thesis work and later, using the DLR model to provide the channel model that is assume to be close to the real signal scenarios. The global comparison in term of position and true errors for the whole trajectory is being compared and analysed.

5.4.1 Simulation using an In-house simulator

An in-house simulator has been developed by creating an artificial trajectory as presented in Figure 103. The simulation methodology for evaluating the impact of MP based on the vector tracking architecture is presented in Figure 104. In this set-up, channel 1 is considered as the channel of interest where different sets of MP scenarios have been introduced during the whole trajectory. At the same time, the other 4 channels are assumed to be operating under nominal condition. The artificial satellite constellation for this simulation is presented in Figure 105. The objective of this test is to evaluate the proposed adaptive approach for mitigating the impact of MP in the tracking mode relative to conventional STL and VTL architectures.

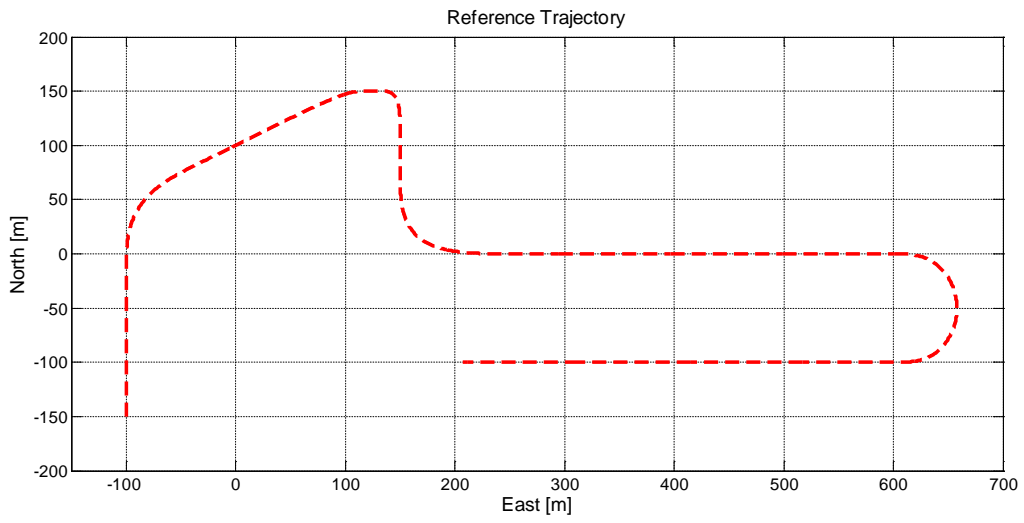


Figure 103: Artificial reference trajectory.

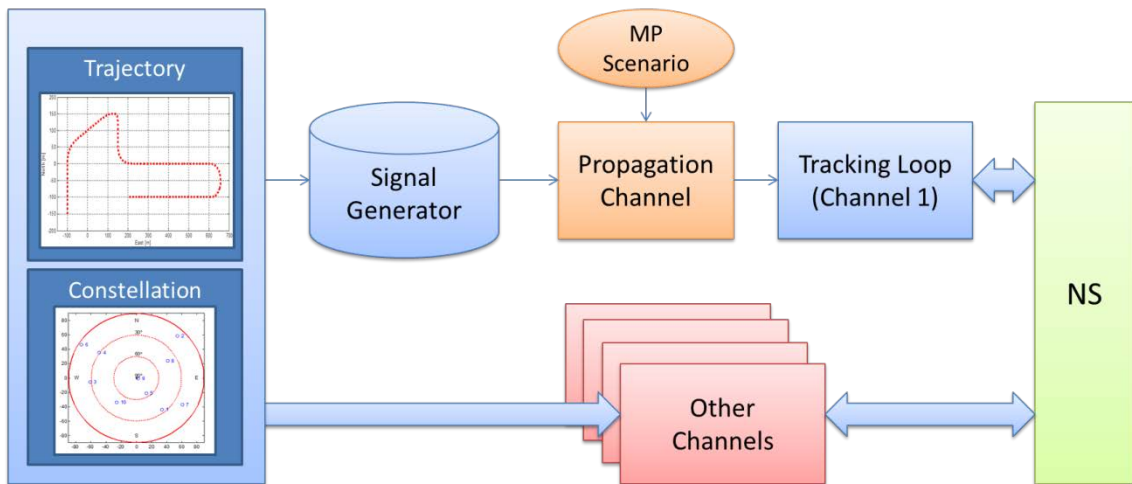


Figure 104: Simulation configuration.

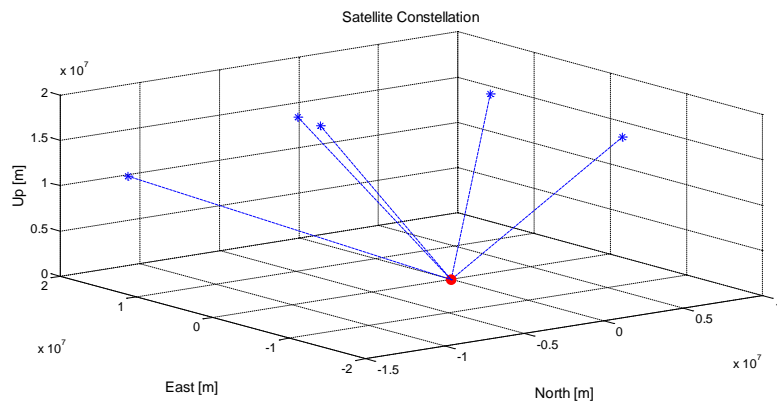


Figure 105: Satellite constellation.

In order to analyse these impacts and the performance enhancement offered by the adaptive approach, different sets of controlled MP scenarios have been created for the simulation which are based on the artificial trajectory. The conditions on the MP will exhibit both coherent and non-coherent MP scenarios. The corresponding parameters of these controlled scenarios are presented in Table 9. All types of different receiver tracking architectures (STL, VTL and AVTL) are used to provide the estimation of the global position which will then be compared to the reference trajectory.

Table 9: Description of the controlled MP scenarios.

	Time Interval [s]	A [unit]	f [Hz]	τ [chips]	φ [rads]	Remark
Scenario 1	3-8	0.6	7	0.1	$\pi/4$	
	4-10	0.7	18	0.2	$\pi/2$	
Scenario 2	31-36	0.4	6	0.2	$\pi/2$	Lost DP from 35s to 40s
	32-38	0.5	-11	0.1	$\pi/4$	
Scenario 3	96-103	0.5	7	0.1	$\pi/4$	
	98-104	0.4	18	0.2	$\pi/2$	
	96-102	0.6	0	0.6	$\pi/4$	
Scenario 4	160-170	0.4	0	0.6	$\pi/4$	
	165-180	0.5	1	0.5	$\pi/2$	

Based from Table 9, Scenario 1 is set-up to be in the presence of non-coherent MP during an acceleration of vehicle towards the North direction. Scenario 2 is characterized by a non-coherent MP during deceleration of the vehicle. In this scenario, the LOS is lost in this scenario 3s after the generated MP. Scenario 3 studies the presence of a mixture of coherent and non-coherent MP. In this scenario, the vehicle is supposed to have constant speed during the first part of the trajectory and decelerates at the end of the scenario. In scenario 4, the vehicle is affected by a coherent MP when it is moving towards west with a constant velocity. All scenarios presented here have been considered to validate the behaviour of the proposed adaptive tracking algorithm. The performance comparison is done by looking at the tracking error between the estimation provided by the navigator and the reference trajectory.

In order to look closer of the MP effects, the VTL approach is used estimate the position as presented in Figure 106. It is clear that at each MP scenarios introduced will corresponds to a certain biases on the estimated positioning provided by the navigator. This means that the VTL architecture

suffers from some biases at the navigator level which results in poor estimation of the receiver's position.

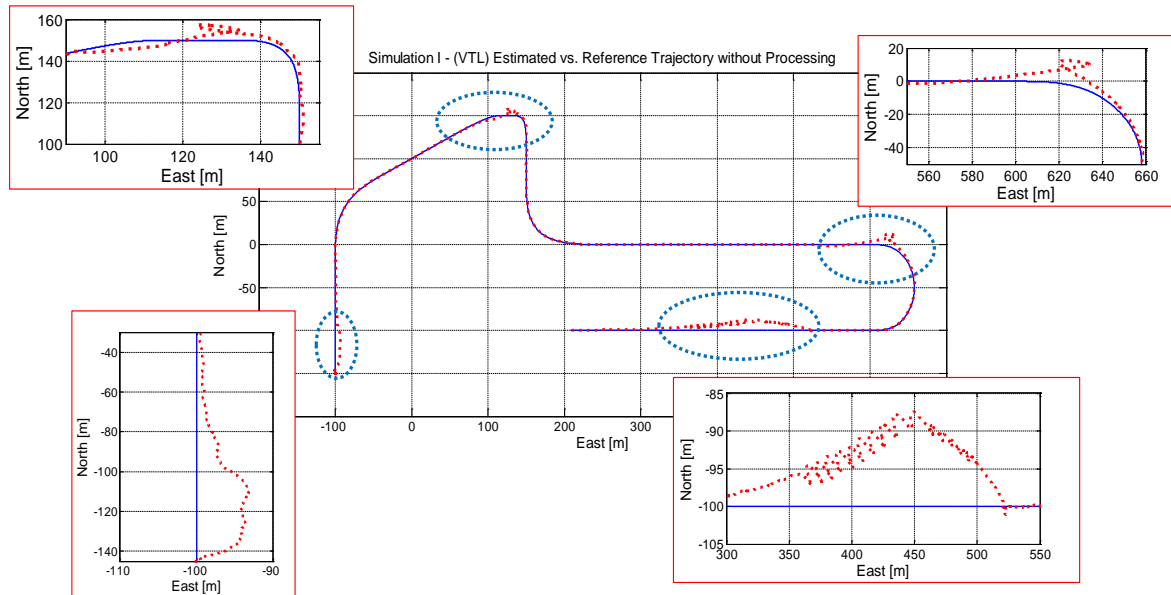


Figure 106: Zoom on the MP scenarios

a) Global Comparison

The global comparison between STL, VTL and proposed AVTL are presented in Figure 107 through Figure 110. The 2D and 3D estimated trajectory by STL, VTL and AVTL architecture are presented in Figure 107 and Figure 108 respectively. On the other hand, the comparison between these architectures versus time in terms of positioning error is presented in Figure 109 and the true error is presented in Figure 110. Lastly, the mean errors and the maximum errors estimated by these architectures are recorded and presented in Table 10.

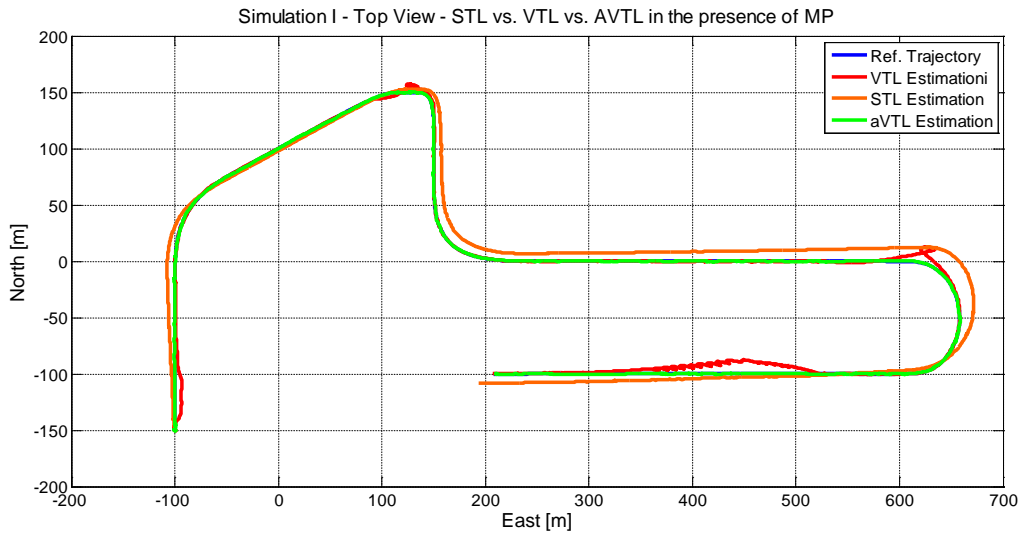


Figure 107: 2D global comparison of position estimation.

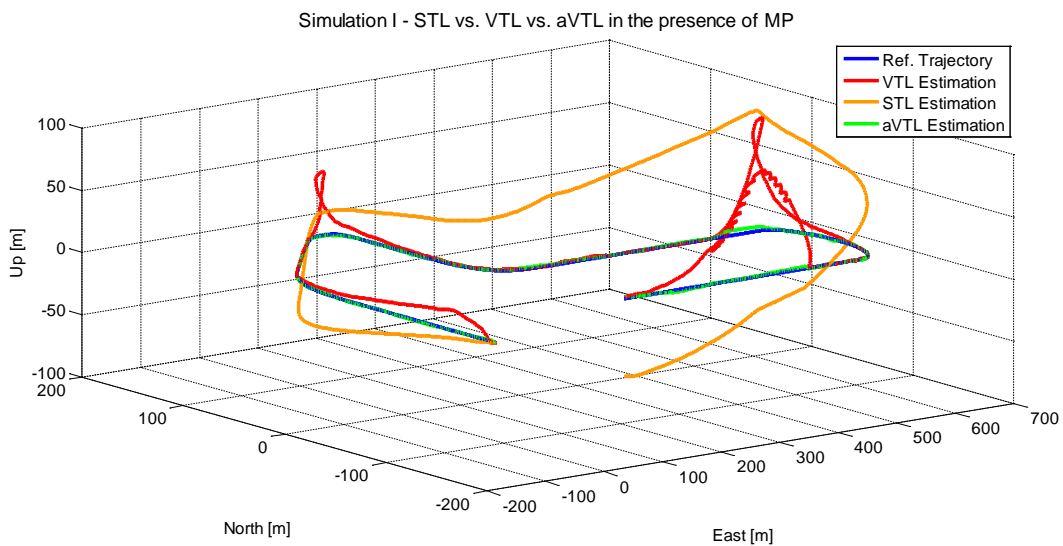


Figure 108: 3D global comparison of position estimation.

Figure 107 and Figure 108 shows that the estimated trajectory performed by STL architectures suffered the worst when compares to the VTL and AVTL approaches. However, the VTL approach also suffered some estimation errors during the MP scenarios introduced during the simulation. This can be explained by the fact that the observation provided by the contaminated channel (channel #1) is being used by the navigator for position estimation.

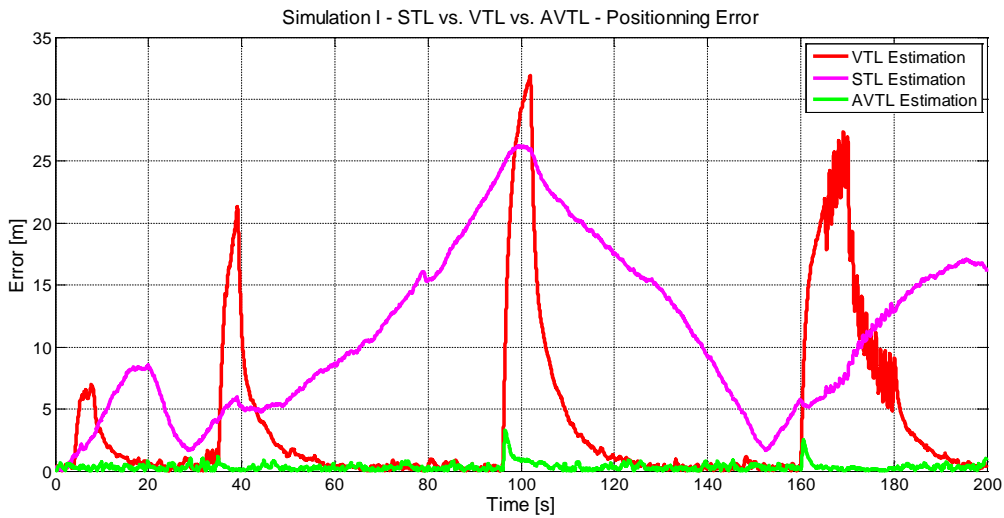


Figure 109: 2D - Positioning Error between STL, VTL and AVTL approaches.

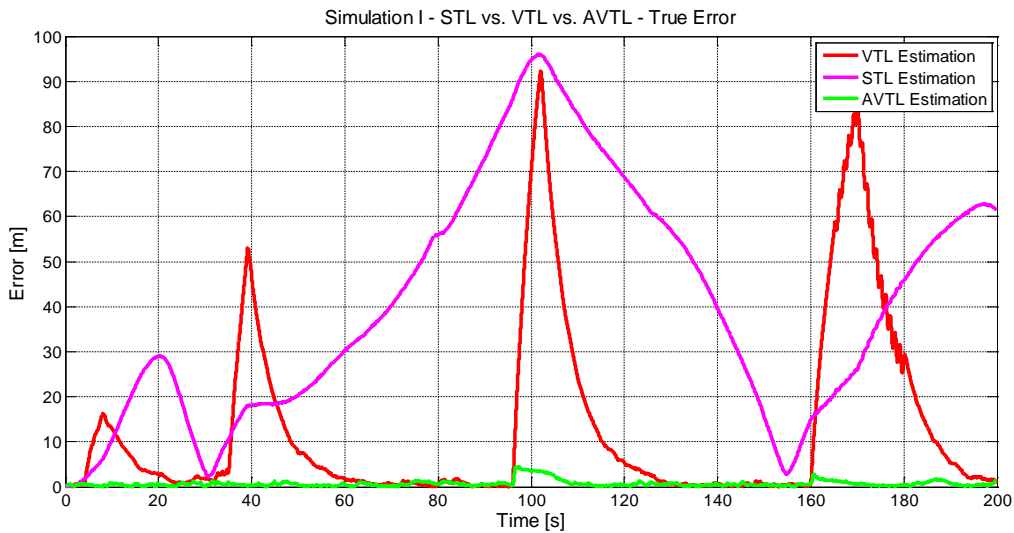


Figure 110: 3D – True Error between STL, VTL and AVTL approaches.

Since the impact of the MP scenarios is not obvious from the figures presented in Figure 107 and Figure 108, therefore, a 2D and 3D positioning errors versus time are presented in Figure 109 and Figure 110 respectively. From this figures, we can observed that for VTL architectures, each MP scenarios introduced during the simulation will correspond to an observable position estimation error but the fact that VTL used the navigator to command the local NCO allows for the estimation to correctly estimated when the MP were absence. In the case of STL, we observed that the biases caused by the MP are not as instantaneous as the VTL approach but cumulatively increases in its positioning errors. In practice for STL architecture, at some point during tracking stage, re-

acquisition is required for the channel that due to loss of locks. But in our simulation, the navigator will continually use the measurement provided by the channels.

Table 10: Mean and maximum values of the positioning error.

	2D Position Error		3D Position Error	
	Mean [m]	Max [m]	Mean [m]	Max [m]
STL	11.05	26.25	40.04	96.04
VTL	3.90	31.90	13.22	92.37
AVTL	0.35	3.30	0.72	4.45

b) Conclusion

Both 2D and 3D tracking errors displayed shows precisely the improvement results from the proposed adaptive tracking algorithm. Both conventional STL and VTL architecture suffers from the presence of the MP. Moreover, these results are confirmed when we calculate the mean and maximum errors for each architectures presented in Table 10. During the whole simulation AVTL manage to keep the mean error to be less than $1m$ for the overall positioning errors.

5.4.2 Simulation using DLR Model

In order to assess the proposed AVTL architectures realistically, a DLR simulator was used to provide the channel model of the receiver. For us to implement this, the DLR model has been handled in a separate simulation to generate the data file containing all the signal parameters independently. We use our artificial trajectory to control the parameters that the DLR model allows for the user to control, such as speed, heading and azimuth which is based on our chosen constellation and trajectory. Other generic parameters associated with the scenario are kept by default. This first stage of the simulation in generating the data file is presented in Figure 111. The generated data file will have the incoming signal profile as what have being presented earlier in Chapter 3 (section 3.4.3). Once the data files were generated, it is used by our simulator as presented in Figure 112. Here, we proposed for the evaluation to be conducted under similar methodology to the one we presented earlier in the case of controlled scenarios.

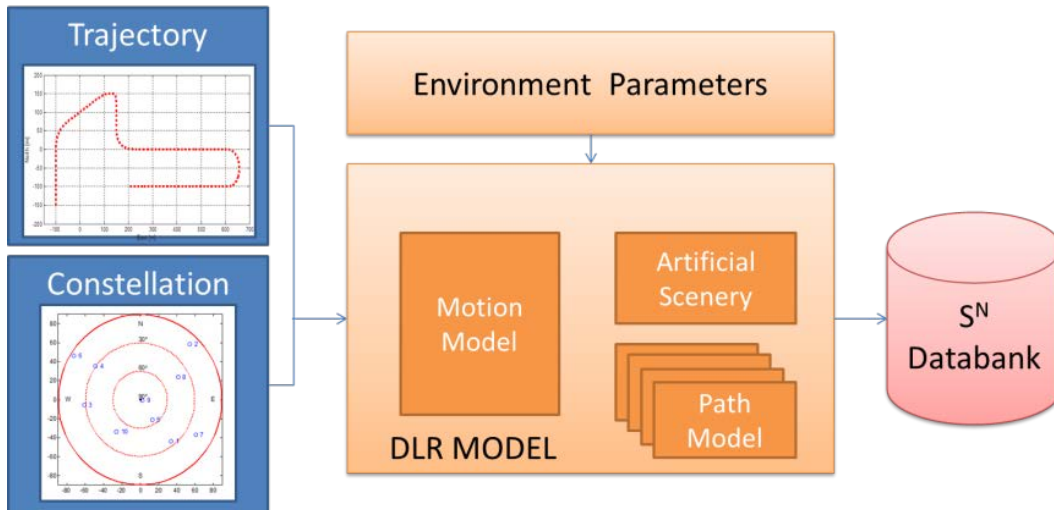


Figure 111: Integrating the DLR to provide the channel profile.

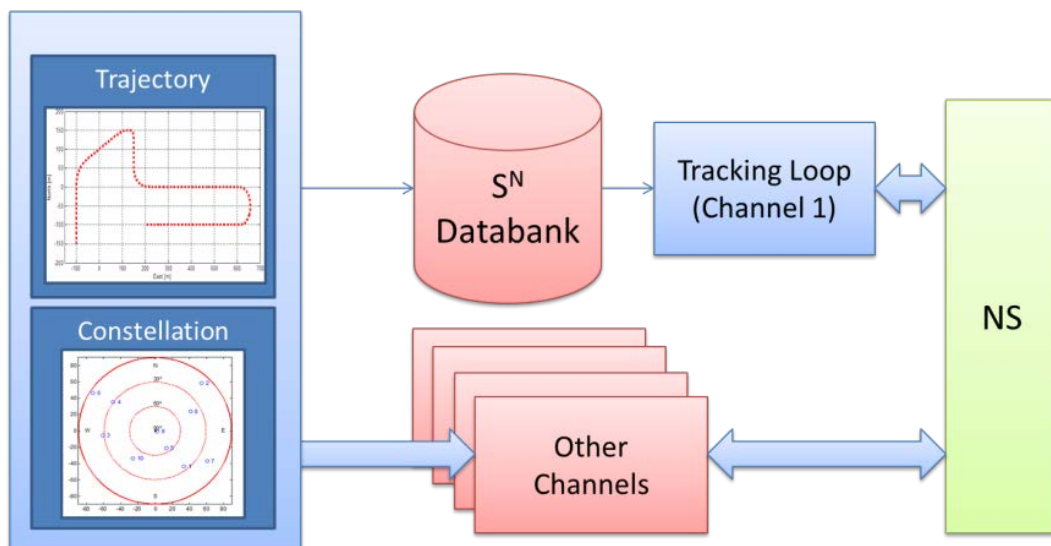


Figure 112: Integrating the data-file generated by the DLR with the in-house simulator.

Overall, we generated nine data files each for both urban and suburban scenarios which are based on a given constellation. For the demonstration however, we choose the channel profile that exhibits harsh condition scenarios where the 3D view of the PSD generated by the DLR model are presented in Figure 113. The use of PSD is considered an effective way to estimate the LOS signal power, the C/N_0 and the signal-to-noise+interference ratio.

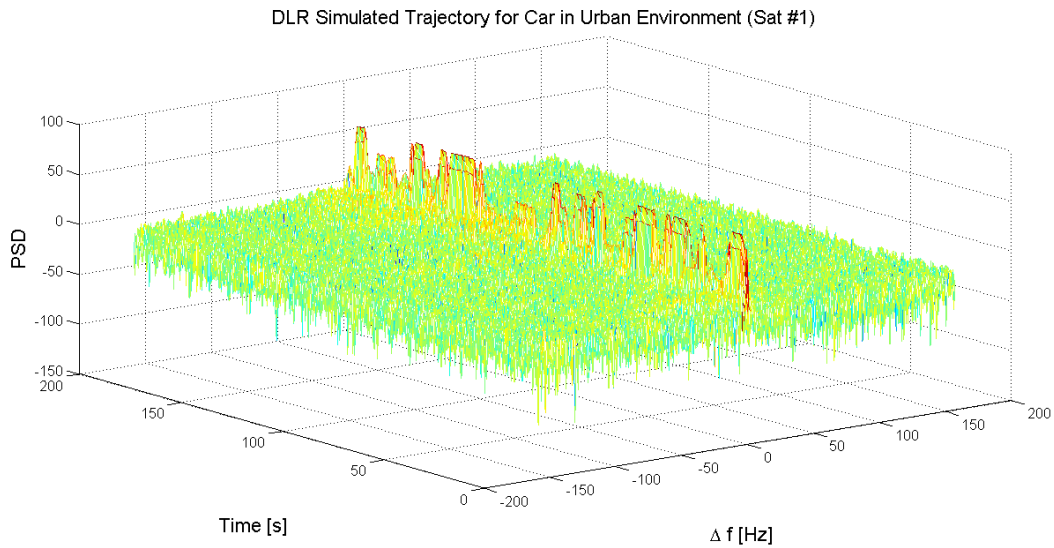


Figure 113: PSD of satellite #1.

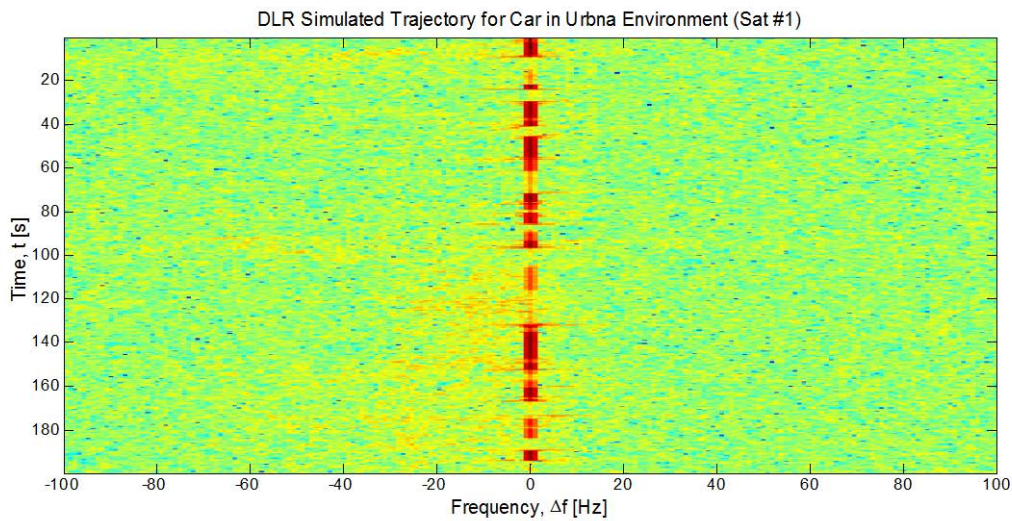


Figure 114: Top view of DLR Simulated Trajectory for Car in Urban Environment (Sat #1)

By referring the PSD provided in Figure 113, we noticed that this channel profile exhibits severe case of channel masking conditions with equally strong attenuation of MP. This condition is more obvious when we look from the top view presented in Figure 114. Note that for this channel model, after approximately 80s during the simulation, strong attenuation of reflection and scattering of MP can be observed. Besides that, during the whole simulation, masking effect consistently occurred throughout the channel which qualified this particular case to be considered as harsh environment. The NLOS signals however are spread in the frequency domain as far as this channel model is concern.

a) Global Comparison

A similar comparison that have been perform in section 5.6.1 is being carried where STL, VTL and AVTL architectures are being compared in term of position estimation where the results were presented from Figure 115 through Figure 118. The position estimation of each architectures superimposed on the reference trajectory are presented in Figure 115 for the 2D position estimation and in Figure 116 for the 3D position estimation. The position error and true error versus time are then presented in Figure 117 and Figure 118 respectively. Later, the mean and maximum errors of STL, VTL and AVTL architecture for both position and true errors are tabulated in Table 12.

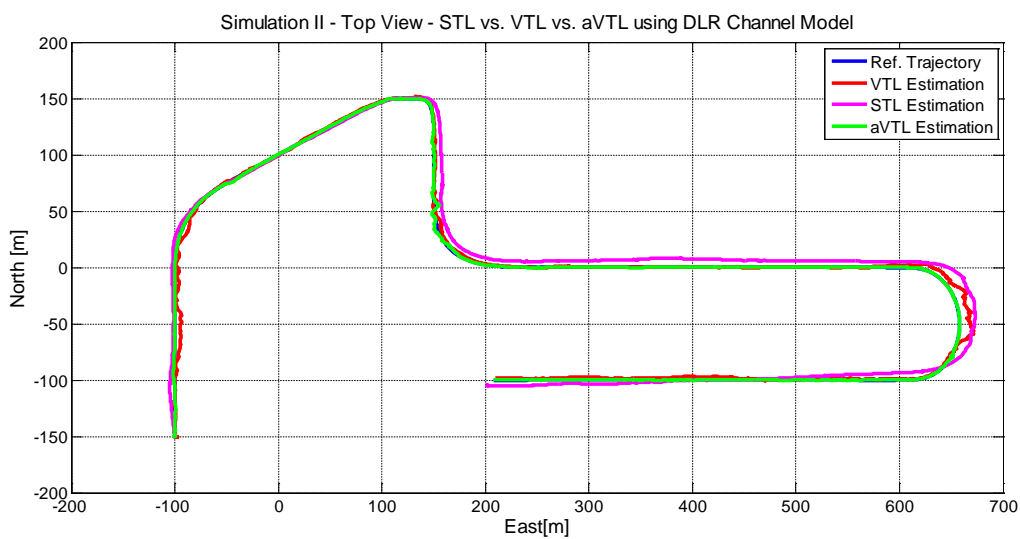


Figure 115: 2D global comparison on position error using DLR Channel Model

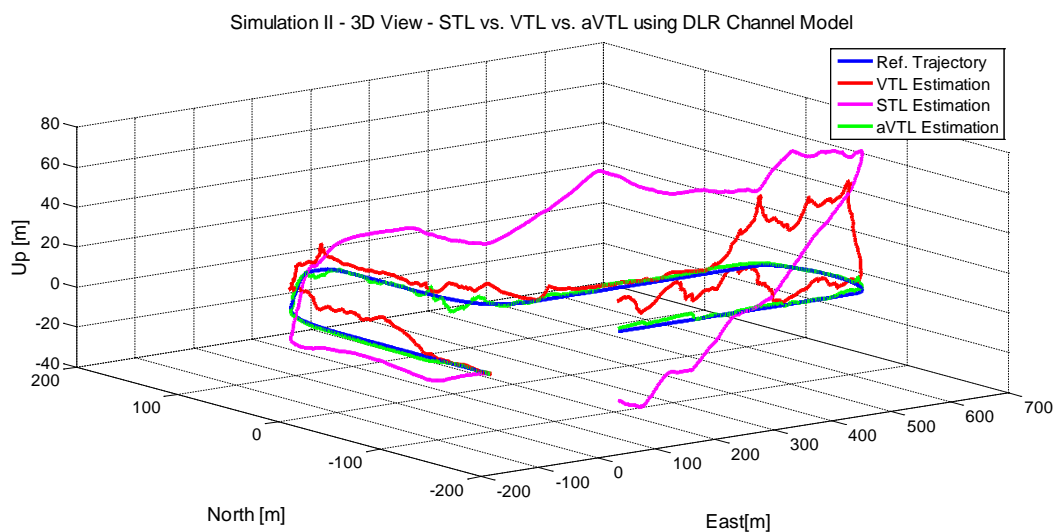


Figure 116: 3D global comparison on true error using DLR Channel Model.

The results presented Figure 115 and Figure 116 shows the position estimation of all architectures where STL suffers the worst relative to VTL and AVTL approaches. In practice, under many severe condition of satellite masking (where the LOS signal is no longer available), re-acquisition is required for the masked channel. In this simulation however, the position estimation is being carried out throughout the simulation so that a global comparison can be performed under the same condition.

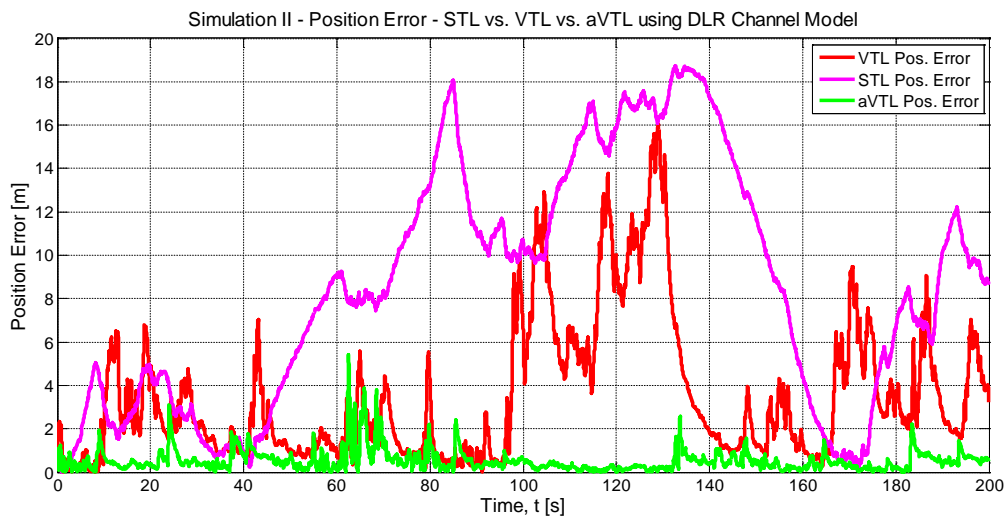


Figure 117: 2D - Positioning Error of STL, VTL and AVTL approaches using DLR channel model.

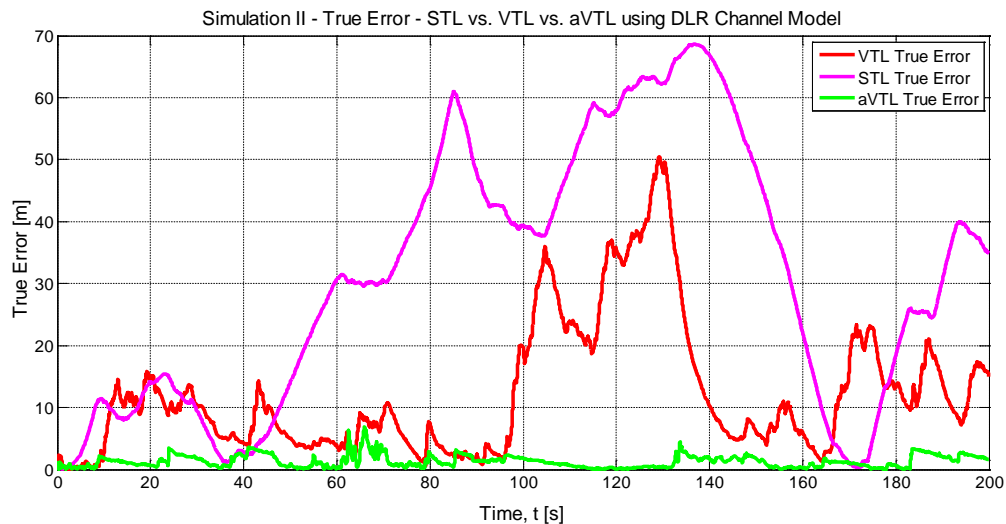


Figure 118: 3D - True Error of STL, VTL and AVTL approaches using DLR channel model.

The positioning errors versus time are presented in Figure 117 for 2D position error and in Figure 118 for the 3D true error respectively in order to evaluate the tracking performance using DLR

channel model. From these figures especially in the case of VTL approach, huge amount of errors occurred between 95s and 135s. This corresponds to a large masking condition if we refer to the PSD presented in Figure 114. Note that at some period during the simulation, STL performed better than VTL, in particular between the period of 165s and 175s. But globally, VTL still outperformed STL under this channel condition. Indeed for DLR channel model, AVTL still outperformed both conventional STL and VTL architectures.

Table 11: Mean and maximum values of the positioning error.

	2D Position Error		3D Position Error	
	Mean [m]	Max [m]	Mean [m]	Max [m]
STL	8.54	18.72	31.09	68.68
VTL	3.53	16.03	12.35	50.54
AVTL	0.53	5.42	1.31	6.88

b) Conclusion

By using the DLR channel model, we are no longer in control of neither the MP scenarios nor the masking effect. The position estimation presented when using the DRL channel model shows that AVTL outperformed both the conventional STL and VTL approach. Note that both STL and VTL approaches suffers significantly under harsh environment condition. Furthermore, these observations and results are verified when the mean and maximum error of each architectures are calculated and presented in Table 11. These results correspond to the results obtained in earlier simulation when controlled MP scenarios were used. Here, the AVTL approach manage to reduce the mean value of the true error to be less than 1.5m.

5.5 Summary

The implementation of the proposed adaptive receiver architecture is based on decentralized VTL approach which also allow seamless switch for an STL mode. The AVTL presented in this chapter proposed to test the quality of the signal inside the local tracking loop by performing test statistics on the incoming signal. Here, we detailed out the specification of each processing techniques which are implemented inside the tracking loop. These techniques concern the channel configuration which can be done by exploiting test statistics for evaluating the quality of the signal

that is being tracked by the local channel. By doing so, we gain both advantages that STL and VTL offers and no longer concern on the issue of contamination of channels. The global comparison shows that the adaptive tracking outperforms better than the conventional STL and VTL architecture. The approach chosen for the architecture assessment will allow specifying and further design for real hardware implementation of a reconfigurable receiver. Indeed, this adaptive approach is considered a good direction on fully developed a GNSS receiver that can adapt its configurations for every environment.

CHAPTER 6

CHAPTER 6 – Conclusions

This chapter summarizes the work invested in this thesis by reiterating the motivations, the approach and benefits of the proposed adaptive tracking architecture, especially what it could offer in term of reliability in the context of harsh environment. The perspective of this study is put into global perspective for further development in the study of GNSS receiver. Lastly, this thesis will be concluded with some prospect of future work that could be of interest for further investigation with respect to GNSS receiver architecture and development.

6.1 Perspective

The present research objective in the field of GNSS is to further improve the overall navigation performance. This means providing better and more robust navigation signals under

every possible scenario. Many of the studies available proposed to process the PR and DR measurement provided by the tracking loop and they perform a statistical analysis on these measurements to improve their reliability. In practice this processing is performed at the navigator rate and this approach doesn't suit for non-stationary MP environment. On the contrary, here, we purposed to process the signal tracked within the local tracking channel, at the discriminator rate, in order to ensure that good measurement are provided to the navigator.

This is done by introducing specific processing inside the local tracking loop in order to detect MP and to soften their effects. Thus, adapting integration time and tracking loop bandwidths allows no-coherent MP impacts, which are not at the LOS frequency, to be mitigated. With regard to NLOS signals which arrive at the LOS frequency, the VTL approach which is proposed here improves the performance of the statistic test which is implemented in the delay domain for detecting the presence of this multipath. A solution is also proposed for mitigating the effect of such MP by selecting adaptively the delay discriminator resolution. By improving the reliability of the measurements which are delivered to the navigator, this approach appears as interesting. As a result, the global performance of the navigator will improve. A step by step evaluation of the received signal inside the tracking loop has been carried out in order to ensure that the adaptive tracking is able to improve the overall performance of the receiver in providing good positioning solution.

To summarize, the contributions of each chapter can be concluded as follows:

Chapter 1 discusses on the problem formulation of this thesis work. The motivation of such studies and detailed objectives of this research are clearly formulated and presented.

In Chapter 2, detailed discussion on the tracking channel is being discussed. Many of the discussion focus on the signal, as well as the tracking loop parameters, and how each of these parameters affects the performance of the tracking loop. At the end of this chapter, an in-house tracking loop was developed and proposed. It will be used for defining an adaptive tracking architecture later in the project.

Chapter 3 however deals with the channel models that will be used to access the performance of the adaptive tracking loop. Here, we proposed to use 2 different approaches with regard to channel models. The first one, based on a deterministic model allows us to control the MP scenarios. This

approach enables a coarse characterization of the channel behaviour to be done. Later, the DLR channel model is proposed to be integrated with our simulator to provide more realistic environment. The main features of this model are described.

The larger perspective of the GPS receiver is addressed in Chapter 4. Here, we discussed on the implementation of the receiver architecture, from the traditional scalar tracking loop (STL) to the vectorial tracking loop (VTL) receiver architectures. We examined both architectures, presenting their advantages and disadvantages, and how an adaptive approach can improve both architectures. In this chapter, we later proposed an STL/VTL approach that is compatible with the implementation of adaptive tracking architecture.

Last but not least, in Chapter 5, we proposed the so called adaptive tracking loop architecture. Here, we detailed out the specification of each processing techniques which are implemented inside the tracking loop. This techniques concern the channel configuration which can be done by exploiting test statistics for evaluating the quality of the signal that is being tracked by the local channel. The simulations presented at the end of this chapter show the global performance of the proposed solution, by comparing the proposed adaptive tracking with the conventional STL and VTL architecture.

6.2 Future Work

This adaptive estimator uses the NS as a command in order to improve the test which are performed within the receiver, by reducing the NCO stress. The approach that has been proposed for coherent LOS mitigation is based on high resolution discriminator. Investigating a measurement which takes into account LOS and MP is also an interesting prospect. In this domain two approaches where considered which can be divided in two main classes. The first one considers an a priori model for LOS and MP. With regard to MP this model is not valid. The second class, which uses a MLE estimator for estimating the LOS and MP parameters without any observations, is not robust in practice. Combining the two approaches by using the VTL approach for exploiting the LOS a priori information could be an attractive solution.

Another aspect of this research that could benefit from this study is the use of an inertial measurement unit (IMU). In that case the VTL approach is referred as a deep integrated INS/GNSS system. This approach allows a reduction of the navigator rate to be obtained.

An interesting study in the continuity of this research could concern the exploitation of MP when 3D representation is available. While the multipath decorrelation which is performed in the frequency and in the time domain doesn't allow MP to be used as measurement in an unknown environment, having the 3D model for a specific environment will allow MP to be handled efficiently. This approach which enables MP to be exploited when the LOS is not available, will lead to an improvement of GNSS availability. The major problem of such methods is that it required a huge computational load for processing.

Further improvement from this concept will then be translated into larger application which ultimately used for higher performance application such as safety and rescue. Last but not least, the realization of such approach on real hardware implementation such as FPGA will be a very interesting prospect. Indeed a lot of efforts need to be done before we could reach this stage, but having a receiver which can adapt to different scenario and still able to provide reliable positioning is something to look forward to in the future.

Bibliography

- [1] P. W. Ward, J. W. Betz and C. J. Hegarty, "Chapter 5: Satellite Signal Acquisition, Tracking and Data Demodulation," in *Understanding GPS: Principles and Applications*, 2nd ed., E. D. Kaplan, Ed., Norwood, MA, Artech House, 2006, pp. 153-241.
- [2] C. Hegarty, M. Tran and J. W. Betz, "Multipath Performance of the New GNSS Signals," in *ION NTM*, San Diego, 2004.
- [3] G. T. Ferreira and D. F. Nunes, "Advanced Multipath Mitigation Techniques For GNSS Receivers," in *ANACOM 2007*, 2007.
- [4] N. Viandier, J. Marais, A. Rabaoui and E. Duflos, "GNSS pseudorange error density tracking using Dirichlet Process Mixture," in *13th Conference on Information Fusion (FUSION)*, Edinburgh, 2010.
- [5] A. Giremus, J.-Y. Tournet and A. Doucet, "A Fixed-Lag Particle Filter for the Joint Detection/Compensation of Interference Effects in GPS Navigation," *IEEE Transactions on Signal Processing*, vol. 58, no. 12, pp. 6066-6079, 2010.
- [6] M. Spangenberg, V. Calmettes, O. Julien, J.-Y. Tournet and G. Duchateau, "Detection of Variance Changes and Mean Value Jumps in Measurement Noise for Multipath Mitigation in Urban Navigation," *NAVIGATION*, vol. 57, no. 1, pp. 35-52, 2010.
- [7] B. Krach, A. Steingass and A. Lehner, "Technical Note on the Implementation of the Land Mobile Satellite Channel Model - Software Usage," German Aerospace Center (DLR), Cologne, 2007.
- [8] J. B.-Y. Tsui, *Fundamentals of Global Positioning System Receivers A Software Approach*, 2nd ed., New Jersey: John Wiley & Sons, Inc., 2005.
- [9] J. J. Spilker Jr., "Chapter 3: GPS Signal Structure and Theoretical Performance," in *Global Positioning System: Theory and Applications Volume I*, Sunnyvale, CA, American Institute of Aeronautics and Astronautics, Inc., 1994, pp. 57-119.
- [10] K. Borre, D. M. Akos, N. Bertelsen, P. Rinder and S. H. Jensen, *A Software-Defined GPS and GALILEO Receiver - A Single Frequency Approach*, Boston: Birkhauser, 2007.
- [11] M. Lashley and D. M. Bevy, "Comparison in the Performance of the Vector Delay/Frequency Lock Loop and Equivalent Scalar Tracking Loops in Dense Foliage and Urban Canyon," in *Proceedings of the 24th International Technical Meeting of The Satellite Division of the Institute of Navigation (ION GNSS 2011)*, Portland, OR, 2011.
- [12] E. D. Kaplan and C. J. Hegarty, *Understanding GPS: Principles and Applications*, 2nd ed., E. D.

Kaplan, Ed., Norwood, MA: Artech House, 2006.

- [13] J.-H. Won, D. Dötterböck and B. Eissfeller, "Performance Comparison of Different Forms of Kalman Filter Approach for a Vector-Based GNSS Signal Tracking Loop," *NAVIGATION*, vol. 7, no. 3, pp. 189-199, 2010.
- [14] A. Lehner, "Multipath Channel Modelling for Satellite Navigation System," Ph.D dissertation, Technischen Fakultät der Universität Erlangen-Nürnberg, Erlangen, 2007.
- [15] B. W. Parkinson, "GPS Error Analysis," in *Global Positioning System: Theory and Applications Volume I*, California, American Institute of Aeronautics and Astronautics, Inc., 1996, pp. 469-483.
- [16] A. Mehmood and A. Mohammad, "Characterisation and Channel Modelling for Mobile Satellite Communication Systems," in *Satellite Communications*, N. Diodata, Ed., Rijeka, InTech, 2010, pp. 133-151.
- [17] F. S. Solheim, J. Vivekanandan, R. H. Ware and C. Rocken, "Propagation delays induced in GPS dry air, water vapors, hydrometeors, and other particulates," *Geophysical Research*, vol. 104, no. D8, pp. 9663-9670, 1999.
- [18] A. Jahn, H. Bischl and G. HeiB, "Channel Characterisation for Spread Spectrum Satellite Communication," in *IEEE 4th International Symposium on Spread Spectrum Techniques and Applications Proceedings*, Mainz, 1996.
- [19] A. Abdi, W. C. Lau, M.-S. Alouini and M. Kaveh, "A new simple model for land mobile satellite channels: First and second order statistics," *IEEE Transactions on Wireless Communication*, vol. 2, no. 3, pp. 519-528, 2003.
- [20] A. Abele, F. Perez-Fontan, M. Bousquet, P. Valtr, J. Lemorton, F. Lacoste and E. Corbel, "A new physical-statistical model of the land mobile satellite propagation channel," in *Fourth European Conference on Antenna and Propagation*, Barcelona, 2010.
- [21] A. Lehner and A. Steingass, "A Novel Channel Model for Land Mobile Satellite Navigation," in *ION GNSS 18th International Technical Meeting of the Satellite Division*, Long Beach, 2005.
- [22] M. S. Karaliopoulos and F. N. Pavlidou, "Modelling the land mobile satellite channel: a review," *Electronics & Communication Engineering Journal*, pp. 235-248, 1999.
- [23] F. P. Fontan, M. Vazquez-Castro, C. E. Cabado, J. P. Garcia and E. Kubista, "Statistical Modelling of the LMS Channel," *IEEE Transactions on Vehicular Technology*, vol. 50, no. 6, pp. 1549-1567, November 2001.
- [24] M. Irsigler, J. A. Avila-Rodriguez and G. W. Hein, "Criteria for GNSS Multipath Performance Assessment," in *ION GNSS Technical Program 2005*, Long Beach, California, 2005.

- [25] C. Oestges, S. Saunders and D. Vanhoenacker-Janvier, "Physical statistical modelling of the land mobile satellite channel based on ray tracing," *IEE Proceedings - Microwave, Antennas and Propagation*, vol. 146, no. 1, pp. 45-49, 1999.
- [26] A. Lehner, "Satellite Navigation Multipath Channel Model," German Aerospace Center (DLR), 12 March 2013. [Online]. Available: <http://.kn-s.dlr.de/satnav/>. [Accessed 10 December 2013].
- [27] S. F. Syed Dardin, V. Calmettes, B. Priot and J.-Y. Tournet, "Design of an Adaptive Vector-Tracking Loop for Reliable Positioning in Harsh Environment," in *26th International Technical Meeting of the Satellite Division of the Institute of Navigation (ION GNSS+ 2013)*, Nashville, 2013.
- [28] S. F. Syed Dardin, V. Calmettes, B. Priot and J.-Y. Tournet, "Adaptive GNSS signal tracking techniques in the context of a deeply integrated GNSS/INS navigation system designed for tackling multipath in urban environment.," in *The European Navigation Conference*, Vienna, 2013.
- [29] J. R. De Boer, W. Vigneau, V. Calmettes, S. Bidon and L. Ries, "Specification of a Simulator to Access the Performance of Adaptive Vector Tracking Loops in Urban Environment," in *6th European Workshop on GNSS Signals and Signals Processing*, Munich, 2013.
- [30] H. Chen, T. Kirubarajan and Y. Bar-Shalom, "Comparison of centralized and distributed tracking algorithms using air-to-air scenarios," *Proc. SPIE 4048, Signal and Data Processing of Small Targets 2000*, pp. 440-451, 13 July 2000.
- [31] P. Axelrad and R. G. Brown, "Chapter 9 - GPS Navigation Algorithm," in *Global Positioning System: Theory and Applications Volume I*, Washington, American Institute of Aeronautics and Astronautics, Inc., 1996, pp. 409-433.
- [32] P. D. Groves, *Principles of GNSS, Inertial, and Multisensors Integrated Navigation Systems*, Boston: Artech House, 2008.
- [33] M. Lashley, D. M. Bevely and J. Y. Hung, "A Valid Comparison of Vector and Scalar Tracking Loops," in *Position Location and Navigation Symposium (PLANS), 2010 IEEE/ION*, Indian Wells, 2010.
- [34] M. Lashley, D. M. Bevely and J. Y. Hung, "Performance Analysis of Vector Tracking Algorithms for Weak GPS Signals in High Dynamics," *IEEE Journal of Selected Topics In Signal Processing*, vol. 3, no. 4, pp. 661-673, 2009.
- [35] S. Peng, J. Morton and R. Di, "A multiple-frequency GPS software receiver design based on a vector tracking loop," in *Proceedings of IEEE/ION PLANS 2012*, Myrtle Beach, SC, 2012.

- [36] M. Spangenberg, V. Heiries, A. Giremus and V. Calmettes, "Multi-Channel Extended Kalman Filter for Tracking BOC modulated signals in the presence of multipath," in *18th International Technical Meeting of the Satellite Division of the Institute of Navigation*, Long Beach, 2005.
- [37] A. Giremus, T. Jean-Yves and V. Calmettes, "A Particle Filter Approach for Joint Detection/Estimation of Multipath Effects on GPS Measurement," *IEEE Transaction on Signal Processing*, vol. 55, no. 4, pp. 1275-1285, 2007.
- [38] N. Viandier, D. Nahimana, J. Marais and E. Duflos, "GNSS Performance Enhancement in Urban Environment Based on Pseudo-range Error Model," in *Proceedings of IEEE/ION PLANS 2008*, Monterey, 2008.
- [39] J. J. Spilker Jr., "Chapter 7: Fundamentals of Signal Tracking Theory," in *Global Positioning System: Theory and Applications Volume I*, Sunnyvale, American Institute of Aeronautics and Astronautics, 1994, pp. 245-327.
- [40] H. So, T. Lee, S. Jeon, C. Kim, C. Kee, T. Kim and S. Lee, "Implementation of a Vector-based Tracking Loop Receiver in a Pseudolite Navigation System," *Sensors*, vol. 10, no. 7, pp. 6324-6346, 2010.
- [41] M. Lashley and D. M. Bevly, "GNSS Solution: What About Vector Tracking Loops?," *InsideGNSS*, pp. 16-21, May/June 2009.
- [42] M. Petovello and G. Lachapelle, "Comparison of Vector-Based Software Receiver Implementations with Application to Ultra-Tight GPS/INS Integration," in *Proceedings of the 19th International Technical Meeting of the Satellite Division of The Institute of Navigation (ION GNSS 2006)*, Fort Worth, 2006.
- [43] W. L. Edwards, B. J. Clark and D. M. Bevly, "Implementation Details of a Deeply Integrated GPS/INS Software Receiver," in *Position Location and Navigation Symposium (PLANS), 2010 IEEE/ION*, Indian Wells, CA, 2010.
- [44] M. Petovello, D. Sun, G. Lachapelle and M. Cannon, "Performance Analysis of an Ultra-Tightly Integrated GPS and Reduced IMU System," in *Proceedings of the 20th International Technical Meeting of the Satellite Division of The Institute of Navigation (ION GNSS 2007)*, Fort Worth, TX, 2007.
- [45] M. Lashley and D. M. Bevly, "Vector Delay/Frequency Lock Loop Implementation and Analysis," in *Proceedings of the 2009 International Technical Meeting of The Institute of Navigation*, Anaheim, CA, 2009.
- [46] T. Pany, R. Kaniuth and B. Eissfeller, "Deep Integration of Navigation Solution and Signal

- Processing," in *Proceedings of the 18th International Technical Meeting of the Satellite Division of The Institute of Navigation (ION GNSS 2005)*, Long Beach, CA, 2005.
- [47] T. Lin, C. O'Driscoll and G. Lachapelle, "Channel Context Detection and Signal Quality Monitoring for Vector-based Tracking Loops," in *Proceedings of the 23rd International Technical Meeting of The Satellite Division of the Institute of Navigation (ION GNSS 2010)*, Portland, OR, 2010.
- [48] S. Zhao and D. Akos, "An Open Source GPS/GNSS Vector Tracking Loop - Implementation, Filter Tuning, and Results," in *Proceedings of the 2011 International Technical Meeting of The Institute of Navigation*, San Diego, CA, 2011.
- [49] D. Benson, "Interference Benefits of a Vector Delay Lock Loop (VDLL) GPS Receiver," in *Proceedings of the 63rd Annual Meeting of The Institute of Navigation*, Cambridge, MA, 2007.
- [50] M. Petovello, C. O'Driscoll and G. Lachapelle, "Carrier Phase Tracking of Weak Signals Using Different Receiver Architectures," in *Proceedings of the 2008 National Technical Meeting of The Institute of Navigation*, San Diego, CA, 2008.
- [51] M. L. Psiaki and H. Jung, "Extended Kalman Filter Methods for Tracking Weak GPS Signals," in *Proceedings of the 15th International Technical Meeting of the Satellite Division of The Institute of Navigation (ION GPS 2002)*, Portland, OR, 2002.
- [52] M. L. Psiaki, "Smoother-Based GPS Signal Tracking in a Software Receiver," in *Proceedings of the 14th International Technical Meeting of the Satellite Division of The Institute of Navigation (ION GPS 2001)*, Salt Lake City, UT, 2001.
- [53] M. Lentmaier, B. Krach and P. Robertson, "Bayesian Time Delay Estimation of GNSS Signals in Dynamic Multipath Environments," *International Journal of Navigation and Observation*, Vols. 2008, Article ID 372651, no. 10.1155/2008/372651, pp. 1-11, 2008.
- [54] E. Copps, G. Geier, W. Fidler and P. Grundy, "Optimal Processing of GPS Signal," *Navigation: Journal of the Institute of Navigation*, vol. 27, no. 3, pp. 171-182, 1980.
- [55] S. Kiesel, C. Ascher, D. Gramm and G. F. Trommer, "GNSS Receiver with Vector Based FLL-Assisted PLL Carrier Tracking Loop," in *Proceedings of the 21st International Technical Meeting of the Satellite Division of The Institute of Navigation (ION GNSS 2008)*, Savannah, GA, 2008.
- [56] T. Pany and B. Eissfeller, "Use of a Vector Delay Lock Loop Receiver for GNSS Signal Power Analysis in Bad Signal Conditions," in *Proceedings of IEEE/ION Position, Location, And Navigation Symposium (PLANS) 2006*, San Diego, CA, 2006.
- [57] M. Zhodzishsky, S. Yudanov, V. Veitsel and J. Ashjaee, "Co-OP Tracking for Carrier Phase," in *Proceedings of the 11th International Technical Meeting of the Satellite Division of The Institute*

- of Navigation (ION GPS 1998)*, Nashville, 1998.
- [58] N. Sokhandan, A. Broumandan, J. T. Curran and G. Lachapelle, "High Resolution Delay Estimation for Urban GNSS Vehicular Navigation," in *Proceedings of the 25th International Technical Meeting of The Satellite Division of the Institute of Navigation (ION GNSS 2012)*, Nashville, TN, 2012.
- [59] K. Dragūnas and K. Borre, "Multipath Mitigation Based on Deconvolution," *Journal of Global Positioning System 2011*, vol. 10, no. 1, pp. 79-88, 2011.
- [60] G. A. McGraw and M. S. Braasch, "Multipath Mitigation Using Gated and High Resolution Correlator Concepts," in *Proceedings of the National Technical Meeting of the Satellite Division of the Institute of Navigation*, San Diego, 1999.
- [61] P. D. Groves, Principles of GNSS, inertial, and multi-sensor integrated navigation systems, Artech House, 2008.
- [62] N. Bergman, "Posterior Cramer-Rao Bounds for Sequential Estimation," in *Sequential Monte Carlo Methods in Practice*, New York, Springer-Verlag, 2001.
- [63] ISAE, "Récepteur GNSS intègre pour environnements difficiles. Patent pending." 2014.
- [64] CNES, M3S and ISAE, "Dispositif de poursuite intègre de signaux GNSS. Patent pending CNES B1454." 2014.
- [65] K. D. Rao, M. Swamy and E. I. Plotkin, "GPS Navigation with Increased Immunity to Modeling Errors," *IEEE Transaction on Aerospace and Electronic Systems*, vol. 40, no. 1, pp. 1-11, 2004.
- [66] A. Van Dierendonck, P. Fenton and T. Ford, "Theory and Performance of Narrow Correlator Spacing in a GPS Receiver," *NAVIGATION: Journal of The Institute of Navigation*, vol. 39, no. 3, pp. 265-283, Fall 1992.
- [67] M. S. Braasch, "Performance Comparison of Multipath Mitigating Receiver Architecture," *IEEE*, vol. 3, pp. 1309-1315, 2001.
- [68] C. Loo, "A Statistical Model for a Land Mobile Satellite Link," *IEEE Transactions on Vehicular Technology*, Vols. VT-34, no. 3, pp. 122-127, August 1985.
- [69] G. E. Corazza and F. Vatalaro, "A Statistical Model for Land Mobile Satellite Channels and Its Application to Nongeostationary Orbit System," *IEEE Transactions on Vehicular Technology*, vol. 43, no. 3, pp. 738-742, August 1994.
- [70] A. Van Dierendonck and M. S. Braasch, "Evaluation of GNSS Receiver Correlation Processing Techniques for Multipath and Noise Mitigation," in *Proceeding of the 1997 National Technical Meeting of the Institute of Navigation*, Santa Monica, 1997.

- [71] M. Irsigler and B. Eissfeller, "Comparison of multipath mitigation techniques with consideration of future signal structures," in *Proceedings of the 16th International Technical Meeting of the Satellite Division of the Institute of Navigation*, Portland, 2003.
- [72] M. Z. H. Bhuiyan, E. S. Lohan and M. Renfors, "Code Tracking Algorithms for Mitigating Multipath Effects in Fading Channels for Satellite-Based Positioning," *EURASIP Journal on Advances in Signal Processing*, vol. 2008, p. 17, 2008.
- [73] L. Garin, F. v. Diggelen and J.-M. Rousseau, "Strobe & Edge Correlator Multipath Mitigation for Code," in *Proceedings of the 9th International Technical Meeting of the Satellite Division of The Institute of Navigation*, Kansas City, 1996.
- [74] A. Steingass and A. Lehner, "Land Mobile Satellite Navigation - Characteristics of the Multipath Channel," in *Proceedings of the 16th International Technical Meeting of the Satellite Division of the Institute of Navigation (ION GPS/GNSS 2003)*, Portland, 2003.
- [75] B. W. Parkinson and J. J. Spilker, *Global Positioning System: Theory and Applications I*, Massachusetts: American Institutr of Aeronautics and Astronautics, Inc., 1996.
- [76] P. Misra and P. Enge, *Global Positioning System: Signals, Measurements, and Performance*, Massachusetts: Ganga-Jamuna Press, 2006.
- [77] M. Lashley and D. M. Bevly, "Analysis of Discriminator Based Vector Tracking Algorithms," in *Proceedings of the 2007 National Technical Meeting of The Institute of Navigation*, San Diego, CA, 2007.
- [78] M. Lashley, "Modeling and Performance Analysis of GPS Vector Tracking Algorithms," Ph.D dissertation, Auburn University, Auburn, AL, 2009.
- [79] P. Mahalanobis, "On the generalized distance in statistics," in *Proceedings of the National Institute of Sciences*, Calcutta, 1936.
- [80] R. D. J. Van Nee, "Spread Spectrum Code and Carrier Synchronization Errors Caused by Multipath and Interference," *IEEE Transaction On Aerospace and Electronic Systems*, vol. 29, no. 4, pp. 1359-1365, 1993.

Rédaction De Mémoire De Thèse

Etude d'Algorithmes de Poursuite du Signal GNSS Permettant d'Améliorer le Positionnement en Environnement Urbain

Par,

Syed Mohd Fairuz Bin Syed Mohd Dardin

ISAE-Supaero

Directeur de Thèse : **Prof. Jean-Yves Tournet**, *ENSEEIH*

Co-Directeur de Thèse : **Dr. Vincent Calmettes**, *ISAE-Supaero*

CHAPITRE 1: Introduction

Objectif

Cette activité de recherche concerne le domaine de la navigation par satellite qui utilise les systèmes GNSS (Global Navigation Satellite Systems). Elle vise à améliorer les performances globales d'un système de navigation, c'est à dire la robustesse, la disponibilité et l'intégrité d'un récepteur utilisant les signaux GNSS pour élaborer sa position et sa vitesse. L'enjeu est important, le nombre d'applications exigeant une information de position ne cessant de croître. Pour atteindre les objectifs de performance cités on note par exemple que les représentations des nouveaux signaux proposés pour GPS et GALILEO visent à améliorer les propriétés d'intercorrélation entre les signaux, faciliter la poursuite de ces signaux en abaissant le niveau des seuils de poursuite, et réduire l'effet des interférences. La navigation basée sur les signaux GNSS reste toutefois dépendante du canal de propagation et est particulièrement affectée en cas réflexion, réfraction, diffraction, diffusion, et de blocage du signal émis par le satellite. Il en résulte une dégradation importante des performances de localisation en environnement urbain. L'objectif de cette recherche est ainsi de proposer, d'analyser et de caractériser des architectures de récepteur robuste, permettant d'adresser efficacement le problème de la navigation dans des environnements difficiles où le signal GNSS est affecté par de fortes perturbations, telles que celles décrites sur la figure 1, où le signal transmis par le satellite peut être masqué, réfléchi, diffracté par les bâtiments. Lorsque le véhicule se déplace il en résulte des fluctuations de la puissance du signal reçu, qui résulte de la combinaison des signaux des divers trajets dont la phase, l'amplitude et la direction varient dans le temps.

Il devient nécessaire de proposer des traitements au sein des récepteurs. Cette thèse propose d'implanter ces traitements au sein des boucles de poursuite des récepteurs, dans des schémas de poursuite vectorielle. L'accent est mis sur la définition d'une architecture reconfigurable utilisant la sortie de détecteurs opérant dans le domaine des retards et le domaine de fréquences, et sur la mise en œuvre de solution pour l'adoucissement des effets des multi-trajets.

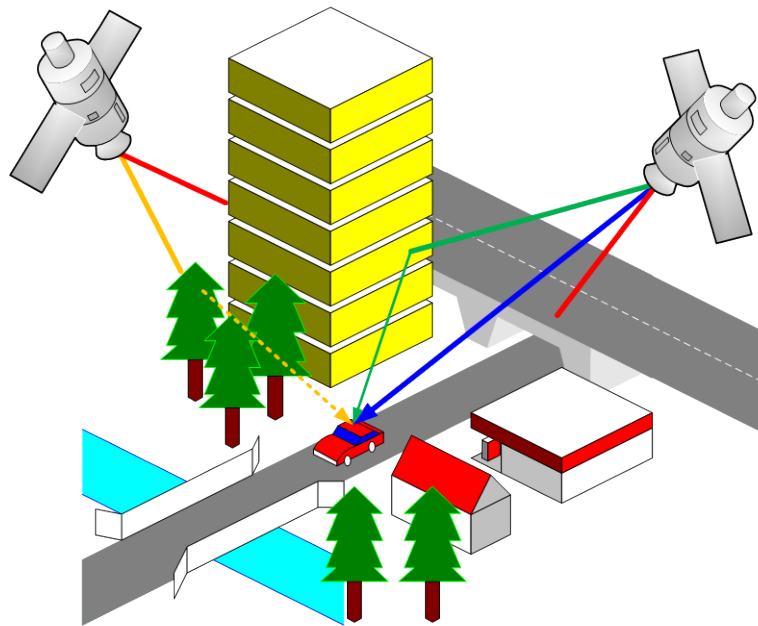


Figure 1: Navigation en environnement difficile

Contexte

Les méthodes explorées pour améliorer la robustesse des récepteurs GPS adressent habituellement le traitement des mesures délivrées par le récepteur. Ces mesures déduites d'une estimation du retard de propagation, et de la fréquence Doppler du signal reçu sont des mesures de pseudo-distances, et de delta-distances. Elles sont délivrées au rythme de fonctionnement du navigateur, qui peut varier de 1Hz à 20Hz selon les récepteurs. Les traitements réalisés sur ces mesures sont ainsi effectués à ce rythme. Plusieurs approches ont été considérées. Dans [1] un modèle de mesure paramétrique est considéré, en considérant le biais induit par un multi-trajet. Ce biais est estimé en utilisant des méthodes de Monte Carlo. Dans [2] le modèle de mesure utilisé en présence de multi-trajets est basé sur un mélange de gaussiennes, et la commutation d'un modèle à l'autre sur un système à saut de Markov. Dans [3] un traitement en ligne est implémenté pour rendre consistant un estimateur basé sur un filtre de Kalman étendu. Ce traitement consiste à estimer la moyenne et la variance de la loi de mesure. Tous ces traitements s'appliquent aux mesures utilisées en entrée du navigateur.

Sur la durée d'élaboration de la mesure le modèle dynamique qui décrit l'évolution du retard de propagation et de la fréquence du trajet direct est en général bien maîtrisé. Par contre les bruits sur

ces mesures de retard et de fréquence Doppler peuvent fluctuer rapidement sur cette durée. On note des variations d'autant plus rapides que la vitesse du véhicule est importante. Il est donc logique d'imaginer des méthodes de traitements plus en amont dans le récepteur. Ces méthodes de traitement ne peuvent s'appliquer au signal reçu, représenté par une suite d'échantillons dont le rythme varie habituellement entre 1MHz et 20MHz. Une compression de l'information est réalisée. Elle consiste en un filtre adapté qui réalise la corrélation du signal reçu avec un signal réplica dont les paramètres sont estimés par le récepteur. Le signal de sortie de ce corrélateur contient tous les paramètres du signal. En pratique plusieurs corrélateurs sont nécessaires. Le nombre de ces corrélateurs dépend du modèle de mesure utilisé par l'estimateur. Ce modèle de mesure évolue au rythme des corrélations qui peut varier, en général, de 1ms à 20 ms. Implanter des traitements à ce rythme permet de définir des fenêtres d'observation sur lesquelles on peut admettre la stationnarité des bruits de mesure, même en présence de multi-trajets. Des méthodes de traitement ont ainsi été proposées. Elles consistent à une décomposition temps fréquence [4], ou à des algorithmes de déconvolution consistant à estimer les paramètres du canal en présence de multi-trajets [5]. La charge de calcul induite ne permet pas d'envisager un traitement en ligne du signal reçu.

Des techniques ont été étudiées pour permettre ce traitement en ligne de la mesure obtenue en sortie de corrélateurs en présence de multi-trajets. Elles peuvent utiliser des modèles d'évolution des paramètres des trajets qui peuvent être pertinents pour le trajet direct puisque ses paramètres suivent la dynamique du véhicule [6]. Ils ne le sont pas pour les trajets réfléchis. Dans ces conditions il peut être envisagé d'utiliser des méthodes basées sur l'estimateur de maximum de vraisemblance, sur une durée d'observation à définir d'après la qualité du signal mesuré [7]. La charge de calcul est importante et la robustesse de cette méthode reste un problème.

L'approche étudiée dans le cadre de cette thèse concerne des techniques de poursuite dites vectorielles (VTL) qui utilisent le navigateur pour construire le signal replica appliqué aux corrélateurs. La poursuite bénéficie donc de toutes les mesures présentées au navigateur [8]. Cette approche a été analysée s'agissant de la poursuite de signaux très bruités. Ces méthodes sont à opposer aux méthodes de poursuite scalaire qui utilisent pour chaque canal un estimateur local pour estimer les paramètres du signal réplica, dont sont déduites les mesures utilisées par le récepteur.

Le principal problème induit par la boucle VTL est le risque de contamination entre canaux. Il devient crucial de détecter une mesure contaminée de manière à garantir l'intégrité du navigateur. En

améliorant l'information a priori sur les paramètres du trajet direct cette approche facilite la détection de multi-trajet.

L'objectif du travail conduit au cours de cette thèse a été défini en s'appuyant sur cette analyse. Il inclut la définition de méthodes faible coût et robustes, utilisant l'architecture VTL pour adresser le problème de la navigation en présence de multi-trajets. Il a pour but d'évaluer l'intérêt de cette approche dans des environnements GNSS défavorables. Ce travail est décrit dans un rapport découpé en 6 chapitres.

- Le chapitre 1 fait un état de l'art des systèmes GNSS et introduit le domaine de recherche exploré dans le cadre de cette thèse.
- Le chapitre 2 présente les formes des signaux GPS. Il décrit par ailleurs le fonctionnement des boucles de poursuite conventionnelles et les paramètres qui impactent les performances de ces boucles. Une présentation des techniques de traitement au sein du récepteur est aussi proposée.
- Le chapitre 3 vise à analyser des modèles du canal Satellite-Mobile, ainsi que les effets des multi-trajets sur un récepteur conventionnel. Un modèle de canal simple déterministe est proposé pour une première analyse des algorithmes alors que la représentation du signal d'interférence est imposée et donc connue. Le modèle de canal défini dans [9] est aussi étudié. Il est exploité pour produire des simulations dans un environnement plus réaliste.
- Le chapitre 4 décrit plusieurs approches qui peuvent être utilisées pour élaborer un récepteur de navigation délivrant la position et la vitesse de ce récepteur. L'analyse qui est faite permet de dériver le récepteur conventionnel, basé sur une architecture STL, mais aussi un récepteur exploitant une poursuite vectorielle du signal. Ces 2 approches sont analysées en termes de complexité et performance. Les avantages et inconvénients de chacune d'elles sont présentés. Finalement une architecture permettant une reconfiguration aisée supportant les modes de poursuite STL et VTL est proposée.
- Le chapitre 5 décrit une architecture adaptative permettant d'exploiter les modes de poursuite STL et VTL pour améliorer les performances de la navigation en environnement urbain. Une première approche consiste à proposer une structure qui permet de détecter et de rejeter efficacement un signal affecté d'un multi-trajet dans un contexte multi-constellation où il est admis que le nombre de satellites non contaminés permet de résoudre le problème du positionnement. Une deuxième approche visant à réduire l'impact d'un signal contaminé est étudiée afin d'adresser le problème du positionnement lorsqu'un petit nombre de mesures disponibles est considéré.

- Le chapitre 6 élabore une synthèse des résultats obtenus permettant une analyse et une comparaison des solutions explorées et propose des évolutions des algorithmes proposés ainsi que de nouveaux axes de recherche.

CHAPITRE 2 : Principe des systèmes GNSS

Ce chapitre rappelle les fondements des systèmes GNSS, et plus spécialement du système GPS. Il décrit les formes d'onde des signaux utilisées en navigation, en s'intéressant plus particulièrement au signal reçu par le récepteur.

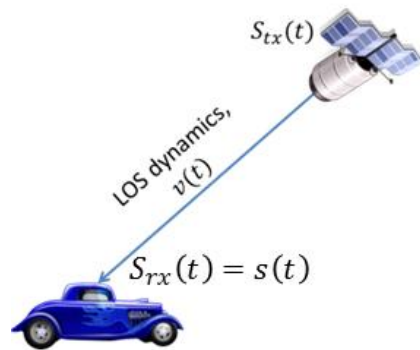


Figure 2: Etude du signal reçu par le récepteur

Ces signaux dérivent des principes mises en œuvre dans les systèmes de transmission à spectre étalé par des séquences directes. Les différents satellites de la constellation partagent la même bande. Des codes d'étalement orthogonaux permettent une séparation des différentes sources au sein du récepteur. L'expression de l'enveloppe complexe du signal obtenu en sortie de l'étage radiofréquence est:

$$s(t) = A.D(t - \tau(t))C(t - \tau(t)) \exp(j[\varphi(t)]) + n(t) \quad (1)$$

où $D(\cdot)$ et $C(\cdot)$ représentent respectivement le signal des données et le code d'étalement.

Dans cette impression apparaissent les paramètres caractéristiques de la propagation. Les paramètres $\tau(t)$ et $\varphi(t)$ représentent respectivement le délai de propagation du code et la phase de la porteuse. Ces 2 paramètres dépendent de la distance du récepteur au satellite. La phase de la

porteuse peut être déduite de la fréquence Doppler qui dépend de la vitesse relative véhicule-satellite :

$$\varphi = \varphi(0) + 2\pi \int_0^t f(u)du \quad \text{où } f = f_{L1} \frac{v(t)}{c}.$$

Ce signal, qui porte donc des informations reliées à la distance et à la vitesse récepteur-satellite, est d'une bonne pertinence s'agissant des applications de navigation. Il permettra d'élaborer une estimation de la position et de la vitesse du véhicule lorsque le nombre de satellites le permet.

On note qu'en présence de multi-trajets le signal reçu d'un satellite est obtenu en cumulant les signaux des différents trajets.

$$s(t) = \sum_{l=0}^{N-1} A_l \cdot D(t - \tau_l(t)) \cdot C(t - \tau_l(t)) \exp(j\varphi_l(t)) + n(t)$$

avec

(2)

$$\varphi_l = \varphi_l(0) + 2\pi \int_0^t f_l(u)du.$$

Dans cette impression l'index l indique le l^{eme} trajet (l'index $l = 0$ est utilisé pour le signal direct, dit « Line Of Sight (LOS)».

Dans un récepteur GNSS ce signal est numérisé et compressé pour permettre son traitement. La compression consiste en un filtre adapté qui réalise la corrélation du signal reçu avec une réplique du signal LOS dont les paramètres sont estimés par le récepteur. La sortie du signal de sortie du corrélateur, délivré à l'instant $t_k = \sum_{t=0}^k T_k$ est décrite par l'équation ci-après, en l'absence du signal de donné qui est supposé connu sur la durée de corrélation :

$$u_z(k) \approx \sum_{l=0}^N \sqrt{2P_l} R(\Delta\tau_{l,k}) \frac{\sin(\pi\Delta f_{l,k} T_k)}{\sin(\pi\Delta f_{l,k} T_s)} \exp(j\Delta\varphi_{l,k}) + n[k] \quad (3)$$

Dans cette expression $R(.)$ représente la fonction d'autocorrélation du code d'étalement et n représente le bruit blanc gaussien qui résulte du bruit dans le canal de transmission. Les paramètres $\Delta\tau_{l,k} = \tau_{l,k} - \hat{\tau}_{0,k}$, $\Delta\varphi_{l,k} = \varphi_{l,k} - \hat{\varphi}_{0,k}$ et $\Delta f_{l,k} = f_{l,k} - \hat{f}_{0,k}$ représentent respectivement les erreurs

sur les estimées du délai, de la phase, de la fréquence pour chaque trajet, le trajet direct étant le trajet de référence.

Il est important de noter que les paramètres du trajet direct sont estimés par des estimateurs locaux dans le cadre d'une poursuite scalaire du signal, dite « Scalar Tracking Loop (STL) », qu'ils sont estimés, s'agissant du délai et de la fréquence, par le navigateur dans la cadre d'une poursuite vectorielle du signal, dite « Vector Tracking Loop (VTL) ». En ce qui concerne la phase une mesure locale est nécessaire, la précision du navigateur n'étant pas suffisante.

Le chapitre 1 rappelle par ailleurs les principes des estimateurs locaux tels qu'ils sont décrits dans [11].

CHAPITRE 3 : Canal de transmission

L'évaluation des algorithmes proposés sur la base de signaux réels demande un effort important nécessitant la mise en œuvre d'un récepteur complet. Dans le contexte de cette thèse il est proposé de valider les algorithmes étudiés sur la base de simulations. Deux approches sont proposées. La première est basée sur un modèle de canal simple permettant de maîtriser la configuration des signaux atteignant le récepteur. La 2^{ème} approche est basée sur un modèle plus réaliste issu de travaux présentés dans [9], [11] et [12]. L'impact des multi-trajets sur les performances d'un récepteur conventionnel est également étudié dans ce chapitre.

Modèle déterministe

Le modèle le plus simple considère un multi-trajet spéculaire et la réponse impulsionnelle du canal est modélisé par :

$$h_c(k) = a_{0,k} \delta(t - \tau_{0,k}) \exp(j\varphi_{0,k}) + a_{1,k} \delta(t - \tau_{1,k}) \exp(j\varphi_{1,k}) \quad (4)$$

où $a_{0,k}$ et $a_{1,k}$ représentent les amplitudes du trajet direct et du trajet réfléchi, $\tau_{0,k}$ et $\tau_{1,k}$ représentent le délai de ces 2 trajets, $\varphi_{0,k}$ et $\varphi_{1,k}$ la phase de ces 2 trajets.

En pratique la variation des paramètres du trajet direct est déduite de la vitesse du véhicule. S'agissant du trajet réfléchi, les simulations permettront de considérer un trajet à la fréquence du trajet direct qui est caractéristique d'un multi-trajet apparaissant alors que le récepteur est à l'arrêt, ou lorsque ce récepteur se déplace parallèlement au bâtiment produisant la réflexion de ce multi-trajet. Des trajets ayant une fréquence Doppler différente de celle du signal LOS pourront aussi être simulés. Ces conditions de simulation pourront être considérées pour une évaluation des performances d'un récepteur GNSS, dans les différentes configurations du étudiées dans le cadre de cette thèse.

Modèle physico-statistique

Des modèles de canaux ont été élaborés et validés à partir de campagnes de mesures. Ces modèles prennent en compte la description de l'environnement, le déplacement du véhicule et les caractéristiques de l'antenne du récepteur. Une description des signaux atteignant l'antenne du récepteur peut être établie au moyen d'un outil de lancer de rayon. Cette description habituellement déterministe nécessite une modélisation précise des surfaces des bâtiments. Le signal reçu est ainsi modélisé par la somme de plusieurs composantes issues de la réflexion, de la diffusion et de la diffraction du signal. Dans le cadre de cette étude le modèle large Bande [12] du DLR (German Aerospace center) a été adopté. Ce modèle considère le trajet direct avec ou sans masquage, des échos proches et des échos lointains. Une représentation retard, puissance des multi-trajets est donnée figure 3.

En pratique le simulateur du DLR utilisé pour ce projet combine des modèles physiques qui nécessitent une description rigoureuse de l'environnement et des modèles statistiques élaborés à partir de campagnes de mesures. Les sorties de ce simulateur ont été analysées, dans le cadre de ce travail, par le biais de simulations proposées pour une trajectoire donnée du véhicule.

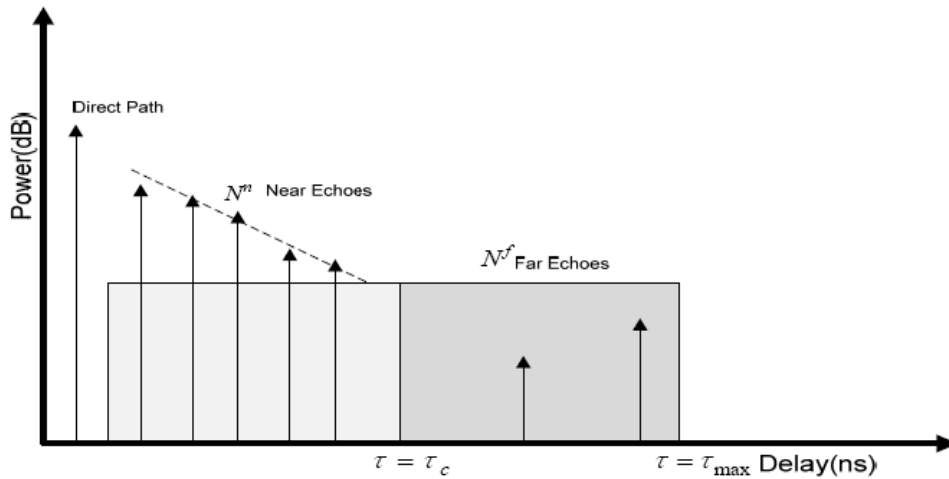


Figure 3: Statistique des paramètres de multi-trajets proposée dans [12].

Mise en œuvre du simulateur du DLR

Le simulateur du DLR est utilisé pour générer un fichier de données qui contient les paramètres de tous les trajets modélisés au sein du simulateur. Ces paramètres sont l'amplitude qui, portant l'information de phase, est complexe, et le retard. Ces données sont délivrées à la fréquence de 1 KHz. L'architecture de ce simulateur est décrite figure 4.

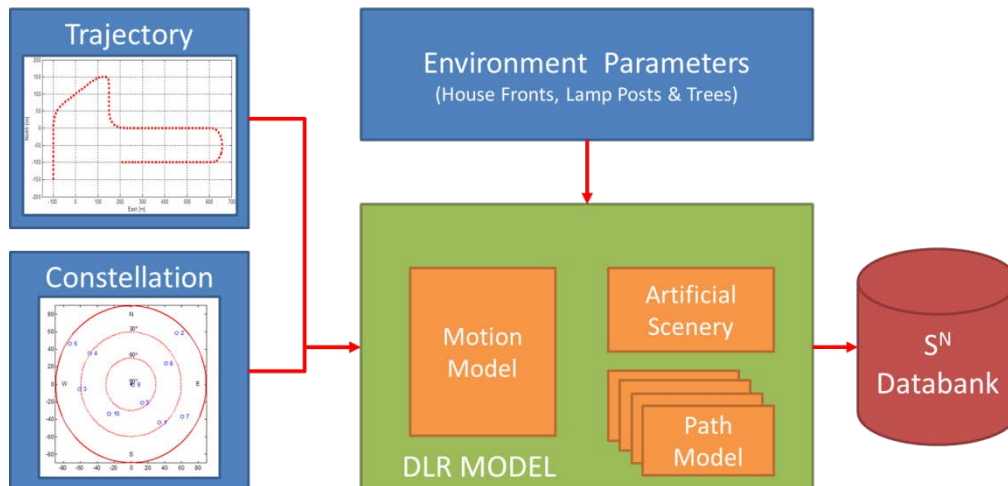


Figure 4: Mise en œuvre du simulateur du DLR.

Le fichier produit est ensuite utilisé par le générateur d'échantillons qui produit le signal d'entrée du récepteur défini par l'équation (2). Ce signal est représenté par des échantillons générés à la fréquence de 10MHz. Comme le simulateur du DLR fonctionne à la fréquence de 1ms, la valeur des

paramètres des différents trajets est supposée constante sur cette durée. Même si cette hypothèse n'est pas toujours vérifiée, l'impact de cette approximation reste faible, la durée d'intégration du corrélateur étant au moins égale à cette durée de 1ms.

Analyse de la distribution des retards

Cette analyse permet d'observer la distribution des retards observés en sortie du canal lorsque le véhicule se déplace. Cette distribution dépend de l'environnement, l'amplitude des retards augmentant avec la largeur des rues. La figure 5 représente les retards observés lorsque le véhicule se déplace pendant 1 sec dans un environnement urbain. Pour cet environnement le retard peut atteindre des valeurs allant jusqu'à 450 mètres (1.5 chip).

Sur les figures 6 et 7 sont représentées les distributions des retards observés sur 3 minutes de simulation, pour un environnement urbain, et un environnement suburbain. On observe une forte représentation des multi-trajets de faibles amplitudes qui seront difficilement détectables. Cela reste vrai pour un environnement suburbain, malgré un étalement temporel des retards plus important que celui observé pour un environnement urbain.

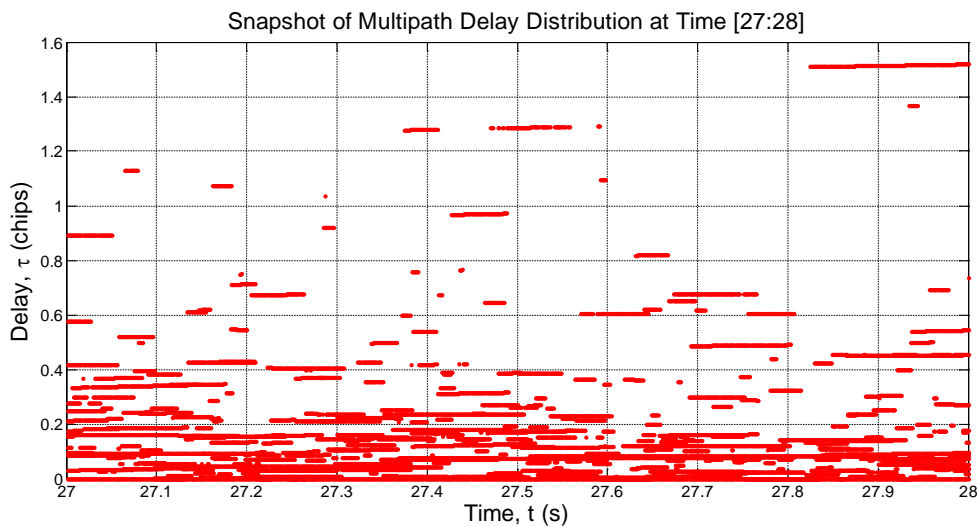


Figure 5: Valeurs des retards observés sur une seconde

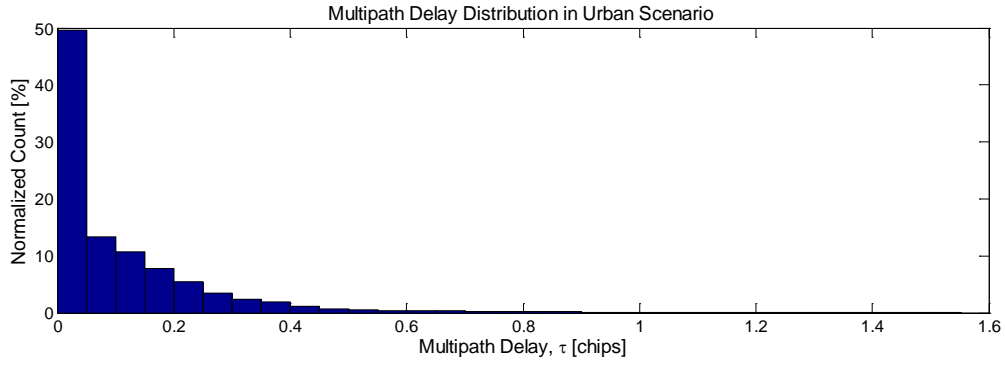


Figure 6: Distribution des retards des multi-trajets pour un environnement urbain.

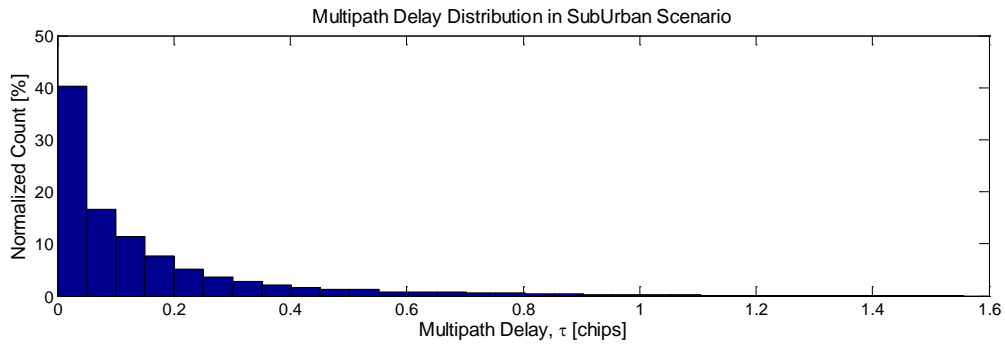


Figure 7: Distribution des retards des multi-trajets pour un environnement suburbain.

Analyse fréquentielle des multi-trajets

Une analyse fréquentielle des multi-trajets est réalisée en sortie du corrélateur, alors que le simulateur du DLR est utilisé pour décrire le signal en sortie du canal. La sortie du corrélateur est définie par l'équation (3). Pour cette étude on considère que le signal replica reproduit le signal LOS, c'est-à-dire que les paramètres du signal direct sont parfaitement estimés. L'équation (3) devient alors :

$$u_z(k) \approx \sqrt{2P_0} + \sum_{l=1}^N \sqrt{2P_l} R(\Delta\tau_{l,k}) \frac{\sin(\pi\Delta f_{l,k} T_k)}{\sin(\pi\Delta f_{l,k} T_s)} \exp(j\Delta\varphi_{l,k}) + n[k] \quad (5)$$

La densité spectrale de puissance (DSP) du signal obtenu est représentée figure 8. On note une fluctuation de la puissance du trajet direct correspondant à des atténuations et à des masquages du signal.

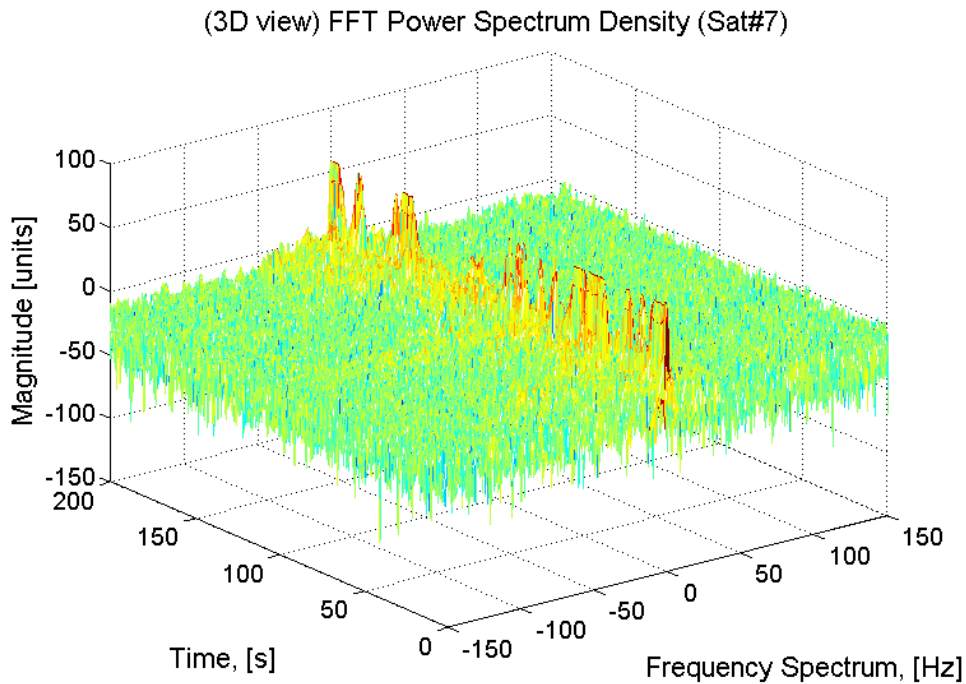


Figure 8: DSP du signal en sortie du corrélateur en présence de multi-trajets.

La figure 9 permet une analyse plus fine des phénomènes observés. Dans le domaine des fréquences les multi-trajets restent concentrer dans une bande autour de la fréquence 0. L'étalement fréquentiel dépend de la vitesse du véhicule. Lorsque le véhicule se déplace les multi-trajets apparaissent de manière diffuse dans le domaine des fréquences, induisant une dégradation du rapport Puissance du signal sur Puissance du bruit, le bruit incluant alors le bruit blanc mais aussi les signaux d'interférence.

Par ailleurs cette représentation montre que l'analyse en fréquence permet :

- le calcul de la puissance du signal LOS en intégrant cette densité spectrale autour de la fréquence nulle,
- le calcul de la puissance du bruit blanc en intégrant cette densité spectrale sur une bande de fréquence telle que $|f| > 30Hz$ pour cette vitesse du véhicule,
- le rapport signal sur bruit (bruit blanc sur interférence) en fonction de la bande du récepteur.

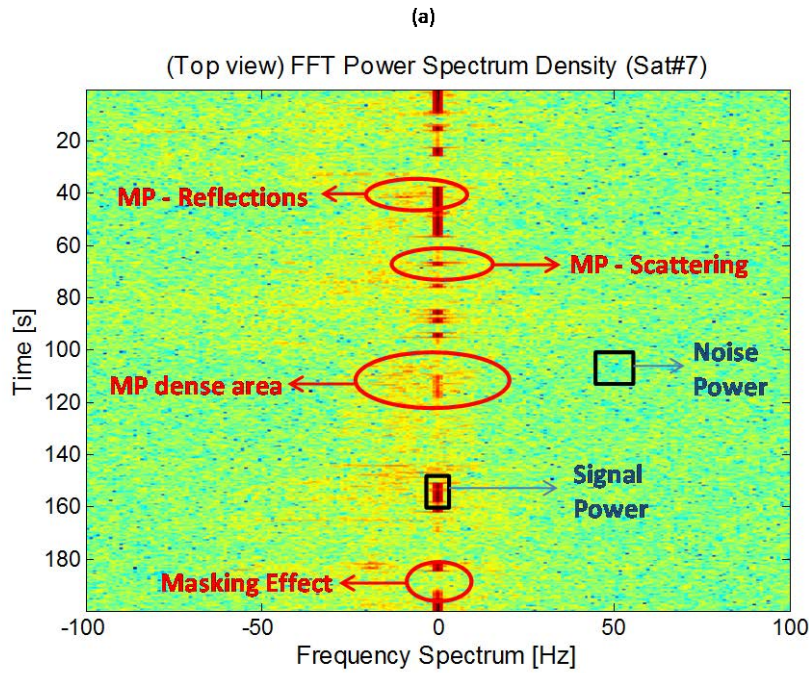


Figure 9: DSP du signal en sortie du corrélateur en présence de multi-trajets.

Effets des multi-trajets

Par ailleurs ce chapitre met en évidence l'impact des multi-trajets sur le récepteur. Des erreurs de vitesse peuvent apparaître en présence de multi-trajets induits par des bâtiments qui ne sont pas orientés dans l'axe de déplacement du véhicule, en particulier en cas de masquage du trajet direct. Toutefois les erreurs des multi-trajets affectent principalement la mesure de position, en raison d'une distorsion des sorties des corrélateurs utilisés pour élaborer cette mesure de retard. Alors que l'analyse en fréquence permet la séparation de trajets de fréquences différentes, la décorrélation dans le domaine des délais restent difficile. Il est rappelé que des corrélateurs « haute résolution » peuvent permettre de réduire l'impact de multi-trajets. Ils nécessitent des fréquences d'échantillonnage du signal élevées.

CHAPITRE 4 : Poursuite du signal dans les récepteurs GNSS

Ce chapitre analyse le principe d'un récepteur GNSS et traite plus particulièrement de la poursuite des signaux au sein de ce récepteur. Les blocs étudiés ici sont représentés sur la figure 10. Le bloc « Navigation System » réalise le calcul de la position et de la vitesse en utilisant les mesures

délivrées par l'étage « Signal Processing ». Cette étape réalise la poursuite du signal LOS et consiste en une estimation en ligne des paramètres de ce signal collecté par l'antenne. Cette estimation est généralement réalisée au moyen de boucles de poursuite qui utilisent les sorties de discriminateurs de retard, de fréquence, et de phase comme observations. Ces sorties peuvent avantageusement être exploitées par un filtre de Kalman pour de faibles rapports signal à bruit du signal traité [13].

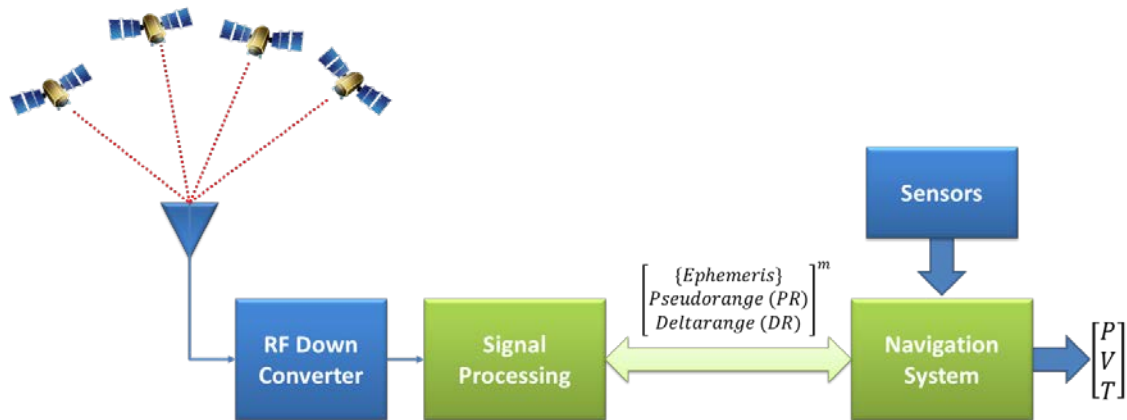


Figure 10: Architecture d'un récepteur GNSS.

Navigateur

On rappelle les différentes approches utilisées pour calculer la position et la vitesse au sein d'un récepteur. La mesure physique utilisée pour le calcul de la position est la mesure de distance satellite-utilisateur. Cette mesure est obtenue en estimant le délai de propagation du signal. Alors que la synchronisation des horloges des satellites est assurée en réalisant, au sein du récepteur, les corrections modélisées par la station de contrôle qui se trouve à Colorado Springs pour GPS, la synchronisation du temps récepteur et du temps satellite nécessite le calcul du biais de l'horloge récepteur. La mesure qui en résulte est une mesure de pseudo-distance.

$$\rho_m = \|\mathbf{r}^m - \mathbf{r}^u\| + b_H + n_{\rho_m} \quad (5)$$

où \mathbf{r}^m et \mathbf{r}^u représentent respectivement la position du satellite et la position de l'utilisateur, b_H représente le biais d'horloge, n_{ρ_m} représente le bruit de mesure.

En pratique la résolution de ce problème nécessite l'utilisation d'au moins 4 satellites pour estimer l'état $X = [\mathbf{r}^u \quad b_H]^T$. Cet état est obtenu de manière récursive en calculant l'erreur sur la valeur de l'état connue.

$$X(k) = X(k-1) + \Delta X(k) \text{ avec } \Delta X(k) = (H_{k-1}^T H_{k-1})^{-1} H_{k-1}^T \Delta \rho(k) \quad (6)$$

où H est la matrice jacobienne obtenue en linéarisant, par rapport aux paramètres inconnues (position, biais d'horloge), autour de l'état défini à l'instant $k-1$, le système d'équations obtenu à partir de l'équation (5), définie pour au moins 4 satellites, et $\Delta \rho$ représente la différence entre la mesure délivrée par le récepteur et la mesure estimée à partir de l'état connu.

La vitesse est obtenue en utilisant la même approche, la mesure utilisée étant la mesure de la delta-distance :

$$\dot{\rho}_m = LOS_m^T \cdot (\mathbf{v}^m - \mathbf{v}^u) + d_H + n_{\dot{\rho}_m} \quad (7)$$

où \mathbf{v}^m et \mathbf{v}^u représentent respectivement la vitesse du satellite et la vitesse de l'utilisateur, d_H représente la dérive du biais d'horloge, $n_{\dot{\rho}_m}$ représente le bruit de mesure.

Dans cette équation LOS_m^T est un vecteur ligne unitaire qui donne la direction du satellite m , montrant l'impact de la géométrie de la constellation sur les performances de l'algorithme. Cette mesure est obtenue à partir d'une estimation de la fréquence Doppler du signal reçu.

$$f_D = - \left[LOS_m^T \cdot \frac{(\mathbf{v}^m - \mathbf{v}^u)}{c} \right] f_{L1}. \quad (8)$$

où c est la vitesse de la lumière et f_{L1} est la fréquence de la porteuse.

Navigateur basé sur un filtre de Kalman étendu (EKF)

Dans le cadre de ce projet un filtre de Kalman étendu est utilisé pour estimer la position et la vitesse du véhicule, le biais et la dérive de biais de l'horloge récepteur. Il nécessite une description espace-état du système.

Modèle d'état

Ce modèle décrit l'évolution de l'état du système qui contient ici la position et la vitesse du véhicule, exprimées dans un repère de navigation (Est, Nord, Up) dont l'origine est la position initiale du véhicule. Il inclut aussi le biais et la dérive de biais de l'horloge.

$$X^{NS} = [r_E \quad v_E \quad r_N \quad v_N \quad r_U \quad v_U \quad b_H \quad d_H]^T \quad (9)$$

Il est décrit par la matrice de transition Φ^{NS} telle que:

$$\Phi^{NS} = \begin{bmatrix} A & 0 & 0 & 0 \\ 0 & A & 0 & 0 \\ 0 & 0 & A & 0 \\ 0 & 0 & 0 & A \end{bmatrix} \quad (10)$$

où

$$A = \begin{bmatrix} 1 & T_{NS} \\ 0 & 1 \end{bmatrix} \quad (11)$$

T_{NS} étant la fréquence de mise à jour du navigateur.

Le modèle de prédiction est donc :

$$\hat{X}_{k+1}^{NS} = \Phi^{NS} \hat{X}_k^{NS} + w_k \quad (12)$$

avec:

$$E\{ww^T\} = Q^{NS} = \begin{bmatrix} Q_{dyn} & 0 \\ 0 & Q_{clk} \end{bmatrix} \quad (13)$$

où:

$$Q_{dyn} = \begin{bmatrix} Q_A & 0 & 0 \\ 0 & Q_A & 0 \\ 0 & 0 & Q_A \end{bmatrix}$$

$$Q_A = \begin{bmatrix} \sigma_a^2 \cdot \frac{T_{NS}^4}{4} & \sigma_a^2 \cdot \frac{T_{NS}^3}{2} \\ \sigma_a^2 \cdot \frac{T_{NS}^3}{2} & \sigma_a^2 \cdot T_{NS}^2 \end{bmatrix} \quad (14)$$

et

$$Q_{clk} = \begin{bmatrix} \sigma_b^2 \cdot T_{NS}^2 + \sigma_d^2 \frac{T_{NS}^4}{4} & \sigma_d^2 \cdot \frac{T_{NS}^3}{2} \\ \sigma_d^2 \cdot \frac{T_{NS}^3}{2} & \sigma_d^2 \cdot T_{NS} \end{bmatrix}. \quad (15)$$

Modèle de mesure

Le modèle de mesure est basé sur les paramètres estimés au niveau des boucles de poursuite, en considérant principalement le délai de propagation et la fréquence Doppler du signal :

$$Y_k^{NS} = \begin{bmatrix} \tilde{\tau}^1 \\ \tilde{f}^1 \\ \vdots \\ \tilde{\tau}^m \\ \tilde{f}^m \\ \vdots \\ \tilde{\tau}^{N_{sat}} \\ \tilde{f}^{N_{sat}} \end{bmatrix} \quad \text{avec } 1 \leq m \leq N_{sat} \quad (16)$$

Le modèle de mesure linéarisé peut se mettre sous la forme :

$$\Delta Y_k^{NS} = H_k \widehat{\Delta X}_k + v_k. \quad (17)$$

La matrice H est la matrice Jacobienne définie ainsi :

$$H_k^{NS} = \begin{bmatrix} \frac{LOS_x^1}{\lambda_c} & 0 & \frac{LOS_y^1}{\lambda_c} & 0 & \frac{LOS_z^1}{\lambda_c} & 0 & \frac{1}{\lambda_c} & 0 \\ 0 & \frac{LOS_x^1}{\lambda_{fL1}} & 0 & \frac{LOS_x^1}{\lambda_{fL1}} & 0 & \frac{LOS_x^1}{\lambda_{fL1}} & 0 & \frac{1}{\lambda_{fL1}} \\ \vdots & \vdots \\ \frac{LOS_x^m}{\lambda_c} & 0 & \frac{LOS_y^m}{\lambda_c} & 0 & \frac{LOS_z^m}{\lambda_c} & 0 & \frac{1}{\lambda_c} & 0 \\ 0 & \frac{LOS_x^m}{\lambda_{fL1}} & 0 & \frac{LOS_y^m}{\lambda_{fL1}} & 0 & \frac{LOS_z^m}{\lambda_{fL1}} & 0 & \frac{1}{\lambda_{fL1}} \\ \vdots & \vdots \\ \frac{LOS_x^{N_{sat}}}{\lambda_c} & 0 & \frac{LOS_y^{N_{sat}}}{\lambda_c} & 0 & \frac{LOS_z^{N_{sat}}}{\lambda_c} & 0 & \frac{1}{\lambda_c} & 0 \\ 0 & \frac{LOS_x^{N_{sat}}}{\lambda_{fL1}} & 0 & \frac{LOS_y^{N_{sat}}}{\lambda_{fL1}} & 0 & \frac{LOS_z^{N_{sat}}}{\lambda_{fL1}} & 0 & \frac{1}{\lambda_{fL1}} \end{bmatrix} \quad (18)$$

où λ_C et $\lambda_{f_{L1}}$ représentent les longueurs d'onde du code et la porteuse.

La matrice de covariance de l'erreur de mesure est définie à partir de la variance des bruits sur les estimées de retard et de fréquence élaborées par les boucles de poursuite.

$$E[vv^T] = R_{Y_k}^{NS} = \text{diag} \left(\sigma_{\tilde{\tau}_1}^2 \sigma_{\tilde{f}_1}^2, \dots, \sigma_{\tilde{\tau}_m}^2 \sigma_{\tilde{f}_m}^2, \dots, \sigma_{\tilde{\tau}_{N_{sat}}}^2 \sigma_{\tilde{f}_{N_{sat}}}^2 \right)_k. \quad (19)$$

Ces variances seront fixées dynamiquement en fonction de la qualité du signal (rapport C/N_0) et de la bande de bruit des boucles de poursuite.

Boucles de poursuite

Le bloc « Signal Processing » représenté sur la figure 10 produit les mesures utilisées par le navigateur pour élaborer une position (équations (16) à (19)). Ce bloc consiste en un estimateur qui utilise les sorties d'un banc de corrélateurs comme observation. Dans un récepteur conventionnel il est basé sur une boucle de poursuite scalaire (boucle STL). Dans ce mode de poursuite chaque canal du récepteur fonctionne de manière autonome. Dans le cadre de cette étude il est proposé de comparer cette approche scalaire à une approche vectorielle pour laquelle la poursuite bénéficie des informations concentrées au niveau du navigateur.

Poursuite scalaire

La boucle scalaire est décrite sur la figure 11. Le récepteur fonctionne en boucle ouverte en utilisant une structure directe dans laquelle chaque boucle de poursuite produit de manière autonome une mesure qui est utilisée par le navigateur pour élaborer le calcul de la position et de la vitesse du véhicule.

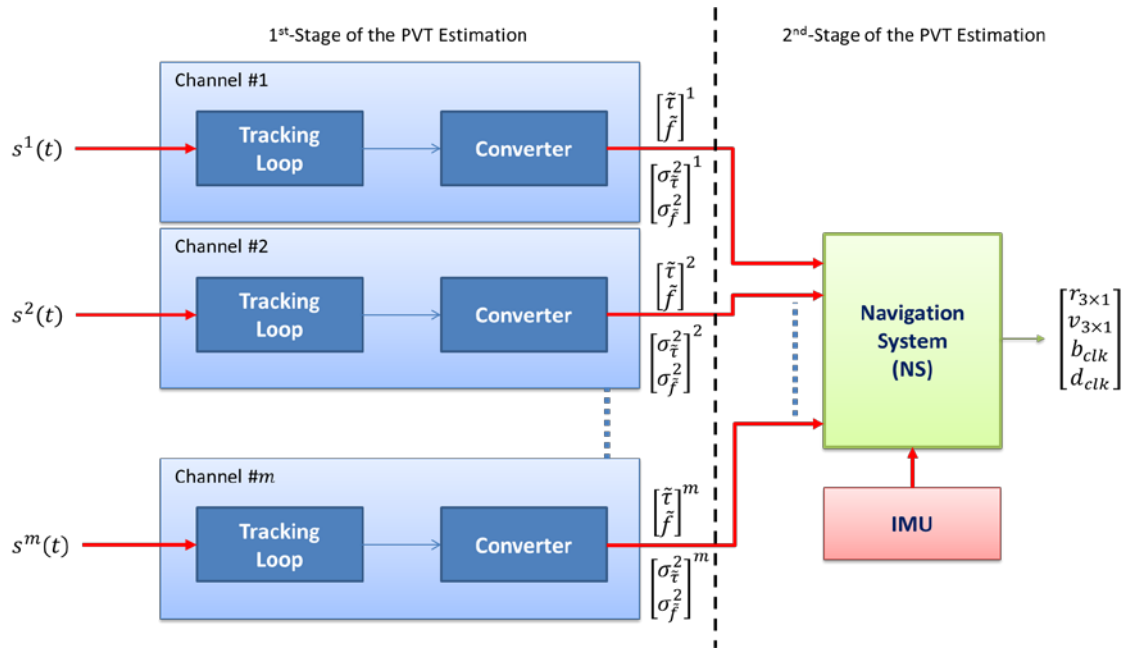


Figure 11: Architecture d'un récepteur basé sur une poursuite scalaire des signaux.

Chaque boucle (DLL pour Delay Lock Loop, PLL pour Phase Lock Loop, FLL pour Frequency Lock Loop) constitue un estimateur, les paramètres à estimer décrivant le vecteur d'état suivant:

$$X_k = [\tau \quad \varphi \quad f]_k^T \quad (20)$$

Une représentation espace-état peut être adoptée pour décrire cet estimateur. L'équation de mise à jour de l'état est régie par l'équation :

$$\tilde{X}_{k+1} = \Phi^{LE} \cdot \tilde{X}_k + K \cdot \Delta Y_k \quad (21)$$

où Φ^{LE} représente la matrice de transition, K est une matrice de gain dont les coefficients sont calculés en ligne en fonction de la bande de bruit requise pour l'estimateur, ΔY_k représente l'innovation sur les mesures qui est produite par des discriminateurs.

$$\Phi^{LE} = \begin{bmatrix} 1 & 0 & K_{\varphi\tau} T_{int} \\ 0 & 1 & T_{int} \\ 0 & 0 & 1 \end{bmatrix} \quad (22)$$

$$K = T_{int} \begin{bmatrix} \omega_{DLL} & 0 & 0 \\ 0 & \sqrt{2}\omega_{PLL} & 0 \\ 0 & \omega_{PLL}^2 & \omega_{FLL} \end{bmatrix} \quad (23)$$

$$\Delta Y_k^{m^{Disc}} = \begin{bmatrix} \Delta\tau \\ \Delta\varphi \\ \Delta f \end{bmatrix}_k^{m^{Disc}} = \begin{bmatrix} \overline{\tau_k - X_{k-1}(1)} \\ \overline{\varphi_k - X_{k-1}(2)} \\ \overline{f_k - X_{k-1}(3)} \end{bmatrix} \quad (24)$$

où :

- T_{int} , durée d'intégration sur laquelle opèrent les discriminateurs, représente aussi la période de mise à jour des estimateurs.
- $K_{\varphi\tau} = R_c/f_{L1} = 1/1540$ est le rapport entre le rythme chips et la fréquence de la porteuse.
- $\overline{\tau_k - X_{k-1}(1)}$, $\overline{\varphi_k - X_{k-1}(2)}$ et $\overline{f_k - X_{k-1}(3)}$ sont les erreurs moyennes de retard, phase et fréquence, obtenues en sorties des discriminateurs.

Les coefficients du gain K sont décrits dans [10], page 180.

Lorsque l'approche scalaire est utilisée les oscillateurs qui produisent le signal réplica sont contrôlés par l'estimateur local. Ce contrôle est assuré par une commande en fréquence des oscillateurs (\tilde{f}_{DLL} pour l'oscillateur qui pilote le générateur de code, \tilde{f}_{PLL} pour l'oscillateur qui produit la porteuse)

$$\begin{bmatrix} \tilde{f}_{DLL} \\ \tilde{f}_{PLL} \end{bmatrix}_{k+1}^+ = \begin{bmatrix} K_{\varphi\tau} & K_{11} & 0 \\ 1 & 0 & K_{22} \end{bmatrix} \begin{bmatrix} X(3) \\ \Delta Y(1) \\ \Delta Y(2) \end{bmatrix}_{k+1} . \quad (25)$$

où les coefficients K_{11} et K_{22} sont décrits dans [10], page 180.

Il est à noter que les paramètres du vecteur d'état (f, τ) constitue la mesure utilisée par le navigateur. La matrice de covariance du bruit de mesure se déduit des gains K_{ij} [10] et du rapport C/N_0 relatif au signal poursuivi.

Poursuite vectorielle

L'étude adressée par cette thèse concerne des récepteurs utilisant une architecture vectorielle. Lorsque cette architecture est utilisée, les oscillateurs qui produisent le signal replica sont contrôlés par le navigateur. Ce contrôle utilise les estimations du délai et de la fréquence élaborées par le navigateur à partir de la position et de la vitesse.

$$\hat{t}^m = \frac{1}{\lambda_c} [LOS_m^T \cdot (\hat{r}^u - r^m) + b_H] \quad (26)$$

$$\hat{f}^m = \frac{1}{\lambda_{L1}} [LOS_m^T \cdot (\hat{v}^u - v^m) + d_H]. \quad (27)$$

Lorsque le navigateur est basé sur un filtre de Kalman, il est possible de délivrer une information sur la qualité de ces estimées. L'écart-type sur ces estimées est alors défini d'après les équations suivantes :

$$\sigma_m^t = \sqrt{H_{2m-1} P^{NS} H_{2m-1}^T} \quad (28)$$

$$\sigma_m^f = \sqrt{H_{2m} P^{NS} H_{2m}^T} \quad (29)$$

où :

- $P^{NS} = E\{X^{NS}[X^{NS}]^T\}$ est la matrice de covariance du bruit, associée au vecteur d'état décrit par l'équation (9),
- H_{2m-1} et H_{2m} sont les $(2m-1)^{ème}$ et $(2m)^{ème}$ de la matrice H^{NS} définie par l'équation (18).

Plusieurs approches sont utilisées pour construire une architecture vectorielle. Une comparaison de ces différentes approches est proposée dans [14]. Un modèle générique est présenté figure 12.

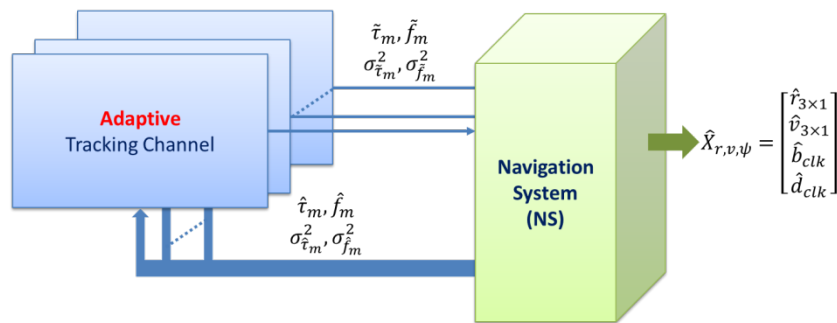


Figure 12: Architecture VTL

L'architecture qui a été retenue pour ce projet est décrite ici. S'agissant du modèle de prédiction, il diffère de celui décrit par l'équation (22) de par le fait qu'il utilise la fréquence estimée par le navigateur.

$$\begin{aligned}\tilde{f}_{m,l}^- &= \hat{f}_{m,l} \\ \tilde{\varphi}_{m,l}^- &= \tilde{\varphi}_{m,l-1}^- + T^{EL} \hat{f}_{m,l-1} \\ \tilde{\tau}_{m,l}^- &= \tilde{\tau}_{m,l-1}^+ + K_{\varphi\tau}^m T^{EL} \hat{f}_{m,l-1}\end{aligned}\quad (30)$$

S'agissant de la phase, la mise à jour utilise la sortie du discriminateur de phase $\delta\varphi_{m,l}$:

$$\begin{aligned}\delta\varphi_{m,l} &= \varphi_{m,l} - \tilde{\varphi}_{m,l-1}^+ \\ \tilde{\varphi}_{m,l}^+ &= \tilde{\varphi}_{m,l}^- + K_{22}^m T^{EL} \delta\varphi_{m,l}\end{aligned}\quad (31)$$

En ce qui concerne le délai, la mise à jour utilise le délai estimé par le navigateur :

$$\begin{aligned}\tilde{f}_{m,l}^+ &= \tilde{f}_{m,l}^- \\ \tilde{\tau}_{m,l}^+ &= \tilde{\tau}_{m,l}^- + K_{11}^m T^{EL} (\hat{\tau}_m - \tilde{\tau}_{m,l-1}^+)\end{aligned}\quad (32)$$

Les mesures utilisées par le navigateur sont obtenues à partir des sorties des discriminateurs de retard et de fréquence ($\delta\tau_{m,l}$, $\delta f_{m,l}$) :

$$\begin{aligned}\delta\tau_{m,l} &= \tau_{m,l} - \tilde{\tau}_{m,l-1}^+ \\ \tilde{\tau}_{m,l} &= \tilde{\tau}_{m,l}^+ + \delta\tau_{m,l} \\ \delta f_{m,l} &= f_{m,l} - \tilde{f}_{m,l-1}^+ \\ \tilde{f}_{m,l} &= \tilde{f}_{m,l}^+ + \delta f_{m,l}\end{aligned}\quad (32)$$

En présence d'interférence les sorties des discriminateurs sont affectées d'une erreur qui conduit à un modèle de mesure non consistant. Il en résulte une erreur sur la trajectoire estimée.

Comparaison des performances des boucles STL et VTL

Analyse globale en environnement urbain

La figure 13 montre les trajectoires estimées par le récepteur opérant dans les 2 modes de fonctionnement STL et VTL, lorsque le simulateur du DLR est utilisé pour décrire le signal issu d'un des satellites d'une constellation de 5 satellites, alors qu'un environnement de type urbain est considéré.

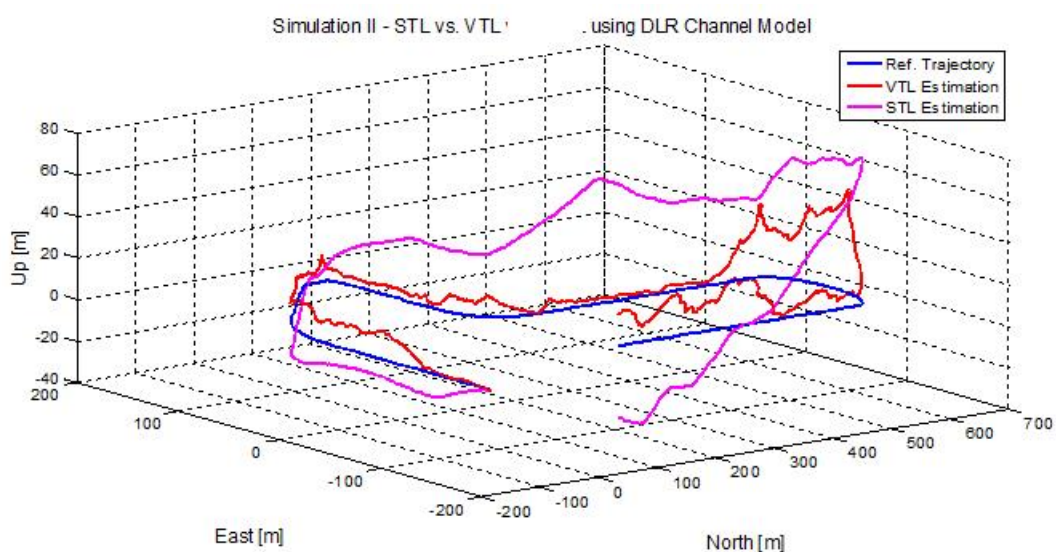


Figure 13: Comparaison des performances des boucles STL et VTL

Une comparaison des trajectoires obtenues montre que la boucle VTL présente de meilleures performances pour cette simulation. Ceci est lié au fait que la boucle DDL dans une architecture STL est fortement impactée par un biais de mesure, ou une absence de mesure, en sortie des discriminateurs. En raison de la faible valeur de la bande de bruit de la boucle DLL ces effets perdurent à la disparition des phénomènes ayant entraîné une dégradation de la poursuite.

Effet de mesures contaminées dans une architecture vectorielle

S'agissant de la boucle VTL, on observe également une erreur de position en présence de mesures contaminées qui dans ce cas peut introduire une erreur de navigation pouvant affecter les performances d'une boucle saine. Ce phénomène peut être observé sur la figure 14. Au moyen du simulateur basé sur un modèle de canal déterministe, un multi-trajet spéculaire est généré pour 4 des satellites durant 10 sec. Après convergence des estimateurs on observe une dégradation de la mesure de retard sur les canaux sains.

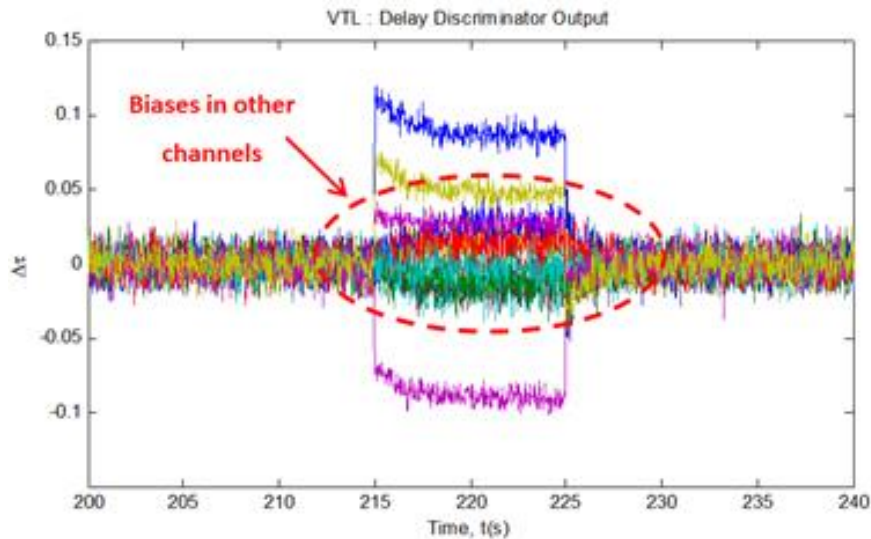
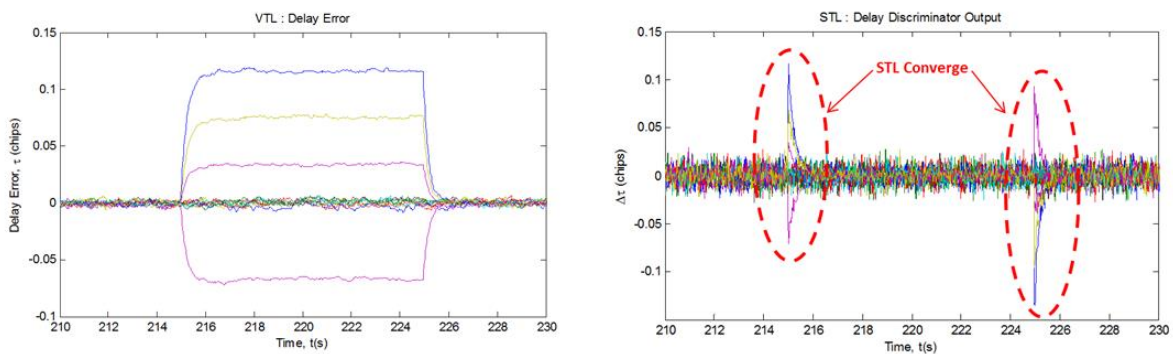


Figure 14: Effets de mesures contaminées.

Ceci montre l'importance du rejet de mesures contaminées au sein d'un récepteur basé sur une architecture vectorielle.

Analyse de la sortie des discriminateurs pour les 2 architectures

Comme précédemment un multi-trajet spéculaire est généré pour 4 des satellites durant 10 sec, au moyen du simulateur basé sur un modèle de canal déterministe. Ici les mesures contaminées sont écartées du modèle de mesure utilisé par le navigateur. On compare alors les signaux délivrés par les discriminateurs de retard dans les 2 configurations (STL et VTL). Sur la figure 15 on observe, pour la boucle VTL, que les discriminateurs de retard associés aux canaux contaminés rapportent sur la valeur de l'erreur due à l'apparition d'un multi-trajet. Au contraire la boucle STL converge de manière à annuler l'erreur induite par ce multi-trajet.



(a)

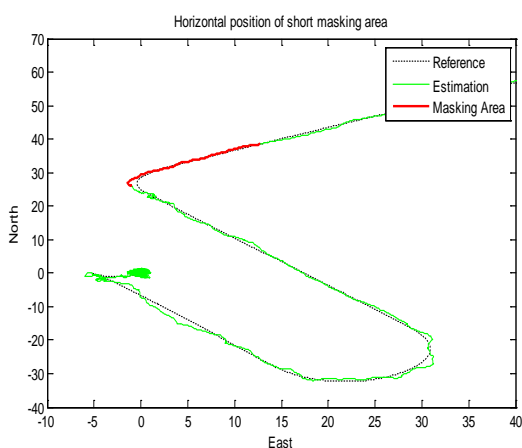
(b)

Figure 15: Sortie des Discriminateurs en mode VTL (a), et STL (b), en présence de multi-trajet.

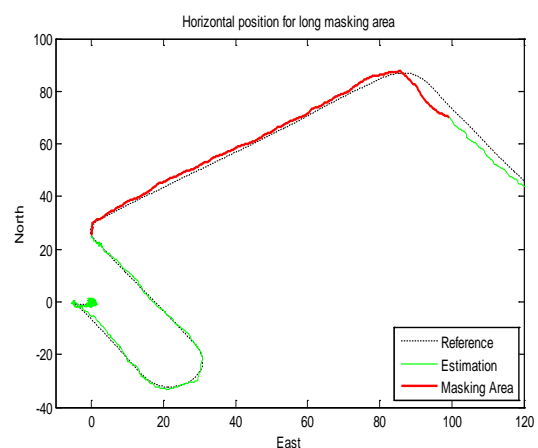
Ceci met en évidence l'intérêt de l'architecture VTL qui facilite la détection de mesures entachées d'une erreur. Par contre il est important de noter qu'en l'absence de rejet un multi-trajet affecte le navigateur quelle que soit l'architecture.

Effet d'un masquage du satellite

En cas de masquage du satellite poursuivi, l'estimateur ne bénéficie d'aucune mesure. Sa capacité à poursuivre le signal dépend de la connaissance a priori des paramètres à estimer. Lorsqu'une boucle STL est utilisée le modèle de prédiction est décrit par les équations (21) et (22). La capacité à poursuivre le signal dépend alors de la pertinence de la fréquence estimée à l'instant de la dernière mesure. S'agissant d'une boucle de poursuite VTL, le modèle de prédiction est décrit par les équations (30) qui utilise en particulier l'information de fréquence élaborée par le navigateur. Il en résulte un bruit de prédiction de puissance d'autant plus faible que la précision sur la vitesse estimée par le navigateur est bonne. Des simulations ont ainsi permis de mettre en évidence l'intérêt de la poursuite vectorielle en cas de masquage. Ces simulations ont été réalisées pour les trajectoires décrites par les figures 16 (a) et 16 (b).



(a)



(b)

Figure 16: Zones de masquage court (a), long (b).

Les résultats sont analysés à partir des observations reproduites sur les figures 17 (a) et 17 (b) pour un masquage court, sur les figures 18 (a) et 18 (b) pour un masquage long.

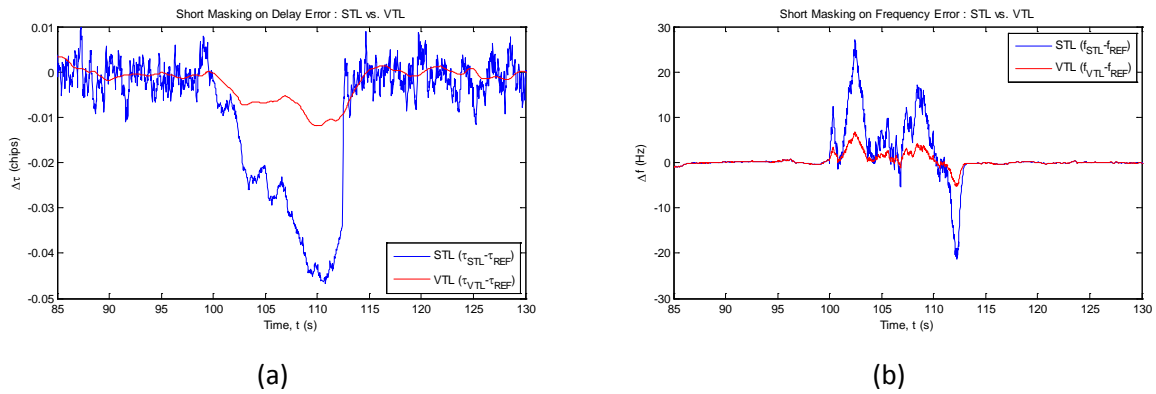


Figure 17: Erreurs sur le délai (a) et la fréquence (b) estimés en cas de masquage court.

Quelle que soit la durée de masquage, la boucle VTL offre comme prévu les meilleures performances mettant en évidence l'intérêt de cette architecture qui l'améliore la disponibilité des mesures. Il faut noter que dans le cas de la boucle STL des masquages de longues durées peuvent entraîner un déverrouillage des boucles de poursuite, rendant nécessaire une ré-acquisition du satellite à la fin de la période de masquage. L'apparition de ce phénomène sera plus ou moins rapide, dépendant des conditions initiales, de la dynamique du véhicule, du stress sur le NCO.

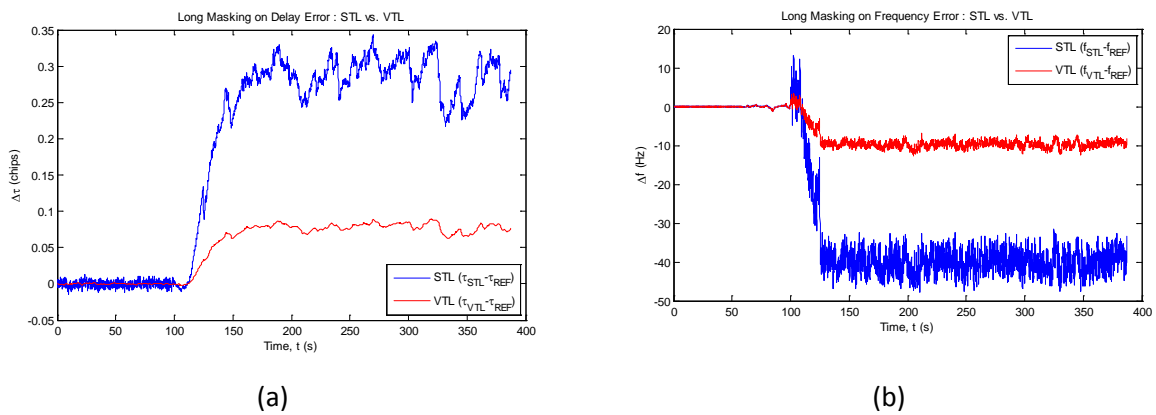


Figure 18: Erreurs sur le délai (a) et la fréquence (b) estimés en cas de masquage long.

Quelle que soit la durée de masquage, la boucle VTL offre comme prévu les meilleures performances mettant en évidence l'intérêt de cette architecture pour l'amélioration de la disponibilité des mesures. Il faut noter que dans le cas de la boucle STL des masquages de longues durées peuvent entraîner un déverrouillage des boucles de poursuite, rendant nécessaire une ré-acquisition du satellite à la fin de la période de masquage. L'apparition de ce phénomène sera plus ou moins rapide, dépendant des conditions initiales, de la dynamique du véhicule, du stress sur le NCO.

Synthèse

Cette analyse met en évidence l'intérêt de la boucle VTL. Cette architecture facilite en particulier la détection de MT dégradant la mesure de pseudo-distance. Elle permet aussi d'améliorer la disponibilité des mesures dans des environnements comme celui décrit figure 19 où des masquages peuvent entraîner le décrochage de boucle STL.

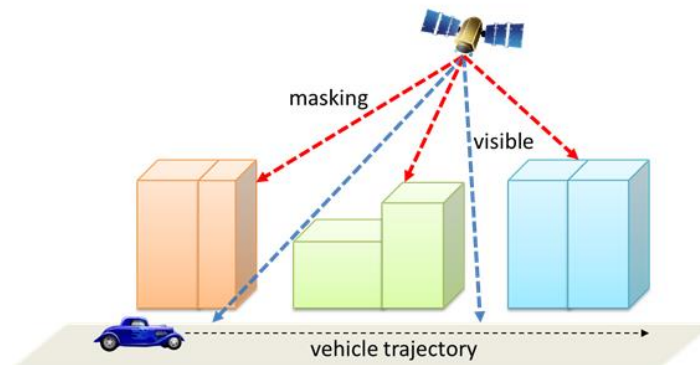


Figure 19: Typiquement urbain environnement.

Enfin il est important de rappeler l'importance du traitement de mesures contaminées, en particulier dans le cas d'une architecture VTL qui rend les canaux dépendants les uns des autres.

CHAPITRE 5 : Poursuite des signaux en présence de multi-trajets

Ce chapitre propose des stratégies de poursuite adaptatives des signaux GNSS en présence de multi-trajets, en exploitant en particulier une architecture vectorielle du récepteur. Cette architecture est représenté figure 20.

Cette architecture intègre 1) des blocs pour la détection de multi-trajets dans le domaine des fréquences et dans le domaine des retards, 2) des discriminateurs de retard de résolution paramétrable, des éléments de contrôle assurant en particulier la configuration des oscillateurs contrôlés numériquement (NCO).

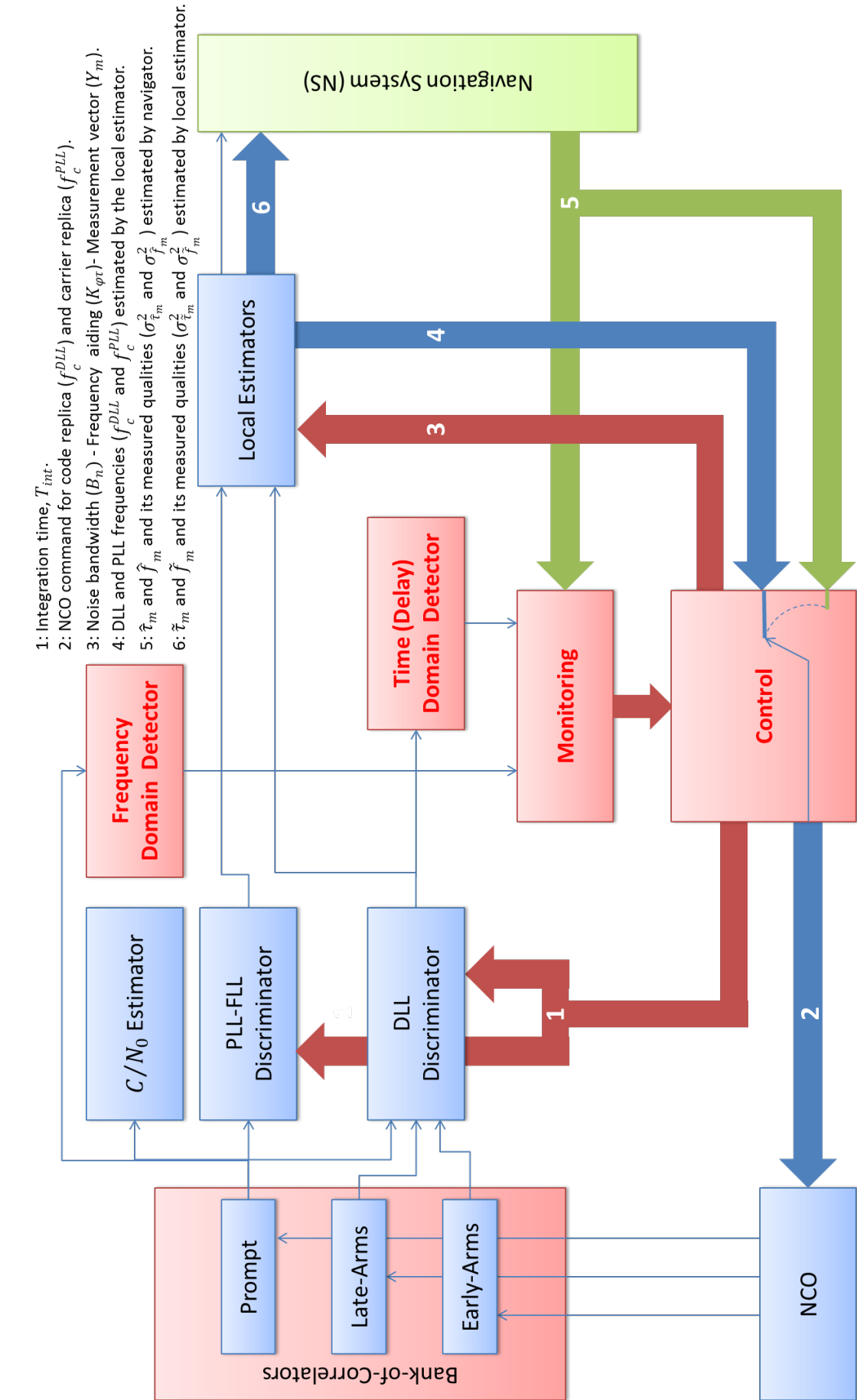


Figure 20 : Architecture du système de poursuite adaptatif

Détection des multi-trajets

Dans le chapitre qui précède l'importance des détecteurs de multi-trajets dans une architecture vectorielle a été mise en évidence. Cette détection peut s'opérer dans le domaine des fréquences ou (et) dans le domaine des retards.

Détection dans le domaine des fréquences

L'analyse est proposée dans le contexte d'une boucle vectorielle. Dans ce cas la sortie du corrélateur prompt s'écrit :

$$u_z(k) = A_{0,k}(\Delta f_{0,k}) R(\Delta \tau_{0,k}) \exp(j\Delta \varphi_{0,k}) + \sum_{l=1}^L A_{l,k}(\Delta f_{l,k}) R(\Delta \tau_{l,k}) \exp(j\Delta \varphi_{l,k}) + n_k \quad (33)$$

S'agissant d'une architecture vectorielle la fréquence et le retard du signal LOS ($\hat{f}_0, \hat{\tau}_0$) sont délivrés par le navigateur :

$$\Delta \tau_0 = \tau_0 - \hat{\tau}_0 \quad \text{avec} \quad \hat{\tau}_0 = \frac{LOS_m^T|_{r=r^{NS}}}{\lambda_c} (\mathbf{r}^{NS} - \mathbf{r}_m) + \frac{b}{\lambda_c} \quad [\text{chips}] \quad (34)$$

$$\Delta f_0 = f_0 - \hat{f}_0 \quad \text{avec} \quad \hat{f}_0 = -\frac{LOS_m^T|_{r=r^{NS}}}{\lambda_{L1}} (\mathbf{v}^{NS} - \mathbf{v}_m) - \frac{d}{\lambda_{L1}} \quad [\text{cycles/s}] \quad (35)$$

Lorsque le navigateur est intègre et lorsque le modèle dynamique de ce navigateur satisfait l'application, on admet que les estimées du retard et de la fréquence du signal direct sont non biaisées. On a alors $E\{\Delta \tau_0\} = 0$ et $E\{\Delta f_0\} = 0$. Et la variance sur ces grandeurs dépend de la qualité de la solution de navigation délivrée par le navigateur. Ces variances peuvent se déduire de la matrice de covariance de l'erreur d'état, et de la matrice d'observation (équations (28) et (29)). Dans ces conditions une transformée de Fourier rapide (FFT) réalisée sur la sortie du corrélateur prompt fait apparaître un pic autour de la fréquence nulle.

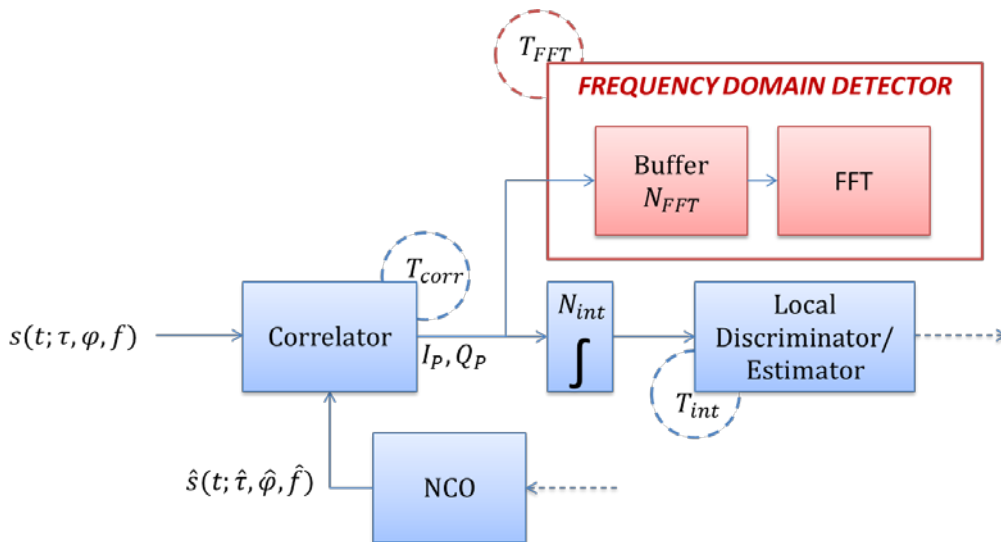


Figure 21: Détecteur dans le domaine de fréquence

Il est proposé ici de réaliser une FFT sur 1024 points utilisant 128 points du signal. L'architecture de ce module est présentée figure 21. La sortie de ce bloc peut être exploitée pour 1) la détection de masquage, 2) l'estimation du rapport C/N_0 , 3) le calcul de la bande de bruit garantissant un rapport signal sur bruit plus interférence donné [14].

Cette analyse permet également la détection de trajet NLOS qui ne sont pas exploités dans le cadre de cette étude. En effet l'exploitation de signaux NLOS nécessite la connaissance du trajet suivi par ce signal, cette connaissance nécessitant une description de l'environnement 3D dans lequel évolue le récepteur.

Détection dans le domaine des retards

L'idée est d'utiliser les spécificités de la boucle vectorielle pour l'implantation de détecteurs de multi-trajets. Ces détecteurs opèrent à la sortie d'un discriminateur de retard comme illustré figure 22 :

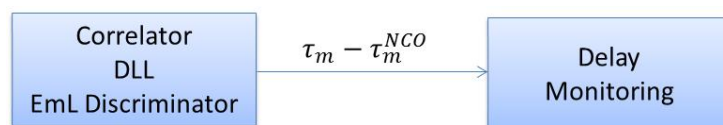


Figure 22: Détection de multi-trajets dans le domaine des retards

Un test statistique est défini. Il porte sur module du signal de sortie du discriminateur avance moins retard [15].

$$|EmL(\Delta\tau)| = |R(\Delta\tau + 2\Delta) - R(\Delta\tau - 2\Delta) + n_{EmL}|. \quad (36)$$

Le test suivant est considéré:

$$\begin{cases} H_0 \text{ (absence de NLOS): } EmL(l) = n_{EmL}(l) \\ H_1 \text{ (présence de NLOS): } EmL(l) = \delta\tau_{MP}(k) + n_{EmL}(l) \end{cases} \quad \text{pour } l \in \{-L + 1, \dots, 0\} + k \quad (37)$$

où $\delta\tau_{MP}$ est l'erreur de retard induite par le trajet NLOS.

La puissance du bruit additif est estimée à partir de l'analyse en fréquence, et le rapport de vraisemblance est obtenu sous l'hypothèse que l'amplitude du signal NLOS n'est pas connue:

$$\frac{H_1}{H_0} \frac{|\overline{EmL}|^2}{\eta} \geq 1 \quad (38)$$

où $\overline{EmL} = \frac{1}{L} \sum_{l=0}^{L-1} EmL(l+k)$ et η est le seuil proposé pour ce test.

Nous considérons ici que le stress de l'oscillateur et du navigateur peuvent être négligé. Dans ce cas la sortie du discriminateur représente l'innovation sur la mesure de retard, qui peut être utilisée pour mettre à jour le navigateur. Le seuil η peut être défini dynamiquement à partir de la matrice de covariance de l'innovation estimée par le navigateur, et du bruit de mesure.

$$\eta = \frac{k}{\sqrt{L}} \sqrt{\sigma_{\tau_m}^2 + \sigma_{\tau}^2} = \frac{k}{\sqrt{L}} \sqrt{H_{2m-1} P^{NS} H_{2m-1}^T + \sigma_{\tau}^2} \quad (39)$$

où k est réglé à 2.5, et $\sigma_{\tau_m}^2$ is la variance de l'erreur de mesure qui dépend du rapport C/N_0 .

Stratégie pour la gestion des multi-trajets

La détection des multi-trajets s'opèrent dans le domaine des fréquences et dans le domaine des retards. L'analyse en fréquence est utilisée pour définir le temps d'intégration des corrélateurs, de façon à garantir un rapport puissance du signal sur puissance du bruit (bruit blanc + interférence) satisfaisant. Lorsque ce rapport ne peut être atteint pour des durées d'intégration de 100ms le signal est déclaré absent. La boucle est positionnée en mode VTL, permettant la poursuite en aveugle du signal. Elle n'est pas utilisée pour l'élaboration du vecteur de mesure utilisé par le navigateur. Lorsqu'un canal satisfait les exigences de l'analyse en fréquence il est soumis à des tests dans le domaine des retards. En cas de contamination dans le domaine des retards deux approches peuvent être retenues :

- Le nombre de mesures délivrées au navigateur est jugé suffisant. Le canal est poursuivi en mode VTL. Les mesures qu'il délivre ne sont pas utilisées tant que le test élaboré au niveau du détecteur qui opère dans le domaine des retards n'est pas satisfait.
- Le nombre de mesures délivrées au navigateur est jugé insuffisant. Le canal est poursuivi en mode VTL. Les mesures qu'il délivre sont utilisées par le navigateur basé sur un filtre de Kalman robuste. Ces mesures sont obtenues en sortie d'un discriminateur étroit qui limite l'impact des multi-trajets.

Traitement le domaine des retards

Dans le cadre de cette étude le traitement dans le domaine des retards est basé sur l'utilisation de discriminateurs réglables en résolution. Des discriminateurs très étroits permettent de réduire l'impact de multi-trajets mais peuvent être affectés par un stress important au niveau des NCOs. Le stress sur un paramètre $\tilde{\theta}$ (pouvant représenter le retard ou la fréquence à estimer) peut être réduit pour une boucle VTL.

Dans le cas d'une boucle STL le bruit sur le paramètre estimé dépend du bruit d'estimation de la boucle STL, de l'erreur due à la dynamique du véhicule non modélisée par la boucle STL $(\sigma_{\tilde{\theta}}^{DYN})^2$, du bruit du à l'oscillateur $(\sigma_{\tilde{\theta}}^{Oscillator})^2$:

$$(\sigma_{\tilde{\theta}}^{NCO})^2 = (\sigma_{\tilde{\theta}}^{DYN})^2 + (\sigma_{\tilde{\theta}}^{Oscillator})^2 + \sigma_{\tilde{\theta}}^2 \quad (40)$$

Dans le cas d'une boucle VTL le bruit sur le paramètre estimé dépend du bruit d'estimation de la boucle VTL, de l'erreur due à la dynamique du véhicule non modélisée par le navigateur $(\sigma_{\theta}^{NAV})^2$, du bruit du à l'oscillateur $(\sigma_{\theta}^{Oscillator})^2$:

$$(\sigma_{\theta}^{NCO})^2 = (\sigma_{\theta}^{NAV})^2 + (\sigma_{\theta}^{Oscillator})^2 + \sigma_{\theta}^2 \quad (41)$$

Le gain qui résulte de l'utilisation d'une boucle VTL vient d'une réduction du bruit d'estimation qui résulte de cette architecture. Il peut venir d'une réduction du bruit sur la dynamique du véhicule lorsque le navigateur est couplé à une centrale inertielle.

Dans le contexte de cette étude nous admettons que l'oscillateur qui équipe le récepteur, de technologie OCXO (*Oven Controlled X-tal(Crystal) Oscillator*), est stable ; que le navigateur est adapté à la dynamique du véhicule. Dans le cas d'une architecture vectorielle, le stress sur le NCO ne dépend alors que de la qualité de la solution de navigation, mesurée à partir de l'équation (28), et la résolution du discriminateur peut être adaptée en fonction de cette qualité.

Pour le récepteur étudié ici un banc de 7 corrélateurs est utilisé pour construire une corrélation en phase, un discriminateur avance-moins-retard (*EML*), et 2 discriminateurs "Double Delta ($\Delta\Delta$)".

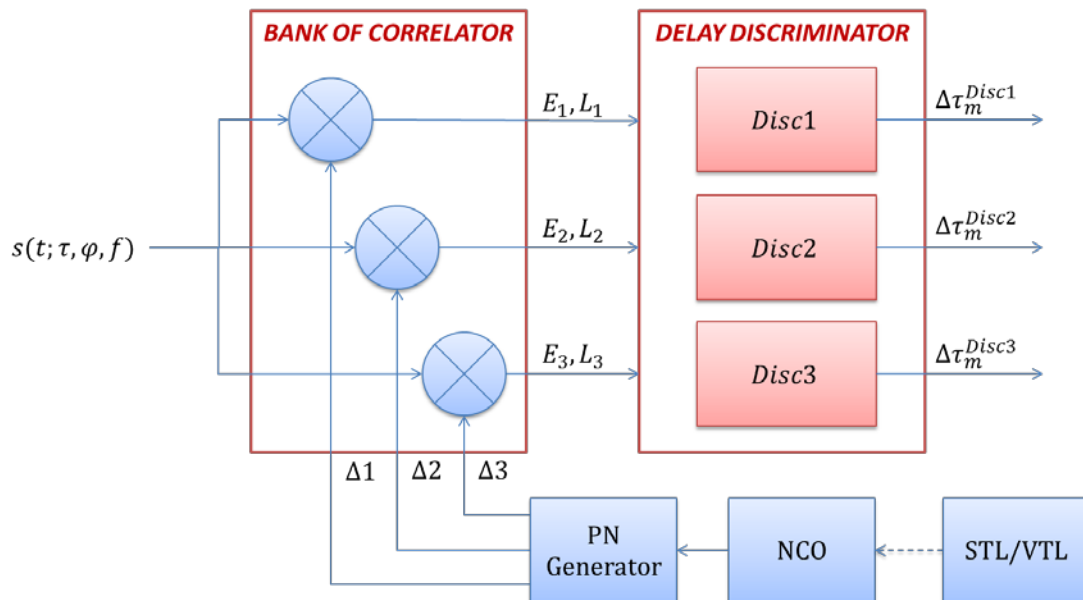


Figure 23: Architecture du discriminateur reconfigurable

Corrélateur Prompt	:	$P(\Delta\tau) = R(\Delta\tau)$
Corrélateur très en avance	:	$E3(\Delta\tau) = R(\Delta\tau + 2\Delta)$
Corrélateur en avance	:	$E2(\Delta\tau) = R(\Delta\tau + \Delta)$
Corrélateur peu en avance	:	$E1(\Delta\tau) = R\left(\Delta\tau + \frac{\Delta}{2}\right)$
Corrélateur peu en retard	:	$L1(\Delta\tau) = R\left(\Delta\tau - \frac{\Delta}{2}\right)$
Corrélateur en retard	:	$L2(\Delta\tau) = R(\Delta\tau - \Delta)$
Corrélateur très en retard	:	$L3(\Delta\tau) = R(\Delta\tau - 2\Delta)$

Le discriminateur avance-moins-retard (*EML*) est obtenu à partir des corrélateurs en avance et en retard :

$$S^{EML}(\Delta\tau) = E3(\Delta\tau) - L3(\Delta\tau).$$

Les discriminateurs avance-moins-retard $\Delta\Delta$ sont obtenus de la manière suivante :

$$S^{\Delta\Delta 1}(\Delta\tau) = E1(\Delta\tau) - L1(\Delta\tau) - \frac{1}{2}(E2(\Delta\tau) - L2(\Delta\tau))$$

$$S^{\Delta\Delta 2}(\Delta\tau) = E2(\Delta\tau) - L2(\Delta\tau) - \frac{1}{2}(E3(\Delta\tau) - L3(\Delta\tau)).$$

Enveloppe d'erreur des discriminateurs

L'enveloppe d'erreur obtenue pour chacun des discriminateurs est représentée figure 24. Elle montre les valeurs extrêmes, obtenues pour des multi-trajets en phase et en opposition de phase par rapport au trajet direct, de l'erreur introduite par un multi-trajet, en fonction du retard que ce multi-trajet présente par rapport au trajet LOS. Cette représentation met en évidence que l'utilisation du discriminateur $\Delta\Delta$, défini pour un espacement de 0.1 chip, permet de limiter l'erreur de poursuite à des valeurs inférieures à 5 mètres.

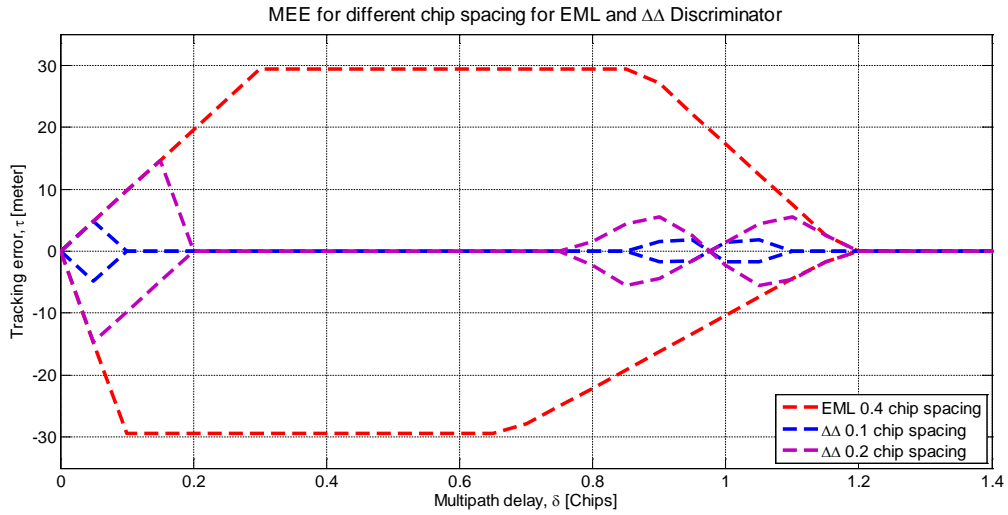


Figure 24: Enveloppe d'erreur des discriminateurs proposés.

En pratique le discriminateur est choisi en fonction de la règle défini dans [10].

$$3\sigma_{\tau} + R_e \leq \frac{D}{2}. \quad (42)$$

où σ_{τ} est l'écart-type de l'erreur de poursuite, R_e est l'erreur induite par l'oscillateur et la dynamique du véhicule, et D est la plage de fonctionnement du discriminateur. La figure 25 permet d'observer cette plage qui est réduite à [-15 mètres, +15 mètres] pour le discriminateur le plus étroit.

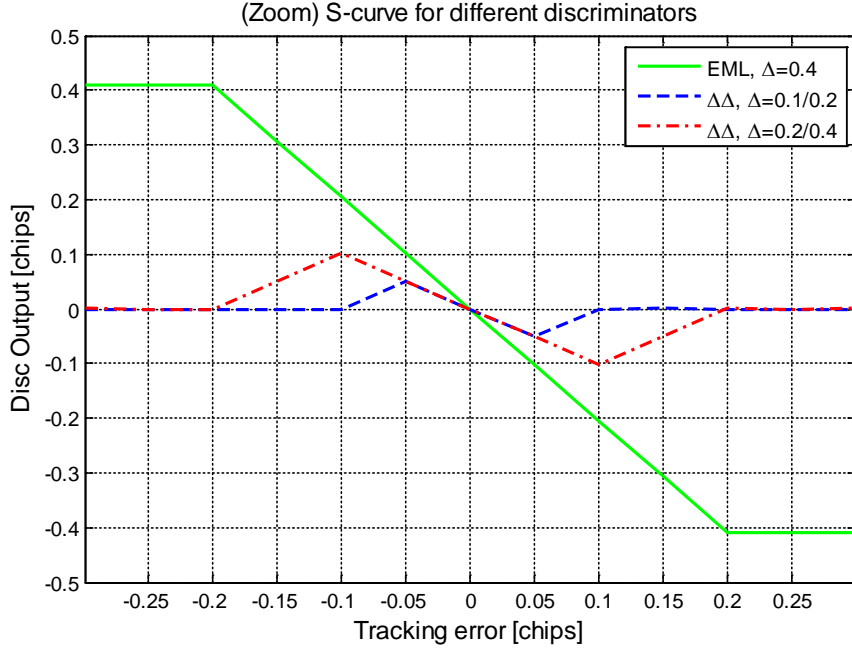


Figure 25: Courbe en S des discriminateurs proposés.

Gestion des mesures de retard

Lorsque des mesures sont utilisées en présence de multi-trajet à la fréquence du trajet direct, ces mesures sont exploitées par un filtre de Kalman robuste. Dans un premier temps un gain est défini en fonction de la puissance de l'innovation en utilisant la fonction d'influence β telle que:

$$\beta_{m,k}^{\Delta\tau} = \beta(\tilde{t}_{m,k} - \hat{t}_{m,k}^-) \quad (43)$$

où $\tilde{t}_{m,k}$ and $\hat{t}_{m,k}^-$ représentent respectivement la valeur de la mesure de retard et la valeur a priori de cette mesure. Cette valeur a priori est déduite de l'état prédit par le navigateur. On note $\sigma_{\Delta\tau} = \sqrt{H_{2m-1} P^{NS} H_{2m-1}^T + \sigma_{\tau}^2}$ l'écart-type de l'erreur sur l'innovation. La fonction d'influence est définie ainsi:

$$\beta(e) = \begin{cases} e, & |e| \leq k_{\Delta\tau,1}\sigma_{\Delta\tau} \\ e + k_{\Delta\tau,1}\sigma_{\Delta\tau} \left(1 - \exp\left\{ \frac{(e + k_{\Delta\tau,1}\sigma_{\Delta\tau})^2}{2(k_{\Delta\tau,2}\sigma_{\Delta\tau})^2} \right\} \right), & k_{\Delta\tau,1}\sigma_{\Delta\tau} < e < 3\sigma_{\Delta\tau} \\ e - k_{\Delta\tau,1}\sigma_{\Delta\tau} \left(1 - \exp\left\{ \frac{(e - k_{\Delta\tau,1}\sigma_{\Delta\tau})^2}{2(k_{\Delta\tau,2}\sigma_{\Delta\tau})^2} \right\} \right), & -3\sigma_{\Delta\tau} < e < -k_{\Delta\tau,1}\sigma_{\Delta\tau} \\ 0, & \text{ailleurs} \end{cases} \quad (44)$$

Cette fonction est représentée figure 26, pour $\sigma_{\Delta\tau} = 1$, $k_{\Delta\tau,1}=1.5$, $k_{\Delta\tau,2}=1$.

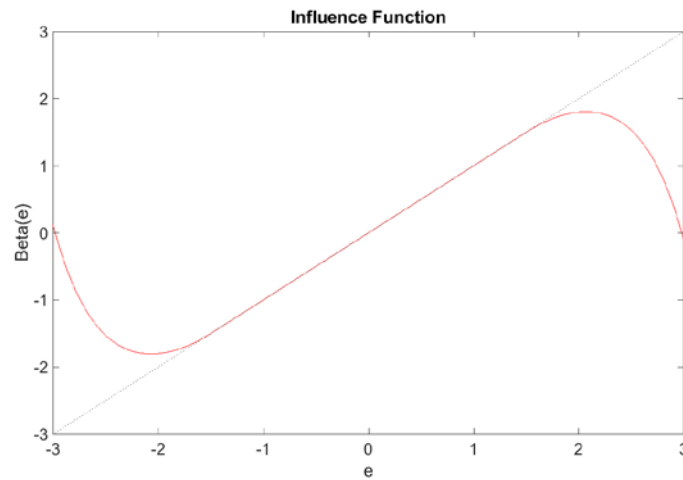


Figure 26: Fonction d'influence β .

Cette fonction est utilisée pour pondérer la matrice d'observation, en fonction de l'amplitude de l'innovation :

$$\gamma_{m,k}^{\Delta\tau} = \frac{\beta(\tilde{t}_{m,k} - \hat{t}_{m,k}^-)}{\tilde{t}_{m,k} - \hat{t}_{m,k}^-} = \frac{\beta_{m,k}^{\Delta\tau}}{\tilde{t}_{m,k} - \hat{t}_{m,k}^-}. \quad (45)$$

Le coefficient de pondération est représenté figure 27, pour $\sigma_{\Delta\tau} = 1$, $k_{\Delta\tau,1}=1.5$, $k_{\Delta\tau,2}=1$.

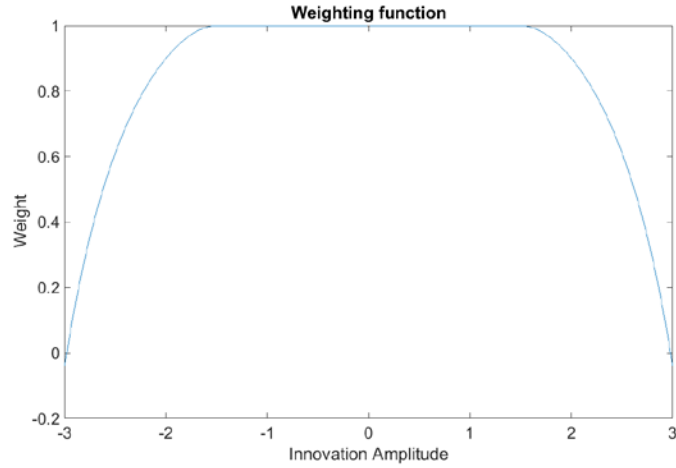


Figure 27: Fonction de pondération.

Le modèle de mesure est alors défini par le vecteur de mesure ΔY_m^{NS} and la matrice d'observation H^{NS} :

$$\Delta Y_{m,k}^{NS} = \begin{bmatrix} \tilde{t}_{m,k} - \hat{t}_{m,k}^- \\ \tilde{f}_{m,k} - \hat{f}_{m,k}^- \end{bmatrix} \quad (46)$$

$$H_k^{NS} = \Gamma_k^{\Delta\tau} H_k^{NS} \quad (47)$$

où $\Gamma_k^{\Delta\tau}$ est une matrice diagonale dont les éléments de la diagonale sont $(\gamma_{1,k}^{\Delta\tau}, 1, \dots, \gamma_{m,k}^{\Delta\tau}, 1, \dots)$.

Performance du récepteur proposé

Les performances de ce récepteur sont évaluées en simulation (figure 28), en utilisant les 2 modèles de canaux présentés précédemment.

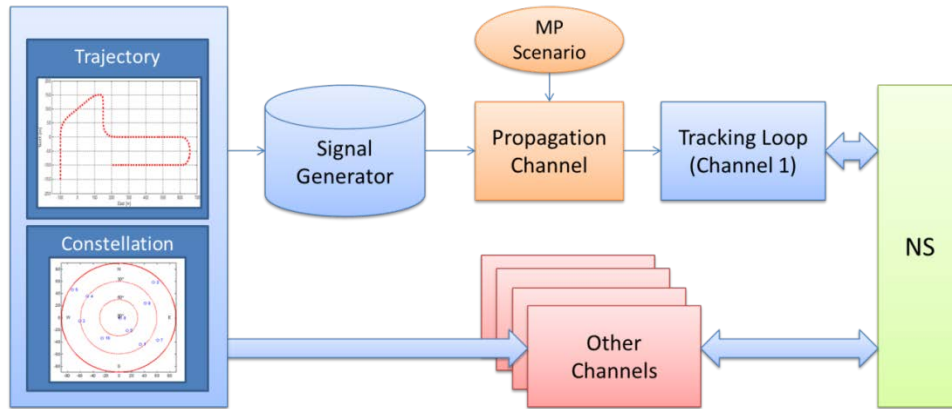


Figure 28: Principe de la simulation.

Une constellation de 5 satellites est considérée. Cette constellation est décrite figure 29. Sur la durée de la simulation les effets des multi-trajets sont pris en compte pour 1 des 5 satellites alors que les 4 autres satellites sont considérés comme sains. La trajectoire suivie par le véhicule est représentée figure 30. Plusieurs scénarios sont simulés, en utilisant le simulateur basé sur un modèle de canal déterministe, ou le simulateur du DLR.

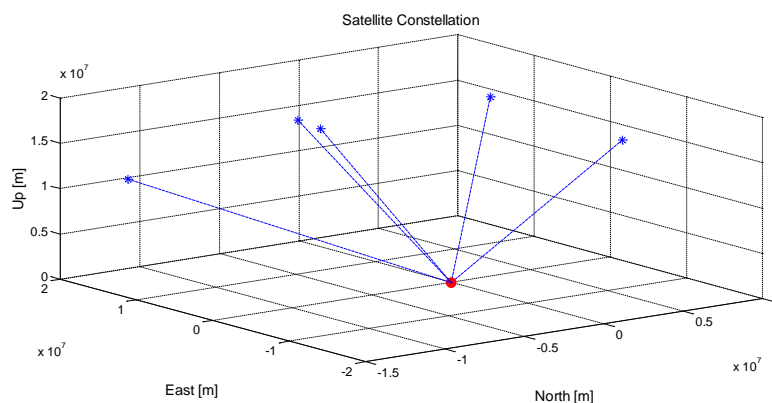


Figure 29: Constellation.

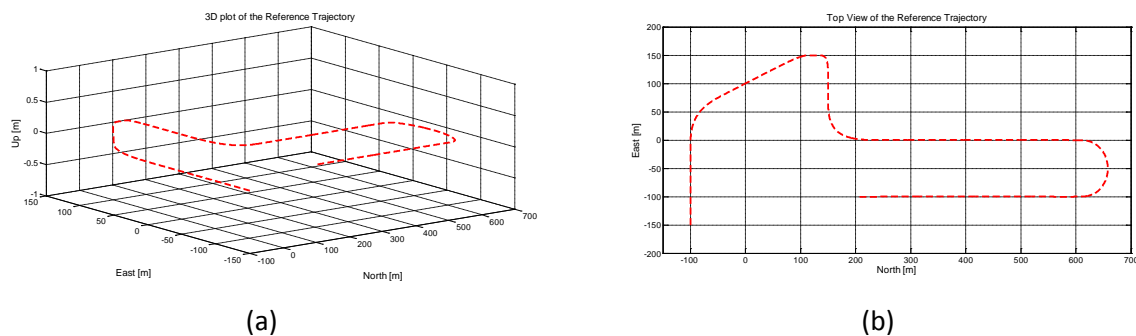


Figure 30: Trajectoire.

Les performances de l’algorithme utilisant les principes décrits dans ce chapitre sont comparés aux performances obtenues avec une architecture basée sur une boucle scalaire et une architecture basée sur une boucle vectorielle conventionnelle.

Modèle de canal déterministe

Des perturbations sont générées pour le canal considéré. Ces perturbations consistent à la prise en compte d’un multi-trajet spéculaire sur des portions de la trajectoire. Les paramètres de ce multi-trajet sont donnés dans le tableau ci-après.

Tableau 12: Description des paramètres d’un multi-trajet spéculaire.

	Time Interval [s]	A [unit]	f [Hz]	τ [chips]	φ [rads]	Remark
Scenario 1	3-8	0.6	7	0.1	$\pi/4$	
	4-10	0.7	18	0.2	$\pi/2$	
Scenario 2	31-36	0.4	6	0.2	$\pi/2$	Lost DP from 35s to 40s
	32-38	0.5	-11	0.1	$\pi/4$	
Scenario 3	96-103	0.5	7	0.1	$\pi/4$	
	98-104	0.4	18	0.2	$\pi/2$	
	96-102	0.6	0	0.6	$\pi/4$	
Scenario 4	160-170	0.4	0	0.6	$\pi/4$	
	165-180	0.5	1	0.5	$\pi/2$	

La trajectoire estimée par l’algorithme adaptatif (aVTL) est comparée aux trajectoires obtenues en mode STL et en mode VTL classique. On observe sur la figure 31 que les bonnes performances obtenues en utilisant une boucle aVTL contrôlée de façon dynamique dépendamment des sorties des détecteurs.

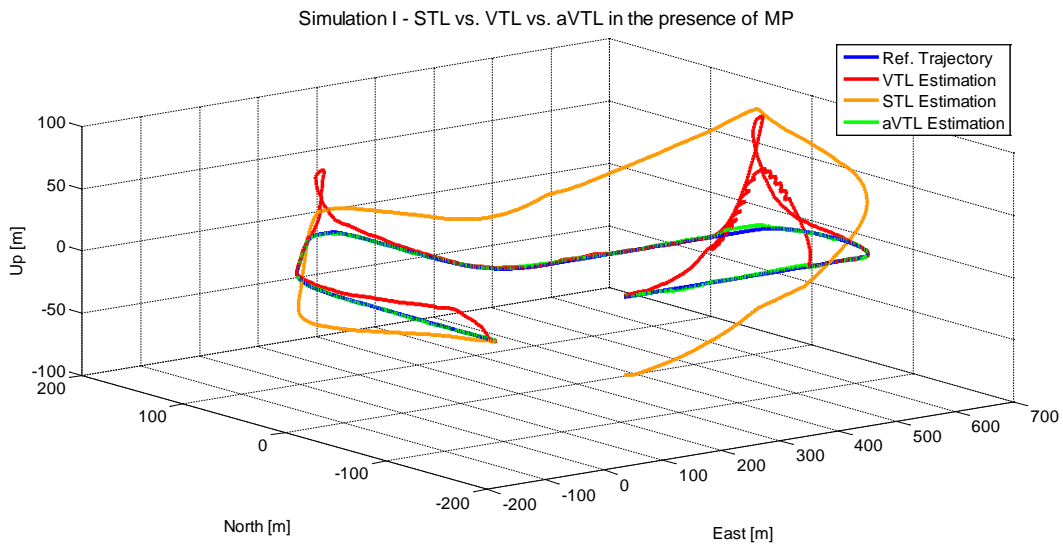


Figure 31: Trajectoire 3D estimée dans les modes STL, VTL et aVTL.

De même la représentation 3D met en évidence les améliorations apportées par l'architecture aVTL.

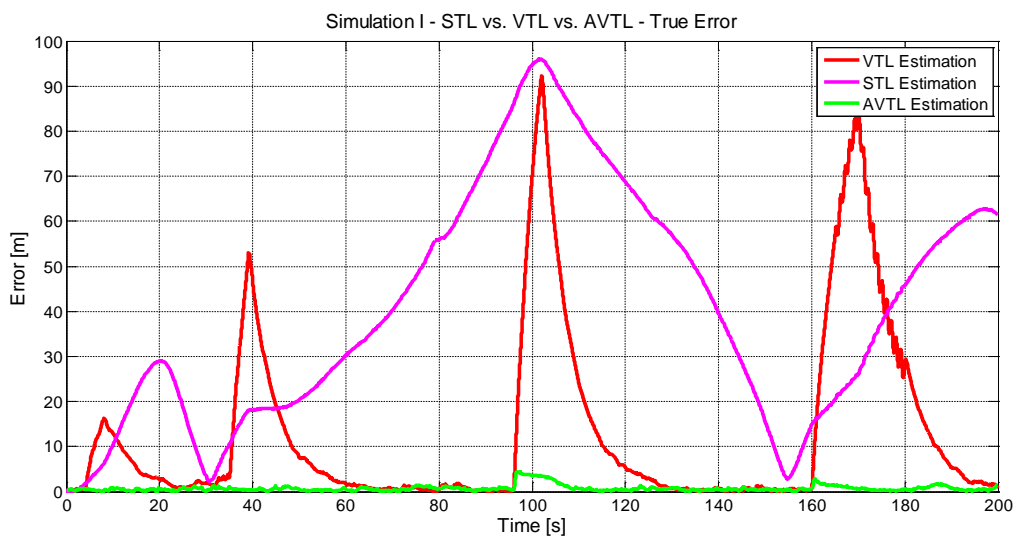


Figure 32: Erreur 3D sur les trajectoires estimées dans les modes STL, VTL et aVTL

Modèle DLR

Des simulations ont ensuite été conduites en utilisant le simulateur de canal du DLR pour modéliser le signal du canal sous test dans un environnement urbain. La trajectoire n'est pas modifiée. Les autres satellites ne sont pas affectés par les multi-trajets. Les figures 32 et 33 montrent le spectre du signal de sortie du corrélateur prompt. Ces figures mettent surtout en évidence l'évolution de la

puissance du trajet direct. On note également une remontée du bruit au voisinage de la fréquence nulle due à des multi-trajets dont l'énergie est étalée dans le domaine des fréquences. Ces multi-trajets n'affecteront pas le récepteur lorsque le temps d'intégration est correctement choisi.

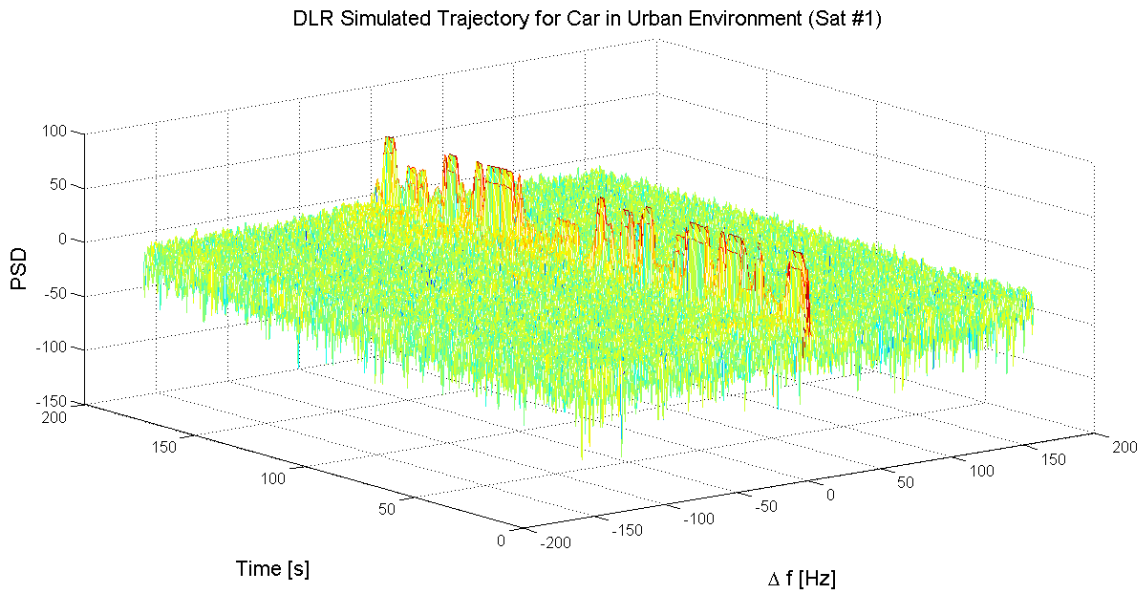


Figure 33: Densité spectrale (3D) en sortie du corrélateur prompt.

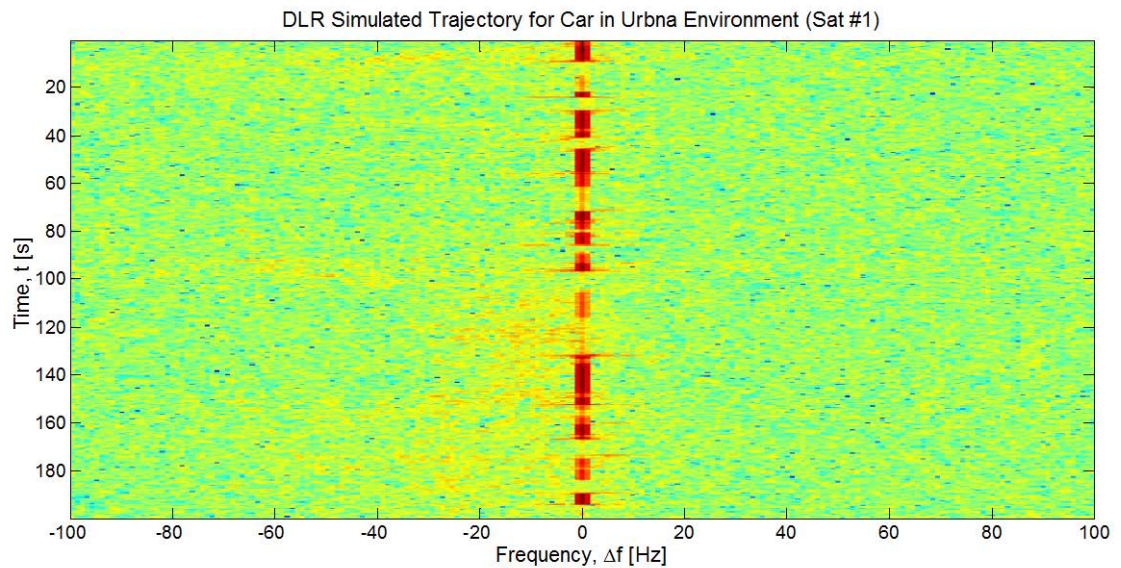


Figure 33: Densité spectrale (2D) en sortie du corrélateur prompt.

Comme pour la simulation précédente les performances de l'algorithme adaptatif (aVTL) sont analysées à partir des figures 34 et 35. Elles mettent en évidence les améliorations apportées par l'algorithme proposé.

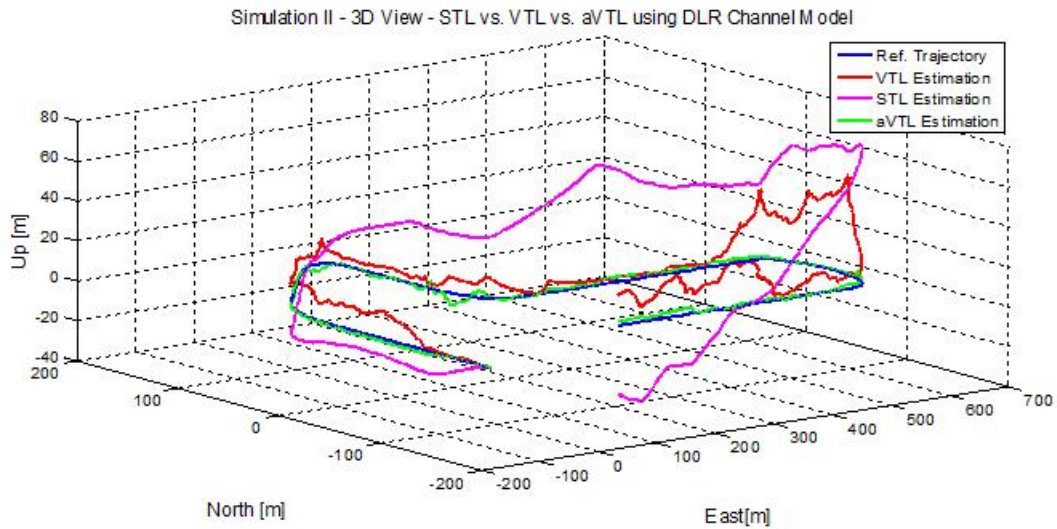


Figure 34: Trajectoire 3D estimée dans les modes STL, VTL et aVTL.

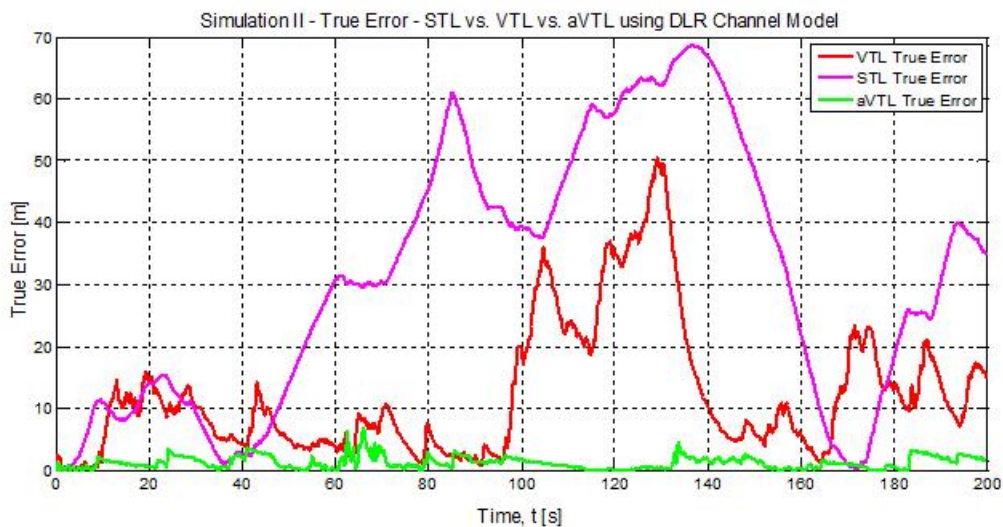


Figure 35: Erreur 3D sur les trajectoires estimées dans les modes STL, VTL et aVTL.

CHAPITRE 6 : Conclusion

L'architecture de récepteur étudiée dans le cadre de cette thèse a montré l'intérêt d'une boucle vectorielle pour adresser la problématique de la navigation en environnement urbain. Des

améliorations ont été apportées sans induire une forte augmentation de la complexité du récepteur. Ces améliorations sont dues principalement à l'architecture retenue qui permet de réduire le stress sur les NCOS du récepteur, à la mise en place de détecteurs de multi-trajets opérant dans le domaine des fréquences et des retards, aux stratégies proposées en présence de mesures contaminées. L'évaluation des solutions proposées repose sur des simulations qui utilisent un modèle de canal représentatif de l'environnement. Des simulations à partir de signaux collectés sur le terrain seraient nécessaires. Elles nécessiteraient l'implantation de toutes les fonctions d'un récepteur fonctionnant sur la base de l'architecture analysée dans le cadre de cette étude

Bibliographies

- [1] A. Giremus, J.Y. Tournet and A. Doucet, "A Fixed-Lag Particle Filter for the Joint Detection/Compensation of Interference Effects in GPS Navigation," *IEEE Transactions on Signal Processing*, vol. 58, no. 12, pp. 6066-6079, 2010.
- [2] N. Viandier, J. Marais, A. Rabaoui and E. Duflos, "GNSS pseudorange error density tracking using Dirichlet Process Mixture," in *13th Conference on Information Fusion (FUSION)*, Edinburgh, 2010.
- [3] M. Spangenberg, V. Calmettes, O. Julien, J.-Y. Tournet and G. Duchateau, "Detection of Variance Changes and Mean Value Jumps in Measurement Noise for Multipath Mitigation in Urban Navigation," *NAVIGATION*, vol. 57, no. 1, pp. 35-52, 2010.
- [4] N. Sokhandan, A. Broumandan, J. T. Curran and G. Lachapelle, "High Resolution Delay Estimation for Urban GNSS Vehicular Navigation," in *Proceedings of the 25th International Technical Meeting of The Satellite Division of the Institute of Navigation (ION GNSS 2012)*, Nashville, TN, 2012.
- [5] K. Dragūnas and K. Borre, "Multipath Mitigation Based on Deconvolution," *Journal of Global Positioning System 2011*, vol. 10, no. 1, pp. 79-88, 2011.
- [6] M. Spangenberg, V. Heiries, A. Giremus and V. Calmettes, "Multi-Channel Extended Kalman Filter for Tracking BOC modulated signals in the presence of multipath," in *18th International Technical Meeting of the Satellite Division of the Institute of Navigation*, Long Beach, 2005.
- [7] R. D. J. Van Nee, J. Sierveld, P. C. Fenton, and B. R Townsend, "The Multipath Estimating Delay Lock Loop: Approaching Theoretical Accuracy Limits", *IEEE Position, Location and Navigation Symposium*, Las Vegas, Nevada, April U-15, 1994.
- [8] M. Lashley and D. M. Bevely, "Analysis of Discriminator Based Vector Tracking Algorithms," in *Proceedings of the National Technical Meeting of The Institute of Navigation*, San Diego, 2007.
- [9] A. Lehner and A. Steingass, "A Novel Channel Model for Land Mobile Satellite Navigation," in *Proc. 18th International Technical Meeting of the Satellite Division of The Institute of Navigation (ION GNSS 2005)*, Long Beach, 2005.

- [10] P. W. Ward, J. W. Betz and C. J. Hegarty, "Chapter 5: Satellite Signal Acquisition, Tracking and Data Demodulation," in *Understanding GPS: Principles and Applications*, 2nd ed., E. D. Kaplan, Ed., Norwood, MA, Artech House, 2006, pp. 153-241.
- [11] A. Lehner, "Multipath Channel Modelling for Satellite Navigation System," Ph.D dissertation, Technischen Fakultät der Universität Erlangen-Nürnberg, Erlangen, 2007.
- [12] A. Jahn, H. Bischl and G. HeiB, "Channel Characterisation for Spread Spectrum Satellite Communication," in *IEEE 4th International Symposium on Spread Spectrum Techniques and Applications Proceedings*, Mainz, 1996.
- [13] J.-H. Won, D. Dötterböck and B. Eissfeller, "Performance Comparison of Different Forms of Kalman Filter Approach for a Vector-Based GNSS Signal Tracking Loop," *NAVIGATION*, vol. 7, no. 3, pp. 189-199, 2010
- [14] J.-R. De Boer, W. Vigneau, V. Calmettes, S. Bidon and L. Ries, "Specification of a Simulator to Access the Performance of Adaptive Vector Tracking Loops in Urban Environment," in *6th European Workshop on GNSS Signals and Signals Processing*, Munich, 2013.
- [15] CENTRE NATIONAL D'ETUDES SPATIALES, et al , "Dispositif de poursuite intègre de signaux GNSS", Brevet B1509- France - Dépôt de demande de brevet français Numéro: 1553315, 15 avril 2015